THE UNIVERSITY OF QUEENSLAND

AUSTRALIA

Phase Equilibria Studies of Zinc-containing Copper Smelting Slags

Hongquan Liu

Master of Engineering

A thesis submitted for the degree of Doctor of Philosophy at

The University of Queensland in 2016

School of Chemical Engineering

Abstract

The smooth operation and productivity of the copper smelters are highly dependent on the comprehension of slag chemistry under the smelting conditions. Phase equilibria of slag principally control the melting temperatures of the slags and proportions of solids at fixed operating temperatures. Due to the decrease of copper ore grade as well as the use of complex feeds, appreciable amount of ZnO is present in the copper smelting slags. The aim of the present study is to investigate the liquid temperature and phase relations of the zinc-containing copper smelting slag systems.

Due to the fast vaporization of zinc under reducing conditions, experimental techniques have been developed to enable the phase equilibrium studies of zinc-containing system at copper smelting conditions to be carried out. The experimental procedures in present studies involve master slags preparation, high temperature equilibration, quenching and electron probe X-ray microanalysis (EPMA). The methodology applied in the present study allows the phase assemblages and compositions of the phases existing in the quenched samples to be spontaneously analysed by EPMA.

The phase equilibria studies on the zinc-containing slag systems have been conducted under fixed oxygen partial pressure (Po_2) at 10^{-8} atm at temperature range from 1443 K (1170 °C) to 1573 K (1300 °C). The slag systems investigated in the present studies including:

(1) A reinvestigation on "FeO"-SiO_2 system at temperature range from 1473 K (1200 °C) to 1573 K (1300 °C). The experimental outcomes improve the accuracy of phase diagram of this system at Po_2 10^{-8} atm.

(2) ZnO-"FeO"-SiO_2 system at temperature range from 1443 K (1170 °C) to 1573 K (1300 °C). The experimental outcomes indicate that the liquidus temperature is much higher than "FeO"-SiO_2 pseudo-binary system with the presence of ZnO in the slag.

(3) ZnO-"FeO"-SiO_2-Al_2O_3 system at temperatures, 1523 K (1250 °C), 1543 K (1270 °C) and 1573 K (1300 °C) with Al_2O_3 varying from 2 to 6 wt pct. The experimental results show that the increase of Al_2O_3 content in the slag phase increases the liquidus temperature in the spinel phase. The distribution of ZnO with the presence of Al_2O_3 tends to be in spinel than the liquid phase.

(4) ZnO-"FeO"-SiO_2-MgO system at temperatures, 1523 K (1250 °C), 1543 K (1270 °C) and 1573 K (1300 °C) with MgO varying from 2 to 6 wt pct. The experimental results

indicate that increasing MgO content in the slag phase significantly increases the liquidus temperature in the spinel primary phase field. The presence of MgO in the ZnO-"FeO"-SiO_2-MgO system has minor effect on partitioning behaviour of ZnO between in the spinel and liquid phases.

(5) ZnO-"FeO"-SiO_2-CaO system at temperatures, 1523 K (1250 °C), 1543 K (1270 °C) and 1573 K (1300 °C) with CaO varying from 2 to 6 wt pct and 2 wt pct sulphur. The experimental outcomes suggest that the increasing of CaO concentration in the slag phase will significantly increases the liquidus temperature in the spinel primary phase field; the introduction of CaO into the slag has minor effect on the ZnO partitioning behaviour between the spinel and liquid phases.

(6) Preliminary experimental work ZnO-"FeO"-SiO_2-CaO-S system at temperatures 1443 K (1170 °C) and 1473 K (1200 °C). The experiment results indicate that 2 wt pct of sulphur in the liquid phase significantly decrease the liquidus temperature, up to 70 K compared to the ZnO-"FeO"-SiO_2-CaO system.

The experimental work from present studies fill the gap of zinc-containing copper smelting slag under conditions relevant to that in industrial practice. With the experimental outcomes obtained in present studies, more accurate information of the slag chemistry of zinc-bearing slag systems are now available for industrial smelter operation as well as for the thermodynamic modelling of the copper smelting slags.

The evaluation of minor elements (arsenic and zinc) distributions among the gas / slag / matte phases during the copper smelting process were carried out. Literature reviews of existing experimental data and models of the distributions show that the operating parameters in smelting process have major impact on the fractional distribution behaviours of As and Zn. Thermodynamic calculation software - FactSage 6.4 was applied to predict the distribution behaviours of As and Zn as function of the operating parameters during the smelting process and compared with the literatures. The study of minor element distributions will improve the understanding of thermodynamic behaviours, and benefit the management of minor elements during copper smelting process.

Declaration by author

This thesis is composed of my original work, and contains no material previously published or written by another person except where due reference has been made in the text. I have clearly stated the contribution by others to jointly-authored works that I have included in my thesis.

I have clearly stated the contribution of others to my thesis as a whole, including statistical assistance, survey design, data analysis, significant technical procedures, professional editorial advice, and any other original research work used or reported in my thesis. The content of my thesis is the result of work I have carried out since the commencement of my research higher degree candidature and does not include a substantial part of work that has been submitted to qualify for the award of any other degree or diploma in any university or other tertiary institution. I have clearly stated which parts of my thesis, if any, have been submitted to qualify for another award.

I acknowledge that an electronic copy of my thesis must be lodged with the University Library and, subject to the policy and procedures of The University of Queensland, the thesis be made available for research and study in accordance with the *Copyright Act 1968*.

I acknowledge that copyright of all material contained in my thesis resides with the copyright holder(s) of that material. Where appropriate I have obtained copyright permission from the copyright holder to reproduce material in this thesis.

Publications during candidature

1. H. Liu, Cui Z., Chen M. and Zhao B., "Phase equilibrium study of ZnO-"FeO"-SiO_2 system at fixed Po_2 10^{-8} atm", Proceedings of High Temperature Processing Symposium, Editors M. Akbar Rhamdhani and Geoffrey Brooks, publisher Swinburne University of Technology, Melbourne, Australia, ISBN 978-0-9875930-2-3, 2014, pp. 117-124.

2. H. Liu, Z. Cui, M. Chen and B. Zhao, "Phase Equilibrium Study of ZnO-"FeO"-SiO_2 System at Fixed Po_2 10^{-8} atm", *Metall. Mater. Trans. B*, 47 (2016): 164-173.

3. Liu H., Cui Z., Chen M. and Zhao B., "Phase equilibria studies in the system ZnO-"FeO"-SiO_2-Al_2O_3 for copper smelting slags", *Proceedings of High Temperature Processing Symposium*, Editors Geoffrey Brooks and M. Akbar Rhamdhani, publisher Swinburne University of Technology, Melbourne, Australia, ISBN 978-0-9875930-3-0, 2015, pp. 99-102.

4. H. Liu, Z. Cui, M. Chen and B. Zhao, "Phase Equilibria Study of the ZnO-"FeO"-SiO_2-Al_2O_3 System at Po_2 10^{-8} atm", *Metall. Mater. Trans. B*, 47 (2016): 1113-1123.

Publications included in this thesis

H. Liu, Z. Cui, M. Chen and B. Zhao, "Phase Equilibrium Study of ZnO-"FeO"-SiO_2 System at Fixed Po_2 10^{-8} atm", *Metall. Mater. Trans. B*, 47 (2016): 164-173. – incorporated as Chapter 5.

Contributor	Statement of contribution
H. Liu	Designed experiments (60%) Wrote the paper (60%)
Z. Cui	Provided industrial smelting operating data and samples
M. Chen	Designed experiments (10%) Wrote the paper (15%)
B. Zhao	Designed experiments (30%) Wrote the paper (25%)

H. Liu, Z. Cui, M. Chen and B. Zhao, "Phase Equilibrium Study of ZnO-"FeO"-SiO_2-Al_2O_3 System at Fixed Po_2 10^{-8} atm", *Metall. Mater. Trans. B*, 47 (2016): 1113-1123 – incorporated as Chapter 6.

Contributor	Statement of contribution
H. Liu	Designed experiments (65%) Wrote the paper (80%)
Z. Cui	Provided industrial smelting operating data
M. Chen	Designed experiments (15%) Wrote the paper (5%)
B. Zhao	Designed experiments (20%) Wrote the paper (15%)

Contributions by others to the thesis

Contributions by Prof. Baojun Zhao and Dr. Mao Chen in experiment design, concept, analysis, interpretation, drafting, and writing in the advisory capacity.

Statement of parts of the thesis submitted to qualify for the award of another degree

None

Acknowledgements

I would like to thank my principle supervisor Prof. Baojun Zhao for his support and guidance all through the candidature. I also wish to thanks my associate supervisor Prof. Anh V. Nguyen for his valuable suggestions and encourage.

I also would like to thank the following for their assistance during my study:

Dr. Mao Chen at the University of Queensland who helped me in experiments design, outcomes interpretation and paper writing.

Ms. Jie Yu at the University of Queensland who helped me developing the high temperature experimental skills.

Ms. Ying Yu, Mr Ron Rasch and Dr. Kim Sewell from the Centre for Microscopy and Microanalysis (CMM) within the University of Queensland who trained and assisted me using the equipment at CMM.

I wish to thank Dongying Fangyuan Nonferrous Metals Co., Ltd. and The University of Queensland for their financial support of this research through “Fangyuan Fellowship” program, and to the University of Queensland International Research Tuition Award (UQIRTA) and China Scholarship Council (CSC) for providing scholarships for Hongquan Liu.

Finally, I would like to thank my parents and beloved wife Min Gao for the supporting and encourage, especially at the tough time during the candidature.

Keywords

Phase equilibria, zinc-containing copper smelting slags, EPMA, fractional distribution behaviour

Australian and New Zealand Standard Research Classifications (ANZSRC)

ANZSRC code: 091407 Pyrometallurgy 100%

Fields of Research (FoR) Classification

FoR code: 0914 Resources Engineering and Extractive Metallurgy 100%

TABLE OF CONTENTS

LIST OF FIGURES

LIST OF TABLES

1 Introduction

1.1 Overview of Pyrometallurgical Copper Production

Copper, due to its malleability and ductility, as well as excellent heat and electrical conductivity, is widely used in many fields such as automobiles, building construction and infrastructure, which makes it the third major industrial metal in the world. It was reported that about 22.4 million metric tons of copper was produced in 2014.[1]

There are two main routes nowadays to produce copper - pyrometallurgical route and hydrometallurgical route. Around 80% of the copper ore originates in Cu-Fe-S ores which was usually treated by pyrometallurgical route as shown in Figure 1.1[2].

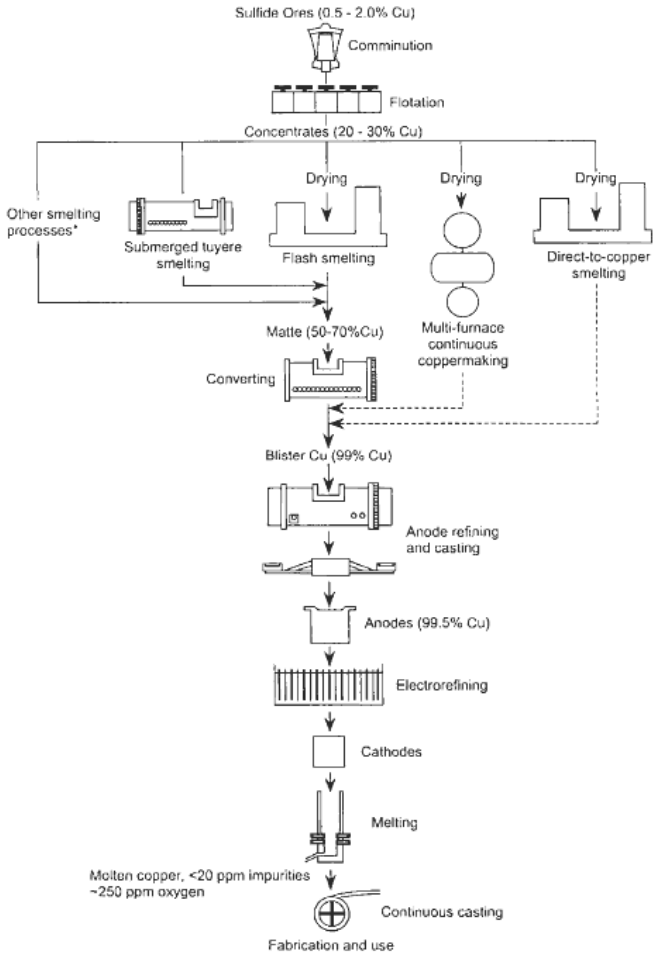

Figure 1.1 Pyrometallurgical route of extracting copper from sulphide ores[2]

Figure 1.1 illustrates the main steps of extracting copper from the ores, which consists of four steps[2]:

1) Flotation of Cu-Fe-S and Cu-S particles in the ore into a concentrate
2) Smelting the concentrate to molten high-Cu matte
3) Converting the matte into impure molten copper

4) Fire- and electro-refining the impure copper into high purity copper

The smelting is one of the key processes in the copper production which generally proceeds in a large and hot furnace. Various techniques were developed these years for the smelting process such as flash smelting process, Noranda process, Ausmelt and etc. A summary of the smelters developed was shown in Table 1.1[2-5]. The Noranda, Teniente, Vanyukov and Fangyuan smelting processes can generally be classified as the submerged tuyere smelting. In all, flash and bath smelting technologies are the major processes used in modern copper making industry[6].

Table 1.1 Summary of smelters used in the pyrometallurgical copper production[2-5]

Smelting type	Furnace Type	Year commercialized	Country of Origin	Current Use (up to 2010)
Flash smelting	OUTOTEC Flash smelting	1949	Finland	30
	INCO Flash Smelting	1952	Canada	4
Submerged Tuyere Smelting	Noranda Process	1973	Canada	3
	Teniente Smelting	1977	Chile	7
	Vanyukov Smelting	1977	Russian Federation and Kazakhstan	3
	Fangyuan Bottom Blowing Process*	2008	China	3
Bath Matte Smelting	Ausmelt/Isasmelt	1999	Australia	16
	Mitsubishi Process	1974	Japan	4

∗The number of copper smelter using SKS Bottom Blowing Process up to 2012

The concepts of the bottom blown oxygen process for both lead and copper smelting developed was originated by Hunan Shuikoshan Mineral Bureau, jointly with China Nonferrous Engineering and Research Institute (now China Enfi Engineering Corp.)[7]. It was the first company, Dongying Fangyuan Nonferrous Metals Co., Ltd., to commercialise the bottom blowing smelter technology in the real industrial production in 2008.

During the development in past few years, great improvements have been achieved, such as oxygen lance design, feed preparation, off-gas handling, operating and process control strategies, *et al*. The target was to find new technologies that could be applied to 1) treat low grade complex copper concentrate; 2) to recover not only copper but also other valuable metals such as gold and silver; 3) to generate off-gases with higher SO_2 concentration for acid plant and 4) to have low operating costs while improving the environmental performance.[7]

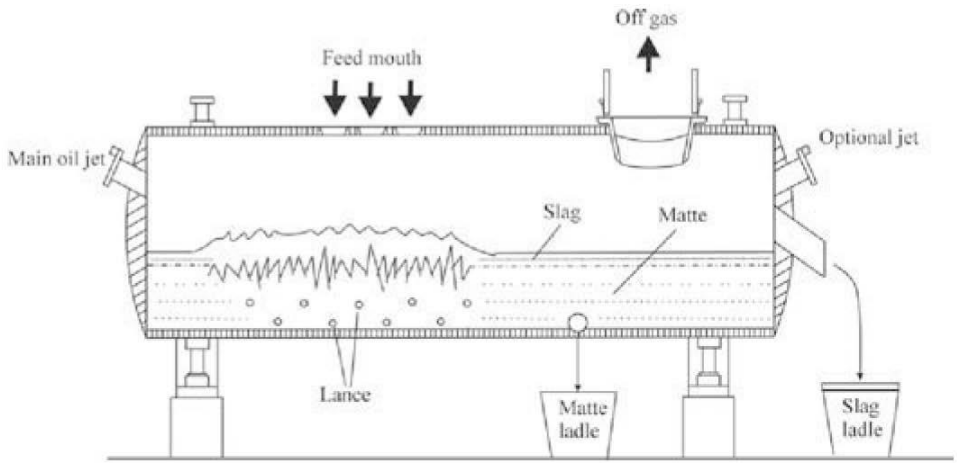

Figure 1.2 Schematic of bottom blown oxygen furnace[7]

The Fangyuan bottom blown oxygen furnace (Figure 1.2) is a horizontal furnace that equips with 9 oxygen lances arranged in two rows at the bottom. During the operation, concentrates are continuously charged into the furnace through the feed mouth located above the reaction zone. Oxygen and air are blown constantly by the oxygen lances into molten copper matte layer, in which iron and sulphur are rapidly oxidized and slag is also formed. Slag formed above the matte layer in the furnace can be tapped regularly through a taphole at one end of the furnace.

The principal role of the slag is to assist in the separation of useful metal from the unwanted chemical species in the slag. During smelting operations, the viscosities of slags, which are determined by the compositions, can have a major influence on mixing rate of charge, separation of different phases, slag tapping rate etc. One of the advantages of the bottom blown oxygen furnace is that it can operate auto-thermally without extra fuel. It was found that the furnace was operated under the liquidus temperature of the slag, which indicates the existence of solid phase and brings high risk of viscosity issues. The phase equilibrium study to fully understand the thermodynamic behaviour of the slag for prediction of the viscosity is essential to optimize the composition of the slag, thus affect efficiency of the smelting process.

1.2 Slag Chemistry

In the smelting process (step 2), the Cu-Fe-S concentrates are smelted to form the matte, which can be described using the reactions as follows:

$$CuFeS_2\ (ore) + O_2 \rightarrow (Cu,Fe)S\ (matte) + FeO + SiO_2$$

$$FeO + SiO_2 \rightarrow FeO{\bullet}\ SiO_2\ (slag)$$

It can be seen that the fayalite slag ($FeO{\bullet}SiO_2$) is one of the major product during the smelting which generally includes silicate glasses, iron oxide and droplets of matte entrained.

Quenched slag samples (Figure 1.3) have been collected from the bottom blown furnace at Dongying Fangyuan Nonferrous Metals. The compositions of the phases present in the slag were measured by EPMA and the results are given in Table 1.2 [7]. The bulk composition of the slag was analysed with XRF by ALS Laboratory Group (Brisbane, Australia). Both EPMA and XRF can only analyse elemental compositions. The oxidation states of the oxides given in Table 1.2 are for presentation purpose, and then all components were normalized to 100 percent as shown in Table 1.2.

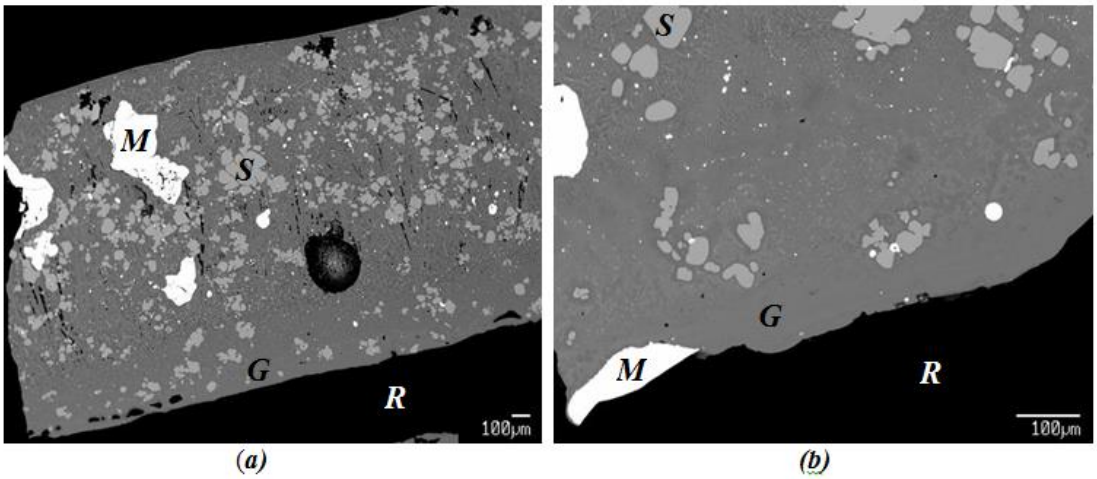

Figure 1.3 Typical microstructures of quenched smelting slag from Fangyuan bottom blown furnace, G = glass; M = matte; R = resin; S = spinel[7]

It can be seen from Table 1.2 that matte, liquid and spinel are the main components existed in the slag. Significant amount of ZnO and Al_2O_3 was found to be present in the liquid and spinel phases. The primary component of the present slag sample from Fangyuan Company is "FeO"-SiO_2-Al_2O_3-ZnO system with small amount of CaO, MgO, S and etc.

Table 1.2 Compositions (wt%) of phases present in copper smelting slag

Phases	"FeO"	Cu_2O	CaO	SiO_2	Al_2O_3	As_2O_3	MgO	S	PbO	ZnO	MoO_3
bulk-XRF	62.2	3.2	1	24.2	3.1	0.1	0.6	1.7	0.5	3.1	0.2
glass	58.4	0.8	1.2	30.5	3.2	0.1	0.7	1.1	0.5	3.3	0.2
spinel	93.7	0.1	0	0.6	3.4	0	0.3	0	0.1	1.7	0.1
matte	10.1	68.9	0	0	0	0.1	0	20.3	0.1	0.2	0.3

The selection of the oxygen partial pressure to investigate the real slag equilibration is essential in the present study. It was reported that the matte grade in the Fangyuan bottom blowing furnace can reach up to 72 %.[7] Figure 1.4 shows the thermodynamic calculation of the relationship of oxygen partial pressure, sulphur partial pressure with the matte grade in the equilibration of slag, matte with spinel[8] which indicates that at matte grade between 70 to 75 %, the oxygen partial pressure is between 10^{-7} to 10^{-8} atm at 1300 ^{o}C. Direct measurement of the oxygen probe in the smelter under

industrial process shows that the average Po_2 was 10^{-8} atm at 1315 °C [9]. Therefore, the oxygen partial at 10^{-8} atm was selected in the present study.

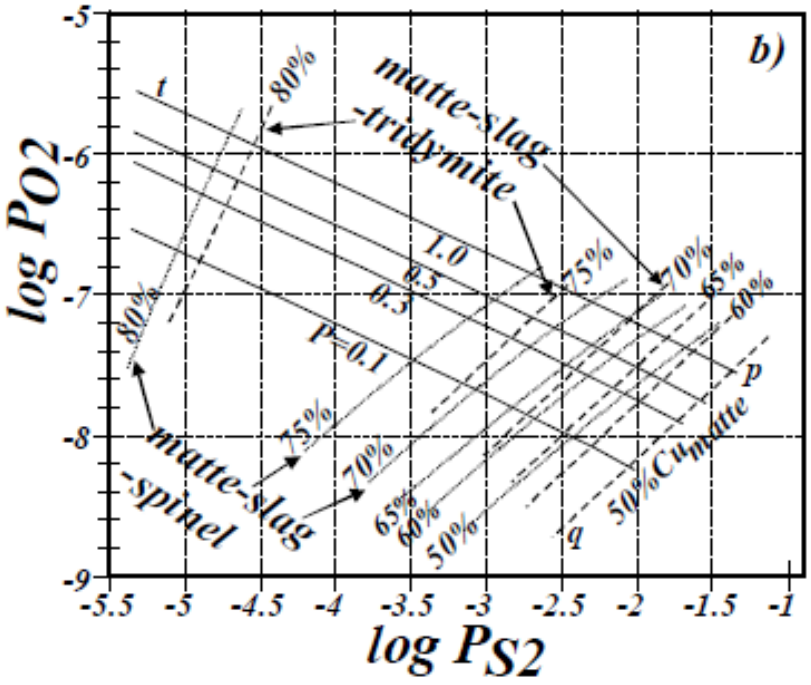

Figure 1.4 S-O predominance diagram for the system Cu-Fe-Si-O-S calculated by FactSage at 1300 °C[8]

1.3 Aim of This Research

In the present slag system, with high content of ZnO in the slag, it is necessary and crucial to understand the effect of the presence of ZnO to the liquidus temperature and phase relationships of the slag under the copper smelting condition. In this case, the first objective is to develop techniques that can be applied to Zn-containing slag systems under Po_2 at 10^{-8} atm; secondly, phase equilibrium studies will be designed and conducted from the ZnO-"FeO"-SiO_2 pseudoternary system to ZnO-"FeO"-SiO_2-based quaternary systems under copper smelting condition which would directly benefit the optimization of the metallurgy process in copper production and the thermodynamic modelling of copper smelting slags.

1.4 References

1. ICSG-Internatinal Copper Study Group. World Copper Production and Usage, 1900–2014p. The World Copper Factbook 2015, 2015. In: http://www.icsg.org/index.php/press-releases/finish/170-publications-press-releases/2092-2015-10-03-icsg-factbook-2015.

2. M. E. Schlesinger, M. J. King, K. C. Sole and W. G. I. Davenport: *Extractive metallurgy of copper*. (Elsevier, Oxford, 2011).

3. K. Jiang, L. Li, Y. Feng, H. Wang and B. Wei, In *T.T. Chen Honorary Symposium on Hydrometallurgy, Electrometallurgy and Materials Characterization*, (2012), pp 165-176.

4. R. R. Moskalyk and A. M. Alfantazi, *Miner. Eng.*, 2003, vol. 16, pp. 893-919.

5. J. Gana, *Resources Policy*, 1992, vol. 18, pp. 21-31.

6. V. Ramachandran, C. Diaz, T. Eltringham, C. Y. Jian, T. Lehner, P. J. Mackey, C. J. Newman and A. V. Tarasov, *Copper-Cobre 2003*, 2003, vol. IV, p. 104.

7. B. Zhao, Z. Cui and Z. Wang, In *4th International Symposium on High-Temperature Metallurgical Processing*, (John Wiley & Sons, Inc.: 2013), p 10.

8. E. Jak, In *Ninth International Conference on Molten Slags, Fluxes and Salts (MOLTEN12)*, (The Chinese Society for Metals: Beijing, China, 2012), p 28.

9. H. M. Henao, C. Nexhip, D. P. George-Kennedy, P. C. Hayes and E. Jak, *Metall. Mater. Trans. B*, 2010, vol. 41B, pp. 767-779.

2 Literatures Review

2.1 FactSage

FactSage is a powerful thermodynamic calculation software that run through the Gibbs energy minimization process based on the reported experimental data.[1, 2] The FactSage contains varied databases and calculation modules for different applications.[1, 2] In present study, the phase diagram module was applied to predict the phase equilibria of ZnO-containing copper smelting slag systems under Po_2 at 10^{-8} atm. During such calculations, the databases of FToxid and Fact were selected for the solution species and pure compounds respectively.

2.2 FeO"-SiO_2 system

2.2.1 "FeO"-SiO_2 system in equilibrium with metallic Fe

Bowen and Schairer[3] investigated the system "FeO"-SiO_2 using electrolytic iron as crucible under the nitrogen atmosphere to prevent iron from oxidation. The experimentally determined phase diagram (Figure 2.1) showed that the congruently melting temperature for fayalite is close to 1205 °C; the eutectic point between fayalite and wüstite at 1177 °C and a third invariant point between tridymite and fayalite at 1178 °C. In addition, the ferric oxide in liquid phase reached its maximum at 11.5 wt pct as composition of the liquid approach the "FeO" end based on wet chemical analysis. Greig[4, 5] studied the immiscibility gap under iron saturation in gas furnace using the quenching method. Studies on this system were also carried out by Schuhmann[6, 7] with gamma-iron saturation using platinum crucible in the furnace where gas mixture of CO_2 and CO passes through, and results show good agreements with those of Bowen and Schairer[3]. Allen *et al*[8] also performed experiments with techniques similar to those adopted by Schuhmann[6, 7], and found a 2 mol pct difference at the eutectic point ("FeO"-Fe_2SiO_4) comparing to that determined by Bowen, *et al* [3]. However, it was reported by Muan[9] that Fe_2O_3 would increase continuously with decrease of temperature. The comparisons of experimental data in phase equilibration and Fe_2O_3 content in liquid was shown in Figure 2.1.

The system was further optimised by Goel *et al*[10]], Bjoerkman[11], Selleby[12], Wu *et al*[13]. A latest thermodynamic optimization of Fe-Si-O system was conducted by Jak[14] based on a critical evaluation of reported data. The calculations combined with

thermodynamics data reported and experimental results show good consistent with the experimental results of Bowen *et al*[3]. However, it is noted that the eutectic temperatures varied from these calculation in some ways.

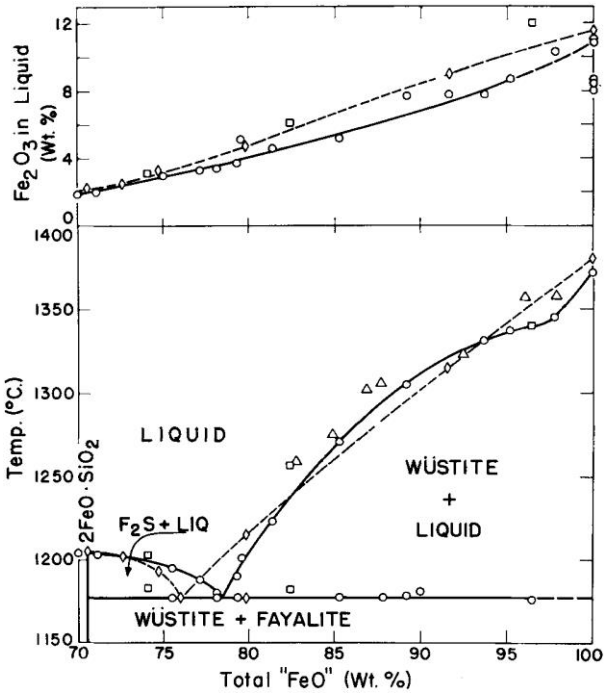

Figure 2.1 Phase diagram of the "FeO"-SiO_2 system (Circle: Allen & Snow in N_2 atmosphere[8]; square, Allen & Snow in controlled CO/CO_2 atmosphere[8]; diamond, Bowen and Schoirer[3]; triangle, R. Schuhmann *et al*[6])

2.2.2 "Fe_2O_3"-SiO_2 system in air

The "Fe_2O_3"-SiO_2 system was investigated by Muan[9, 15] in furnace with air circulating through, of which the result was presented shown in Figure 2.1. The eutectic temperature between magnetite and tridymite was identified at 1455 °C, and two inversion points at 1490 °C, 1470 °C between cristobalite and tridymite, magnetite and hematite, respectively. The immiscibility gap on of this system in air was conducted by Greig[4, 5]. Jak *et al*[14] conducted a critical review and thermodynamic optimization for the Fe-Si-O system using FactSage[2] based on the existing experimental data. According to the calculated phase diagram of the "Fe_2O_3"-SiO_2 system under air condition, the eutectic point between magnetite and tridymite was determined at 1447 °C with the liquid containing 18 wt pct SiO_2 and 82 wt pct Fe_2O_3 and an inversion point close to 1387 °C between magnetite and hematite which is consistent with the reported results[4, 16].

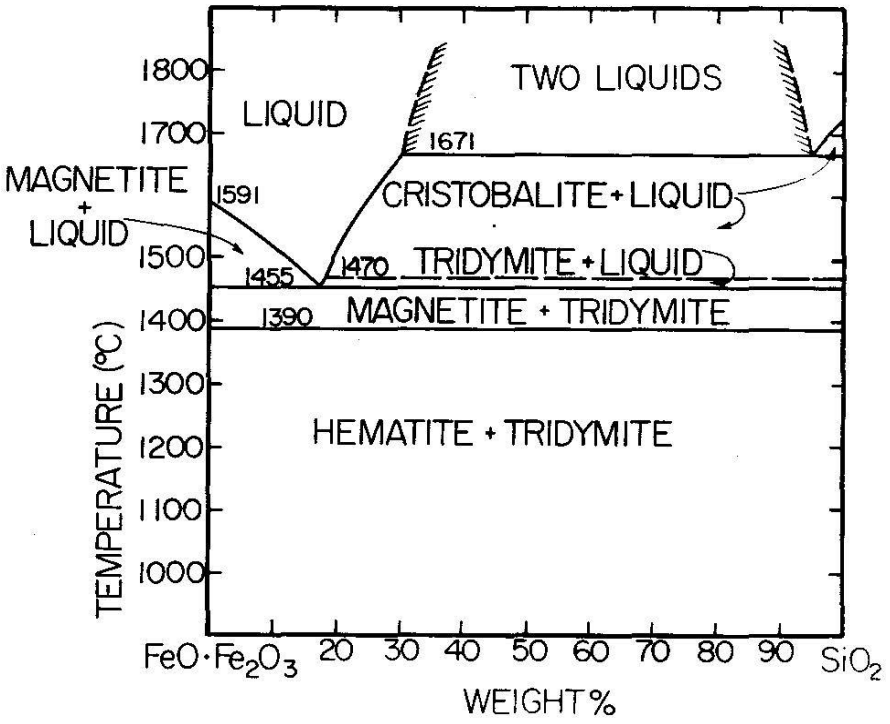

Figure 2.2 Phase diagram of the "FeO"-SiO_2 system in air[17]

2.2.3 "FeO"-SiO_2 system under intermediate oxygen partial pressures

There is limited information of this system under intermediate Po_2 that closely relates to pyrometallurgy of non-ferrous metals, such as copper smelting process, of which the oxygen partial pressure (Po_2) is around 10^{-8} atm[18]. Darken and Gurry[19] investigated the melting point of iron oxide in contact with silica as a function of the Po_2 which was controlled by varied CO_2/CO ratio. Muan[16] systematically studied the FeO-Fe_2O_3-SiO_2 system with Po_2 ranging from $10^{-10.9}$ to 1 atm using different H_2/CO_2 to produce variant oxygen partial pressure in platinum crucible as shown in Figure 2.3 and the phase diagram is now widely accepted and used in the industrial production. Several experiments carried out by Hidayat[20] during the investigation of the CaO-"FeO"-SiO_2 system from 1150 to 1350 °C using Pt as container with Po_2 range from 10^{-6} and 10^{-9} atm by adjusting the CO_2/CO ratio, and result show a good agreement with that from Muan[16].

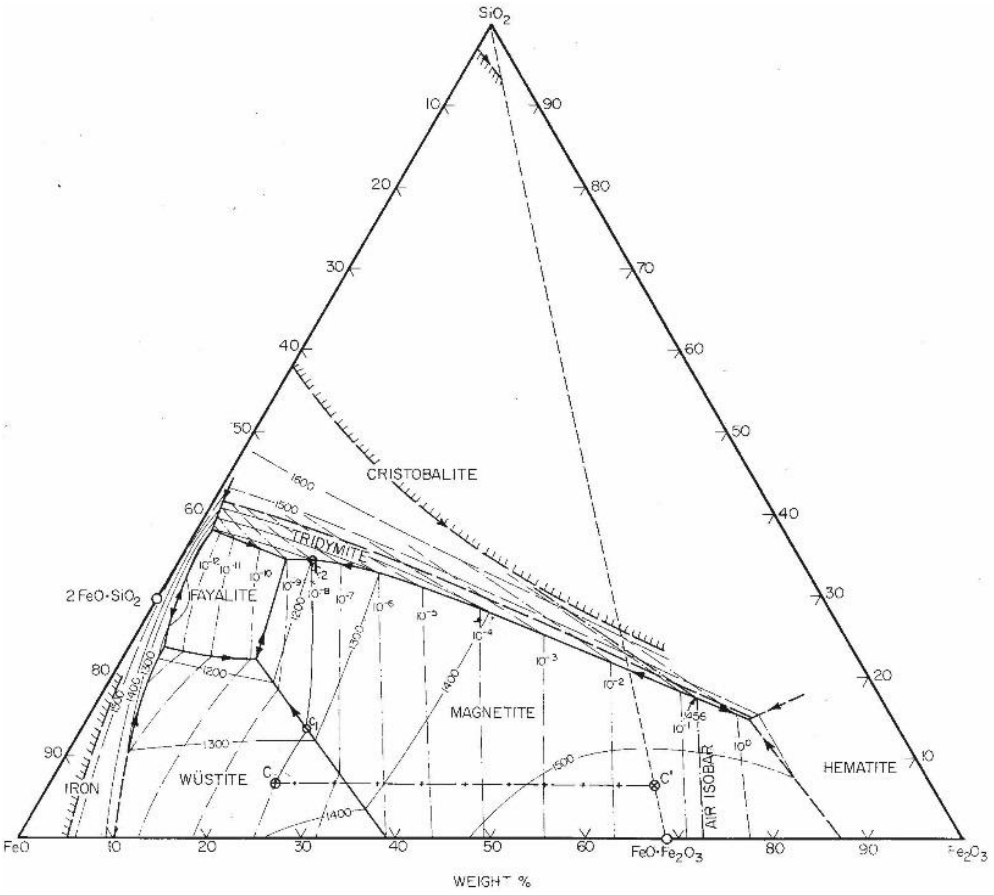

Figure 2.3 Phase diagram of the FeO-Fe_2O_3-SiO_2 system under different oxygen partial pressures[16]

It should be noticed that control the Po_2 has been a key factor to successfully evaluate this system due to the coexisting of ferrous and ferric iron. A summary of the methods that have been reported to control the Po_2 under the intermediate range, was listed in Table 2.1.

Table 2.1 Methods in controlling intermediate Po_2 in quasi binary system "FeO"-SiO_2

Source	Po_2/atm	Method	Comment
L. S. Darken[19, 21]	$6*10^{-7}$~$5.01*10^{-14}$	CO_2-CO gas mixture	Can precisely control the Po_2 in wide range
A. Muan[16]	1~$10^{-10.9}$	CO_2-H_2 gas mixture	Higher thermal diffusion effect, but inappreciable
R. L. Benner[22]	1~10^{-4}	Ar, O_2 gas mixture	Limited Po_2 can be achieved by this method
T. Hidayat[23, 24]	10^{-6}~10^{-9}	CO_2-CO gas mixture	Experiments conducted in CaO-"FeO"-SiO_2 system

As shown above Table 2.1, intermediate po_2 can be achieved by mixing inert gas with O_2 (1-10^{-4} atm) and CO_2 with CO (or CO_2 with H_2) for those between 10^{-5}-10^{-10} atm. It is also reported that intermediate Po_2 can be achieved in closed system using EMF

method of which is controlled by primary phase filed that in equilibrium with the liquid phase[25].

2.3 ZnO-SiO_2 system

This system can be treated as condensed system that the equilibrium between condensed phases and the gas phase can be neglected since sublimation pressure of ZnO under air condition is close to 10^{-3} torr[26] and the boiling point of ZnO under is reported to be 1972 ± 25 °C[27]. Bunting[28] conducted phase equilibria experiments on the system in platinum capsule using quenching methods, following by examinations under the petrographic microscope, and X-ray spectrometer was applied for quantitative analysis (Figure 2.4). Williamson and Glasser[29] reinvestigated the system with SiO_2 ranging from 33 to 55 mol% using similar techniques, of which the result shows good agreements with that by Bunting[28] except that small deviation of the liquidus temperature (less than 15 K) was observed. Their results also suggests that willemite (Zn_2SiO_4) has melting point at 1512 ± 3 °C and ZnO at 1975 ± 25 °C. Two experiments were carried out by Reyes and Gaskell[30] at 1560 °C show good consistency with those of Bunting[28] (Figure 2.4). A comprehensive assessment of the system ZnO-SiO_2 was completed by Bjoerkman[31] combining the reported data. Thermodynamic optimization on the system was also conducted by Jak[32] of which the result shows good agreement with reported results although the eutectic point between zincite and willemite tends to be different form that by determined by Bunting[28].

A reinvestigations of this system were conducted by Hansson *et al*[33] (Figure 2.4) using quench method following by Electron Probe X-ray Microanalysis (EPMA). The obtained phase diagram was presented in Figure 2.4 and compared with those determined by Bunting[28]. The temperatures and compositions of the two eutectic points were determined to be 1448 ± 5 °C, 0.52 ± 0.01 mol fraction ZnO between SiO_2 and willemite and 1502 ± 5 °C, 0.71 ± 0.01 mol fraction ZnO between zincite and willemite. It can be seen that the liquidus temperatures from Hansson *et al*[33] tends to higher than those from Bunting[28] in SiO_2 and zincite as shown in figure 2.4, while lower in the willemite primary phase field. The discrepancy should due be the vaporisation of ZnO at elevated temperature which was omitted in studies by Bunting[28].

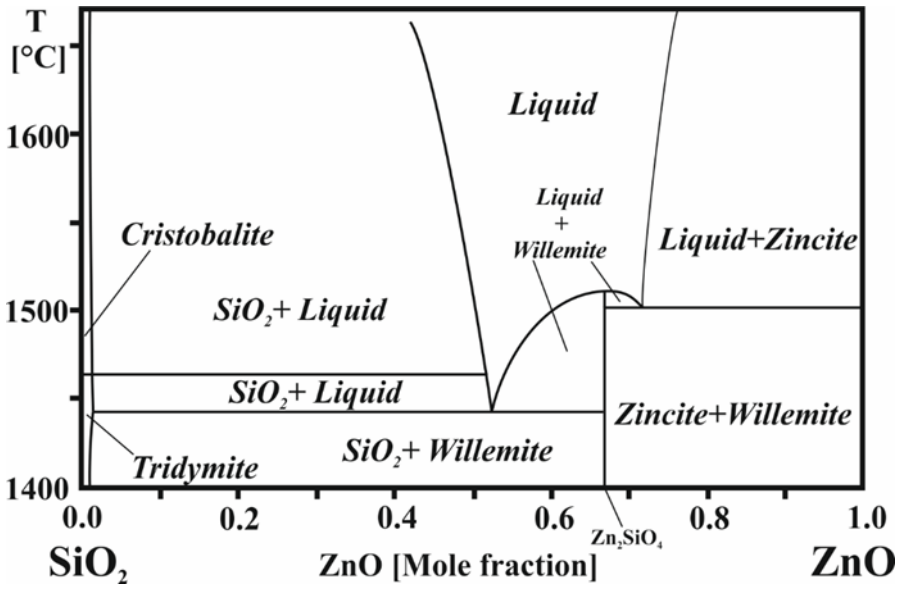

Figure 2.4 Phase diagram of the system ZnO-SiO_2[33]

2.4 ZnO-"FeO" system

2.4.1 ZnO-"FeO" system in equilibrium with metallic Fe

Claude *et al*[34] conducted phase equilibrium study on the system by sealed-tube technique to determine the miscibility between wüstite and zincite under metallic iron saturation at 900 °C during quenching method. Their results show that the solubility of ZnO in wüstite ($Fe_{1-x}O$) was 17% which was independent of x while the $Fe_{1-x}O$ solubility in ZnO was 3.5%. Lykasov *et al*[35] studied the two-phase wüstite-zincite equilibria using electromotive-force measurements (EMF) with a solid electrolyte of yttrium oxide and zirconium dioxide at 847 °C, 897 °C, and 997 °C accompanying by Mossbauer Spectrum, chemical and X-ray analysis to unravel the solute behaviour of ZnO in wüstite. Lykasov *et al*[36] investigated the "FeO"-Fe_3O_4-$ZnFe_2O_4$-ZnO system in the temperature range from 727 °C to 1077 °C using EMF technique. A new phase with composition located between the wüstite and spinel primary phase fields was reported while there is no information regarding the ferric and ferrous iron concentration in zincite was given. Itoh and Azakami[37, 38] investigated the phase relations of the Fe-Zn-O system using evacuated sealed quartz tube at at 827 °C and 927 °C by a quenching technique, of which the results are shown in Figure 2.5 (a) and (b). The results indicated that the phase relations tend to be similar under temepratures at 927 °C and 827 °C with minor difference on the mutual solid solubilities between ZnO and FeO. A number of studies were also conducted in the way that the Po_2 is self-built in close systems where the oxygen potential can be determined by EMF[39-43].

Jak *et al*[44] extensively studied the system under iron saturation using quench technique coupling with EPMA with the temperature ranging from 900 to 1200 °C. Good agreements can be seen between Jak[44] with others (Figure 2.6). Degterov *et al*[45] assessed the available phase equilibria data in the Fe-Zn-O system and performed a thermodynamic optimization of the system by combining different solution models. It can be seen from Figure 2.6 that the model fits well the experimental data between 800 to 1200 °C and reasonably predicts the phase equilibria at temperatures higher than 1200 °C.

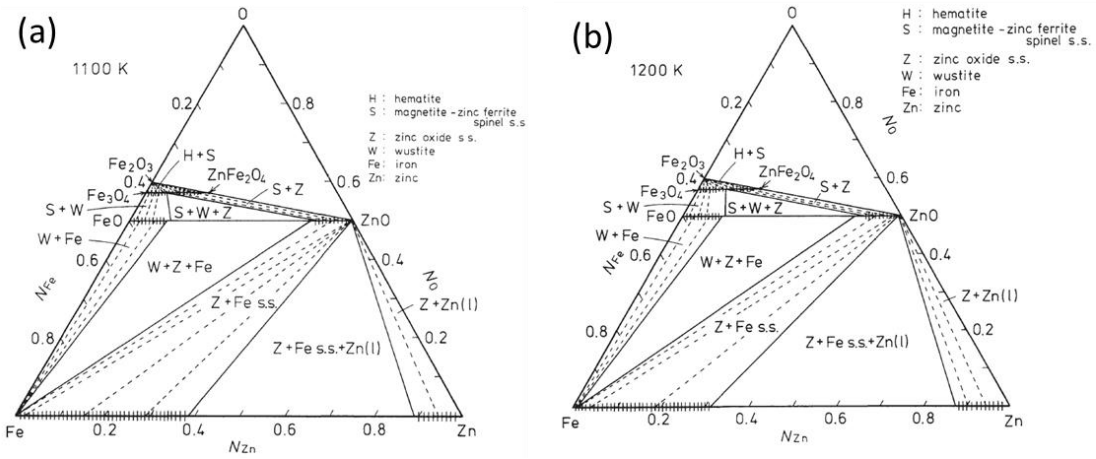

Figure 2.5 Phase diagram of Zn-Fe-O system in equilibrium with metallic iron: (a) at 827 °C[38]; (b) at 927 °C[37]

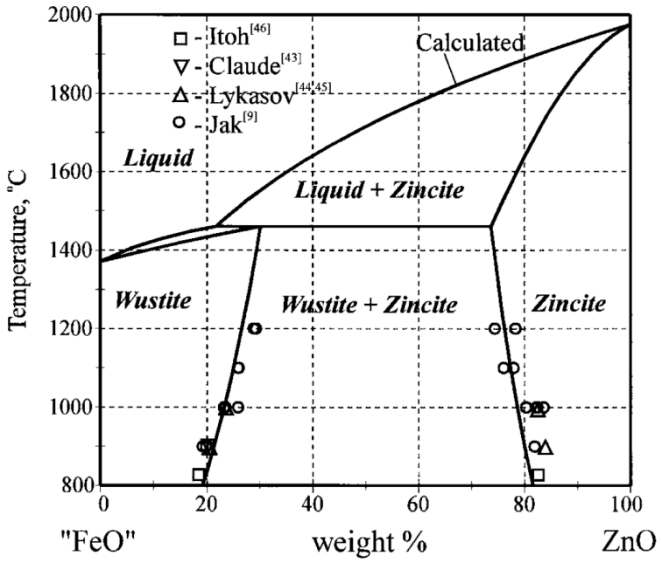

Figure 2.6 Phase diagram of the system "FeO"-ZnO under metallic iron saturation[45]

It should be noticed that ZnO will be reduced by metallic iron under iron saturation according the following reaction:

$$Fe\ (s) + ZnO\ (s) \rightarrow Zn\ (g) + FeO\ (solid\ solution)$$

Even at intermediate Po_2, ZnO may evaporate through the decomposition of ZnO. In this case, experimental techniques should be taken care of to deal with the loss of ZnO from evaporation. A summary of the experimental techniques to inhibit the vaporisation of ZnO is presented in Table 2.2. It is admitted that ZnO evaporation would not be a problem when closed system applied, but systematically investigations on systems involving elements with varied oxidation states can not be conducted by using this method since Po_2 is controlled by the condensed phases in equilibration. A compromise technique had been developed by Jak *et al*[44] to investigate ZnO-containing systems under metallic iron saturation. As shown in Figure 2.7 (a), a pie-type sample technique was adopted in their experiments to minimize the evaporation of ZnO, where the bulk composition change during equilibration is show in the Figure 2.7 (b). This method has been widely applied to conduct phase equilibrium studies on ZnO-containing system by other authors.

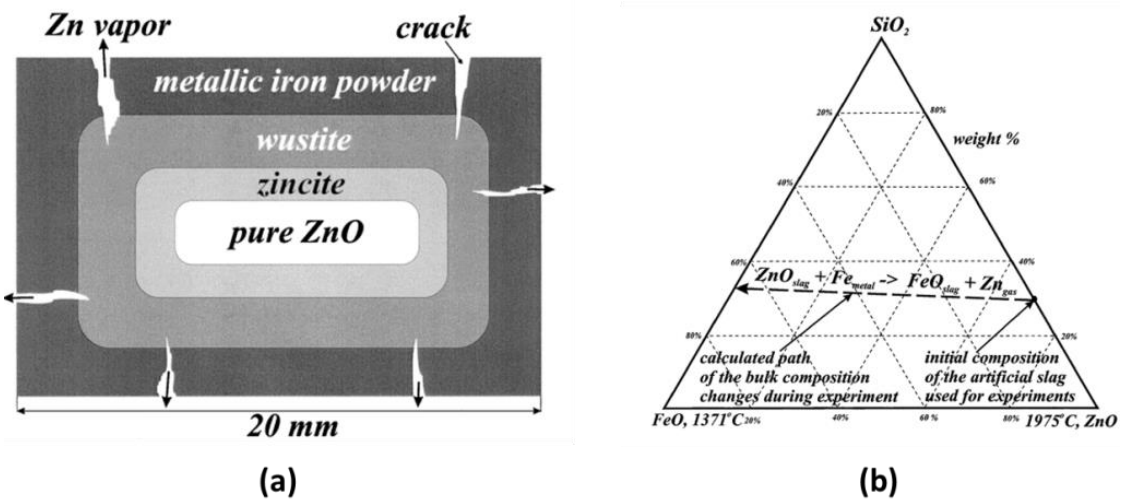

Figure 2.7 Experimental technique applied under metallic iron saturation: (a) - schematic of the pie-type sample; (b) - bulk composition changes during the equilibration.

Table 2.2 Techniques in minimizing the vaporisation of ZnO relating to ZnO-"FeO" system

Source	Po_2	Method	comment
E. Jak[44]	Iron saturation	Pie-type sample applied with ZnO in the centre	Po_2 close to 10^{-12} atm
J.M. Claude[34]	Iron saturation	Sealed-tube	Closed system
R. L. Benner[22]	1~10^{-4} atm	Firmly pack in Pt crucible	No information on ZnO evaporation
I. Katayama[39]	$10^{-3.5}$~10^{-14} atm	closed galvanic cell applied	Closed system while Po_2 can be determined
S. Schaefer[42]	10^{-5}~10^{-7} atm (Fe_2O_3 saturation)	closed galvanic cell applied	Closed system while Po_2 can be determined
S. Itoh[38]	10^{-18}~10^{-22} (Fe-Zn alloy saturation)	closed galvanic cell applied	Closed system while Po_2 can be determined
A. A. Lykasov[46]	Wüstite saturation	closed galvanic cell applied	Closed system while Po_2 can be determined
S. Itoh[37, 47, 48]	10^{-3}~10^{-20} atm	Evacuated sealed-tube	Po_2 controlled by condensed phase
R. Hansson[49]	10^{-4}~10^{-8}, 10^{-10} atm	Mixture placed in Pt crucible	No information on ZnO evaporation

2.4.2 ZnO-Fe_2O_3 system in air

Tanida *et al*[50-52] investigated the iron oxide-ZnO system under air atmosphere at temperatures between 900 to 1450 °C using a quench method coupling with EPMA analyses. The phase relations at sub-solidus temperatures were experimentally determined and the spinel solution present was further characterized by X-ray diffraction and Mössbauer Spectrum to understand the structural details. Degterov *et al*[45] performed the experiments in the Fe-Zn-O system under air condition with temperature ranging from 900 °C to 1500 °C. The quenched samples were further analysed by EPMA. Thermodynamic optimizations of the system were also performed within the temperatures, 800 to 1500 °C based on solution models. Further predictions on the phase equilibria at temperatures higher than 1500 °C were also performed as shown in Figure 2.8. Good consistency can be seen between the model predictions and reported results[22, 39, 52] at sub-solidus temperatures. Another investigation on the same system was conducted by Hansson *et al*[49, 53] in air at temperatures up to 1580 °C using similar methodologies as those adopted by Degterov[45]. The wet chemical analysis was performed to determine the amount of ferrous iron in the quenched samples. Their results show good agreement with the those obtained by Degterov *et al*[45] at all temperatures.

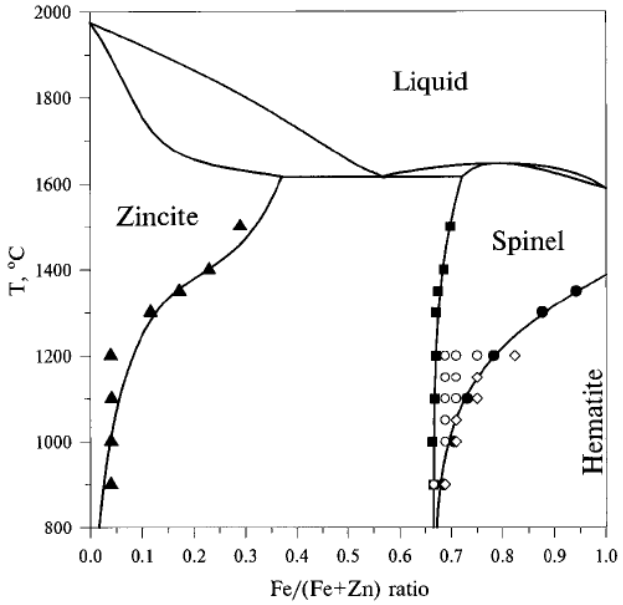

Figure 2.8 Phase diagram of ZnO-Fe_2O_3 under air condition[53] (Open: Tanida[52], solid: Degterov[45])

2.4.3 ZnO-"FeO" system under intermediate Po_2

The phase equilibria behaviours of the FeO-Fe_2O_3-ZnO system have been widely studied due to its importance to non-ferrous pyrometallurgy. Benner and Kenworthy[22] investigated the Fe-Zn-O system with Po_2 varied from 1 to 10^{-4} atm by using different ratio of oxygen-argon gas mixture at 1100 °C, 1300 °C and 1400 °C. The quenched samples were synthetically analysed by wet chemical analysis for determining content of ferrous iron, fluorescent analysis to measure the total amount of Zn and iron and XRD to identify the phases presented. The phase relations based on isobar at the three target temperatures were acquired and further thermodynamic properties of this system also conducted by the authors which suggests that $ZnFe_2O_4$ tend to be more easily decomposed at elevated temperatures.

Hansson *et al*[49, 54] explored the system at temperatures ranging from 1200 to 1400 °C with Po_2 fixed at 10^{-6} atm, and at 1200 °C with Po_2 ranging from 10^{-4} to 10^{-8} atm using quenching method and EPMA technique. The phase relations at sub-solidus temperatures were extensively explored in their studies as shown in the Figure 2.9. Figure 2.9 (A) shows the experimentally determined isotherms in the ZnO-rich corner at $po_2 = 10^{-6}$ atm where the spinel and zincite are coexisting at all temperatures. The Figure 2.9 (B) shows the experimentally determined O_2 isobars in the ZnO-rich corner at 1200 °C where spinel phase tends to be table at higher Po_2.

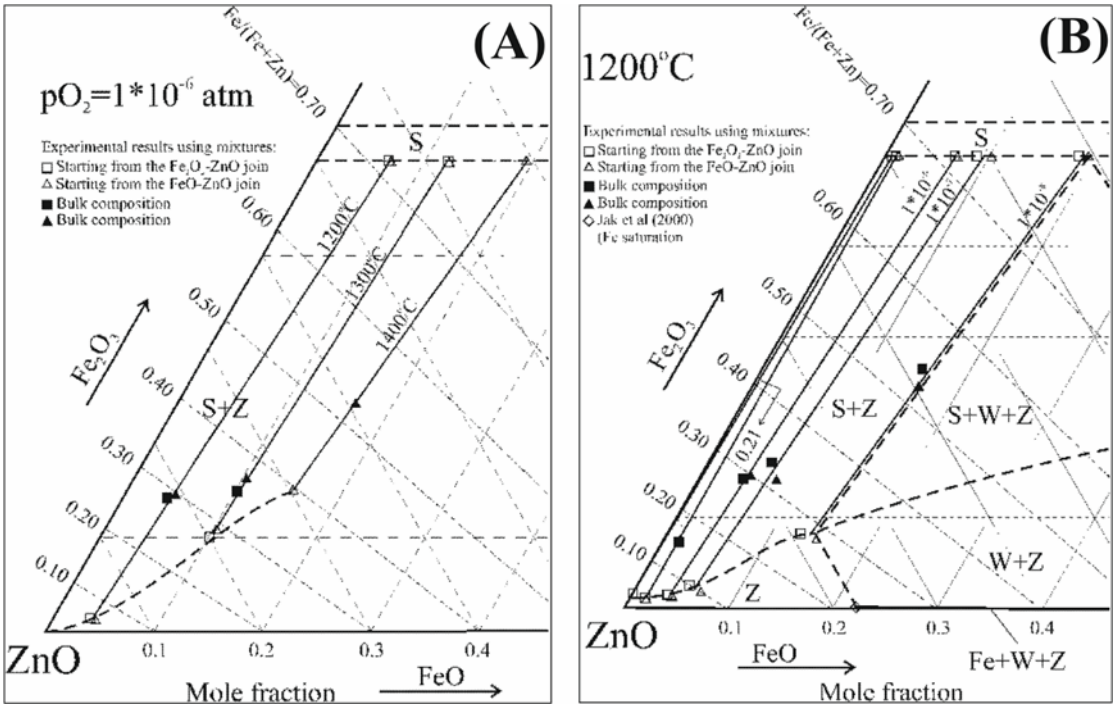

Figure 2.9 Phase diagrams of the FeO-Fe_2O_3-ZnO, (A) - isotherms at $Po_2 = 10^{-6}$ atm and (B) - isobars at 1200 °C [49]

2.4.4 Summary of ZnO-"FeO" system

The vaporisation of ZnO at elevated temperatures and coexistence of ferric and ferrous iron in the system ZnO-"FeO" bring difficulties in phase equilibria studies on the system under intermediate Po_2. Hence, it is imperative to develop experimental techniques that can enable the exploration of the system under intermediate Po_2. A summary of the experimental techniques regarding this issue was listed in Table 2.3.

In developing the thermodynamic model for the Zn-containing systems, the information of the solid solutions is particularly important. Meanwhile, the industrial smelting processes generally operate under the conditions approaching spinel saturation. As such, the details on spinel solid solution are believed to be critical factor thermodynamics modelling of ZnO-bearing copper smelting slags. An extensive review on the $ZnFe_2O_4$-Fe_3O_4 system was performed by Graydon and Kirk[43]. It was confirmed that there is miscibility gap between spinel zinc ferrite ($ZnFe_2O_4$) and magnetite (Fe_3O_4). The spinel solid solution under air condition has been studied by many authors[44, 45, 53], and relationship between ZnO solubility in spinel and temperature is present in Figure 2.10. It is obvious that the solubility of ZnO in spinel decreases when increasing temperature under air atmosphere.

Table 2.3 Intermediate Po_2 controlled involving ZnO-"FeO" pseudobinary system

Source	Po_2/atm	Method	Comment
R. L. Benner[22]	$1\sim10^{-4}$	Ar, O_2 gas mixture	Limited Po_2 can be achieved by this method
S. Itoh[48]	$10^{-3}\sim10^{-14}$ (Determined by EMF)	Vacuum sealed-tube	Po_2 can't be specifically controlled
Hansson[49]	$10^{-4}\sim10^{-8}$	H_2, N_2 and CO_2 gas mixture	Evaporation of ZnO was not discussed
	10^{-10}	CO_2, CO gas mixture	

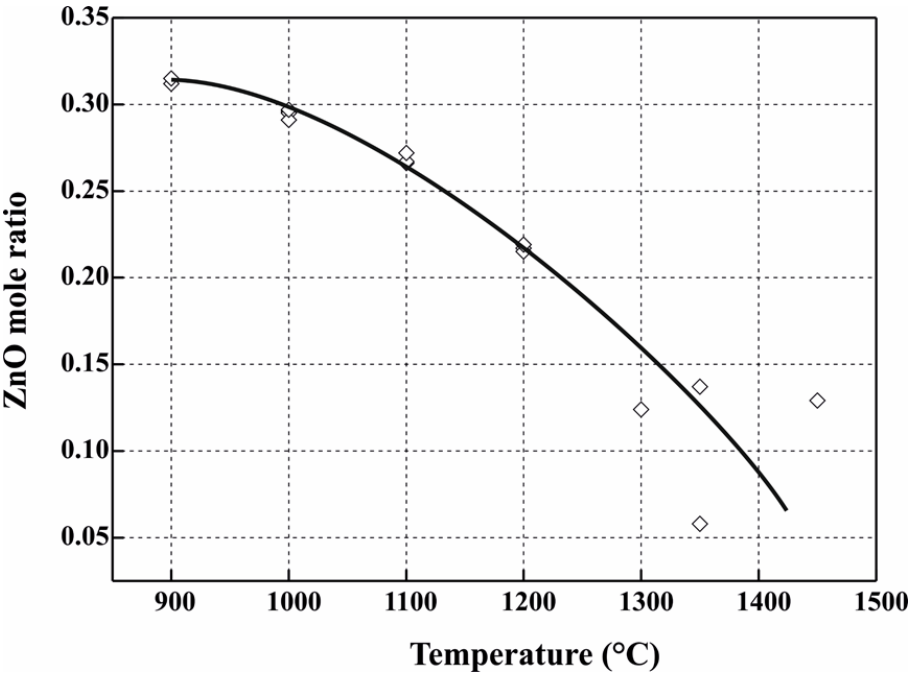

Figure 2.10 ZnO concentration in spinel in equilibrium with hematite and air as function of temperature[45]

2.5 ZnO-"FeO"-SiO_2 system

2.5.1 ZnO-"FeO"-SiO_2 system in equilibrium with metallic Fe

The system was firstly investigated by Davenport[55] under metallic iron saturation using quench method. The isoactivity lines of ZnO and "FeO" were obtained at 1300 °C which were extrapolated to 1600 °C using the regular solution model. However, no other information was reported regarding the phase relations and liquidus at 1300 °C. Dobrotsvetov *et al*[56] explored the join Fe_2SiO_4-Zn_2SiO_4 under the nitrogen atmosphere with temperatures ranging from 1205 to 1512 °C. The fayalite (Fe_2SiO_4) was prepared from $Fe_2C_2O_4$ and SiO_2 in an iron crucible under nitrogen at 1250 °C and willemite (Zn_2SiO_4) was obtained by heating the mixture of ZnO and SiO_2 at 1350 °C for 25-30 hours. Sealed iron crucibles were applied up to 1430 °C, while open Pt envelops were used at those temperatures higher than 1430 °C where Fe softens. The quenched

samples were analysed by wet chemical method and examined by microscopy, DTA and XRD to determine the phase assemblages. The sub-solidus miscibility gap was estimated based on optical properties and X-ray diffraction data on mixture composition.

Itoh and Azakami[57] conducted phase equilibria study on the system "FeO"-ZnO-SiO_2 coexisting with metallic iron at 827 °C. In the study, the sample was placed in an iron crucible which was then sealed in an evacuated quartz tube. The sample was first sintered at 1127 °C for 12 hours followed by equilibration at 827 °C for more than 60 hours and then quenching in water. The phase assemblages of the quenched samples were identified using XRD and corresponding compositions were determined by EPMA. The results showed that the phase relation in the "FeO"-ZnO-SiO_2 system under iron saturation were composed by four two-phase fields, two three-phase fields and two single phase fields. The mutual solubilities between "FeO" and ZnO, as well as Fe_2SiO_4 and Zn_2SiO_4 were also determined.

Jak *et al*[44] conducted extensive experimental investigations on this system under iron saturation at temperatures ranging from 1000 to 1350 °C in "FeO"-rich area by applying high-temperature equilibration coupling with EPMA analyses. The boundaries between tridymite and fayalite, fayalite and willemite, fayalite and wüstite and wusitite and willemite were identified (Figure 2.11). Thermodynamic optimizations[58] were also performed thereafter based on the experimental results (Figure 2.11). Generally, good agreement on liquidus temperatures under metallic iron saturation can be seen between prediction and experimental measurements at constant wt pct ZnO.

Ericsson and Filippidis[59] studied the system ZnO-"FeO"-SiO_2 on the join Fe_2SiO_4-Zn_2SiO_4 at 1000 °C. The mixtures of oxides were equilibrated at 1000 °C in evacuated SiO_2 tubes for two weeks. After equilibration, the tubes were quenched in water and the samples were examined using XRD, SEM, EPMA and Mössbauer Spectrum. The solubilities of Fe_2SiO_4 in willemite and Zn_2SiO_4 in fayalite were found to be 52 mol% and 17 mol%.

Umetsu *et al*[60] studied part of the system "FeO"-ZnO-SiO_2 and the join Fe_2SiO_4-Zn_2SiO_4 between 1150 to 1350 °C under purified nitrogen. The starting mixtures were obtained by heating the briquettes in Pt crucible at 1350 °C for one hour. The final compositions of the starting mixtures were determined by wet chemical analyses. About 20 mg of crushed starting mixtures was wrapped in a Pt foil envelope and heated at the

target temperature for one hour under purified nitrogen. The sample was then quenched into ice-cold water and then examined by XRD. Significant difference was found between the results of Dobrotsvetov *et al*[56] and of Umetsu *et al*[60].

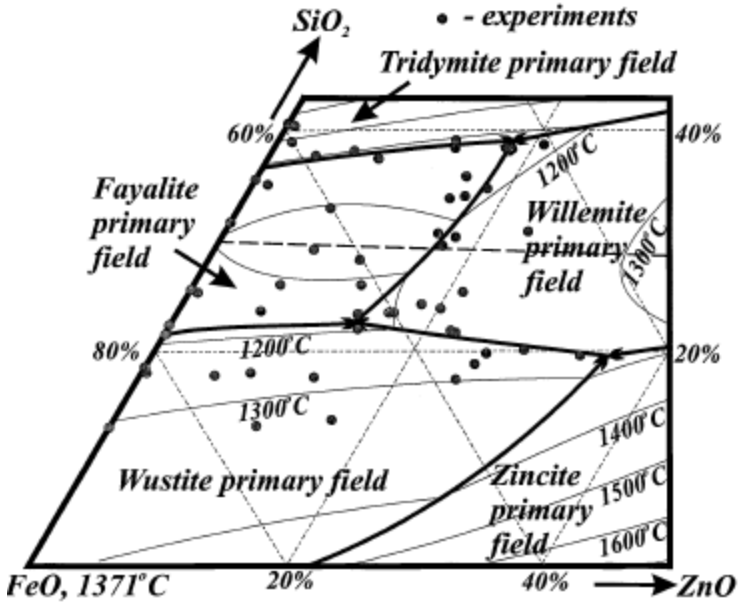

Figure 2.11 Predicted phase diagram of ZnO-"FeO"-SiO_2 system with experimental data[44]

2.5.2 ZnO-"FeO"-SiO_2 system in air

Limited experimental attempts were performed by Jak *et al*[58]. The experimental procedures applied involve high-temperature equilibration and quenching techniques followed by electron probe X-ray microanalysis (EPMA). Liquidus temperatures and solid solubilities of the crystalline phases were measured in the temperature range from 1200 °C to 1450 °C in the zinc ferrite, zincite, willemite, and tridymite primary phase fields of the Zn-Fe-Si-O system under air atmosphere. The phase diagram was mainly constructed by the thermodynamic model (Figure 2.12).

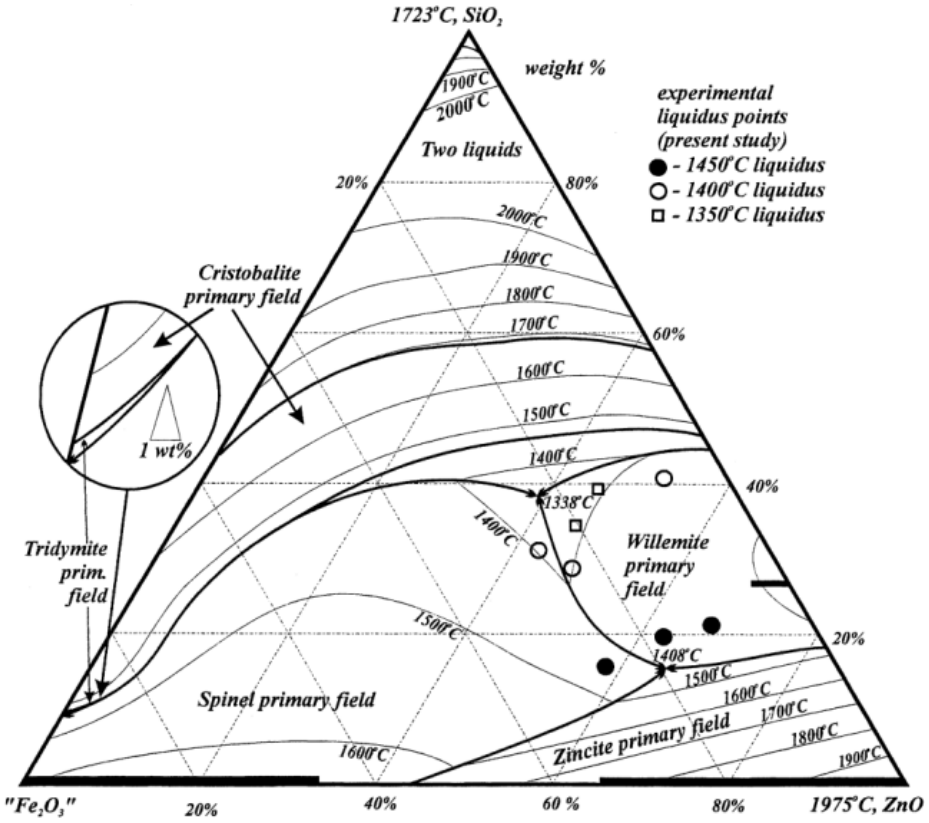

Figure 2.12 Phase diagram of ZnO-"Fe_2O_3"-SiO_2 in air[58]

2.5.3 ZnO-"FeO"-SiO_2 system at intermediate oxygen partial pressures

There is no information found in this system.

2.5.4 Summary of ZnO-"FeO"-SiO_2 pseudo-ternary system

This system forms the main chemical components of the copper smelting slags. As such, the information is particularly important to copper smelting operations. However, no information of this system regarding the phase rations and liquidus temperature under intermediate Po_2 was found to the best of our knowledge. The major difficulty when investigating the phase equilibria of ZnO-bearing system is the high evaporation of ZnO in reducing condition. The procedures in controlling the ZnO vaporisation were summarized in Table 2.4. It can be seen that several studies[47, 56, 57, 59, 60] used the closed systems. A pie-type sample technique was applied in the studies performed by Jak *et al*[44]. Although these experimental techniques could successfully minimise the loss of ZnO during the equilibration, their feasibilities to those conditions under intermediate Po_2 are questionable.

Table 2.4 Methods to reduce the loss of ZnO in pseudoternary system ZnO-"FeO"-SiO_2

Source	Po_2	Method	Comment
B. L. Dobrotsvetov[56]	Ar atmoshpere	Sealed Fe crucibles	Experiments conducted on join: Zn_2SiO_4-Fe_2SiO_4
Y. Umetsu[60]	N_2 atmosphere	Wrapped in a Pt foil envelope	Less reducing condition
T. Ericsson[59]	Vacuum	Sealed-tube	Closed system Po_2 can't be controlled
S. Itoh[47]	Vacuum		
S. Itoh[57]	Iron saturation	Sealed-tube	
E. Jak[44]	Iron saturation	Pie-type sample applied with ZnO-SiO_2 in the centre	Po_2 close to 10^{-12} atm

2.6 ZnO-"FeO"-SiO_2-Al_2O_3 system

There is no information found in this system.

2.7 ZnO-"FeO"-SiO_2-MgO system

There is no information found in this system.

2.8 ZnO-"FeO"-SiO_2-CaO system

This system forms the major chemical compositions of the industrial slags from the non-ferrous pyrometallurgical processes[61, 62], as such, extensive studies had been conducted to gain details on the thermodynamic properties relevant to practical production. Davenport[55] firstly conducted phase equilibria study on the system by using quenched under iron saturation to determine the activity of ZnO. The ZnO activity was evaluated at five SiO_2 concentration levels with no information of the phase relations and liquidus reported. Dobrotsvetov *et al*[63] studied the system on the Zn_2SiO_4-$CaFeSiO_4$ join using Zr crucibles at temperatures ranging from 1250 to 1500 °C with 0 - 50% Zn_2SiO_4. The phases presented were identified by optical microscope and XRD. There are four primary phase fields determined: willemite, willemite-hardystonite, hardystonite-fayalite and monticellite. Meanwhile, the limit solubility of willemite in monticellite was determined to be 21 wt pct. Further experiments were also conducted by Dobrotsvetov *et al*[64] to unravel the mechanism how Zn loss during lead smelting process. Their results were presented in Figure 2.13.

Another study on the system was performed by Lenz and Lee[65] by DTA techniques under a gas mixture of 90 pct N_2, 5.2 pct CO_2 and 4.8 pct CO in slags compositions close to those in lead blast furnace slags. The authors only determined the liquidus

temperatures without further quantitative analysis on the quenched samples. The results were present in the Figure 2.14. It can be seen that the liquidus temperature increased with the CaO/SiO_2 ratio at constant ZnO content in both silica and wüstite primary phase fields. It is also noticed that liquidus temperature in the silica phase is almost independent of FeO content at low CaO/SiO_2 ratio while changes dramatically with FeO content in wüstite phase field. The effect of ZnO content on the liquidus temperature was also evaluated by the authors.

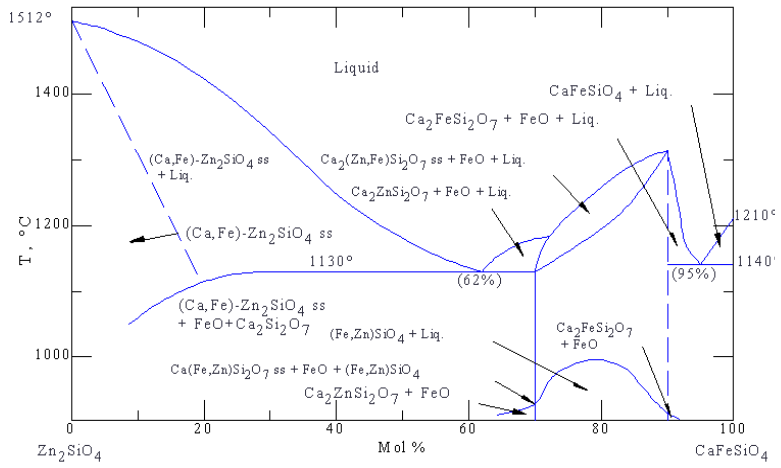

Figure 2.13 Phase diagram of the join $CaFeSiO_4$-Zn_2SiO_4[64]

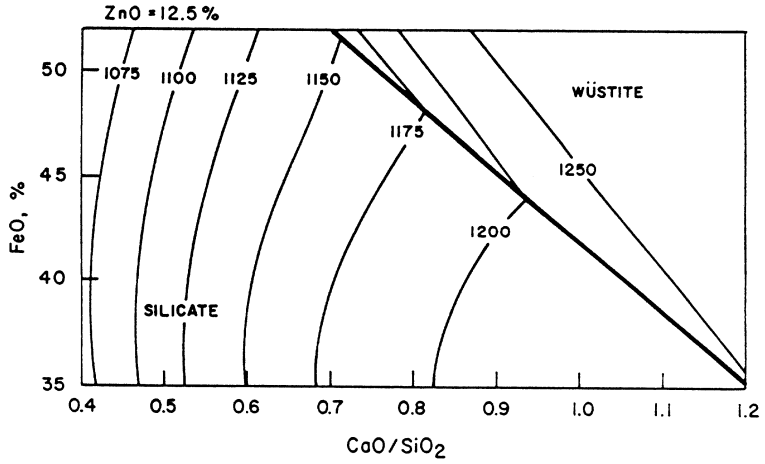

Figure 2.14 Portion of the system CaO-"FeO"-ZnO-SiO_2[65], Temperature: °C

Extensive studies on the system were conducted by Jak *et al*[62, 66] with four CaO/SiO_2 ratios: 0.33, 0.71, 0.93 and 1.2, under iron saturation using quench method and EPMA in temperature range: 1000 - 1300 °C. Both liquid phase and the solid phases in the quenched samples were measured by EPMA. The obtained results were presented on pseudo-ternary system ZnO-"FeO"-($CaO + SiO_2$) with fixed CaO/SiO_2 ratio. As shown in Figure 2.15, the primary phase fields tend to be different between pseudo-sections

with fixed CaO/SiO_2 ratio. The fayalite phase field substantially shrinks with increasing CaO/SiO_2 ratio, and disappears when that reach 1.2. The composition relationship between liquid phase and the solid solution in equilibrium was also discussed in the paper.

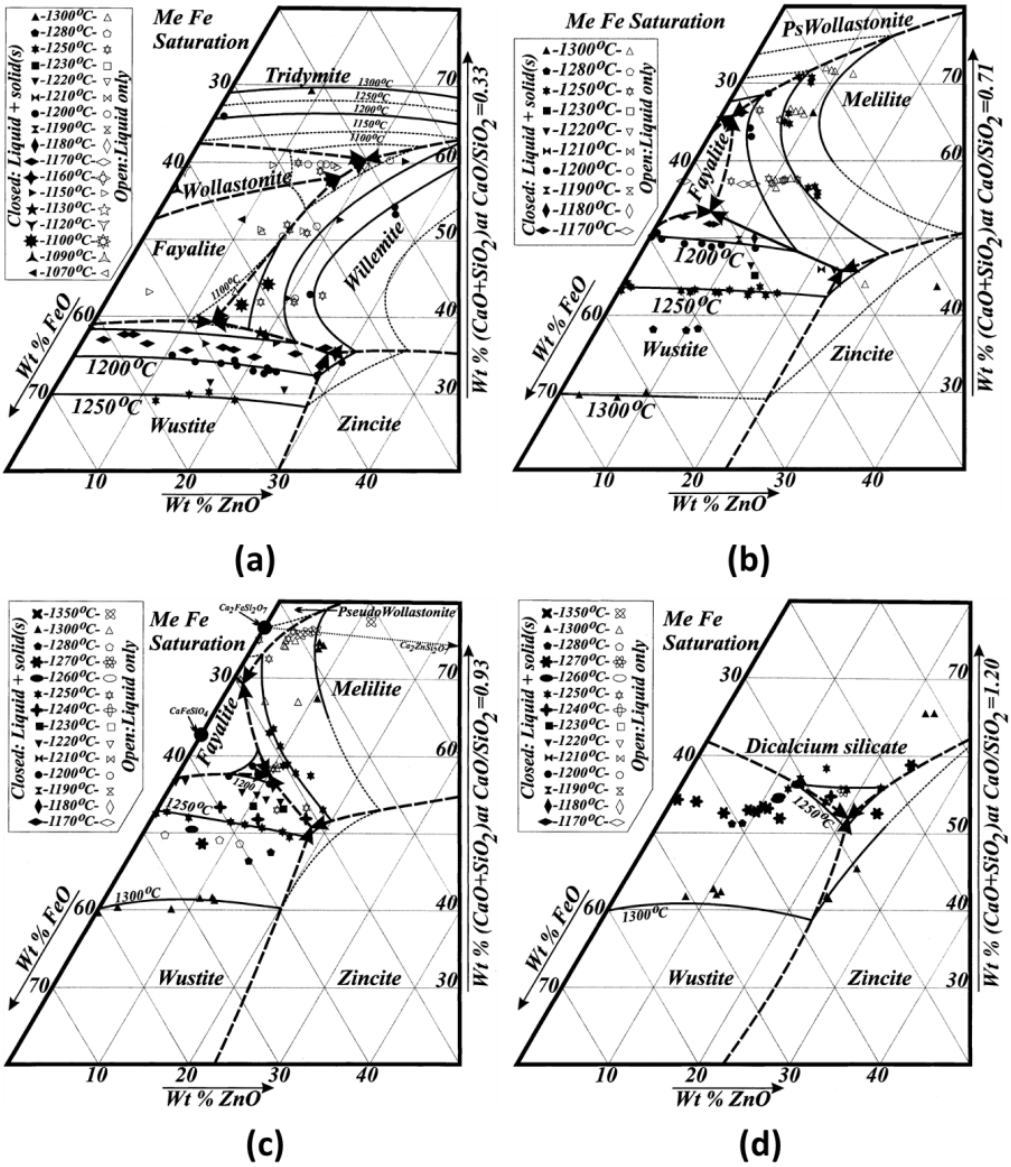

Figure 2.15 Portion of the phase diagram in psuedoternary ZnO-"FeO"-($CaO+SiO_2$) system with varied CaO/SiO_2 ratio: (a) - 0.33, (b) - 0.71, (c) - 0.93 and (d) - 1.2, under iron saturation[62, 66]

The system Ca-Fe-Si-O-Zn forms the basis for the chemical description of a range of non-ferrous smelting slag[62]. Phase equilibria studies on the system had been carried out under iron saturation of which the Po_2 is close to 10^{-12} atm. There is no information available on the system that investigations were conducted under intermediate Po_2As the Po_2 in the copper smelting process is generally close to 10^{-8} atm, so that those results

can not directly be applied to the copper smelting processes. Similarly, the techniques applied in ZnO-containing systems regarding minimise the vaporisation of ZnO are summarized in Table 2.5.

Table 2.5 Experimental techniques applied in the system ZnO-"FeO"-SiO_2-CaO

Source	Po_2	Method	comment
V. I. Bershak[67]	No specific	Stoichiometric starting materials used	Experiments conducted along the join: Zn_2SiO_4-$CaFeSiO_4$
J. G. Lenz[65]	90% N_2, 5.2% CO_2, 4.8% CO	No specific	Examine the region close to Brunswick lead blast furnace slags
W. G. Davenport[55]	Zn-Cu-Fe alloy saturation	No specific	No information on ZnO evaporation
B. L. Dobrotsvetov[63]	Iron saturation	Stoichiometric starting materials used	Experiments conducted on the join: Fe_2SiO_4-$CaFeSiO_4$
E. Jak[62, 66]	Iron saturation	CaO-ZnO-SiO_2 master slag surrounded by metallic powder and pelletized	Po_2 close to 10^{-12}

2.9 Zn-Containing Multi-Component Systems

2.9.1 Phase equilibrium studies on ZnO-containing multi-components system

The phase equilibria studies on the multi-component systems can provide direct information to the slags system from industry copper production. However, to presents the phase diagrams of high-order systems requires accurate information of the low-order systems.

The first investigation on the system ZnO-"FeO"-CaO-Al_2O_3-SiO_2 was conducted by Tan and Vix[68] with composition range relevant to those in ISF furnace and lead blast furnace. The authors developed a program to predict liquidus temperatures and phase compositions combining Factsage slag database with mathematical model of slag based on revised urbain formalism. Further experimental studies also performed to validate the developed program. Yamaguchi *et al*[69] conducted experimental studies on the system under metallic iron saturation with the desire to recover base metals from copper converter slag. The activity of ZnO in the system ZnO-CaO-SiO_2-"FeO"-Al_2O_3 system at 5 wt pct Al_2O_3 was obtained at 1300 °C. Their results suggest that the ZnO activity increases in the SiO_2-rich side and decreases at the CaO-rich side with the presence of Al_2O_3 comparing to ZnO-CaO-SiO_2-"FeO" system. No information on the phase relations and liquidus was reported in their study.

Extensive investigations on the system ZnO-"FeO"-CaO-Al_2O_3-SiO_2 were also performed by Zhao *et al*[70-74] under metallic iron saturation with varied ratios of

CaO/SiO_2 and $(CaO+SiO_2)/Al_2O_3$ using quenching method and EPMA technique. The compositions investigated were planned in the region relating to non-ferrous metal pyrometallurgical processes. The obtained results were presented in pseudo-terneray ZnO-"FeO"-(Al_2O_3+SiO_2+CaO) at constant CaO/SiO_2 and $(CaO+SiO_2)/Al_2O_3$ ratios, as shown in the Figure 2.16 (A) to Figure 2.16 (H). Their results suggest that the $(CaO+SiO_2)/Al_2O_3$ ratio tends to increase the full liquid area at 1250 °C. Meanwhile, the liquidus temperatures in the spinel primary phase field increase when the Al_2O_3 and ZnO concentrations in the slag increasing.

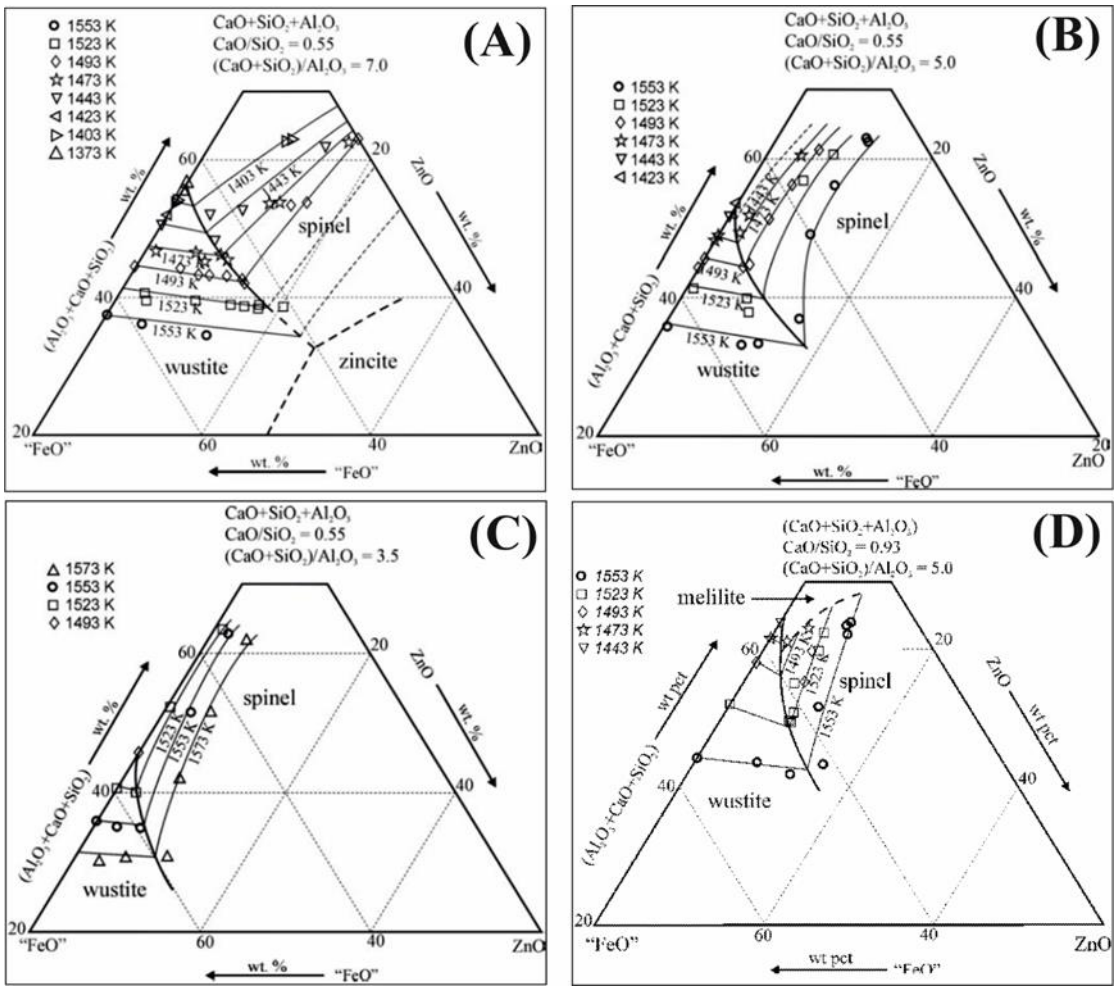

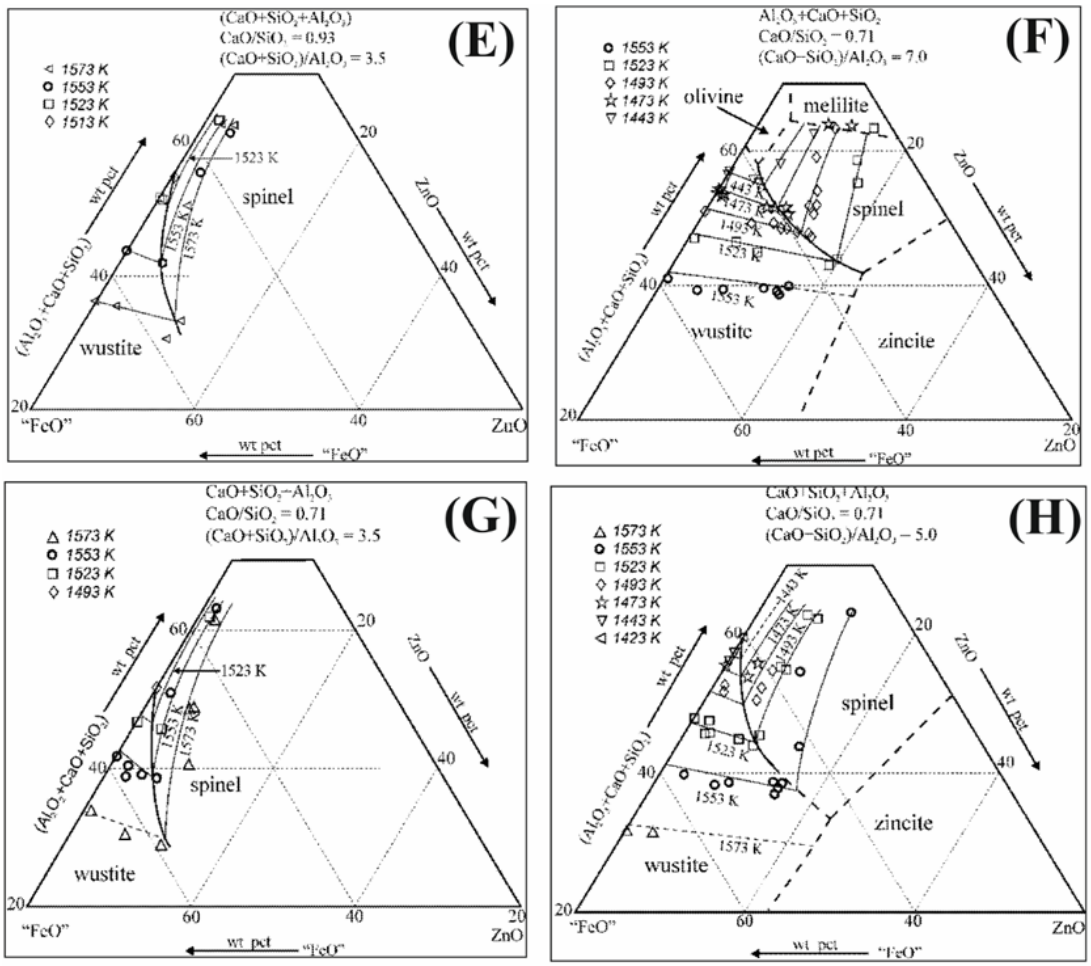

Figure 2.16 Liquidus in the pseudo-ternary system ZnO-‘‘FeO’’-(Al_2O_3+CaO+SiO_2) with varied CaO/SiO_2 and (CaO+SiO_2)/Al_2O_3 ratios as under metallic iron saturation[70, 71, 73-75]

Further investigations on six-component systems ZnO-“FeO”-Al_2O_3-CaO-SiO_2-MgO[76] and ZnO-“FeO”-Al_2O_3-CaO-SiO_2-S[77] were carried out by Zhao *et al*[76, 77] using the similar techniques[70-74] aiming to acquire direct knowledge on the slags in non-ferrous metal pyrometallurgical processes. The CaO/SiO_2 and (CaO+SiO_2)/Al_2O_3 ratios maintained the same as those studies in system ZnO-“FeO”-CaO-Al_2O_3-SiO_2[70-74]. Similarly, the obtained results were present in the pseudo-ternary ZnO-“FeO”-(Al_2O_3-CaO-SiO_2) system, as shown in Figure 2.17 and Figure 2.18 for the ZnO-“FeO”-Al_2O_3-CaO-SiO_2-MgO[76] and ZnO-“FeO”-Al_2O_3-CaO-SiO_2-S[77] respectively. Their results indicate that the full liquid at 1250 °C significantly decrease with increasing MgO concentration in the liquid phase, while that will increase with the presence of S in the slag. Meanwhile, the liquidus temperatures in the spinel primary phase field increase with the MgO concentration in the liquid increasing, while that decrease with the presence of S in the liquid. Further discussions on the partitioning

behaviours of ZnO between spinel (or wüstite) and liquid phases will also performed in the studies[76, 77].

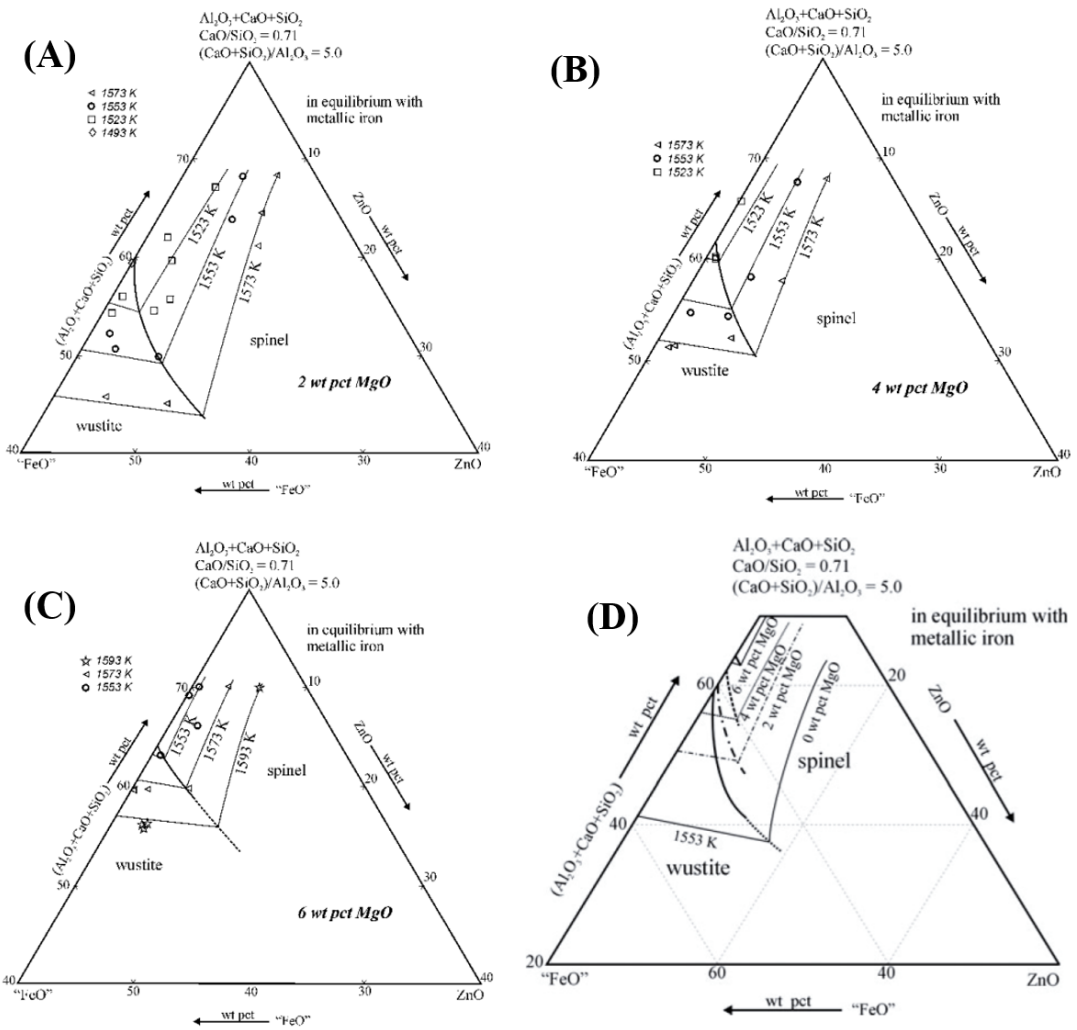

Figure 2.17 Liquidus in the section ZnO-‘‘FeO’’-(Al_2O_3+CaO+SiO_2) at fixed CaO/SiO_2 = 0.71 and (CaO+SiO_2)/Al_2O_3 = 5.0 with varied MgO (as indicated) under metallic iron saturation: (A)-(C); (D)-Effect of Mg to the boundary between wüstite and spinel and 1280 °C isotherm[76]

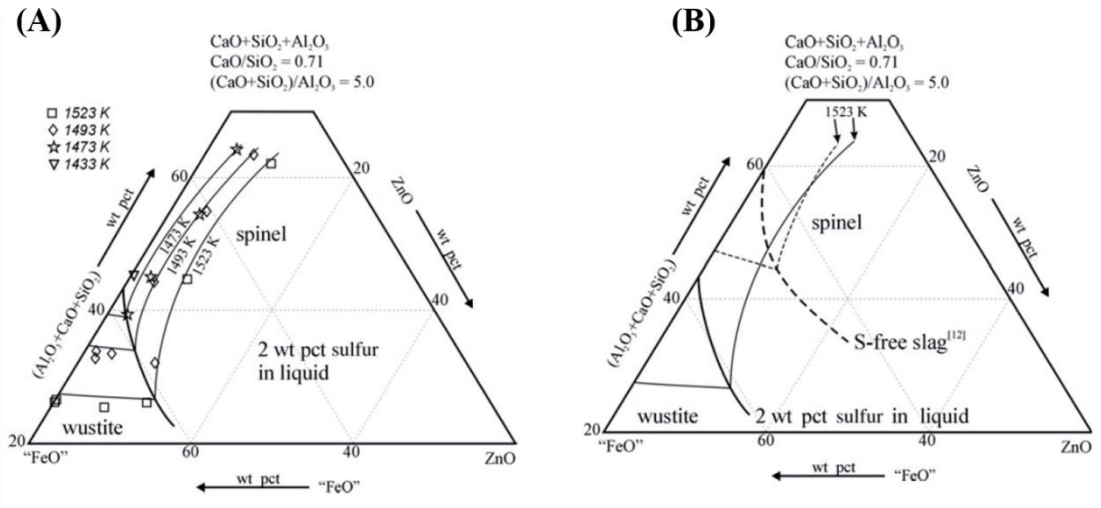

Figure 2.18 Experimental data present on pseudo-terany section ZnO-‘‘FeO’’-(Al_2O_3+CaO+SiO_2) at fixed CaO/SiO_2 =0.71 and (CaO+SiO_2)/Al_2O_3 = 5.0 with 2.0 wt pct S in slag under metallic iron saturation, (A) - the liquidus at varied temperatures and (B) - Comparison on the 1250 °C isotherm in S-containing and S-free systems[77]

2.9.2 Summary on ZnO-containing multi-component systems

The explorations on the Multi-components system critically important to non-ferrous pyrometallurgical processes in ways not only provide direct implications for the industrial practices but also valuable information that can be applied to develop thermodynamic models on the industrial slags. The review suggests that all those reported experimental works were conducted under metallic iron saturation with particular interests to the lead and zinc smelting processes. No information was reported under the intermediate Po_2. A summary on techniques that developed in the multi-component systems is present Table 2.6, Table 2.7 and Table 2.8. There are two main approaches applied, including quenched method under metallic iron saturation and EMF with closed galvanic cell, to investigate the ZnO-containing multi-component systems.

Table 2.6 Experimental technique applied ZnO-“FeO”-Al_2O_3-CaO-SiO_2-S system

Source	Po_2	Method	comment
Zhao[77]	Iron saturation	Mixture pellet surrounded by metallic powder and pelletized	Po_2 close to 10^{-12} atm

Table 2.7 Experimental technique applied ZnO-FeO-CaO-Al_2O_3-SiO_2-MgO system

Source	Po_2	Method	comment
Zhao[76]	Iron saturation	Mixture pellet surrounded by metallic powder and pelletized	Wrapped in Pt crucible

Table 2.8 Experimental techniques applied ZnO-FeO -CaO-SiO_2-Al_2O_3 system

Source	Po_2	Method	comment
K. Azuma[78]	SiO_2 saturation	closed galvanic cell applied	Closed system, Po_2 can't be specifically controlled
N. J. Filipovska[79]	No specific	closed galvanic cell applied	Closed system
K. Yamaguchi[69]	Iron saturation	No specific	Po_2 can't be controlled in this method
B. Zhao[70-74]	Iron saturation	Pie-type sample applied with ZnO-containing master slag in the centre	Po_2 close to 10^{-12} atm

When developing the thermodynamic models on the industrial slags, the accurate information on the solid solutions of interests is required. As the copper smelters generally operate under the conditions approaching spinel saturation, the partitioning behaviours of the components between spinel and liquid phases will be vital for the thermodynamic models on the copper smelting slags. As such, the partitioning effect of ZnO between spinel and liquid phases will be useful to the thermodynamic modelling of the ZnO-containing copper smelting slags. In this case, the information regarding the partitioning effect of ZnO between spinel and liquid phases were summarized, as shown in Figure 2.19 and Figure 2.20. It can be seen that the ZnO concentrations in spinel primary phase filed are generally higher than that in the liquid phase.

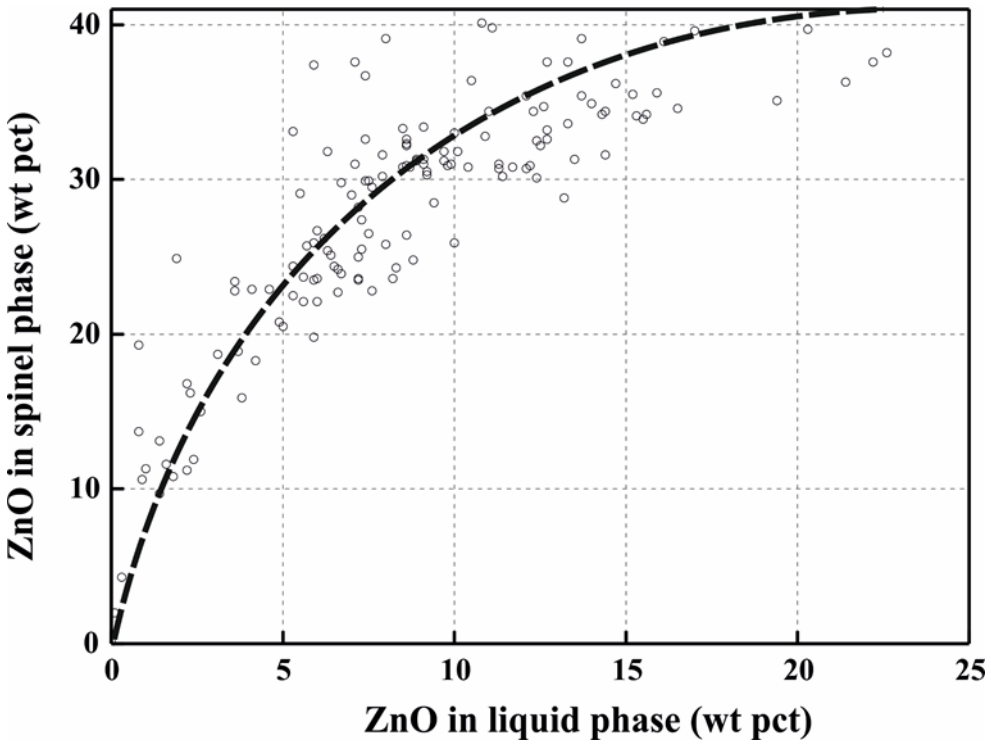

Figure 2.19 Partitioning effect of ZnO between liquid and spinel for temperatures between 1130 °C and 1300 °C under metallic iron saturation with fixed CaO/SiO_2 = 0.55- 0.93 and $(CaO+SiO_2)/Al_2O_3$ = 3.5-7 of system ZnO-FeO-Al_2O_3-CaO-SiO_2[70-74]

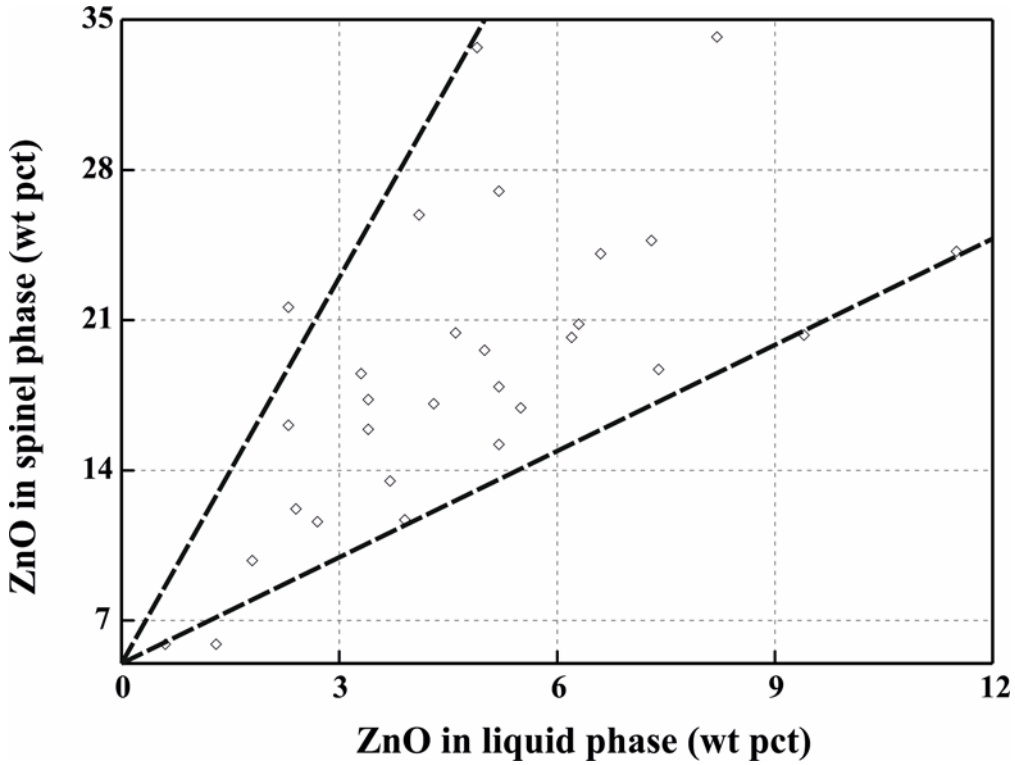

Figure 2.20 Partitioning of ZnO between liquid and spinel for temperatures between 1200 °C and 1320 °C under metallic iron saturation with fixed CaO/SiO_2 = 0.55 and $(CaO+SiO_2)/Al_2O_3$ = 5 at varied MgO concentration (2, 4 and 6 wt pct) for Zn-containing multi-component system[76]

2.10 Summary

Extensive literature review has been conducted on the ZnO-contianing systems, including the auxiliary systems, low-order systems and multi-component systems under varied oxygen partial pressure(air condition, metallic iron saturation and intermediate Po_2), which can be categorized into following systems,

"FeO"-SiO_2;

"FeO"-ZnO;

ZnO-SiO_2;

ZnO-"FeO"-SiO_2;

ZnO-"FeO"-SiO_2-Al_2O_3

ZnO-"FeO"-SiO_2-MgO;

ZnO-"FeO"-SiO_2-CaO;

ZnO-"FeO"-SiO_2-based high-order systems.

Due to the quick loss of ZnO through vaporisation under reducing conditions, proper experimental techniques are required to minimise the ZnO loss during equilibration. As

such, attentions also have been paid to the experimental techniques in the reported literatures. In most of the phase equilibria studies of the ZnO-containing systems under reducing conditions, closed system was generally adopted in the experimental set-up. However, such approach obviously is not suitable for the explorations on the ZnO-containing systems under intermediate Po_2 that requires a direct contact between the condensed phase and gas atmosphere. In this case, further discussion on the experimental technique development will be present in the chapter 4.

Current review also focused on the partitioning behaviour of ZnO between spinel and liquid phases on ZnO-containing systems. The reported results suggest that the ZnO concentrations in the spinel under metallic iron saturation are generally higher than those in the liquid phase. However, there is no information regarding the phase relations and liquidus temperatures of the system ZnO-"FeO"-SiO_2 (or higher-order systems) under intermediate Po_2 are available. For this reason, present study will focus on the development of suitable techniques to enable the exploration of phase equilibria on ZnO-containing slag systems under intermediate Po_2, and improve the understandings of the copper smelting slags in the copper production.

2.11 Thermodynamic Behaviour of Arsenic and Zinc in the Pyrometallurgical Copper Smelting Process

2.11.1 Occurrence behaviours of As and Zn during copper smelting

Yazawa[80] thermodynamically investigated the stable forms of Zn in the matte-slag system at 1300 °C. Using the thermodynamic date, the stability of Zn in the smelting process can be depicted as function of matte grade, as shown in the Figure 2.21, where a_{Zn}, a_{ZnO} and a_{ZnS} refer to the activity of metallic zinc, zinc oxide (ZnO), zinc sulphide (ZnS) respectively. It can be seen that the metallic Zn is hardly stable in the matte-slag system during the copper smelting process, while ZnS is considerable stable intermediate matte grade. The slagging of ZnO can be easily attained as the a_{ZnO} proportion significantly increases with matte grade as showing in Figure 2.21.

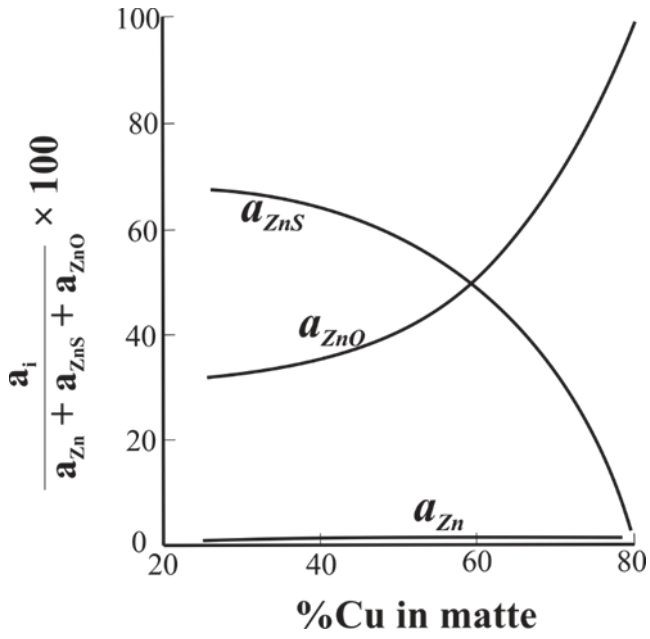

Figure 2.21 Proportion of activity as function of matte grade (pct Cu), reproduced from Yazawa[80]

Jimbo *et al*[81] investigated the phase equilibria between SiO_2-saturation iron silicate slag and molten Cu-As alloys at 1473 and 1523 K under controlled oxygen partial pressure (Po_2). As shown in Figure 2.22 (a) and (b), the AsO and $AsO_{1.5}$ both present in the slag, while the AsO is prevailing at lower Po_2, and the proportion of $AsO_{1.5}$ increases with the increasing Po_2.

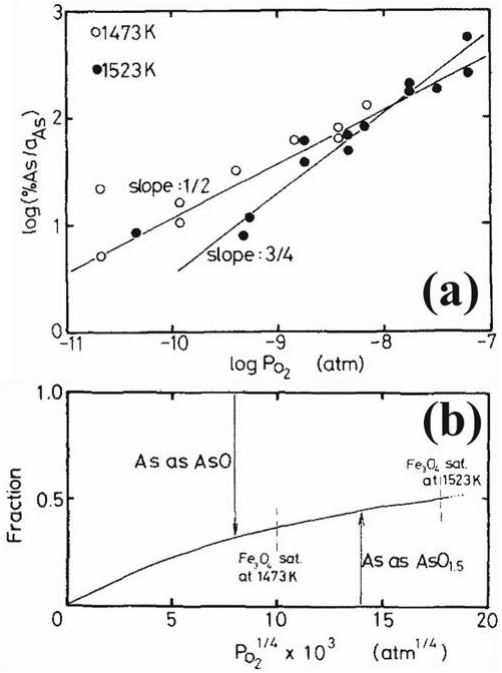

Figure 2.22 Occurrences of As at varied temperature and fraction as a function of Po_2[81]

Steinhauser *et al*[82] reviewed the the probable forms of Zn in the copper smelting process. As shown Table 2.9, the Zn mainly present as sulfidic form in the matte phase, and tends to be oxidic form in the slag. Although, there are varied znic species may present in the gas phase, the Zn gas is predominant during the smeting process.

Table 2.9 Probable forms of Zn in copper smelting[82]

Phase	Znic
Gas	Zn, ZnS, ZnO
Slag	Oxidic
Matte	Sulfidic

Chen and Jahanshahi[83] investigated the thermodynamic behaviour of arsenic in the silver-saturated calcium ferrite slag and calcium iron silicate slag under with controlled oxygen partial pressure (Po_2) at 1300 °C. Using the thermodynamic data in the literature, combing with the obtained experimental results, the variation of distribution coefficient between slag and liquid silver as a function of Po_2 can be deduced, as shown in the Figure 2.23, it can be seen that the slopes better fits the $AsO_{1.5}$ which indicates that the arsenic presents as $AsO_{1.5}$ in the slags investigated.

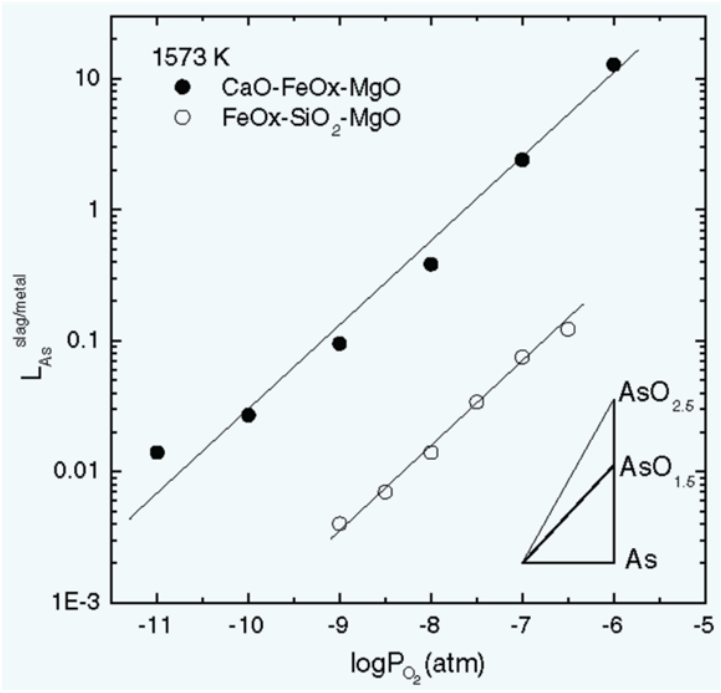

Figure 2.23 Variation of the distribution coefficient of arsenic between slag and liquid silver as function of Po_2 at 1300 °C[83]

2.11.2 Partitioning behaviour of As and Zn during copper smelting

Yazawa[84] investigated the distribution behaviour of As and Zn by considering the possibility and extend of As and Zn removal by slagging and volatilization during the copper smelting process on a thermodynamic basis. By applying the similar methodology, with estimated thermodynamic date, the distribution coefficients between slag and matte were calculated for the As and Zn at 1200 °C. As listed in Table 2.10, the zinc will distribute equally in both slag and matte phase under intermediate matte grade. The vapour pressure arsenic sulphide suggests that volatilization of As from the matte phase during copper smelting could be easily attained, while that of Zn is hardly possible.

Table 2.10 Distribution behaviours of As and Zn and corresponding vapour pressure at 1200 °C[84]

Elements	Distribution coefficient (slag/matte)	Sulphide vapour pressure (atm)
As	[-]	>> 1
Zn	2	$9 \cdot 10^{-3}$

Nagamori and Mackey[85] developed a thermodynamic model to predict distribution coefficients ($\frac{M\ concentration\ in\ matte}{M\ concentration\ in\ slag}$) of As and Zn in the fayalitic slag – matte system based on the reported thermodynamic data by assuming that oxidic dissolution for Zn and monatomic dissolution for As in the fayalite slag. Using the developed model, the effect of operation parameters on the distribution behaviours of As and Zn can be evaluated, e.g., oxygen enrichment and operating temperature. As shown in Figure 2.24, higher oxygen enrichment, lower operating temperature and higher matte grade tend to decrease Zn distribution coefficient which suggest higher slagging effect Zn under these conditions. The details calculated results for As and Zn during matte smelting are presented in Table 2.11. It can be seen that As appear to be concentrated in the matte phase instead of slag phase while Zn tends to enrich in slag phase instead of matte phase during the smelting process.

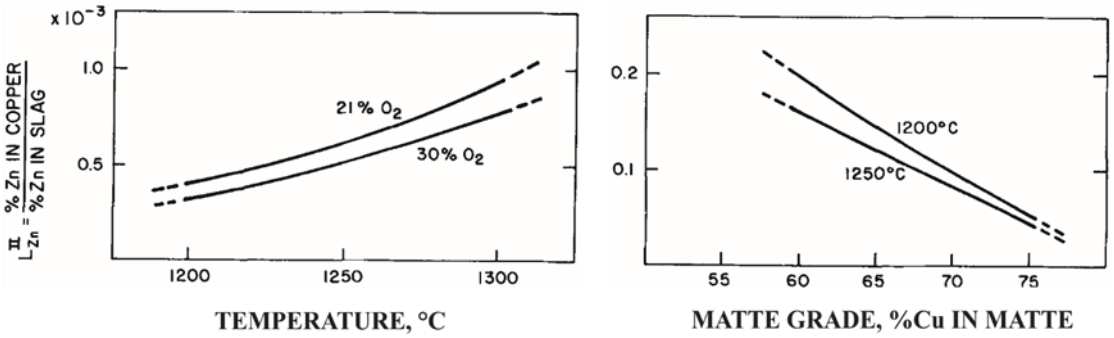

Figure 2.24 Distribution coefficient of Zn as function smelting temperature (left), and matte grade (right)[85]

Table 2.11 Calculated distribution coefficient in the matte-making Noranda process[85]

Elements	Distribution coefficient	Inputs	Factors Enhance slagging
As	1.7	%Cu = 68, 1200 °C; magnetite saturation; tuyere air = 30 % O_2	Higher oxygen enrichment; Higher smelting Temperature; Lower target %Cu
Zn	0.1		

Roine[86] investigated the possibility to remove the As from the matte phase during the smelting process on a thermodynamic basis by considering the As distribution coefficient ($\frac{As\ concentration\ in\ slag}{As\ concentration\ in\ matte}$) as function of Ps_2 (sulphur partial pressure) and Po_2 (oxygen partial pressure). As shown in the Figure 2.25, the results show that the distribution coefficient for As increases with Ps_2 at fixed Po_2. However, the enhanced effect is not sufficient from the viewpoint of industrial removal As by slagging.

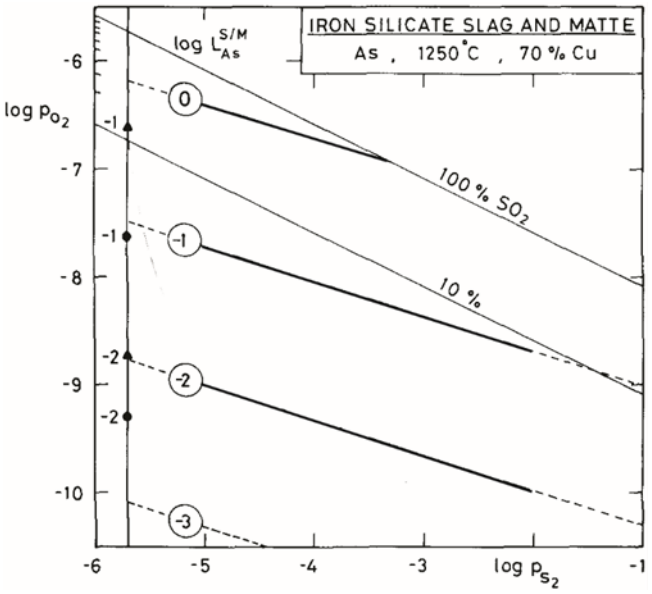

Figure 2.25 Arsenic distribution coefficients as function of Ps_2 and Po_2 at 1250 °C with 70 pct matte grade[86]

Roghani *et al*[87, 88] investigated the distribution behaviour of As between magnesia ferrite silicate slag and copper matte under controlled P_{SO_2} and Ps_2 at 1300 °C. By applied the developed experimental techniques, the effect of P_{SO2} and matte grade on the partitioning effect of As can be evaluated, as shown in Figure 2.26. It can be seen that the distribution coefficient ($\frac{As\ concentration\ in\ slag}{As\ concentration\ in\ matte}$) remains almost constant when the matte grade increases, while following by a dramatically decrease as the matte grade approaching white metal. Meanwhile, higher distribution coefficient can be attained at higher P_{SO2}.

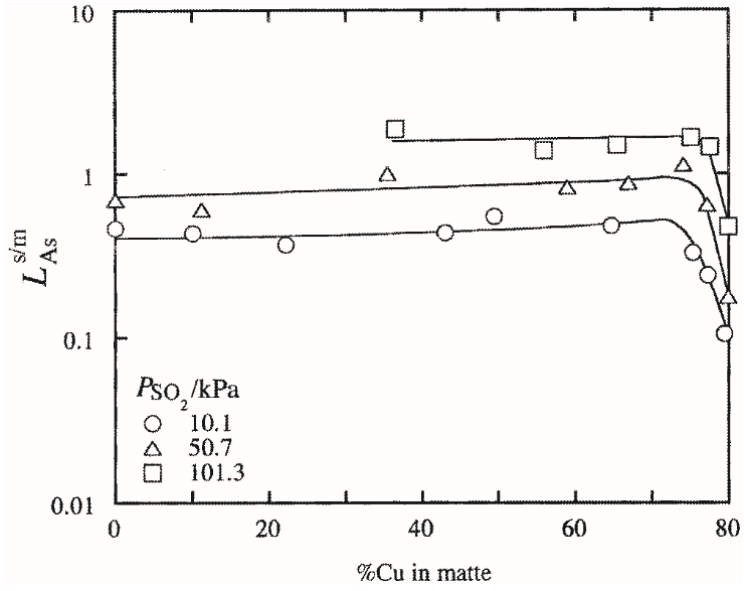

Figure 2.26 Variation of distribution coefficient as function of matte grade under varied P_{SO2}[88]

Reddy and Font[89, 90] thermodynamically evaluated the arsenate (the most stable arsenic-bearing species in the copper slag) in ferrite slags and silicate slags at 1300 °C. As shown in the Figure 2.27 (a), the arsenate capacity substantially increases with FeO content in both fayalite slag (upper) and olivine slag (below), while stays almost unchanged when the matte grade increasing excepts that approaching 70 pct where sharp decreases can be observed. By applying the obtained arsenate capacity, the distribution coefficient of As between slag and matte can be deduced and extrapolated to other slag compositions and temperatures where limited experimental data are available. As can be seen in Figure 2.28, the distribution coefficient slightly decreases with increasing matte grade and following by a dramatically decrease as matte grade approaching white metal.

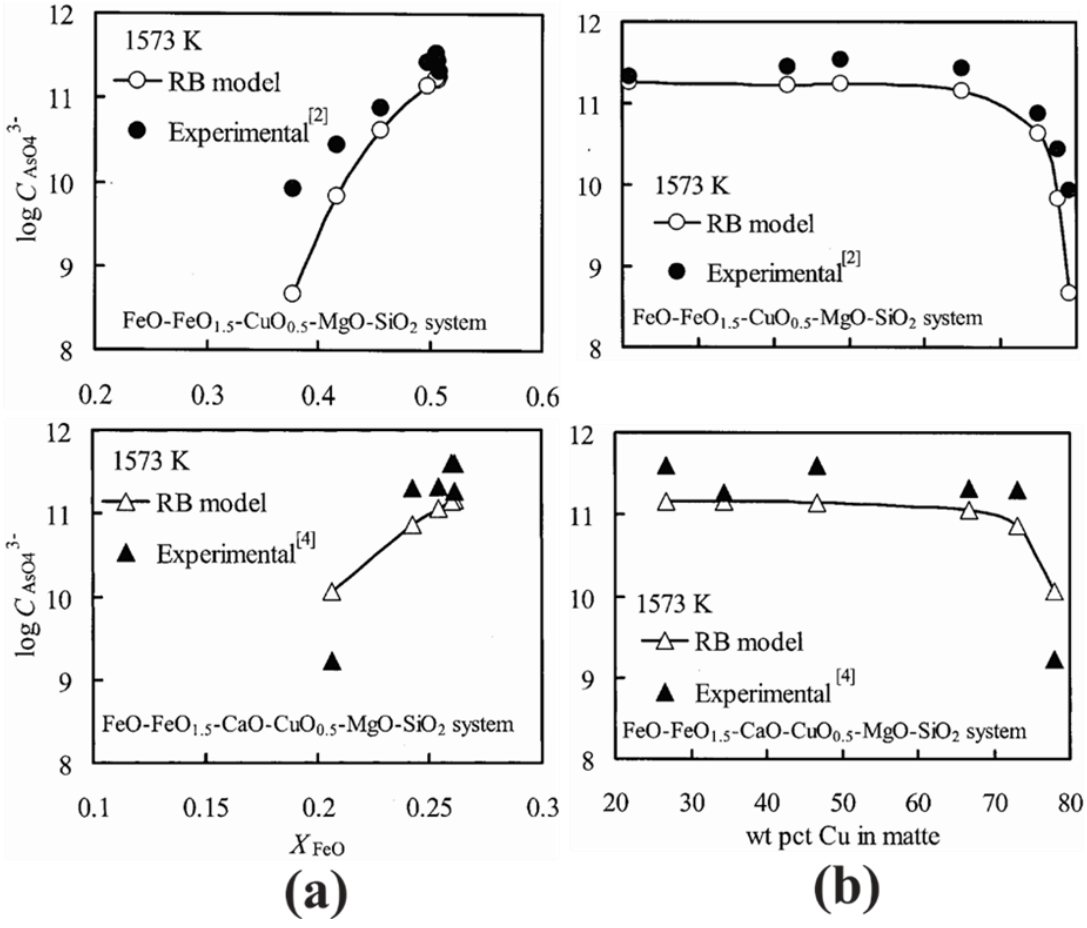

Figure 2.27 The arsenate capacity in varied type of slags as function of, (a) - FeO content and (b) - matte grade[89]

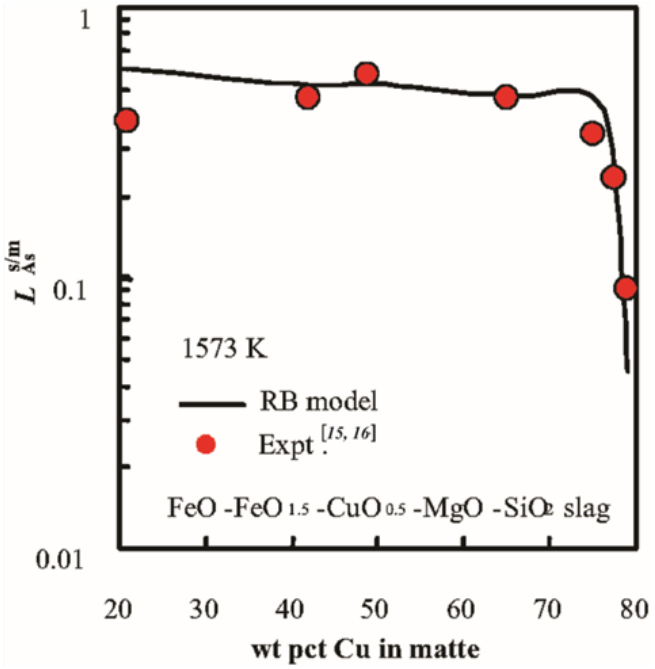

Figure 2.28 Variation of distribution coefficient of As as function of matte grade[90]

Acuna and Sherrington[91] investigated the As distribution coefficient as function of the ratio of slag mass to matte mass. Equilibration tests were carried out in magnesia crucible at 1250 °C with CO/CO_2 gas mixture flowing through. Three different slag/matte ratios (mass) were considered where the slag and matte were both obtained from Teniente Converter (CT) process. As shown in the Figure 2.29, the distribution coefficient of As between slag and matte is independent of the slag/matte mass ratio. Besides, the distribution coefficients obtained in lab-scale tests tend to be lower than that from industrial observations.

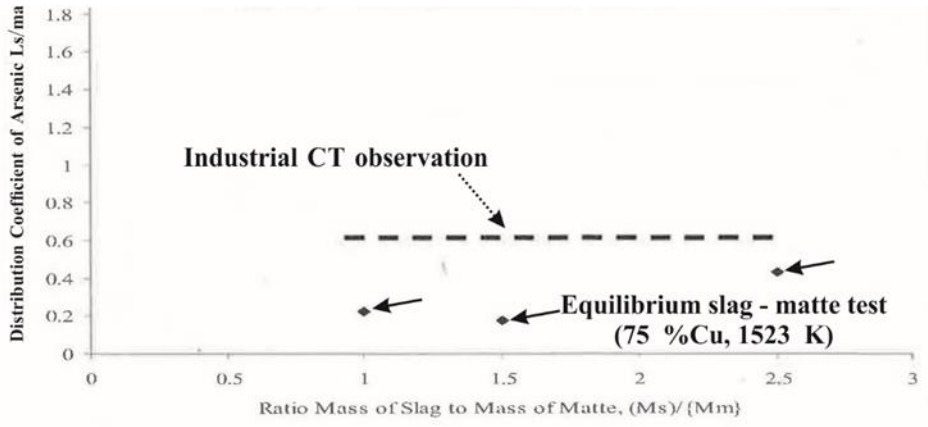

Figure 2.29 Relationship between distribution coefficient of arsenic between slag and matte, and the mass ratio of slag to matte[91]

2.11.3 Fractional distribution behaviours of As and Zn during copper smelting

Weisenberg[92] examined the arsenic distribution in the copper smelter based on the industrial operation data, as listed in the Table 2.12. They concluded that the volatilization rate of arsenic in the flash smelter furnaces were in the order of 76 – 85 wt pct with slagging range varying from 7 to 17 wt pct. In the case of Noranda process, the As elimination rate is much higher at lower matte grades. Due to the important role of volatilization in As removal in the smelting furnaces, the process parameters should be chosen to enhance to As vaporisation. Based on this consideration, the author also suggests that, 1) mineralization of As species might contribute to higher elimination rate as some As compounds have higher vapour pressures; 2) a green-charge furnace should be favourable to As vaporisation; 3) higher operation temperature will lead to higher volatilization; 4) avoiding the over occupancy of the free slag surface by the charge material which can enlarge the contact area between slag and gas phase. In the case of converting process, the As partitioning tends more variable depending on the initial matte grade, up to 92 wt pct of the arsenic can report to the off-gases stream in converting low-grade matte. However, in normal practice, about 70 wt pct of the As is volatilized and 16 wt pct reports in the slag in the converter.

Table 2.12 Fractional distribution of As during the smelting and converting processes[92]

Smelting					Converting				
Furnace type	wt pct As in feed	matte	slag	gas	Furnace type	matte grade %Cu	matte	slag	gas
Noranda	0.06 ~ 0.14	5 ~ 8	13 ~ 7	82 ~ 85	Reverberatory	35 ~ 55	3 ~ 18	35 ~ 0	50 ~ 92
"KCS" Process	N. A.	10	11	79	Outokumpu	45	10	11	79
Outokumpu	0.17	7	17	76	KCS Smelting[1]	70	27	0	73
					KCS Smelting[2]	N. A.	0.3	29.5	70.2

* N.A. = Not available, KCS Smelting[1] = KSC Smelting Converting, KSC Smelting[2] = KSC Smelting Shaft Furnace

Steinhauser *et al*[82] firstly reviewed the fractional distribution behaviour of zinc by comparing the industrial data from different types of copper-smelting processes. As shown in the Figure 2.30, the deportment of Zn to the gas phase is general in the range 18 - 25 wt pct except that from the Sirosmelt process of which the result was obtained from the small pilot-plant trials, while that in the matte slag phase comes to 50 - 60 wt pct. It is also noticed that the Noranda processes generally have better performance on

overall elimination of zinc over other technologies as the removal by slagging is much higher than the other processes.

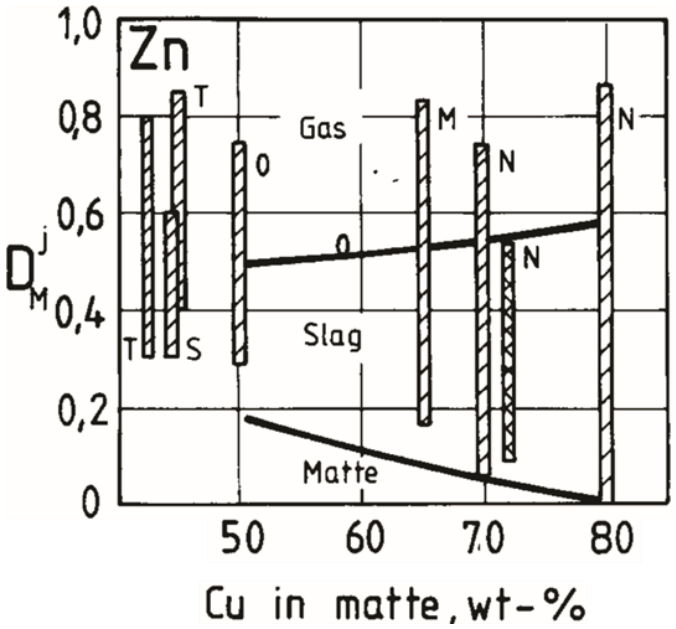

Legend: Index	Process	wt.% Cu in Matte
T	TBRC	40 - 45
S	Sirosmelt	44.5
T	TBRC	45
O	Outokumpu	50
M	Mitsubishi	65
N	Noranda (chalcopyrite concentrates)	70 and 80
N	Noranda (chalcocite concentrates)	72
K	Kennecott converter smelting	70 - 80

Figure 2.30 Fractional distribution of Zn, Pb, Bi and Sb in varied smelting processes[82]

Nagamori and Chaubal[93] developed a computation model to predict the fractional behaviour distribution of As and Zn in the Noranda process by incorporating mechanical entrainments between molten phases into a steady-state volatilization model[94]. By applying the developed computational model, the effect of operating parameters on fractional distribution behaviour of As and Zn can be evaluated, as shown in the Figure 2.31. The Figure 2.31 (a) shows the effect of matte grade on the fractional distribution behaviour, it can be observed that the deportment of As to gas phase continuously decreases with matte grade following by a dramatically decreasing when the approaching white metal. Similar trend can also be seen for Zn, although the much lower volatilization of Zn compared to that of As. The slagging effect of Zn, however, substantially increases with increasing matte grade. The Figure 2.31 (b) shows the effect of oxygen enrichment on the fractional distribution behaviour, which tends to inhibit the volatilization of As and Zn, while increases the slagging effect of Zn. The effect of slag composition on the distribution behaviour, as shown in the Figure 2.31 (c), appears to suppress the volatilization of As and Zn. Meanwhile, the increase of smelting temperature tends to promote the volatilization effect for both As and Zn, as shown in the Figure 2.31 (d). A comparison between the computational model and the industrial observation was also considered, as shown in the Table 2.13. A general good prediction

for As can be seen, while that of Zn elimination by slagging tend to be a bit lower in the industrial operation.

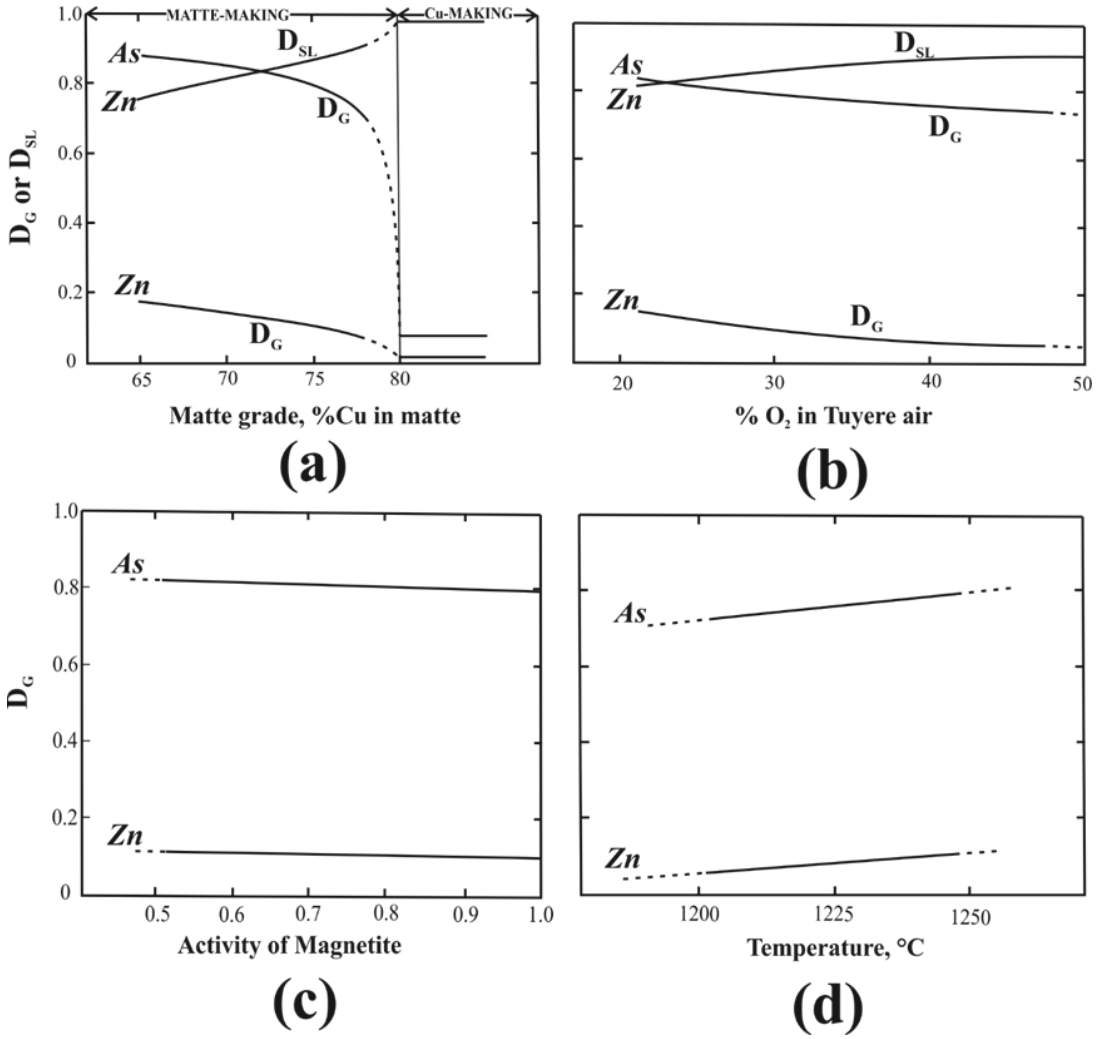

Figure 2.31 Distribution coefficients D_G or D_{SL} as function of Matte grade - (a), oxygen enrichment - (b), slag composition - (c) and temperature - (d), reproduced from Nagamori[93]

Table 2.13 Fractional distribution of impurities elements in smelting from both modelling and industrial plant observation[93]

Element	Fractional distribution (wt pct)						Inputs	Factors enchance slagging	Factors enhance volatilization
	Modelling			Industrial data					
	Matte	Slag	Gas	Matte	Slag	Gas			
As	8	12	80	8	7	85	Target pct = 65, 0.1 impurities elements, 1250 °C and magnetite saturation, oxygen 30 pct in tuyere air	[-]	
Zn	5	84	11	6	68	27		Higher matte grade, Higher oxygen enrichment	Lower matte grade, Higher operating temperature, Lower oxgyen enrichment

Itagaki[95, 96] conducted a thermodynamic evaluation of distribution behaviour on As in copper smelting process by building up a stepwise equilibria model. With the

developed model, the effects of operating parameters on the distribution behaviour of As were considered, as shown in the Figure 2.32 (a) to (d). The deportment of As to the exhaust gas substantially increases with increasing matte grade followed by moderate increment at the end of smelting (approaching 60 pct Cu), as shown in Figure 2.32 (a). The effect of oxygen enrichment on the distribution behaviour, as shown in Figure 2.32 (b), appears to inhibit the As volatilization while significantly enhances the As slagging. An increase of initial As content in the charge, meanwhile, will contribute to higher deportment of As to gas phase, as shown in the Figure 2.32 (c). A higher of degree of vapour saturation (S), as shown in the Figure 2.32 (d), will improve the overall elimination of As.

Table 2.14 Fractional distribution of impurities elements in smelting[96]

Element	Fractional distribution (wt pct)			Factors enhanced volatilization	Factors enhanced slagging	Inputs
	Slag	Gas	Matte			
As	4	90	6	Higher matte grade; Lower oxygen enrichment;	Higher matte grade; Higher oxygen enrichment;	%Cu = 60, 0.3 %X in charge air blowing, S = 1 Temperature = 1300 °C

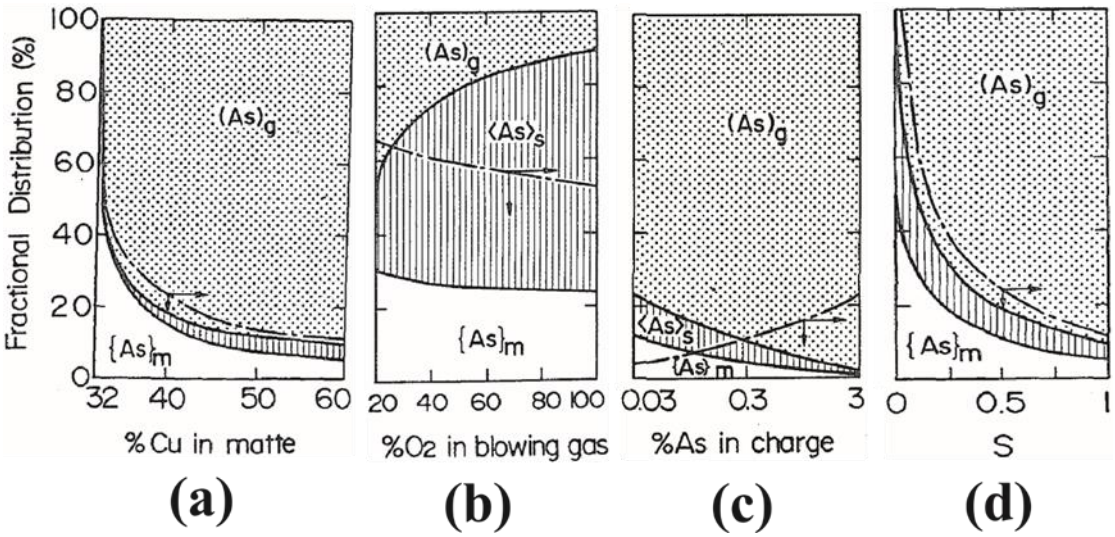

Figure 2.32 Factional distribution of As in copper smelting as function of operating parameters, (a) - matte grade, (b) - oxygen enrichment, (c) - pct As in the charge and (d) - degree of vapour saturation; reproduced from Itagaki[96]

H. Sohn *et al*[97] investigated the distribution behaviours of As and Zn through thermodynamic modelling which was developed based on the previous works done by Chaubal and Nagamori[93, 98, 99]. By applying the developed steady-state bath smelting model, the effects of operational parameters, including smelting temperature, final

matte grade and oxygen enrichment, on the distribution behaviours of As and Zn were considered. The Figure 2.33 (a) shows the fractional distribution behaviour of As under varied operating conditions as denoted by varied symbols. It can be seen that the volatilization rate tends to be stable with increasing target matte grade only until matte grade exceeds 70 pct Cu where a dramatically decrease can be observed. Meanwhile, higher smelting temperature and lower oxygen enrichment can benefit the volatilization. The slagging effect of As, however, tends to be independent of operation temperature. The overall elimination of As remains almost unchanged when target matte target increases. Similar trends can be seen in the Figure 2.33 (b) for Zn, except that the overall elimination rate of Zn significant increases with increasing final matte grade due to the dramatically increase of slagging effect.

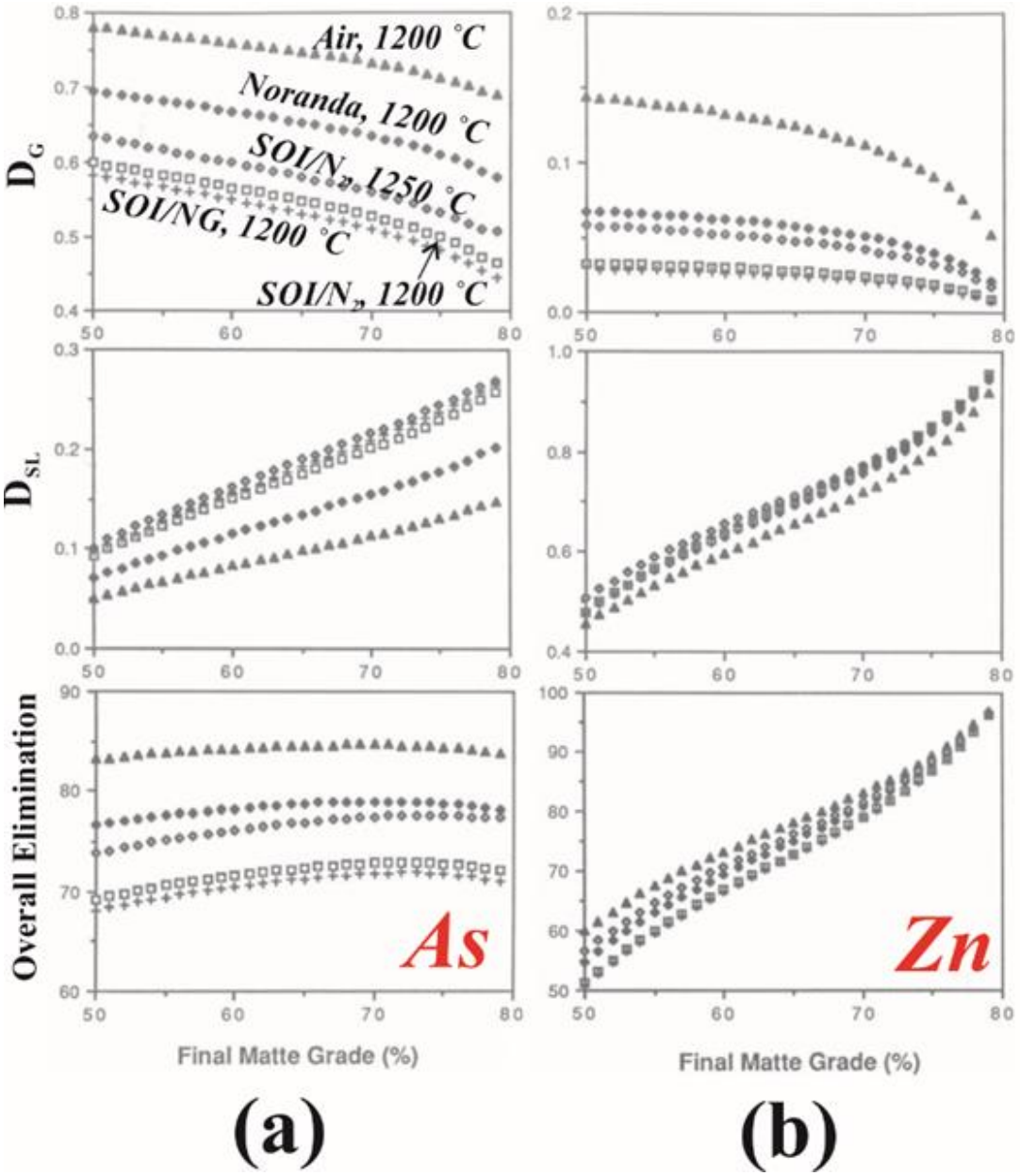

Figure 2.33 The fractional distribution of impurities elements in gas (upper) and slag (middle), and overall elimination rate (bottom) as function of final matte grade in smelting process, (a) - As, (b) - Zn[97]

Cerna *et al*[100] investigated the As distribution during copper smelting process based on a thermodynamic model similar to that reported by Itagaki[96]. Validation of the developed model was carried out by applying the operation parameters from Teniente Converter as inputs in developed model. The developed model has good prediction the fractional distribution of As in the smelting processes. The impacts of operational parameters on the fractional distribution behaviour of As were also evaluated by the developed model, as shown in Figure 2.34. It can be seen that the overall removal rate of As in Teniente Reactor can be enhanced at higher initial As concentration in the

charge. As shown in Figure 2.34 (a), total elimination rate tends be higher at lower oxygen enrichment applied, as can be seen from Figure 2.34 (a), which also promoted at lower target matte grade as shown in Figure 2.34 (b).

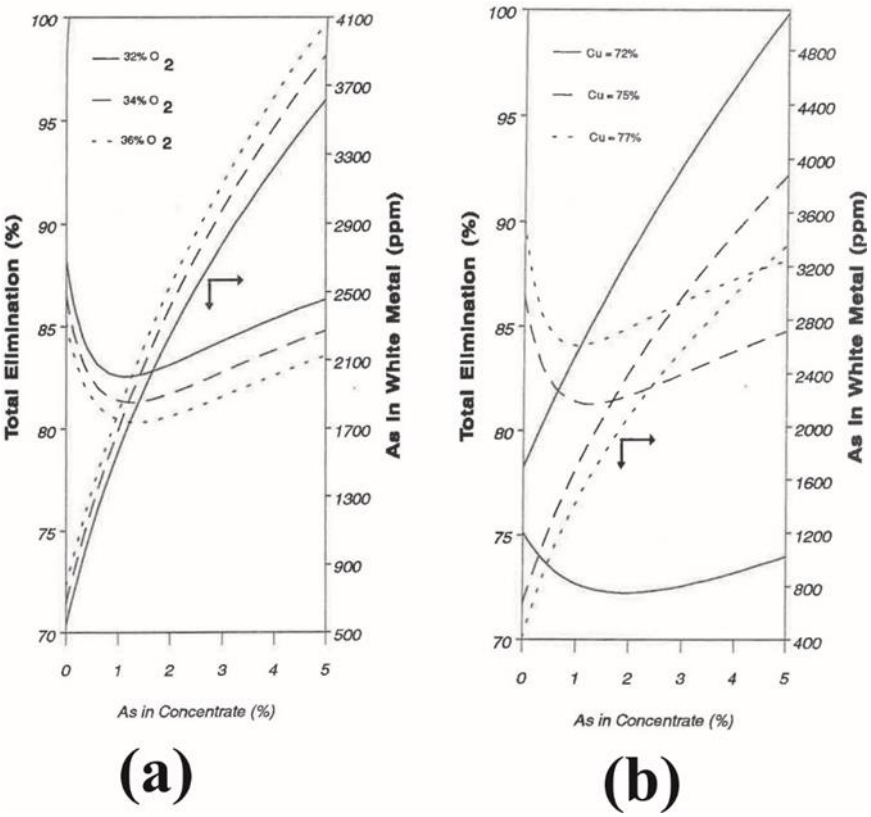

Figure 2.34 The overall elimination rate of varied impurities elements as function of, (a) - oxygen enrichment and (b) - matte grade[100]

Larouche[101] investigated the removal of As through volatilization in the copper smelting processes based on the industrial operation data from personal visit to the smelters and also those reported in literatures. As shown in Figure 2.35 (a), there is no clear trend of the volatilization rate for arsenic when the matte grade increases which should partially due the fact that the no operation parameters and furnace types were specified during the comparisons. However, an increase on the target matte grade generally inhibits the volatilization from a point of view of thermodynamics. An increasing of oxygen enrichment will lead to significantly decrease of volatilization significantly decreases as shown in Figure 2.35 (b).

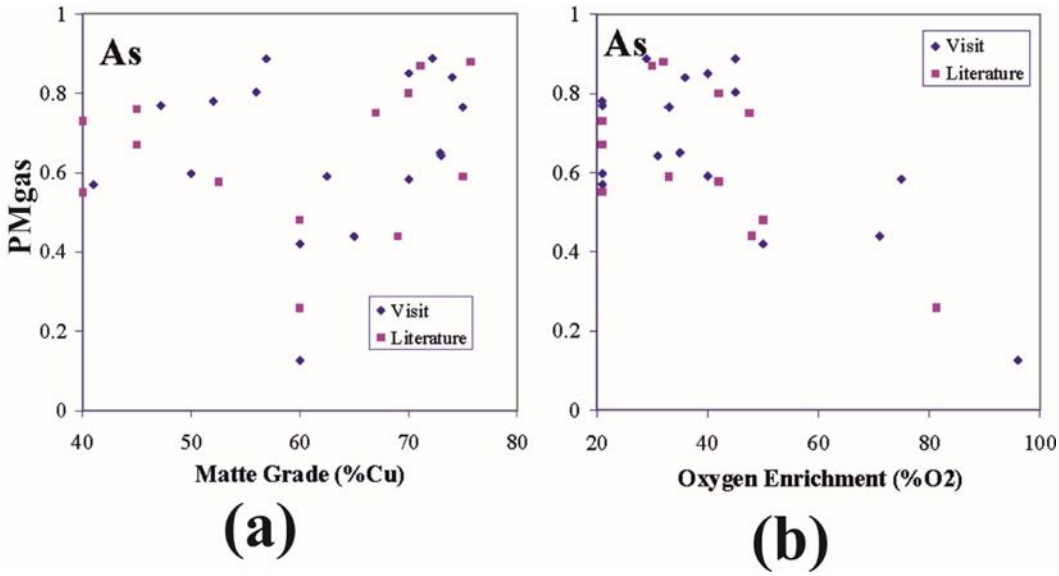

Figure 2.35 The volatilization rate of arsenic as function of, (a) - matte grade and (b) - oxygen enrichment[101]

Sohn *et al*[102] investigated the kinetics of As volatilization by blowing varied oxygen and argon gas mixture into industrial copper matte at 1250 and 1400 °C in a gas tight vertical furnace tube, of which the results are shown in Figure 2.36. In can be seen that the As content in the matte phase substantially decreases with blowing time. A higher blowing temperature somewhat benefit the As volatilization, while the impact by input oxygen partial pressure appears to be rather small.

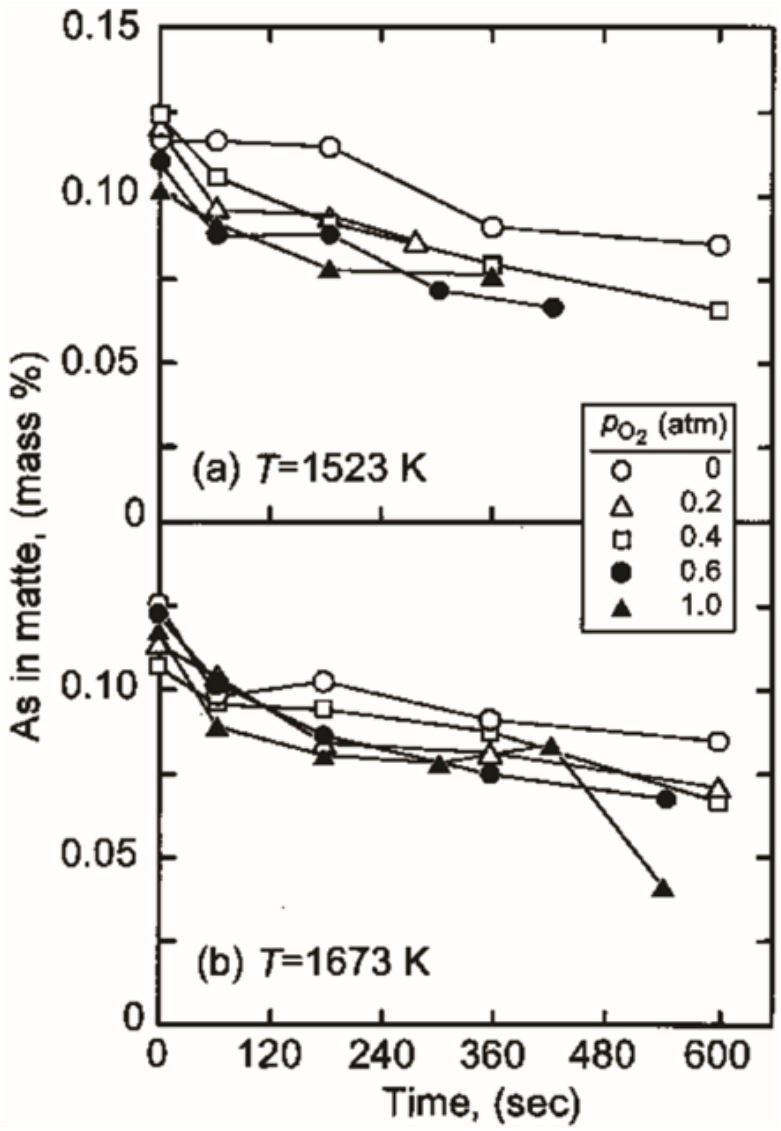

Figure 2.36 Variation of arsenic content in matte as function of blowing time at 1250 °C and 1400 °C[102]

Acuna and Sherrington[91] investigated the As fractional distribution behaviour during smelting in Teniente Converter by applying a thermodynamical model similar to that reported by other researchers[96, 103, 104]. Using the developed model, they evaluated the effect of operating parameters on the As fractional distribution behaviour. The model suggests that the deportment of As decreases with increasing oxygen enrichment. The increasing of As in feed, however, can promote the volatilization and decreases the deportment to matte and slag phases. In the case of matte grade increasing, the volatilization and slagging effect both increase for As. Meanwhile, the increasing on gas saturation factor appears to enhance the volatilization effect while inhibits the slagging of As.

Moyano *et al*[105] investigated the feasibility of treatment high As-bearing concentrate via Teniente Converter from both lab-scale experiment and industrial smelter testing. The lab scale experiments were conducted at 1250 °C with 37 vol% O_2 in tuyere air, of which the results are shown in the Figure 2.37 (a). It can be seen that the volatilization of As substantially increases with the As content in the charge which contributes to higher overall elimination rate. For Teniente Converter testing, the overall elimination rate, as shown in Figure 2.37 (b), however, tends to lower than that in lab scale experiments as higher volatilization rate can be achieved in this case.

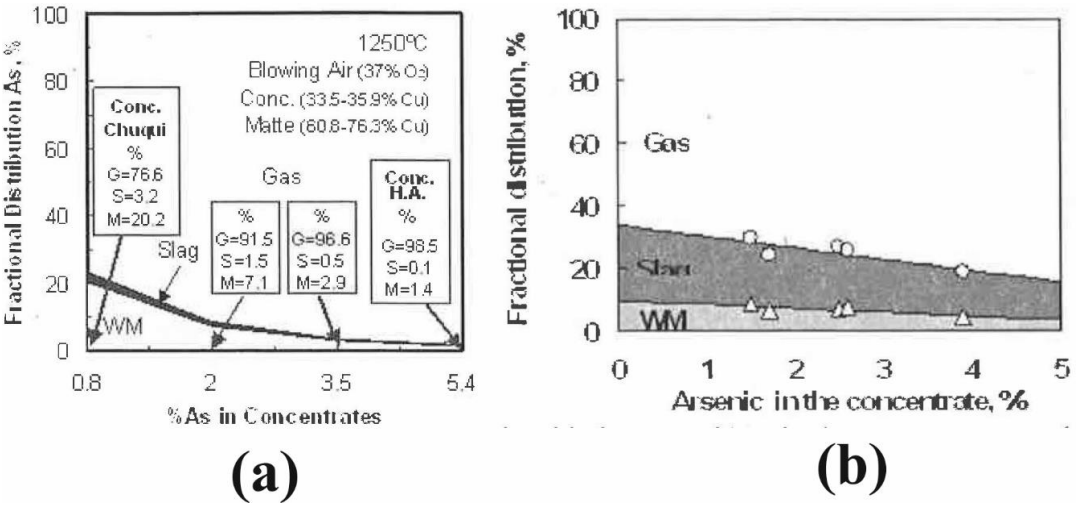

Figure 2.37 Arsenic fractional distribution as function of As wt pct in charge, (a) - lab-scale and (b) - Teniente Converting testing

Montenergro *et al*[106, 107] investigated technical feasibility of recirculating high impurities element - bearing copper smelting dust into the smelter by conducting lab-scale dust-recirculation test with conditions similar to that in the industrial smelting process. The dust recirculation testings were conducted in an electric furnace with blowing temperature range from 1250 to 1300 °C. The smelting process was simulated by blowing N_2-O_2 into the charge at target temperature which was prepared by mixing different ratios of industrial concentrate, matte, slag and dust. By carrying out series of dust recirculation testings, the effects of operation parameters on the fractional distribution behaviour can be evaluated. The Figure 2.38 shows the distribution behaviour of arsenic under varied operating conditions. It can be seen that the deportment of As to the slag phase increases with matte grade in the charged copper matte which tends to have minor effect on the arsenic volatilization. When higher dust circulation rate was applied, the volatilization rate of As increases only until the dust recirculation approaching 13 wt pct. The oxygen enrichment appears to has minor effect

on the As fractional distribution, while the temperature tends to slightly increases the overall elimination of As. The Figure 2.39 shows the fractional distribution behaviour of Zn as function of varied operation parameters. It can be observed that, with the matte grade in the charged copper matte increasing, the overall elimination of Zn tends to slightly increases contributing by the enhanced slagging of Zn. As the dust recirculation rate increases, as opposite to that of arsenic, the overall elimination of Zn tends to decreases due to the inhibited volatilization of Zn. The oxygen enrichment and smelting temperature appear to have minor effect on the overall elimination of Zn.

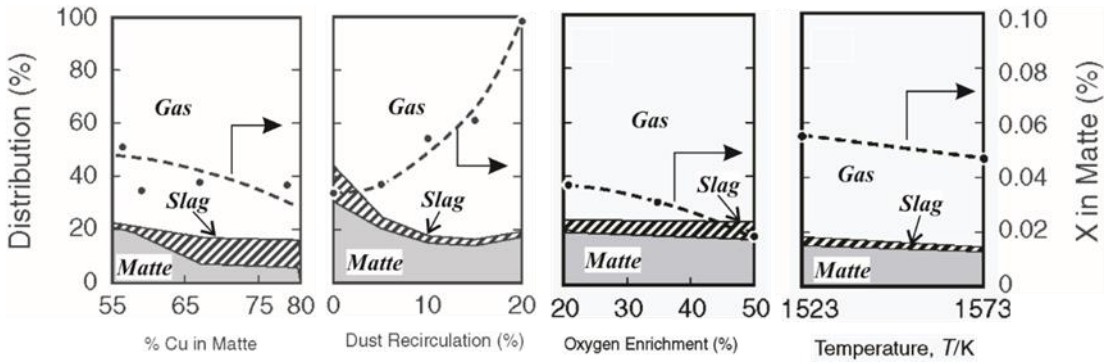

Figure 2.38 Fractional distribution behaviour of arsenic as function of, (a) - starting matte grade, (b) - dust circulation rate, (c) - oxygen enrichment and (d) - operating temperature[106, 107]

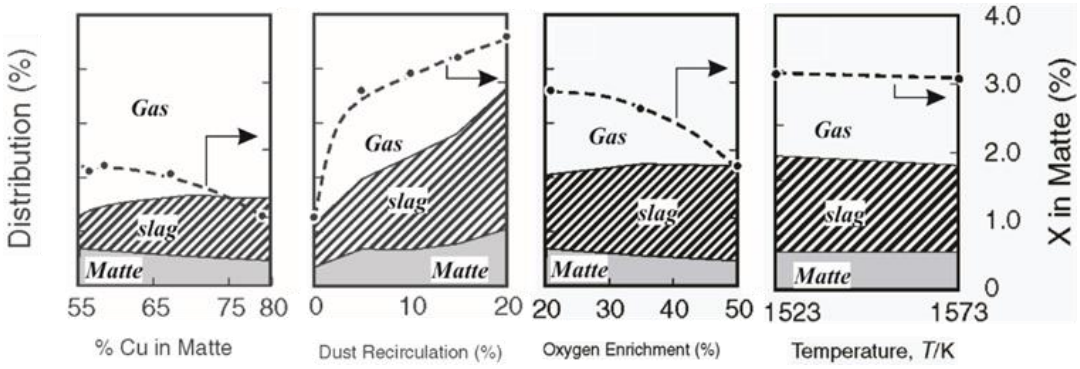

Figure 2.39 Fractional distribution behaviour of zinc as function of, (a) - starting matte grade, (b) - dust circulation rate, (c) - oxygen enrichment and (d) - operating temperature[106, 107]

Chen *et al*[108] developed a thermodynamic model with updated database to investigate the arsenic fractional distribution behaviour during the matte smelting process. By applying, the effect of operation parameters in copper making processes on As distribution behaviour can be accessed, of which the results are shown in the Figure 2.40. During the matte smelting, with increasing final smelting matte grade, as shown in the Figure 2.40 (a), the deportment of As to slag and matte phase tends to increase, while that to the gas phase dramatically decreases. As shown in the Figure 2.40 (b), a

higher deportment of arsenic to slag phase can be seen with increasing Fe/SiO_2 ratio and leads to a lower volatilization. An increasing of Pso_2, as shown in the Figure 2.40 (c), would markedly decreases the volatilization of arsenic and promotes the deportment to the slag phase. An increasing on the slag basicity, as shown in the Figure 2.40 (d), tends to be similar that of increasing Fe to SiO_2 ratio. In case of higher initial arsenic in charge, as shown in Figure 2.40 (e), the volatilization of As tends to increases and contributes to a higher overall elimination rate. However, the overall removal rate of As slightly decreases when smelting temperature increasing, while a higher volatilization can be obtained under the situation.

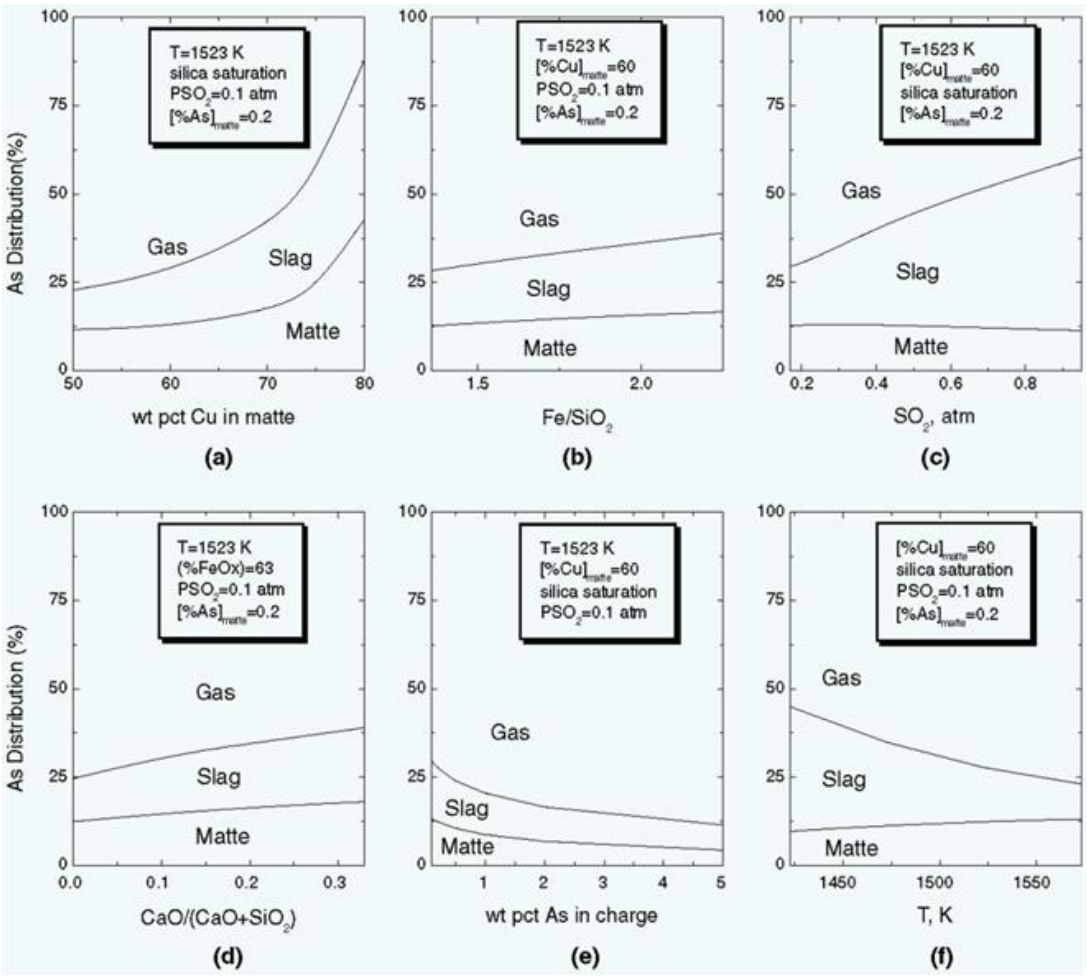

Figure 2.40 Variations of the fractional distribution of arsenic between gas, slag and matte as function of, (a) - matte grade, %Cu, (b) - Fe/SiO_2 ratio, (c) - Pso_2, (d) - $CaO/(CaO+SiO_2)$ ratio, (e) - initial As content charge and (f) - operation temperature[108]

2.12 Reference

1. C. W. Bale, E. B. P. Chartrand, S. A. Decterov, G. Eriksson, A. Gheribi, K. Hack, I. H. Jung, J. Melançon, A. D. Pelton, S. Petersen and C. Robelin, In *Celebrating the Megascale*, (John Wiley & Sons, Inc.: 2014), pp 141-148.

2. C. W. Bale, E. Bélisle, P. Chartrand, S. A. Decterov, G. Eriksson, K. Hack, I. H. Jung, Y. B. Kang, J. Melançon, A. D. Pelton, C. Robelin and S. Petersen, *CALPHAD: Comput. Coupling Phase Diagrams Thermochem.*, 2009, vol. 33, pp. 295-311.

3. N. L. Bowen and J. F. Schairer, *Am. J. Sci.*, 1932, vol. Series 5 Vol. 24, pp. 177-213.

4. J. W. Creig, *Am. J. Sci.*, 1927, vol. Series 5 Vol. 13, pp. 133-154.

5. J. W. Greig, *Am. J. Sci.*, 1927, vol. Series 5 Vol. 14, pp. 473-484.

6. R. Schuhmann, Jr. and P. J. Ensio, *J. Met.*, 1951, vol. 3, pp. 401-11.

7. R. Schuhmann, Jr., R. G. Powell and E. J. Michal, *J. Met.*, 1953, vol. 5, pp. 1097-1104.

8. W. C. Allen and R. B. Snow, *J. Am. Ceram. Soc.*, 1955, vol. 38, pp. 264-80.

9. A. Muan, *J. Met.*, 1955, vol. 7, pp. 965-76.

10. R. P. Goel, H. H. Kellogg and J. L. Rrain, *Metallurgical Transactions B*, 1980, vol. 11, pp. 107-117.

11. B. Björkman, *Calphad-Computer Coupling of Phase Diagrams and Thermochemistry*, 1985, vol. 9, pp. 271-282.

12. M. Selleby, *Metall. Mater. Trans. B*, 1997, vol. 28, pp. 577-596.

13. P. Wu, G. Eriksson, A. D. Pelton and M. Blander, *ISIJ Int.*, 1993, vol. 33, pp. 26-35.

14. E. Jak, P. Hayes, A. Pelton and S. Dectero, *Int. J. Mater. Res.*, 2007, vol. 98, pp. 847-854.

15. A. Muan, *Am. J. Sci.*, 1958, vol. 256, pp. 171-207.

16. A. Muan, *Jom-J Min Met Mat S*, 1955, vol. 7, pp. 965-976.

17. A. Muan and E. F. Osborn: *Phase equilibria among oxides in steelmaking*. (Addison-Wesley Pub. Co., 1965).

18. E. Jak, In *Ninth International Conference on Molten Slags, Fluxes and Salts (MOLTEN12)*, (The Chinese Society for Metals: Beijing, China, 2012), p 28.

19. L. S. Darken, *J. Am. Chem. Soc.*, 1948, vol. 70, pp. 2046-53.

20. T. Hidayat, P. C. Hayes and E. Jak, *Metall Mater Trans B*, 2012, vol. 43, pp. 27-38.

21. L. S. Darken and R. W. Gurry, *J. Am. Chem. Soc.*, 1945, vol. 67, pp. 1398-1412.

22. R. L. Benner and H. Kenworthy: *Thermodynamic properties of the ZnO-Fe_2O_3-Fe_3O_4 system at elevated temperatures part 1: the Thermodynamic Properties as Related to the Spinel Structure*. (U.S. Department of the Interior, Bureau of Mines, 1966).

23. T. Hidayat, P. Hayes and E. Jak, *Metall. Mater. Trans. B*, 2012, vol. 43, pp. 27-38.

24. T. Hidayat, P. C. Hayes and E. Jak, *Metall Mater Trans B*, 2012, vol. 43, pp. 14-26.

25. T. Oishi, T. Goto, Y. Kayahara, K. Ono and J. Moriyama, *Metall. Trans., B*, 1982, vol. 13B, pp. 423-7.

26. W. Hirschwald, F. Stolze and I. N. Stranski, *Z. Phys. Chem. (Muenchen, Ger.)*, 1964, vol. 42, pp. 96-111.

27. H. A. Wriedt, *J. Phase Equilib.*, 1987, vol. 8, pp. 166-176.

28. E. N. Bunting, *J. Am. Ceram. Soc.*, 1930, vol. 13, pp. 5-10.

29. J. Williamson and F. Glasser, *Phys. Chem. Glasses*, 1964, vol. 5, pp. 52-59.

30. R. A. R. a. D. R. Gaskell, *Metall. Mater. Trans. B*, 1983, vol. 12B, p. 7.

31. B. Bjoerkman, *Scand. J. Metall.*, 1986, vol. 15, pp. 185-90.

32. E. Jak, S. Degterov, P. Wu, P. C. Hayes and A. D. Pelton, *Metall. Mater. Trans. B*, 1997, vol. 28B, pp. 1011-1018.

33. R. Hansson, B. Zhao, P. C. Hayes and E. Jak, *Metall. Mater. Trans. B*, 2005, vol. 36, pp. 187-193.

34. J. M. Claude, M. Zanne, C. Gleitzer and J. Aubry, *Mem. Sci. Rev. Metall.*, 1977, vol. 74, pp. 229-36.

35. A. A. Lykasov, V. V. D'Yachuk and G. I. Sergeev, *Izv. Akad. Nauk SSSR, Neorg. Mater.*, 1985, vol. 21, pp. 604-7.

36. A. A. Lykasov, V. V. D'Yachuk and M. S. Pavlovskaya, *Vopr. Pr-va i Obrab. Stali, Chelyabinsk*, 1985, pp. 22-5.

37. S. Itoh and T. Azakami, *Mater. Trans. JIM*, 1995, vol. 36, pp. 1074-80.

38. S. Itoh, K. Sato, S. Nakazawa and T. Azakami, *Shigen to Sozai*, 1989, vol. 105, pp. 739-43.

39. I. Katayama, J. Shibata, M. Aoki and Z. Kozuka, *Transactions of the Japanese Institute of Metals*, 1977, vol. 18, p. 6.

40. G. I. Sergeev, A. A. Lykasov and V. V. D'Yachuk, *Tsvetn. Met. (Moscow)*, 1985, vol. 1, pp. 20-2.

41. G. I. Sergeev, A. A. Lykasov, G. G. Mikhailov and I. F. Khudyakov, *Elektrokhimiya*, 1985, vol. 21, pp. 455-60.

42. S. Schaefer and R. McCune, *Metallurgical Transactions B*, 1986, vol. 17, pp. 515-521.

43. J. W. Graydon and D. W. Kirk, *Metallurgical Transactions B*, 1988, vol. 19, pp. 919-925.

44. E. Jak, B. Zhao and P. Hayes, *Metall. Mater. Trans. B*, 2000, vol. 31, pp. 1195-1201.

45. S. Degterov, A. Pelton, E. Jak and P. Hayes, *Metall. Mater. Trans. B*, 2001, vol. 32, pp. 643-657.

46. A. A. Lykasov, V. V. D'Yachuk and M. S. Pavlovskaya, *Neorg. Mater.*, 1991, vol. 27, pp. 2153-6.

47. S. Itoh and T. Azakami, *Metall. Rev. MMIJ*, 1993, vol. 10, pp. 113-33.

48. S. Itoh and T. Azakami, *Nippon Kinzoku Gakkaishi*, 1994, vol. 58, pp. 1288-93.

49. R. Hansson, P. Hayes and E. Jak, *Metall. Mater. Trans. B*, 2005, vol. 36, p. 7.

50. K. Tanida, T. Kitamura and A. Ohkawa, *Bulletin of the Research Institute of Mineral Dressing and Metallurgy, Tohoku University*, 1985, vol. 40, pp. 155-162.

51. K. Tanida and T. Kitamura, *Bulletin of the Research Institute of Mineral Dressing and Metallurgy, Tohoku University*, 1984, vol. 39, pp. 105-114.

52. K. Tanida and T. Kitamura, *Bulletin of the Research Institute of Mineral Dressing and Metallurgy, Tohoku University*, 1984, vol. 40, pp. 71-76.

53. R. Hansson, P. C. Hayes and E. Jak, *Scand. J. Metall.*, 2004, vol. 33, pp. 294-304.

54. R. Hansson, P. C. Hayes and E. Jak, *Trans. Inst. Min. Metall., Sect. C*, 2005, vol. 114, pp. 141-146.

55. W. G. Davenport, *University of British Columbia, Master Thesis*, 1960.

56. B. L. Dobrotsvetov, E. I. Bogoslovskaya and E. I. Sobel'man, *Dokl. Akad. Nauk SSSR*, 1964, vol. 158, pp. 189-91.

57. S. Itoh and T. Azakami, *Shigen to Sozai*, 1993, vol. 109, pp. 325-329.

58. E. Jak, S. Degterov, A. D. Pelton and P. C. Hayes, *Metall. Mater. Trans. B*, 2001, vol. 32, pp. 793-800.

59. T. Ericsson and A. Filippidis, *Am. Mineral.*, 1986, vol. 71, pp. 1502-1509.

60. Y. Umetsu, T. Nishimura, K. Tozawa and K. Sasaki, *Symp. Ser. - Australas. Inst. Min. Metall.*, 1980, vol. 23, pp. 95-106.

61. B. Zhao, Z. Cui and Z. Wang, In *4th International Symposium on High-Temperature Metallurgical Processing*, (John Wiley & Sons, Inc.: 2013), p 10.

62. E. Jak, B. Zhao and P. C. Hayes, *Metall. Mater. Trans. B*, 2002, vol. 33, pp. 877-890.

63. B. L. Dobrotsvetov, *Vestn. Mosk. Univ., Khim.*, 1967, vol. 22, pp. 44-53.

64. B. L. Dobrotsvetov, E. I. Bogoslovskaya and V. E. Rudnichenko, *Zh. Neorg. Khim.*, 1967, vol. 12, pp. 2190-8.

65. J. G. Lenz and I. Lee, In *Metall. Slags Fluxes, Int. Symp., Proc., 2nd*, ed. H. Alan; Gaskell Fine, David R (Metall. Soc. AIME: 1984), pp 823-35.

66. E. Jak, B. Zhao and P. C. Hayes, *Metall. Mater. Trans. B*, 2002, vol. 33B, pp. 865-876.

67. V. I. Bershak, *Zh. Fiz. Khim.*, 1972, vol. 46, pp. 1534-5.

68. P. Tan and P. Vix, In *EPD Congress 2005*, ed. Mark E. Schlesinger (Minerals, Metals & Materials Society: 2005), pp 713-721.

69. K. Yamaguchi, M. Kudo, Y. Kimura, S. Ueda and Y. Takeda, In *2006 TMS Fall Extraction & Processing Meeting: Sohn International Symposium*, (Minerals, Metals & Materials Society: San Diego, CA, 2006), pp 199-208.

70. B. Zhao, P. C. Hayes and E. Jak, *Metall. Mater. Trans. B*, 2010, vol. 41, pp. 374-385.

71. B. Zhao, P. C. Hayes and E. Jak, *Metall. Mater. Trans. B*, 2010, vol. 41, pp. 386-395.

72. B. Zhao, P. C. Hayes and E. Jak, *Metall. Mater. Trans. B*, 2011, vol. 42, pp. 50-67.

73. B. Zhao, P. C. Hayes and E. Jak, *Int. J. Mater. Res.*, 2011, vol. 102, pp. 269-276.

74. B. Zhao, P. C. Hayes and E. Jak, *Int. J. Mater. Res.*, 2011, vol. 102, pp. 134-142.

75. B. Zhao, P. C. Hayes and E. Jak, *Metall. Mater. Trans. B*, 2010, vol. 42, pp. 50-67.

76. B. Zhao, P. C. Hayes and E. Jak, *Metall. Mater. Trans. B*, 2011, vol. 42, pp. 490-499.

77. B. Zhao, P. C. Hayes and E. Jak, *Metall. Mater. Trans. B*, 2011, vol. 42, pp. 978-986.

78. K. Azuma, S. Goto and O. Ogawa, *J. Fac. Eng., Univ. Tokyo, Ser. A.*, 1967, vol. No. 5, pp. 54-5.

79. N. J. Filipovska and H. B. Bell, *Trans. - Inst. Min. Metall., Sect. C*, 1978, vol. 87, pp. 94-8.

80. A. Yazawa, *Can. Metall. Q.*, 1974, vol. 13, pp. 443-453.

81. I. Jimbo, S. Goto and O. Ogawa, *Metallurgical Transactions B*, 1984, vol. 15, pp. 535-541.

82. J. Steinhauser, A. Vartiainen and W. Wuth, *JOM*, 1984, vol. 36, pp. 54-61.

83. C. Chen and S. Jahanshahi, *Metall. Mater. Trans. B*, 2010, vol. 41, pp. 1166-1174.

84. A. Yazawa and T. Azakami, *Can. Metall. Q.*, 1969, vol. 8, pp. 257-261.

85. M. Nagamori and P. J. Mackey, *Metallurgical Transactions B*, 1978, vol. 9, pp. 567-579.

86. A. Roine, *Metallurgical Transactions B*, 1987, vol. 18, pp. 213-223.

87. G. Roghani, M. Hino and K. Itagaki, *Mater. Trans. JIM*, 1997, vol. 38, pp. 707-713.

88. G. Roghani, Y. Takeda and K. Itagaki, *Metall. Mater. Trans. B*, 2000, vol. 31, pp. 705-712.

89. R. Reddy and J. Font, *Metall. Mater. Trans. B*, 2003, vol. 34, pp. 565-571.

90. J. C. Font and R. G. Reddy, (Minerals, Metals & Materials Society: 2005), pp 51-60.

91. C. M. Acuna and M. Sherrington, In *The Carlos Diaz Symposium on Pyrometallurgy*, (Canadian Institute of Mining, Metallurgy and Petroleum: 2007), pp 273-285.

92. I. J. Weisenberg, P. S. Bakshi and A. E. Vervaert, *JOM*, 1979, vol. 31, pp. 38-44.

93. M. Nagamori and P. C. Chaubal, *Metallurgical Transactions B*, 1982, vol. 13, pp. 331-338.

94. M. Nagamori and P. C. Chaubal, *Metallurgical Transactions B*, 1982, vol. 13, pp. 319-329.

95. K. Itagaki and A. Yazawa, *Trans. Jpn. Inst. Met.*, 1982, vol. 23, pp. 759-67.

96. K. Itagaki, *Metall. Rev. MMIJ*, 1986, vol. 3, pp. 87-100.

97. H. Y. Sohn, H. Kim and K. W. Seo, In *EMC '91: Non-Ferrous Metallurgy—Present and Future*, (Springer Netherlands: 1991), pp 205-217.

98. P. C. Chaubal and M. Nagamori, *Metallurgical Transactions B*, 1988, vol. 19, pp. 547-556.

99. P. Chaubal and M. Nagamori, *Metallurgical Transactions B*, 1983, vol. 14, pp. 303-306.

100. M. Cerna, R. Bustos, G. Riveros and J. Soto, *Proceedings of the Pyrometallurgy 95,(Cambridge, England: The Institution of Mining and Metallurgy, IMM, 1995), 143-156*, 1995, pp. 143-156.

101. P. Larouche: Minor elements in copper smelting and electrorefining. (McGill University, Montreal, Canada, 2001).

102. H. S. Sohn, Y. Fukunaka, T. Oishi, H. Y. Sohn and Z. Asaki, *Metall. Mater. Trans. B*, 2004, vol. 35, pp. 651-661.

103. K. W. Seo and H. Y. Sohn, *Metallurgical Transactions B*, 1991, vol. 22, pp. 791-799.

104. M. Nagamori, P. J. Mackey and P. Tarassoff, *Metall. Trans., B*, 1975, vol. 6B, pp. 197-8.

105. A. Moyano, C. Caballero, R. Mackay, P. Morales and K. ltagaki, In *The Carlos Diaz Symposium on Pyrometallurgy*, (Canadian Institute of Mining, Metallurgy and Petroleum: 2007), pp 301-313.

106. V. Montenegro, H. Sano and T. Fujisawa, *Miner. Eng.*, 2013, vol. 49, pp. 184-189.

107. V. Montenegro, H. Sano and T. Fujisawa, *Mater. Trans.*, 2008, vol. 49, pp. 2112-2118.

108. C. Chen, L. Zhang and S. Jahanshahi, *Metall. Mater. Trans. B*, 2010, vol. 41, pp. 1175-1185.

3 Scope of Present Study

The scope of present study was defined so as to:

1. Develop and improve the experimental techniques to enable the investigation on the phase equilibria behaviour of Zn-containing smelting slags under reducing condition.

2. Explore the effect of slag composition on the liquidus temperature and phase relations with Po_2 fixed at 10^{-8} atm

   (1) "FeO"-SiO_2 and "FeO"-ZnO-SiO_2

   (2) "FeO"-ZnO-SiO_2-Al_2O_3 with three pseudo-sections at 2, 4 and 6 wt pct Al_2O_3

   (3) "FeO"-ZnO-SiO_2-CaO with three pseudo-sections at 2, 4 and 6 wt pct CaO

   (4) "FeO"-ZnO-SiO_2-CaO-(S) with three pseudo-sections at 2, 4 and 6 wt pct CaO

3. Extensive literature review on the arsenic and zinc distribution in the copper smelting processes, further comparisons between different modellings and FactSage 6.4 were conducted.

4 Experimental Procedures

4.1 Overview of Experimental Techniques in the ZnO-containing Slag Systems

Reviews on the experimental techniques applied to phase equilibria studies of complex slags and principles the for selection of suitable techniques have been conducted by Lenz[1] and Jak[2, 3]. Basically, there are two main approaches in the determination of phase equilibria for the complex slags, namely, the static method and dynamic method as shown in Table 4.1[3]. Briefly, dynamic techniques are suitable for those systems with sluggish phase transformations, while the static methods are particularly suitable for slags systems of high viscosity, such as silicate-based slag systems in present studies.

The most powerful static method applied to phase equilibria studies is the quenching technique. Normally, this technique involves preparing a small portion of sample with desired compositions in the system under consideration. The prepared samples were then heated up in the furnace with desired gas condition and held for sufficient time to establish the final equilibrium. The samples were rapidly cooled down in low temperature media, such as ice-water, by which the phase assemblages prevailing at high temperature equilibration can be frozen. The microstructure of solid phase at high temperature equilibration can be retained, and liquid phase will be preserved as homogeneous glasses. The quenched samples can be analysed by XRD or EPMA.

The use of EPMA in phase equilibrium studies has many advantages over conventional approaches. First, it improves the efficiency of the phase equilibria study; secondly, more information and details are achieved for the liquid phase as well as the solid phase in one sample; most importantly, the bulk compositions change will not affect the final results since measurements were conducted after equilibration rather than before the experiment. In this case, the technique scheme involves high temperature equilibration, quenching and EPMA analyses was adopted in the present studies.

Table 4.1 Summary of the principal experimental methods used in phase equilibrium determination in oxide systems[3]

Methods		**Suitability for oxide systems**
Statics method	Electrochemical	Thermodynamic props, e.g. ai,ΔG and ΔS
	Vapour pressure	Knudsen: low metal vapour pressure, non-aggressive
		Reactive gas equilibration: low metal vapour pressure (PO_2 control) Isopeistic equilibria: high metal vapour pressure
	X-ray powder diffraction	phase detection/identification; extensive solid solution: lattice parameters at temperatures
	Hot stage microscopy	Liquidus of low vapour pressure systems, transparent liquid
	Calorimetry	Enthalpies ΔH of formation, of solution and of phase transition
	Equilibration/quench/analysis techniques	Liquidus of hig viscosity liquids, e.g. high silica slags; solid state phase equilibria
Dynamic methods	Thermogravimetric analysis (TG)	Gas/solid and gas/liquid reactions
	Differential thermal analysis (DTA)	Rapid phase transitions (melting point of congruently melting compounds); liquidus/solutions of low viscosity liquids

4.2 Experimental Techniques Development in Present Studies

Due to the rapidly loss of ZnO from evaporation under the reduction conditions, special attention has to been paid to develop techniques to prohibit this process. As discussed in the Chapter 2, most of the investigations on ZnO-containing system under reducing condition had been proceed in sealed-container of which the oxygen partial pressure is controlled by the condensed phases. In current study, the Po_2 is maintained at 10^{-8} atm by CO_2/CO gas mixture all through temperature from 1170 to 1300 °C. In the conventional method, long holding time (from several hours to days) was generally applied, which was firstly adopted in my experimental procedure. However, the preliminary experiments showed that ZnO cannot be preserved in the slag under the reducing condition when conventional method was applied. In this case, preserving the ZnO in the slag should be first priority. As such, two approaches were considered,

1) Decrease the ZnO activity in the starting mixture which was attained by using zinc silicate master slag as zinc-source instead of ZnO;

2) Quick establishment of equilibration (Tens of minutes) between slag and the atmosphere which was achieved by pre-equilibrating the “iron” with the atmosphere and used in the starting mixture.

Overall, the conventional method cannot be successfully applied to phase equilibria study of ZnO-containing slag which involves varied oxidation states under reducing condition, while the present experimental technique works well in such case.

The attainment of equilibration can be confirmed in the following aspects:

A) The master slag was prepared in the conditions similar (temperature and Po_2) to the target one to shorten the equilibration time;

B) The homogeneity of the phase can be confirmed by the EPMA measurements in different areas of the quenched sample. As an example, the EPMA measurements for Sample #145 is listed in Table 4.2, of which the microstructure was shown in Figure 4.1 11 compositions of the liquid phase were measured from different areas and 4 compositions of the willemite phase were measured from different areas by EPMA. The standard deviations are 0.4 and 0.2 for the liquid and willemite, respectively. This confirms that the equilibrium has been achieved within the sample. Usually the sample with the standard deviation of the compositions less than 1% will be accepted and used to construct the phase diagram. In fact, the cooling rate is more important in the research technique which has to be fast enough to convert the liquid phase to homogeneous glass for EPMA measurements.

Table 4.2 EPMA measure results of sample 145#

Comments	FeO	ZnO	Al_2O_3	CaO	SiO_2
Standards	90.2	0	0.0	0.0	0.0
	0.0	0.0	0.0	48.7	51.4
	0.0	0.0	100.0	0.0	0.0
	0.0	99.3	0.0	0.1	0.0
Sample 145#	33.8	34.6	0.0	0.0	31.6
1573 K (1300 °C)	32.7	35.4	0.0	0.0	31.9
Holding time: 30 min	32.5	35.5	0.0	0.0	32.0
Liquid	33.3	34.7	0.0	0.0	32.0
	33.6	34.8	0.0	0.0	31.6
	33.8	34.4	0.0	0.0	31.8
	32.9	35.2	0.0	0.0	31.8
	33.1	35.0	0.0	0.0	31.9
	33.7	34.7	0.0	0.0	31.5
	33.7	34.6	0.0	0.0	31.7
	33.5	34.5	0.0	0.0	31.9
Average:	33.3	34.9	0.0	0.0	31.8
Standard Deviation:	0.4	0.3	0.0	0.0	0.2
Willemite	11.0	60.9	0.0	0.0	28.1
	10.7	61.0	0.0	0.0	28.3
	10.7	61.0	0.0	0.0	28.4
	10.6	61.2	0.0	0.0	28.2
Average	10.7	61.0	0.0	0.0	28.2
Standard Deviation:	0.2	0.1	0.0	0.0	0.1

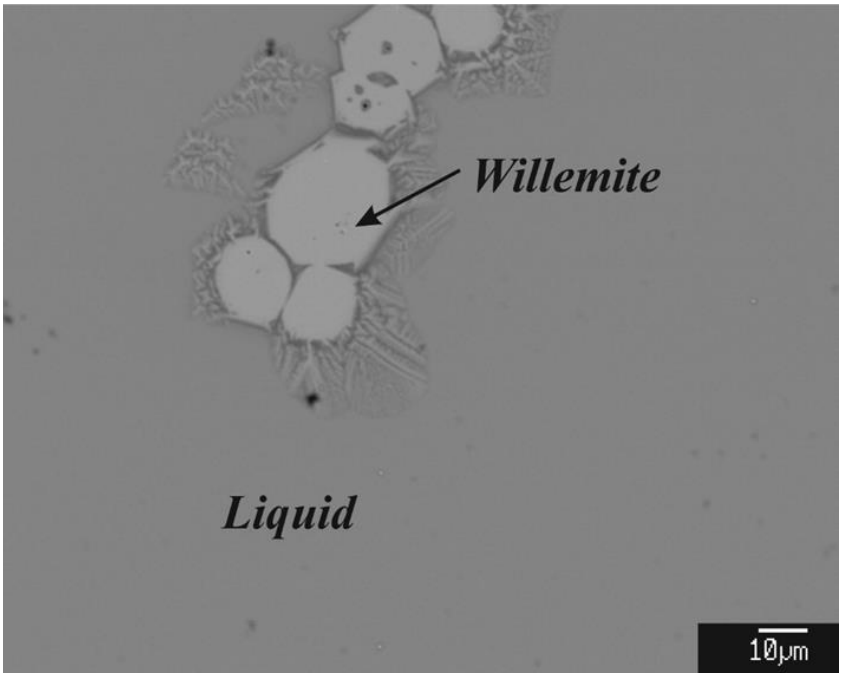

Figure 4.1 Microstructure of sample 145 showing the equilibration between willemite and liquid

C) The self-consistency of the EPMA results will be confirmed again when they are used to construct the isotherms at each temperature.

4.3 Experimental Details in the Present Studies

In phase equilibria studies, it is important to precisely control the temperature, as well as oxygen partial pressure, especially in the present system ZnO-"FeO"-SiO_2 where Fe^{2+} and Fe^{3+} coexist. Moreover, it is crucial to select a proper experimental technique to carry out the experiments with high volatile component ZnO under reducing conditions.

4.3.1 Raw materials

High purity chemicals were used in the phase equilibria study. The chemicals used are listed in Table 4.3. The iron foil was used to prepare the spinel and Fe_2O_3 substrate. The design of the substrates will be discussed in 4.3.2, substrate and master slag preparation. The oxygen partial pressure is controlled by high purity CO and CO_2 gases mixture. The detailed procedure will be discussed in 4.3.3, Control of atmosphere.

Table 4.3 Chemicals used in the present study

Materials	Purity	Supplier
Iron foil (Fe)	99.5+ %	Goodfellow Cambridge Ltd
Platinum foil (Pt)	99.9%	Cookson Ltd
SiO_2	99.9%	Alfa Aesar
ZnO	99.9%	Sigma Aldrich
Fe_2O_3	99.99%	Alfa Aesar
Iron powder (Fe)	99.0%	Goodfellow Cambridge Ltd
CO	99.97%	Coregas
CO_2	99.995%	Coregas

4.3.2 Substrate and master slag preparation

In order to hold the sample and avoid contamination by other elements, the selection of suitable containers is essential. Based on the target equilibrations in different primary phase fields, quartz (SiO_2), spinel (Fe_3O_4) and platinum (Pt) envelop were selected and series of tests have been carried out (Figure 4.2).

The spinel (Fe_3O_4) substrate (Figure 4.2A) was called as the finger-like substrate. Iron foil (0.1-mm thick) that had been folded to specific shapes Figures. The iron foil was equilibrated for 1 hour at 1200 °C or higher under fixed oxygen partial pressure of 10^{-8} atm to ensure magnetite, close to the stoichiometric composition of Fe_3O_4, was formed. These spinel substrates were mainly used for the investigation of the spinel primary phase field. Quartz (SiO_2) crucibles (Figure 4.2B) with diameter of 13-mm and depth of 6.7-mm were made by fusing high-purity silica rod. Open and folded platinum envelopes were also used to test the feasibility of the experiments. Figure 4.2C shows the platinum basket wired up from the Pt wire, while the folded envelop was used to slow down the vaporization rate of the ZnO in the slag.

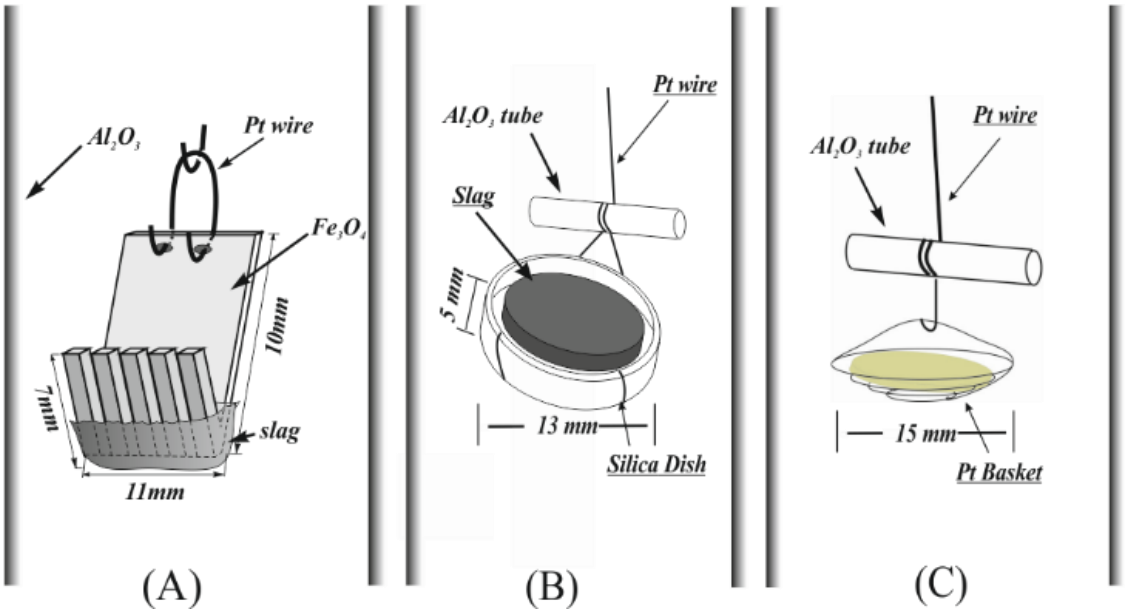

Figure 4.2 Schematic of crucible and suspension used in the present study, (A) - Figure-like spinel substrate; (B) - Quartz crucible; (C) - Platinum envelop

As discussed in Section 4.2, two types of master slags were prepared, including the zinc silicate master slag and iron silicate master slag. The composition of the zinc silicate master slag was chosen to reach the eutectic point close to ZnO-rich side in ZnO-SiO_2 system so that the amount of ZnO required in starting materials can be satisfied without add extra ZnO. The mixture of higher purities of ZnO and SiO_2 in Pt crucible with desired proportion was then heated in maffle furnace under air condition at 1500 °C. After homogenization, the liquid phase was cooled in air to glassy phase which was crushed and milled into fine power using agate mortar. Similar, the compositions f iron silicate the iron silicate master slag was obtained by heating the mixture Fe_2O_3 and SiO_2 in Pt crucible at conditions similar that in the final equilibrations. Details of the master slags preparations were summarized in Table 4.4.

Table 4.4 Master slags used in current research

Master slag	Temperature	Po_2 (atm)	Time (h)	Composition (wt pct)		
				ZnO	SiO_2	"FeO"
Zinc silicate	1773 K (1500 °C)	0.21	0.5	74.4	25.6	0.0
Iron silicate	Same as final equilibration temperature	10^{-8}	16	0.0	33.0	67.0

4.3.3 Control of atmosphere

Mixture of CO-CO_2 gases was used to obtain required oxygen partial pressure. The advantage of this method is that the constant O_2 pressure can be achieved independent of

temperature and mixture compositions. This is a convenient technique in phase equilibria studies, particularly in ranges where the gas ratios can be accurately controlled.

The required oxygen partial pressure was achieved by introducing a stream of high-purity CO-CO_2 gas. The ratios CO/CO_2 can be calculated by FactSage 6.2[4] to reach $Po_2=10^{-8}$ atm at different temperatures. Table 4.5 shows the CO/CO_2 ratios to obtain the $Po_2=10^{-8}$ atm at temperature range from 1170 to 1300 ºC calculated by FactSage 6.2.

Table 4.5 ΔH of CO and CO_2 gas to reach $Po_2=10^{-8}$ atm at different temperatures

Temperature (ºC)	Log(Po_2)	CO/CO_2	CO_2 (ml/s)	ΔH(CO_2) (mm)	CO (ml/s)	ΔH((CO) (mm)
1170	-8	0.0197	400.0	21.0	7.9	12.1
1200	-8	0.0317	400.0	21.0	12.7	21.5
1220	-8	0.0431	400.0	21.0	17.2	27.4
1250	-8	0.0672	400.0	27.4	26.9	22.6
1270	-8	0.0896	400.0	27.4	35.8	30.0
1300	-8	0.1358	400.0	27.4	54.3	11.7

The gas flow rates were controlled by the different liquid level in the U-type capillary (ΔH) (Figure 4.3). Two capillary flow meters connected to two furnaces were calibrated separately before use. Figure 4.4 and Figure 4.5 show the linear relationship of CO and CO_2 in two furnaces between ΔH and the flow rate. Optimum CO and CO_2 flow rates were determined based on the CO/CO_2 ratios and the ΔH of CO_2 and CO are re-calculated from the line equations (Figure 4.5). Generally, the total gas flow rate is adjusted to close to 500 $ml*s^{-1}$. During the experiments, gases are first mixed by gas mixer before being introduced into the furnace tube to obtain the target Po_2.

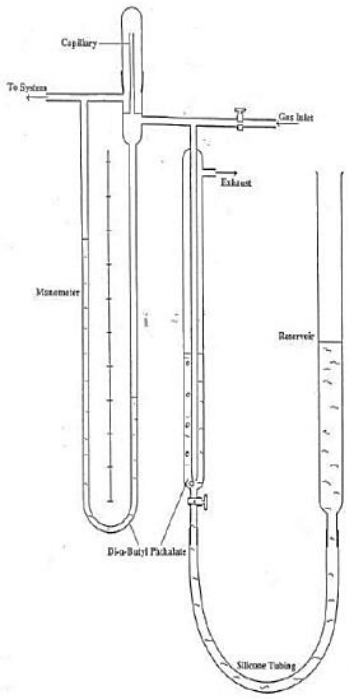

Figure 4.3 Schematic diagram of a glass capillary gas flow meter

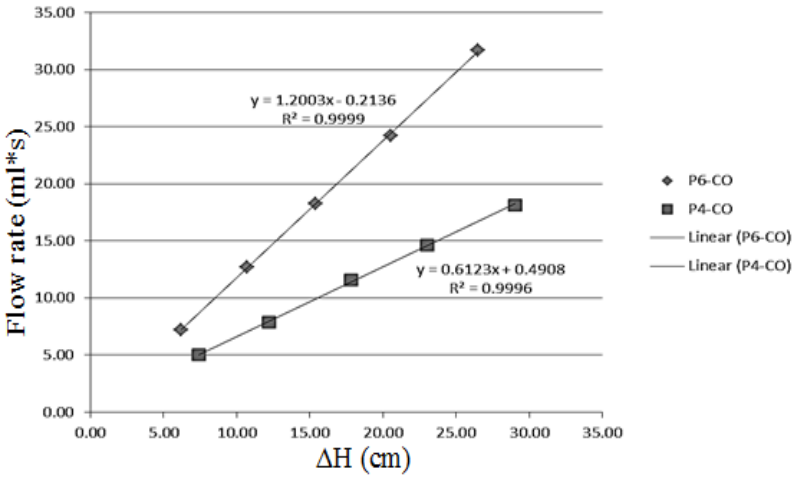

Figure 4.4 Calibration of CO_2 flow rate in two different furnaces P4 and P6

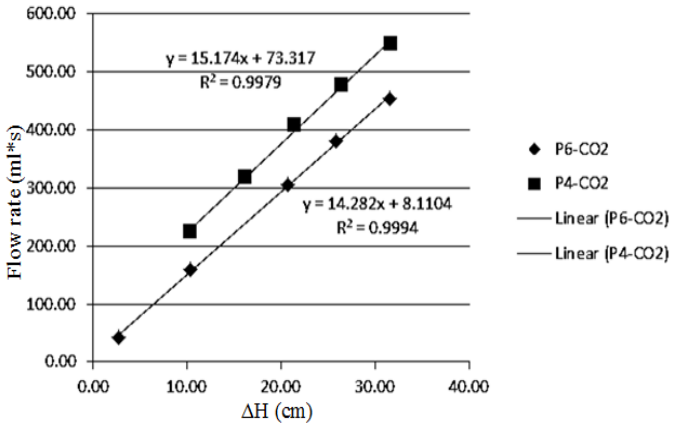

Figure 4.5 Calibration of CO flow rate in two different furnaces P4 and P6

The oxygen partial pressures were later confirmed by an oxygen probe made of yttria-stabilized zirconia solid electrolyte cell ($SIRO_2$, DS-type oxygen probe, Australian Oxytrol Systems, Victoria, Australia). The results of the measurements were within the accuracy of the DS-type oxygen probe, *i.e.* ±0.1 log (Po_2) unit[5].

4.3.4 Equilibration technique

Equilibration experiments were carried out in a vertical reaction tube (impervious recrystallized alumina, 30-mm inner diameter) within an electrical resistance silicon carbide (SiC) heated furnaces (Figure 4.6). A working thermocouple in a re-crystallised alumina sheath was placed to monitor the actual temperature surrounding the sample. The working thermocouple was periodically calibrated against a standard thermocouple (supplied by the National Measurement Institute of Australia, NSW, Australia). The overall absolute temperature accuracy of the experiment was estimated to be ±3 K.

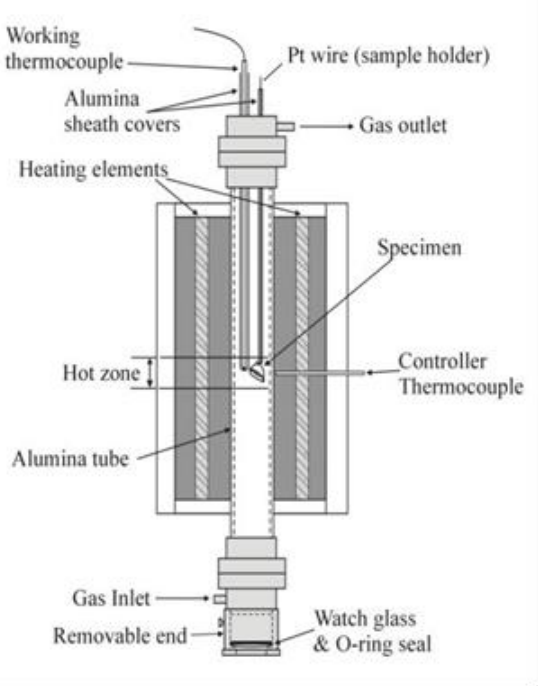

Figure 4.6 Schematic of vertical tube furnace used in the present study[6]

Due to the individual difference of each furnace during the installation, each furnace has its different hot zone, in which temperature was maintained constant (±1 ^oC) at high temperature. Figure 4.7 shows the temperature profile when setting the furnace controller at 1200 ^oC. It can be seen that at the distance 49 to 51 cm from the bottom, the temperature was maintained at 1200 ±1 ^oC. The 4 cm within the furnace was called the hot zone of the furnace.

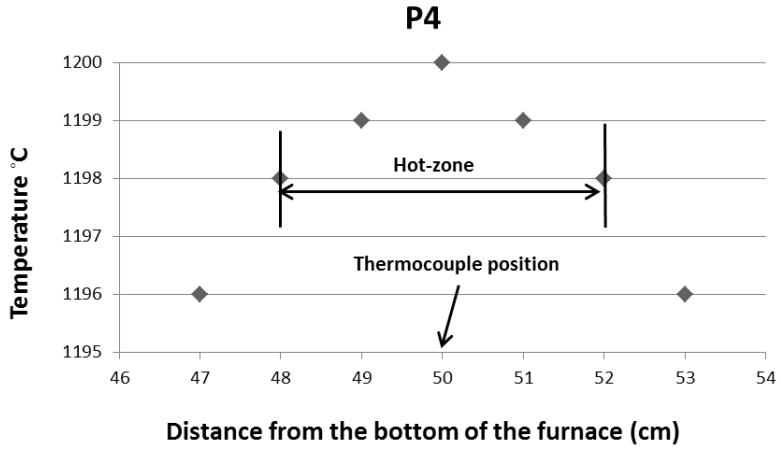

Figure 4.7 Temperature profile of the furnace P4 set at 1200 °C

The sample was introduced from the bottom of the reaction tube and was left at the cold base of the tube while the reaction tube was preconditioned for more than 30 minutes at the required atmosphere condition. The sample was then raised and was suspended in the hot zone of the reaction tube by platinum support wire (0.5-mm diameter). Different pre-melting temperatures that 20 or 50 °C above the equilibration temperatures were adopted for those experiments in ZnO-free systems. Basically, 30 minutes was applied prior to the final equilibration at the target conditions.

After the holding time, the base of the reaction tube was immersed in ice water and the lower lid sealing the tube was removed. Then, the sample would drop directly into the water when pulling up the platinum wire. The specimen was rapidly quenched into water, dried on a hot plate, mounted in epoxy resin, and cross-sectioned by using conventional metallographic polishing technique.

4.3.5 Electron probe X-ray microanalysis (EPMA)

The quenched samples were sectioned, mounted and polished for the Electron Probe X-ray Microanalysis (EPMA). The polished samples were coated with carbon using QT150T (Quorum Technologies) Carbon Coater for electron microscopic examination. A JXA 8200 Electron Probe Microanalyser with Wavelength Dispersive Detectors was used for microstructure and composition analysis. The analysis was conducted at an accelerating voltage of 15 kV and a probe current of 15 nA. The standards used for analysis were from Charles M. Taylor Co. (Stanford, California): Fe_2O_3 for Fe and $CaSiO_3$ for Si. ZnO was prepared from high purity ZnO and recalibrated to the standard willemite Zn_2SiO_4 (Charles M. Taylor Co.). The ZAF correction procedure supplied with the electron probe was applied. The average accuracy of the EPMA measurements is within 1 wt pct. Both Fe^{2+} and Fe^{3+} are present

in the samples, however, only the metal cation concentrations can be measured using EPMA. For the presentation purpose only, “FeO” is used in all the discussion.

4.4 References

1. M. K. Reser, E. M. Levin and H. F. MacMurdie: *Phase diagrams for ceramists*. (American ceramic society, 1964), p.^pp. 29-33.

2. E. Jak, P. Hayes and H.-G. Lee, *Metals and Materials*, 1995, vol. 1, pp. 1-8.

3. E. Jak and P. C. Hayes, *Trans. Inst. Min. Metall., Sect. C*, 2008, vol. 117, pp. 1-17.

4. C. W. Bale, E. Bélisle, P. Chartrand, S. A. Decterov, G. Eriksson, K. Hack, I. H. Jung, Y. B. Kang, J. Melançon, A. D. Pelton, C. Robelin and S. Petersen, *CALPHAD: Comput. Coupling Phase Diagrams Thermochem.*, 2009, vol. 33, pp. 295-311.

5. R. A. Mendybaev, J. R. Beckett, L. Grossman, E. Stolper, R. F. Cooper and J. P. Bradley, *Geochim Cosmochim Ac*, 2002, vol. 66, pp. 661-682.

6. M. Chen and B. Zhao, *J. Am. Ceram. Soc.*, 2013, vol. 96, pp. 3631-3636.

5 Phase Equilibrium Study of ZnO-"FeO"-SiO_2 System at Fixed Po_2 10^{-8} atm

Abstract: Experimental studies of phase equilibria and liquidus temperatures have been carried out in the systems "FeO"-SiO_2 and ZnO-"FeO"-SiO_2 at Po_2 10^{-8} atm. Research techniques have been developed to enable the ZnO-containing system to be investigated under reducing conditions controlled by CO-CO_2 gas mixture. The experimental approach includes master slag preparation, high-temperature equilibration, quench and electron probe x-ray microanalysis (EPMA). Phase compositions in the quenched samples were measured by EPMA and used for construction of phase diagram. It was found that the isotherms of the system ZnO-"FeO"-SiO_2 at Po_2 10^{-8} atm are significantly different from those in equilibrium with metallic iron and those predicted by FactSage. Presence of ZnO in copper smelting slag significantly increases the liquidus temperature in spinel primary phase field. Partitioning of ZnO in liquid and spinel is also discussed in this paper.

Key words: phase equilibrium, copper smelting slag, ZnO-"FeO"-SiO_2, EPMA

5.1 Introduction

Pyrometallurgical process continues to be the principal technology in copper production which include smelting, converting and refining[1]. The objective of the smelting is to partially oxidize sulphur and iron from the Cu-Fe-S concentrate to produce a Cu-enrich molten sulphide phase (matte). Simultaneously, the gangue components in the concentrate form the molten slag by reacting with added flux (SiO_2). Slag properties play critical roles in the copper production, which closely related to metal recovery, slag tapping and refractory corrosions under operating conditions.[2] Currently, approximately 50 pct copper concentrate smelting is carried out by bath smelting furnaces that include top-blown (Ausmelt and Isasmelt), side-blown (Noranda and Teniente) and recently developed bottom-blown technology[3]. The first commercial bottom blown oxygen copper smelting furnace (BBF) at Dongying Fangyuan Nonferrous Metals Co., Ltd has shown excellent performance and drawn significant interest [3-5]. However, as a new copper smelting technology, the knowledge of thermodynamics and physic-chemistry in this smelting process is limited, and current research is part of the comprehensive research program to narrow the knowledge gap. A detailed analyses[3] on BBF slag compositions showed that in addition to the major components "FeO" (both Fe^{2+} and Fe^{3+}), and SiO_2, significant amount of ZnO is also present and spinel is the primary phase present under the

BBF smelting condition in which the oxygen partial pressure (Po_2) was estimated to be 10^{-8} atm.

Phase equilibria of ZnO-SiO_2 system have been well determined by a number of studies. The first study on this system was reported by Bunting[6] which did not consider the loss of zinc at high temperatures. A reinvestigation on this system was conducted by Hansson *et al*[7] using equilibration and quenching followed by EPMA analysis approach. Sub-solidus studies on the Fe-Zn-O system were systematically conducted by Hansson *et al*[8-10] under air and intermediate Po_2, while the experiments under metallic iron saturation on the same system were conducted at 1100 K (827 °C) by Itoh *et al*[11] using EMF method. Phase equilibria studies on Fe-Zn-O system were also carried out by Itoh *et al*[12, 13] at 1100 and 1200 K (827 and 927 °C) in closed quartz capsule where the oxygen partial pressure was determined to be in a wide range 10^{-3} to 10^{-20} atm.

As a base of the copper smelting slags, the pseudo-binary "FeO"-SiO_2 system has been extensively studied under different conditions including metallic iron saturation,[14] air atmosphere[15, 16] and the intermediate Po_2[16-18]. Significant differences on the liquidus temperatures and primary phase fields were observed under various equilibration conditions.

Previous studies in Fe-O-ZnO-SiO_2 system have been focused in air[19] and at metallic iron saturation[19-22]. No information was found in this system relevant to the copper smelting conditions around Po_2 10^{-8} atm. In order to evaluate the effect the ZnO content on phase equilibria of the copper smelting slags, present study is focused on the phase equilibria of ZnO-"FeO"-SiO_2 system at Po_2 10^{-8} atm.

5.2 Experimental Methodology

Experimental techniques used in present research are similar to that described in previous papers.[23, 24] Briefly, the sample was directly quenched into ice water after the equilibration at assemblages and composition of each phase present. However, in the present study the oxygen partial pressure of the slag was controlled by the CO-CO_2 gas mixture and the bulk composition of the slag could be changed during the equilibration due to the vaporisation of zinc. As a first study in the system ZnO-"FeO"-SiO_2 system at Po_2 10^{-8} atm, the research technique has been further developed. controlled temperatures and Po_2 10^{-8} atm, followed by EPMA analysis to determine the phase

5.2.1 Sample and substrate preparation

The oxygen partial pressure of the slag was controlled by the CO-CO_2 gas mixture and the reactions between liquid slag and gas are relatively slow. Long reaction time at given temperature is required to achieve equilibrium. On the other hand, zinc oxide in the slag could be reduced and zinc metal will vaporise from the slag. To ensure the final equilibrium can be achieved in the controlled time and to reduce the vaporisation of zinc, master slags have been prepared in the conditions close to the temperature and oxygen partial pressure required for the final equilibration.

Approximately 0.1 g pelletized mixture was used in each experiment. The mixtures were prepared by mixing the desired amounts of iron silicate master slag and zinc silicate master slag with additional "FeO", ZnO or SiO_2. The "FeO" was prepared from iron foil at the same temperature and oxygen partial pressure required for the final equilibration.

Two master slags, as shown in Table 5.1, were prepared from high purity ZnO, SiO_2, Fe_2O_3 and Fe (Table 5.2). It can be seen from Figure 5.1, excess ZnO was always added in the starting mixture to compensate the loss of ZnO during the equilibration. All the iron oxides used in the present study were pre-conditioned according to the target equilibrium conditions to ensure the equilibrium to be attained. The compositions of the phases were measured by EPMA after the equilibration so that the changes in bulk composition during high temperature equilibration do not affect the phase diagrams to be constructed.

Table 5.1 Master slags used in current research

Master slag	Temperature	Po_2 (atm)	Time (h)	Composition (wt pct)		
				ZnO	SiO_2	"FeO"
Zinc silicate	1773 K (1500 °C)	0.21	0.5	74.4	25.6	0.0
Iron silicate	Same as final equilibration temperature	10^{-8}	16	0.0	33.0	67.0

Table 5.2 Chemical used in present study

Materials	Purity (pct)	Supplier
Iron foil (Fe)	99.5+	Goodfellow Cambridge Ltd
Platinum foil (Pt)	99.9	Cookson Ltd
SiO_2	99.9	Alfa Aesar
ZnO	99.9	Sigma Aldrich
Fe_2O_3	99.99	Alfa Aesar
Iron powder (Fe)	99.0	Goodfellow Cambridge Ltd
CO	99.97	Coregas
CO_2	99.995	Coregas

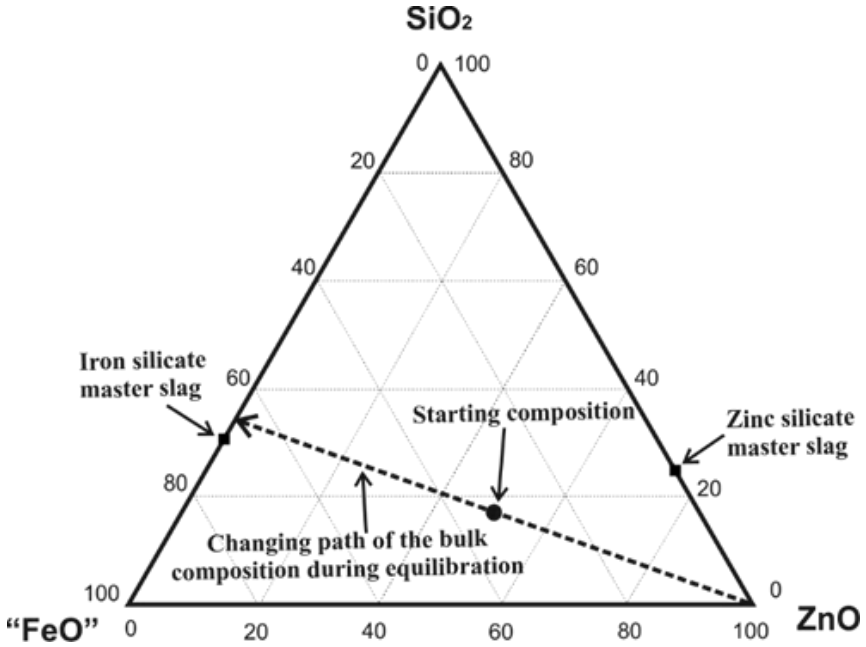

Figure 5.1 Bulk composition changes during the equilibration of the "FeO"- ZnO-SiO_2 slags at Po_2 10^{-8} atm

In order to increase the reaction rate between slag and gas and the cooling rate after the equilibration, the substrates made from quartz (SiO_2)[23] and spinel (Fe_3O_4)[25] were used to hold the mixtures for the experiments targeted in the SiO_2 and spinel primary phases respectively. Pt baskets were used as a container to determine the liquidus in willemite primary phase field. It should be noted that the small amount of iron may be dissolved into Pt wire and the bulk composition of the slag could change[26, 27].

5.2.2 Equilibration

Equilibration experiments were carried out in a vertical reaction tube furnace. A working thermocouple protected by a recrystallized alumina sheath was placed inside the reaction tube to monitor the actual temperature of the sample. The working thermocouple was periodically

calibrated against a standard thermocouple (supplied by the National Measurement Institute of Australia, NSW, Australia). The overall absolute temperature uncertainty was estimated to be ±3 K.

Mixtures of CO-CO_2 gases at different CO/CO_2 ratios were used to obtain the required oxygen partial pressure 10^{-8} atm. The oxygen partial pressures at different temperatures were confirmed by the yttria-stabilized zirconia solid electrolyte cell oxygen probe ($SIRO_2$, DS-type oxygen probe; Australian Oxytrol Systems, Victoria, Australia). The results of the measurements were within the accuracy of the DS-type oxygen probe, *i.e.* ±0.1 log (Po_2) unit[28], details as shown in Table 5.3.

Table 5.3 Gas ratios in current study at varied temperatures and the calibration results

Temperature [K (°C)]	Flow rate (ml/min)		Log (Po_2)	
	CO_2	CO	Theoretical	Calibration
1443 (1170)	400.0	7.9	-8.0	-7.9
1473 (1200)	400.0	12.7	-8.0	-7.9
1493 (1220)	400.0	17.2	-8.0	-8.0
1523 (1250)	400.0	26.9	-8.0	-8.0
1543 (1270)	400.0	35.8	-8.0	-8.0
1573 (1300)	400.0	54.3	-8.0	-8.0

The sample was introduced from the bottom of the reaction tube and held at the cold zone with flush of gas mixture for 15-30 minutes to remove the air. The sample was then raised and kept in the hot zone of the reaction tube for required period.

After the equilibration, the bottom of the reaction tube was immersed in ice water and the lid was removed. Then, the sample was drop directly into the water by pulling up the iron wire which suspended the sample. The quenched sample was dried on a hot plate, mounted in epoxy resin, and polished for metallographic examinations.

5.2.3 Sample analysis

The polished samples were first examined with optical microscopy to observe the phases present and then coated with carbon using QT150TES (Quorum Technologies) Carbon Coater for electron microscopic analyses. A JXA 8200 Electron Probe X-ray Microanalyser (EPMA) with Wavelength Dispersive Detectors was used for microstructure and composition analyses. The analyses were conducted with an accelerating voltage of 15 kV and a probe current of 15 nA. The standards used for analysis were from Charles M. Taylor Co. (Stanford, CA): Fe_2O_3 for Fe and $CaSiO_3$ for Si; and from Micro-Analysis Consultants Ltd (Cambridge, UK): ZnO

for Zn. The ZAF correction procedure supplied with the EPMA was applied. The overall accuracy of EPMA measurements is determined by precision and accuracy. Precision refers to the reproducibility of the measurements and thus the ability to be able to compare compositions, whether within a sample, or between samples, or between analytical sessions. It is a relative description. Accuracy refers the "truth" of the analysis, and is directly tied to the standards used and the matrix correction applied to the raw data, as well equipment conditions and parameter. It is an absolute description. The overall accuracy of EPMA quantitative error analysis is a combination of both. In the present study the liquid phase was relatively hard to be quenched to a homogenous glass and 10-20 points were usually measured from different areas for liquid. The composition of the solid phase was more stable during cooling and 3-5 points were usually measured. The compositions of the phases were the average of 10-20 measurements for liquid and 3-5 measurements for solid. The precision for each phase composition is stated by the standard deviation which is usually below 1 pct. The accuracy of the EPMA measurements is determined by comparing the measured concentration of each element with the given value for the standards. The difference is always controlled below 1 pct. The overall accuracy of the EPMA measurements including both precision and accuracy is within 1 wt pct. Both Fe^{2+} and Fe^{3+} are present in the quenched samples, however, only metal cation concentrations can be measured by EPMA. All iron was recalculated to FeO for presentation purpose only.

5.3 Results and Discussion

5.3.1 Experimental results in the "FeO"-SiO_2 system

The experiments were first carried out for the base system "FeO"-SiO_2 at $Po_2=10^{-8}$ atm in temperature range between 1473 K (1200 °C) and 1573K (1300 °C). It was found that wüstite, spinel and tridymite are the primary phases in the composition range investigated. The typical microstructures of the quenched samples are shown in Figure 5.2, where the equilibrium of liquid phase with one or two solid phases is shown in Figure 5.2(a) - 2(d) respectively. The normalized compositions of the phases measured by EPMA are shown in Table 5.4. It can be seen that the solubilities of SiO_2 in the wüstite and spinel are less than 1 wt pct. The maximum solubility of "FeO" in the tridymite was determined to be 1.0 wt pct. The phase diagram of "FeO"-SiO_2 system constructed from the experimental data is shown in Figure 3. The univariant point between wüstite and spinel primary phase fields was determined to be 1549 ± 10 K (1276 ± 10 °C) at 17.8 wt pct SiO_2. The univariant point between spinel and tridymite

primary phase fields was determined to be 1473 ± 3 K (1200 ± 3 °C) at 34.3 wt pct SiO_2 in the present study.

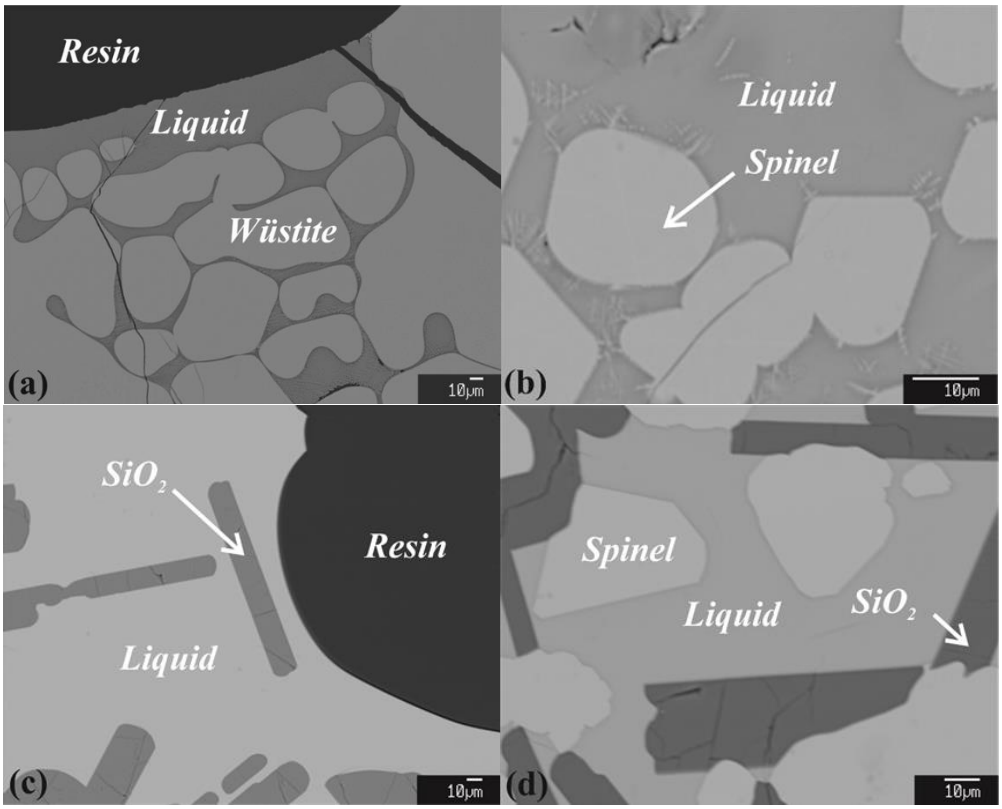

Figure 5.2 Typical microstructures of quenched samples showing equilibrium of liquid with (a) wüstite - 1573k; (b) spinel - 1523 K; (c) tridymite - 1543 K and (d) spinel and tridymite - 1473 K

Table 5.4 Experimental determined phases composition in the "FeO"-SiO_2 system at Po_2 10^{-8} atm

Experiment No.	Temperature [K (°C)]	Phase	Composition (Wt Pct)	
			SiO_2	"FeO"
8	1573 (1300)	Liquid	15.7	84.3
		Wüstite	0.5	99.5
35	1573 (1300)	Liquid	15.8	84.2
		Wüstite	0.5	99.5
84	1573 (1300)	Liquid	15.7	84.3
		Wüstite	0.6	99.4
90	1573 (1300)	Liquid	15.9	84.1
		Wüstite	0.5	99.5
197	1563 (1290)	Liquid	13.8	83.2
		Wüstite	0.7	99.3
137	1543 (1270)	Liquid	20.7	79.3
		Spinel	0.2	99.8
150	1543 (1270)	Liquid	20.4	79.6
		Spinel	0.7	99.3
156	1543 (1270)	Liquid	20.7	79.3
		Spinel	0.7	99.3
101	1523 (1250)	Liquid	25.4	74.6
		Spinel	0.3	99.7
201	1523 (1250)	Liquid	25.1	74.9
		Spinel	0.8	99.2
196	1493 (1220)	Liquid	31.2	68.8
		Spinel	0.8	99.2
21	1473 (1200)	Liquid	34.3	65.4
		Spinel	0.3	99.7
		SiO_2	99.0	1.0
129	1493 (1220)	Liquid	34.8	65.2
		SiO_2	99.7	0.3
39	1523 (1250)	Liquid	36.5	63.5
		SiO_2	99.1	0.9
66	1523 (1250)	Liquid	36.0	64.0
		SiO_2	99.3	0.7
133	1543 (1270)	Liquid	36.7	63.3
		SiO_2	99.2	0.8
138	1543 (1270)	Liquid	36.5	63.5
		SiO_2	99.4	0.6
38	1573 (1300)	Liquid	38.1	61.9
		SiO_2	99.0	1.0
40	1573 (1300)	Liquid	37.9	62.1
		SiO_2	99.4	0.6

Table 5.5 Experimental determined phases composition in the ZnO-"FeO"-SiO_2 system at Po_2 10^{-8} atm

Experiment No.	Temperature [K (°C)]	Phase	Composition (Wt Pct)		
			ZnO	SiO_2	"FeO"
10	1443 (1170)	SiO_2	0.1	98.8	1.1
		Spinel	9.2	0.1	90.7
11	1443 (1170)	SiO_2	0.1	99.1	0.9
		Spinel	8.0	0.3	91.6

Experiment No.	Temperature [K (°C)]	Phase	Composition (Wt Pct)		
			ZnO	SiO_2	"FeO"
12	1443 (1170)	SiO_2	0.1	98.8	1.1
		Spinel	7.7	0.2	92.1
103	1493 (1220)	Liquid	7.9	34.6	57.5
		Spinel	2.8	0.1	97.1
114	1493 (1220)	Liquid	6.3	34.3	59.4
		Spinel	2.8	0.5	96.7
115	1493 (1220)	Liquid	15.2	35.0	49.8
		Spinel	7.2	0.4	92.4
20	1523 (1250)	Liquid	0.4	26.3	73.3
		Spinel	0.1	0.0	99.9
62	1523 (1250)	Liquid	2.4	34.7	63.0
		SiO_2	0.4	99.0	0.7
99	1523 (1250)	Liquid	19.1	33.9	47.1
		Spinel	9.3	0.4	90.3
100	1523 (1250)	Liquid	12.7	34.2	53.1
		Spinel	8.1	0.1	91.8
104	1523 (1250)	Liquid	6.2	30.2	63.6
		Spinel	3.5	1.1	95.4
113	1523 (1250)	Liquid	1.6	26.3	72.1
		Spinel	0.8	0.3	98.9
127	1523 (1250)	Liquid	28.7	34.9	36.4
		Spinel	14.7	0.3	85.0
128	1523 (1250)	Liquid	0.8	25.9	73.3
		Spinel	0.3	0.0	99.6
130	1523 (1250)	Liquid	13.6	33.9	52.4
		Spinel	7.3	0.5	92.2
126	1523 (1250)	Liquid	0.2	36.4	63.5
		SiO_2	0.0	99.0	1.0
131	1523 (1250)	Liquid	16.3	34.8	48.9
		SiO_2	0.4	98.8	0.8
111	1543 (1270)	Liquid	0.7	21.2	78.1
		Spinel	0.3	0.4	99.3
112	1543 (1270)	Liquid	21.0	30.0	49.1
		Spinel	10.1	0.4	89.5
123	1543 (1270)	Liquid	28.8	32.1	39.1
		Spinel	14.2	0.4	85.4
124	1543 (1270)	Liquid	28.2	30.6	41.2
		Spinel	14.4	0.3	85.3
133	1543 (1270)	Liquid	16.6	35.8	47.7
		SiO_2	0.4	98.8	0.8
168	1543 (1270)	Liquid	31.6	34.8	33.6
		Spinel	17.7	0.3	82.0
		Willemite	59.6	28.1	12.3
169	1543 (1270)	Liquid	32.0	34.8	33.3
		Spinel	17.9	0.3	81.8
		Willemite	59.9	28.5	11.6
177	1543 (1270)	Liquid	31.9	35.5	32.6
		Willemite	59.8	28.5	11.6
		SiO_2	0.8	98.4	0.8
75	1573 (1300)	Liquid	4.9	17.0	78.2
		Wüstite	2.5	0.3	97.2
109	1573 (1300)	Liquid	0.7	20.8	78.5

Experiment No.	Temperature [K (°C)]	Phase	Composition (Wt Pct)		
			ZnO	SiO_2	"FeO"
		Spinel	0.2	0.4	99.4
134	1573 (1300)	Liquid	1.6	15.5	82.9
		Wüstite	1.0	0.3	98.8
140	1573 (1300)	Liquid	28.0	26.6	45.3
		Spinel	15.2	0.3	84.5
144	1573 (1300)	Liquid	6.8	18.7	74.5
		Wüstite	3.5	0.4	96.0
145	1573 (1300)	Liquid	34.9	31.8	33.3
		Willemite	61.0	28.2	10.7
163	1573 (1300)	Liquid	34.1	30.0	35.9
		Spinel	18.3	0.3	81.3
		Willemite	59.5	28.5	12.0
164	1573 (1300)	Liquid	34.1	29.7	36.2
		Spinel	18.9	0.3	80.8
171	1573 (1300)	Liquid	37.0	35.8	27.2
		Willemite	63.7	28.4	7.8
		SiO_2	1.1	98.2	0.6
173	1573 (1300)	Liquid	30.9	29.3	39.8
		Spinel	16.6	0.3	83.1
174	1573 (1300)	Liquid	32.9	29.4	37.8
		Spinel	16.2	0.3	83.5
180	1573 (1300)	Liquid	16.2	36.5	47.3
		SiO_2	0.4	98.9	0.7
342	1573 (1300)	Liquid	17.5	36.2	46.3
		SiO_2	0.3	98.9	0.8

The comparisons between the present results and previous studies[16, 17]and FactSage 6.2[29] calculations at Po_2 10^{-8} atm are also shown in Figure 5.3. It can be seen that the present results are in good agreements with the results from Hidayat *et al*[17] and are significantly different from that of Muan[16] and FactSage predictions[29] in wüstite and spinel primary phase fields.

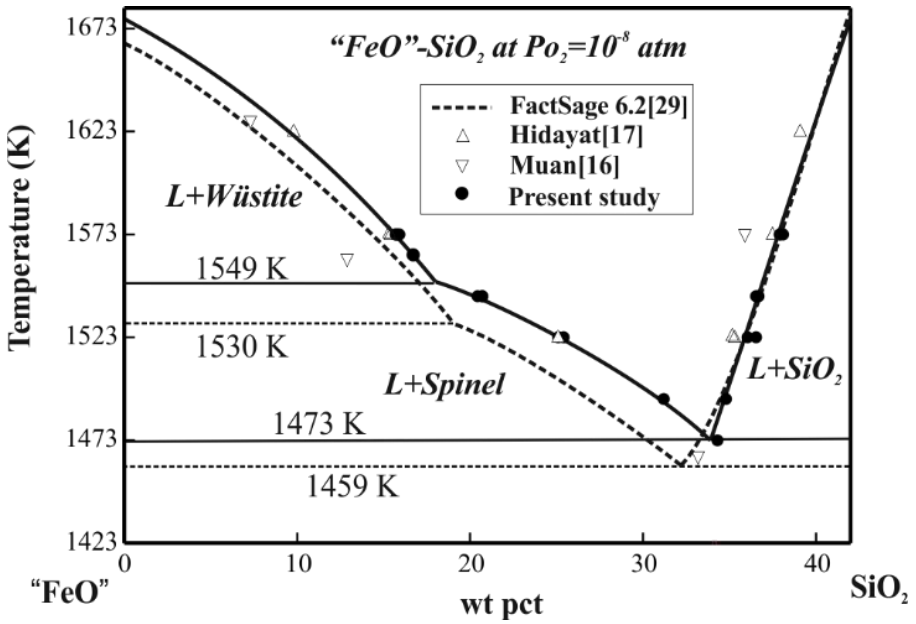

Figure 5.3 Comparisons among the present and previous experimental results[16, 17] and FactSage 6.2[29] predictions on "FeO"-SiO_2 system at Po_2 10^{-8} atm

"FeO"-SiO_2 is a base system for copper smelting slags and phase diagram of this system measured at metallic iron saturation[22] has been used for long time to characterise the copper smelting slags. A comparison of present study with that under metallic iron saturation is shown in Figure 5.4. It can be seen that the fayalite (Fe_2SiO_4) primary phase at iron saturation is replaced by spinel primary phase when Po_2 is fixed at 10^{-8} atm. The liquidus temperatures at Po_2 10^{-8} atm are generally higher than those at metallic iron saturation[22]. Up to 70 K difference in liquidus temperature is observed for these two different conditions. The comparison indicates that primary phase fields and liquidus temperatures of the "FeO"- SiO_2 system can be significantly influenced by oxygen partial pressure. The phase diagram measured previously at iron saturation cannot be used to accurately predict the liquidus temperatures of copper smelting slags.

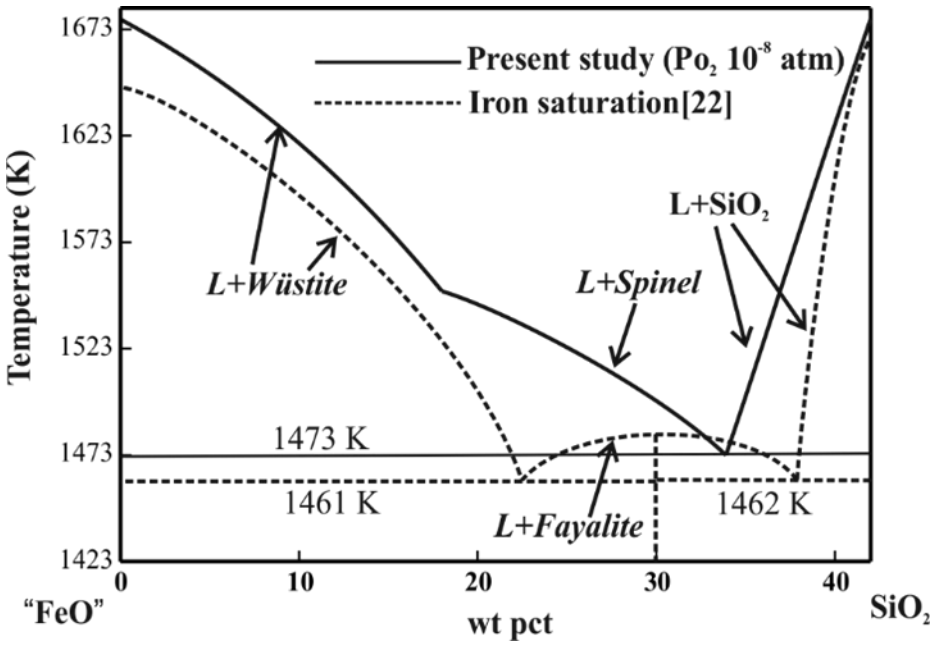

Figure 5.4 Comparisons between the present study at Po_2 10^{-8} atm and the results at metallic iron saturation[22] on the system "FeO"-SiO_2

5.3.2 Experimental results in ZnO-"FeO"-SiO_2 system

The liquidus temperatures in ZnO-SiO_2 binary system have been determined in air by different authors.[6, 7] The eutectic points between tridymite and willemite primary phase fields, and between willemite and zincite primary phase fields were reported[7] to be 1721 ± 5 K (1448 ± 5 °C) at 59 wt pct ZnO and 1775 ± 5 K (1502 ± 5 °C) at 76.8 wt pct ZnO, respectively. No experimental data were reported in ZnO-"FeO'' system at Po_2=10^{-8} atm. The invariant point between wustitie and zinc primary phase fields used in construction of the phase diagram was taken from FactSage 6.2 prediction[29].

In the present study, the liquidus temperatures in the ZnO-"FeO"-SiO_2 system have been experimentally determined at Po_2 10^{-8} atm between 1473 K (1200 °C) and 1573 K (1300 °C) (Table 5.5). The primary phase fields in this system include tridymite, spinel, wustitie and willemite. The typical microstructures of the quenched samples are shown in Figure 5.5. Figure 5.5 (a) shows equilibrium of liquid with spinel at 1573 K (1300 °C). In Figure 5.5b, the liquid was in equilibrium with tridymite at 1543 K (1270 °C). Figure 5.5c shows the liquid was in equilibrium with willemite at 1573 K (1300 °C). In Figure 5.5d, the liquid was in equilibrium with both spinel and tridymite at 1543 K (1270 °C). Figure 5.5e shows that the liquid was in equilibrium with spinel and willemite at 1543 K (1270 °C), and Figure 5.5f shows that the liquid was in equilibrium with both tridymite and willemite at 1543 K (1270 °C).

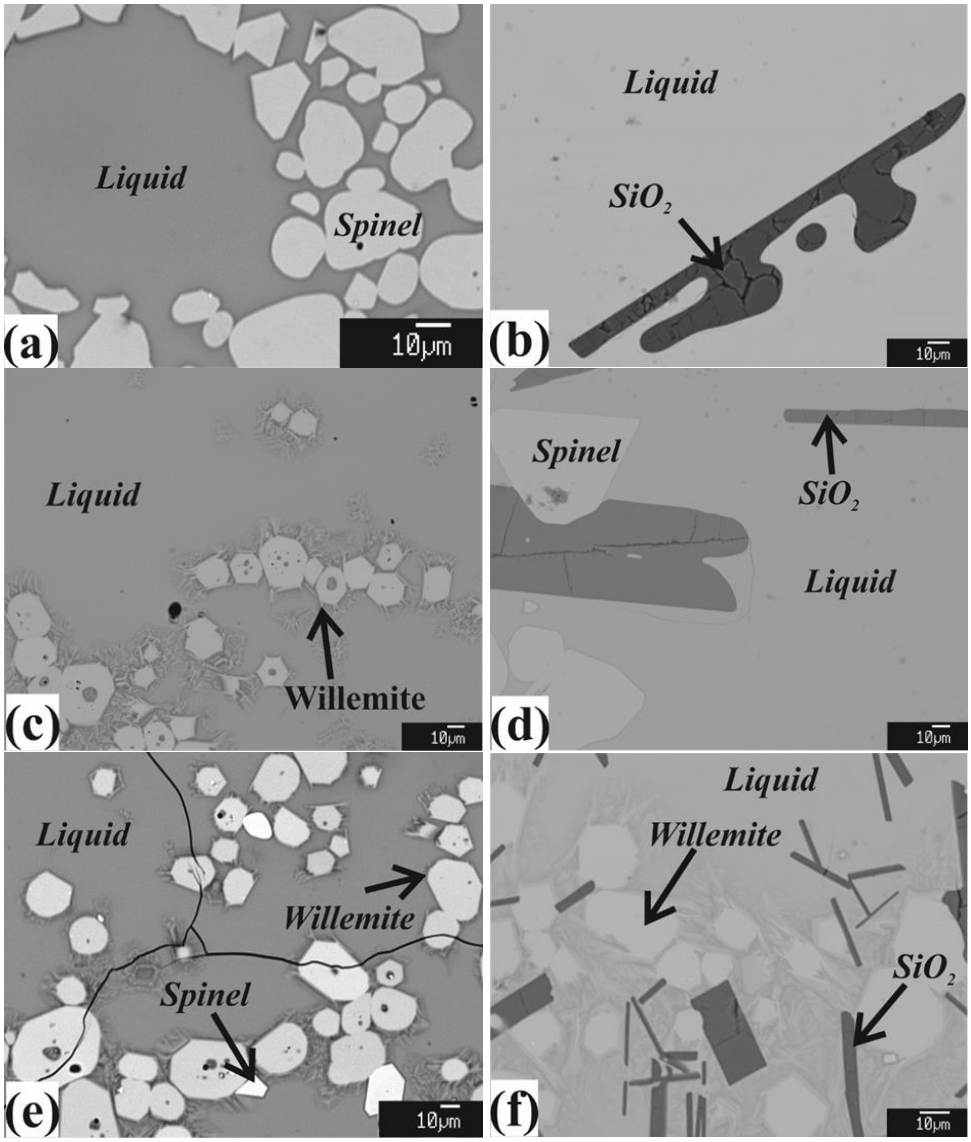

Figure 5.5 Typical microstructures of the quenched samples in ZnO-"FeO"-SiO_2 system at Po_2 10^{-8} atm showing equilibrium of liquid with (a) spinel - 1573 K; (b) tridymite - 1543 K; (c) willemite - 1573 K; (d) spinel + tridymite - 1543 K; (e) spinel + willemite - 1543 K; (f) tridymite + willemite - 1543 K

The phase diagram of ZnO-"FeO"-SiO_2 system at Po_2 10^{-8} atm constructed based on the experimental data is shown in Figure 5.6. The thick solid lines represent experimentally determined boundaries between primary phase fields, while the thick dash lines are hypothetical boundaries. The thin solid lines are experimentally determined isotherms. It should be noted that the spinel [$(Fe^{2+},Zn)O{\cdot}Fe^{3+}{}_2O_3$], wüstite [$(Fe^{2+},Zn)O$] and willemite [$(Zn,Fe^{2+})SiO_4$] are all present as solid solutions in the slag.

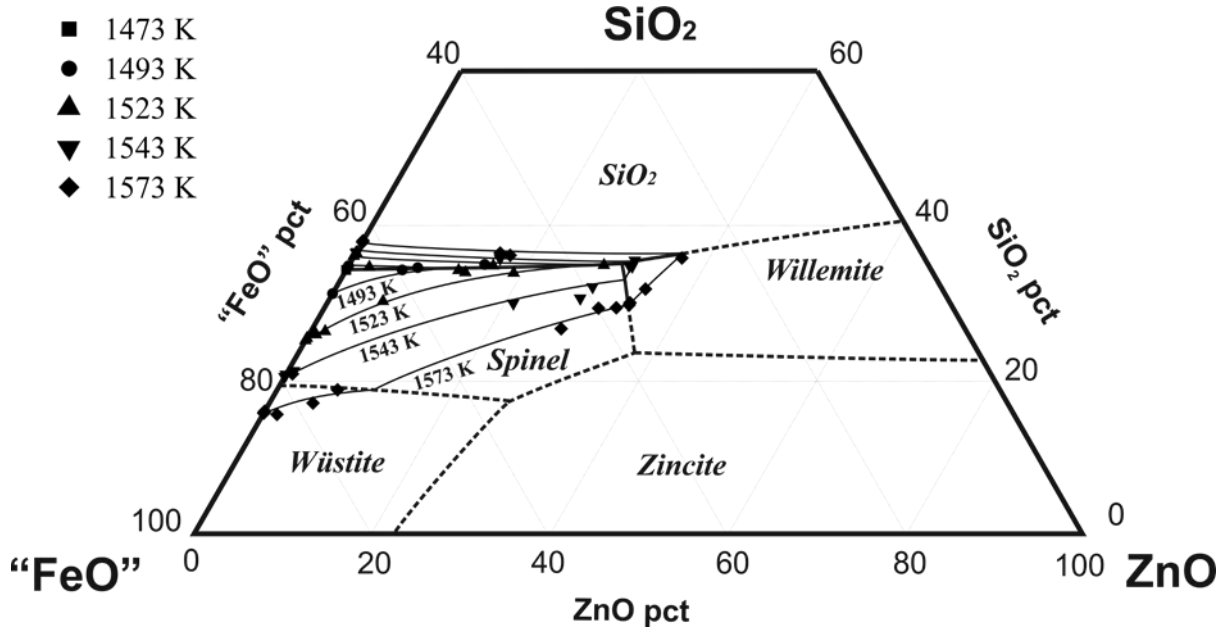

Figure 5.6 Phase diagram with experimental data in ZnO-"FeO"-SiO_2 system at Po_2 10^{-8} atm

Comparisons of 1523 K (1250 °C) isotherms between the present study and FactSage 6.2[29] predictions at Po_2 10^{-8} atm are shown in Figure 5.7. The experimentally determined 1523 K (1250 °C) isotherms at iron saturation[22] are also shown in the figure for comparison. The fully liquid area formed by the isotherms in different primary phase fields represents the operating range of the slag compositions at given temperature. It can be seen from the figure that the fully liquid area at 1523 K (1250 °C) determined in the present study is much smaller than that predicted by FactSage 6.2[29] which is almost same as the liquid region under metallic iron saturation[22]. Clearly the experimental results obtained in equilibrium with metallic iron cannot accurately predict the liquidus temperatures of ZnO-containing copper smelting slags. The database of FactSage 6.2 needs to be improved to accurately characterise the ZnO-containing copper smelting slags.

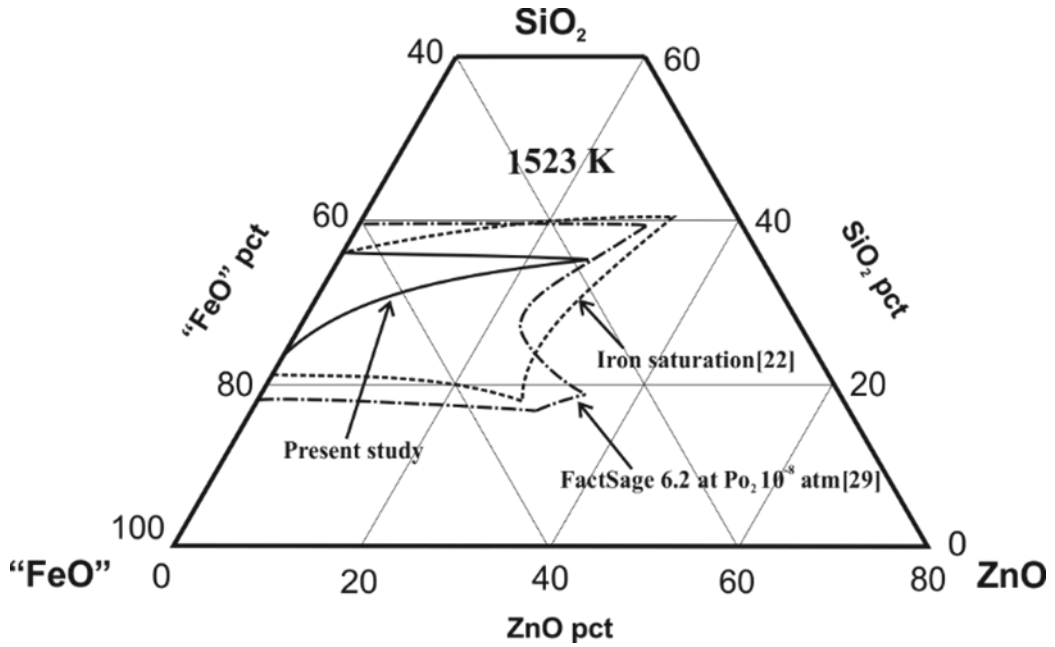

Figure 5.7 Comparison of 1523 K (1250 $^{\circ}C$) isotherms between the present study and FactSage 6.2[29] predictions on ZnO-"FeO"-SiO_2 system at Po_2 10^{-8} atm and metallic iron saturation[22]

Different types of pseudo-binary phase diagrams are easy to be used by operators. Figure 5.8 presents a pseudo-binary diagram ("FeO"+SiO_2) - ZnO at fixed Fe/SiO_2 = 2 (mass) at Po_2 10^{-8} atm. Effect of ZnO on primary phases and liquidus temperatures is demonstrated in this figure. The predictions from FactSage 6.2[29] at Po_2 10^{-8} atm and that at metallic iron saturation[22] are also given in the figure for comparisons. It can be seen that spinel is the only primary phase with up to 30 wt pct ZnO as determined by the present study. The liquidus temperatures increase continuously with increasing ZnO. For instance, the liquidus temperature in the spinel primary phase field is increased by 35 K when ZnO content in liquid increases from 0 to 10 wt pct. At the same Po_2 10^{-8} atm the liquidus temperatures predicted by FactSage 6.2[29] are much lower and willemite phase also appears at 25 wt pct ZnO. The experimentally determined phase diagram at metallic iron saturation[22] shows different primary phases and much lower liquidus temperatures.

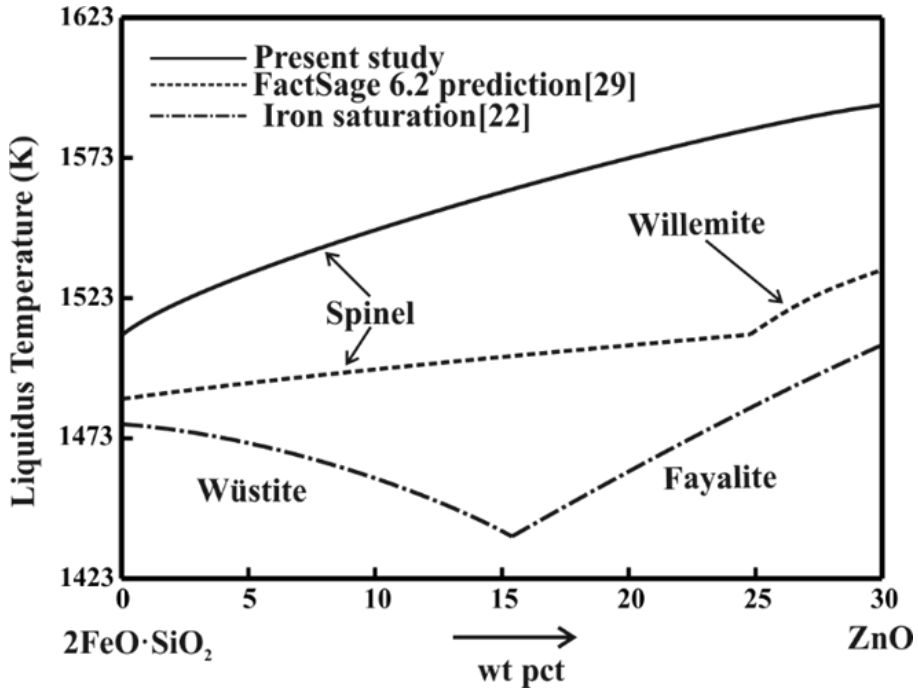

Figure 5.8 Comparisons of pseudo-binary ("FeO"+SiO_2)-ZnO at fixed Fe/SiO_2=2 (mass) between present results and FactSage predictions[29] at Po_2 10^{-8} atm, and also that at iron saturation[22]

To investigate the effect of fluxing condition represented by Fe/SiO_2 ratio, on the liquidus temperature in the ZnO-"FeO"-SiO_2 system, pseudo-binary phase diagram "FeO"-SiO_2 is constructed at fixed 5 wt pct ZnO as shown in Figure 5.9. The phase diagram of ZnO-free system at Po_2 10^{-8} atm and that at metallic iron saturation[22] are also given in the figure for comparisons. It can be seen from Figure 5.9 that presence of 5 wt pct ZnO in the slag does not change the primary phase fields. The liquidus temperatures of the slag with 5 wt pct ZnO are generally higher in wüstite and spinel primary phase fields and lower in SiO_2 primary phase field than those of ZnO-free slag.

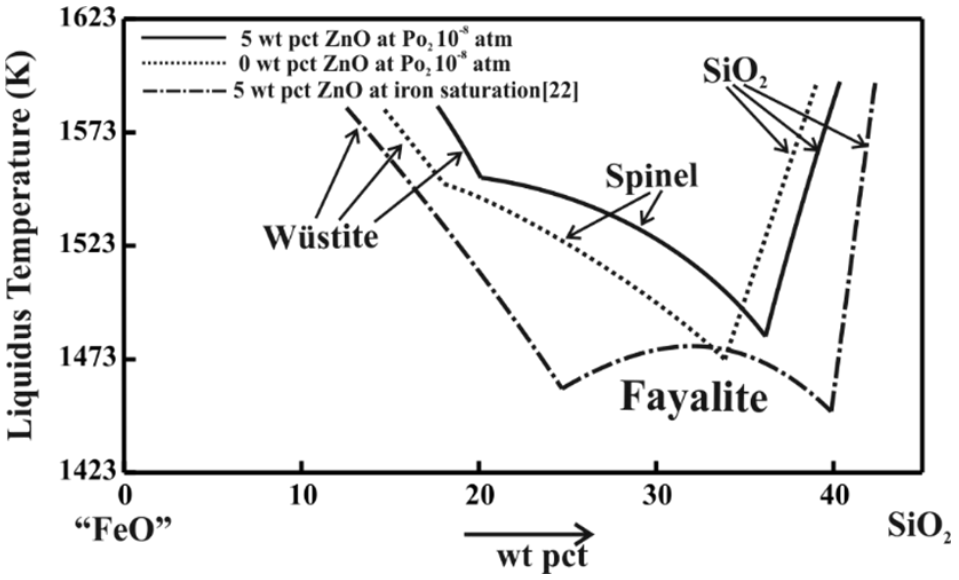

Figure 5.9 Pseudo-binaries "FeO"-SiO_2 at fixed 0 and 5 wt pct ZnO at Po_2 at 10^{-8} atm and iron saturation[22]

One of the advantages using EPMA technique is the compositions of the solid phases can be measured simultaneously with the corresponding liquid phase. The partitioning of ZnO between liquid and solid is important to understand the thermodynamics of ZnO-containing slags. The partitioning of ZnO between spinel and liquid phases has been reported previously in the system ZnO-"FeO"-Al_2O_3-CaO-SiO_2 at metallic iron saturation[24, 30-34]. The comparisons on the partitioning of ZnO between spinel and liquid at iron saturation, FactSage 6.2[29] predictions and present study at Po_2 10^{-8} atm are shown in Figure 5.10. A linear relationship was found between ZnO in spinel phase and in liquid phase from present study and FactSage 6.2[29] predictions at $Po_2=10^{-8}$ atm. The ZnO concentration in the spinel phase is approximately half of that in the liquid phase. The solubility of ZnO in the spinel determined in the present study is higher than that predicted from FactSage 6.2[29] which explains the reason for their difference on the liquidus temperatures.

The ZnO concentration in the spinel phase is much higher than that in liquid phase under metallic iron saturation as illustrated by the circles in Figure 5.10, which can be caused by Po_2 and/or slag compositions. In the present study (system ZnO-"FeO"-SiO_2) the spinel phase is a solid solution of $ZnFe_2O_4$ and Fe_3O_4. In the ZnO-"FeO"-Al_2O_3-CaO-SiO_2 system, the spinel phase is a solid solution of $ZnAl_2O_4$, $FeAl_2O_4$, $ZnFe_2O_4$ and Fe_3O_4. The Gibbs free energy of formation (ΔG^o_f) is -2247, -2181, -1462 and -1440 $kJ \cdot mol^{-1}$ for $ZnAl_2O_4$, $FeAl_2O_4$, $ZnFe_2O_4$ and Fe_3O_4, respectively, at 1573 K (1250 °C) according to FactSage[29]. Clearly the Al_2O_3–containing compounds ($ZnAl_2O_4$ and $FeAl_2O_4$) are much stable than Al_2O_3–free compounds ($ZnFe_2O_4$ and Fe_3O_4). The accurate compositions of the spinel phase measured by EPMA

enable the concentrations of the spinel-forming compounds to be calculated by mass balance. It has found that the concentrations of $ZnAl_2O_4$ and $FeAl_2O_4$ are much higher than that of $ZnFe_2O_4$ and Fe_3O_4 in the spinel phase under metallic iron saturation[24, 30-34]. Effect of Po_2 on partitioning of Zn to spinel will be evaluated when the data in the system ZnO-"FeO"-Al_2O_3-SiO_2 at Po_2 10^{-8} atm are available.

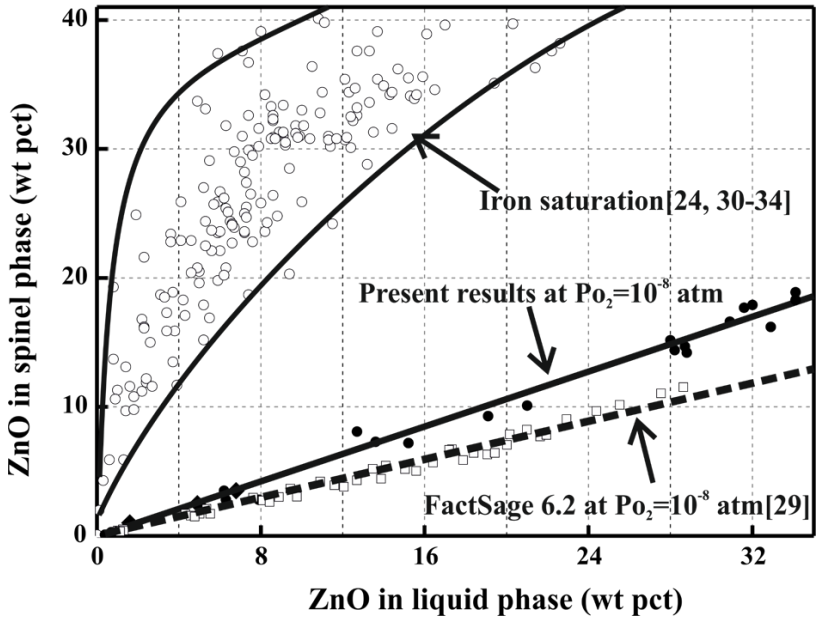

Figure 5.10 Comparison of partitioning effect of ZnO between liquid phase and spinel phase, from current experiments, Factsage prediction[29] and results under metallic iron saturation[24, 30-34]

5.4 **Conclusion**

Phase equilibrium studies have been conducted at oxygen partial pressure 10^{-8} atm relevant to copper smelting conditions in the temperature range from 1473 to 1573 K (1200 to 1300 °C). The liquidus temperatures and primary phase fields in the "FeO"-SiO_2 and ZnO-"FeO"-SiO_2 systems have been experimentally determined. The liquidus temperatures obtained from the present study in spinel primary phase field are higher than that predictions by FactSage 6.2 and that measured at metallic iron saturation. The liquidus temperatures in spinel primary phase field increase with increasing ZnO concentration in slag. ZnO partitioning between spinel phase and liquid phase has been compared at Po_2=10^{-8} atm and metallic iron saturation. The findings in the present study fill the knowledge gap of Zn-containing system relevant to copper smelting slags, and have direct implications to the industrial operations.

5.5 References

1. M. E. Schlesinger, M. J. King, K. C. Sole and W. G. I. Davenport: *Extractive metallurgy of copper*. (Elsevier, Oxford, 2011).

2. M. Chen, S. Raghunath and B. Zhao, *Metall. Mater. Trans. B*, 2013, vol. 44, pp. 506-515.

3. B. Zhao, Z. Cui and Z. Wang, In *4th International Symposium on High-Temperature Metallurgical Processing*, (John Wiley & Sons, Inc.: 2013), p 10.

4. M. Chen, Z. Cui and B. Zhao, In *6th International Symposium on High-Temperature Metallurgical Processing*, (John Wiley & Sons, Inc.: 2015), pp 257-264.

5. Z. Cui, Z. Wang and B. Zhao, In *Copper 2013: Copper International Conference*, (2013), pp 923-933.

6. E. N. Bunting, *J. Am. Ceram. Soc.*, 1930, vol. 13, pp. 5-10.

7. R. Hansson, B. Zhao, P. C. Hayes and E. Jak, *Metall. Mater. Trans. B*, 2005, vol. 36, pp. 187-193.

8. R. Hansson, P. C. Hayes and E. Jak, *Trans. Inst. Min. Metall., Sect. C*, 2005, vol. 114, pp. 141-146.

9. R. Hansson, P. Hayes and E. Jak, *Metall. Mater. Trans. B*, 2005, vol. 36, p. 7.

10. R. Hansson, P. C. Hayes and E. Jak, *Scand. J. Metall.*, 2004, vol. 33, pp. 294-304.

11. S. Itoh, K. Sato, S. Nakazawa and T. Azakami, *Shigen to Sozai*, 1989, vol. 105, pp. 739-43.

12. S. Itoh and T. Azakami, *Mater. Trans. JIM*, 1995, vol. 36, pp. 1074-80.

13. S. Itoh and T. Azakami, *Nippon Kinzoku Gakkaishi*, 1994, vol. 58, pp. 1288-93.

14. N. L. Bowen and J. F. Schairer, *Am. J. Sci.*, 1932, vol. Series 5 Vol. 24, pp. 177-213.

15. A. Muan, *Am. J. Sci.*, 1958, vol. 256, pp. 171-207.

16. A. Muan, *Jom-J Min Met Mat S*, 1955, vol. 7, pp. 965-976.

17. T. Hidayat, P. Hayes and E. Jak, *Metall. Mater. Trans. B*, 2012, vol. 43, pp. 27-38.

18. L. S. Darken, *J. Am. Chem. Soc.*, 1948, vol. 70, pp. 2046-53.

19. E. Jak, S. Degterov, A. D. Pelton and P. C. Hayes, *Metall. Mater. Trans. B*, 2001, vol. 32, pp. 793-800.

20. E. Jak, B. Zhao and P. Hayes, *Metall. Mater. Trans. B*, 2000, vol. 31, pp. 1195-1201.

21. S. Itoh and T. Azakami, *Shigen to Sozai*, 1993, vol. 109, pp. 325-329.

22. B. Zhao: Phase equilibria for copper smelting and lead/zinc reduction slags. (University of Queensland, Brisbane, Australia, 1999).

23. M. Chen and B. Zhao, *J. Am. Ceram. Soc.*, 2013, vol. 96, pp. 3631-3636.

24. B. Zhao, P. C. Hayes and E. Jak, *Int. J. Mater. Res.*, 2011, vol. 102, pp. 134-142.

25. B. Zhao, P. Hayes and E. Jak, *Journal of Mining and Metallurgy, Section B: Metallurgy*, 2013, vol. 49, pp. 153-159.

26. E. Jak and P. C. Hayes, *Trans. Inst. Min. Metall., Sect. C*, 2008, vol. 117, pp. 1-17.

27. H. M. Henao and K. Itagaki, *Metall. Mater. Trans. B*, 2007, vol. 38, pp. 769-780.

28. R. A. Mendybaev, J. R. Beckett, E. Stolper and L. Grossman, *Geochim. Cosmochim. Acta*, 1998, vol. 62, pp. 3131-3139.

29. C. W. Bale, E. Bélisle, P. Chartrand, S. A. Decterov, G. Eriksson, K. Hack, I. H. Jung, Y. B. Kang, J. Melançon, A. D. Pelton, C. Robelin and S. Petersen, *CALPHAD: Comput. Coupling Phase Diagrams Thermochem.*, 2009, vol. 33, pp. 295-311.

30. B. Zhao, P. C. Hayes and E. Jak, *Int. J. Mater. Res.*, 2011, vol. 102, pp. 269-276.

31. B. Zhao, P. C. Hayes and E. Jak, *Metall. Mater. Trans. B*, 2011, vol. 42, pp. 490-499.

32. B. Zhao, P. C. Hayes and E. Jak, *Metall. Mater. Trans. B*, 2011, vol. 42, pp. 978-986.

33. B. Zhao, P. C. Hayes and E. Jak, *Metall. Mater. Trans. B*, 2010, vol. 41, pp. 386-395.

34. B. Zhao, P. C. Hayes and E. Jak, *Metall. Mater. Trans. B*, 2010, vol. 41, pp. 374-385.

6 Phase Equilibria Study of the "FeO"-ZnO-Al_2O_3-SiO_2 System at Po_2 10^{-8} atm

Abstract: Phase equilibria studies on ZnO-"FeO"-SiO_2-Al_2O_3 system have been carried out in the temperature range between 1523 and 1573 K (1300 °C) at Po_2 10^{-8} atm. Experimental techniques applied in the present study include high temperature equilibration, quenching and Electron Probe X-ray Microanalysis (EPMA). The compositions of the phases present in the quenched samples were measured by EPMA and used to construct phase diagrams of the pseudo-ternary sections at fixed Al_2O_3 content. The experimental results show that, spinel, SiO_2 and willemite are the major primary phase fields in the composition range investigated. With 2 wt pct Al_2O_3 content in the liquid phase, the liquidus temperature can be increased by 35 K in the spinel primary phase in comparison with Al_2O_3-free system. The partitioning of ZnO and Al_2O_3 between the spinel and liquid phases are also discussed in the paper.

Key words: phase equilibrium, copper smelting slag, "FeO"-ZnO-Al_2O_3-SiO_2, EPMA

6.1 Introduction

Slagging is critical important in the pyrometallurgical processes to produce metals which closely relates to the slag chemistry under the operational conditions[1, 2]. In order to optimize the operational parameters, e.g., concentrates, flux compositions and temperature for pyrometallurgical processes with high efficiency, less energy consumption and high metal recovery, it is imperative to obtain accurate information of phase equilibria for the slag system.

Zn-Fe-Al-Si-O system forms the basis of the slags in non-ferrous metal pyrometallurgical processes, such as Imperial smelting furnace (ISF), Kivcet, QSL, Ausmelt and Isamelt processes,[3] as well as oxygen bottom blowing copper smelting process[4]. The oxide components are introduced into the slag phase from the concentrates and fluxes. Meanwhile, zinc-bearing slags are also produced in the secondary metal production and in the zinc-bearing waste recycling processes.[5, 6] However, these processes are generally operated at varied temperatures and oxygen partial pressure (Po_2), e.g., the operating temperature is 1423 K (1150 °C) with Po_2 close to 10^{-11} to 10^{-13} atm in lead blast furnace[7], while operating temperature is around 1453 K (1180 °C) with Po_2 close to 10^{-8} atm in a Fangyuan oxygen bottom blowing copper smelting furnace[4, 8], which both have a profound effect on the phase equilibria behaviour and physicochemical properties of the slag.[9]

Previous studies on the ZnO-containing copper smelting slag systems had been carried out under metallic iron saturation,[3, 10-19] of which the composition range investigated was relevant to the lead and zinc blast furnace slags. By applying "pie-type" sample of which inner part was ZnO-containing master slag wrapped by metallic iron foil approach, Zhao *et al*[3, 10-15] studied ZnO-"FeO"-Al_2O_3-CaO-SiO_2 and higher order systems with varied CaO/SiO_2 and $(CaO+SiO_2)/Al_2O_3$ ratios under the metallic iron saturation. The results showed that Al_2O_3 content increases the liquidus temperature in the spinel primary phase field. Yamaguchi *et al*[5] measured the activities of ZnO in the CaO-SiO_2-FeO_x-Al_2O_3 slag with Po_2 fixed at around 10^{-11} atm. They found that the ZnO activities were increased with the addition of Al_2O_3 in the slag, and no phase relations were reported in their study. Our previous work on the ZnO-"FeO"-SiO_2 system at 10^{-8} atm[20] indicated major difference on the phase equilibria behaviour under varied Po_2. The results at iron saturation cannot be directly applied to the copper smelting slags due to the significant difference of Po_2 between these processes.

Meanwhile, no phase equilibria work has been reported on the ZnO-"FeO"-SiO_2-Al_2O_3 system at Po_2 10^{-8} atm. With an aim to further improve the understanding of the ZnO-containing copper smelting slags, the phase equilibria studies on the ZnO-"FeO"-SiO_2-Al_2O_3 system with Al_2O_3 concentration up to 6 wt pct have been carried out at Po_2 10^{-8} atm.

6.2 Experimental

The detailed experimental procedure used in the present study is similar to that reported in the previous works[3, 20]. Briefly, two master slags, SiO_2-Fe-O and ZnO-SiO_2-Al_2O_3 were firstly prepared. The zinc-silicate master slag was prepared by preheating the mixture of ZnO, SiO_2 and Al_2O_3 at 1500 °C in air to obtain homogeneous liquid. The iron-silicate master slag was obtained by pre-equilibration of the mixture of Fe_2O_3 and SiO_2 in the target temperature and Po_2. The final mixture was prepared by mixing the desired proportions of iron-silicate and zinc-silicate master slags with the third component Fe_3O_4, SiO_2 or ZnO. Primary-phase substrate technique was applied for the experiments in the primary phase fields of spinel and SiO_2. A platinum basket was used for the experiments in the willemite primary phase field. After pelletising, the mixture (around 0.15 g) was placed in a suitable container and suspended in the hot-zone of the reaction tube with the CO_2/CO mixture passing through to maintain Po_2 at 10^{-8} atm to achieve final equilibration. After equilibration, the sample was quenched into ice water. The obtained sample was then then mounted and polished for EPMA.

Optical microscopy was firstly applied to examine the phase assemblages present in the sample. Carbon coating was performed on the QT150TES (Quorum Technologies) prior to electron probe microanalysis (EPMA). A JXA 8200 Electron Probe Microanalyser equipped with wavelength-dispersive X-ray spectroscopy (Japan Electron Optics Ltd) was applied to microstructures and phase compositions analyses. The working voltage and probe current were 15 kV and 15 nA, respectively. The standards used for the analyses were from Charles M. Taylor Co. (Stanford, California): Fe_2O_3 for Fe, Al_2O_3 for Al and $CaSiO_3$ for Si, and Micro-Analysis Consultant Ltd (Cambridge, UK): ZnO for Zn. The ZAF correction procedure supplied with the EPMA was applied. Although Fe^{2+} and Fe^{3+} are both present in the quenched samples, only metal cation concentrations can be measured by EPMA. Therefore, all the iron was recalculated to "FeO" for presentation purpose only.

6.3 Results and Discussion

In the present study, phase equilibria in the ZnO-"FeO"-SiO_2-Al_2O_3 system have been determined between 1523 K (1250 °C) and 1573 K (1300 °C) under Po_2 fixed at 10^{-8} atm with Al_2O_3 content up to 6 wt pct. The EPMA results are presented in Table 6.1 to Table 6.3. The phase diagrams are presented in the form of pseudo-ternary at constant Al_2O_3 concentration as indicated in Figure 6.1. Three primary phase fields were identified in the composition range studied, including spinel [$(Fe^{2+}, Zn)O\bullet(Fe^{3+}, Al)_2O_3$], tridymite ($SiO_2$) and willemite [$(Fe^{2+}, Zn)_2SiO_4$]. The typical microstructures from the quenched samples are presented in Figure 2 that include the equilibrium of liquid with spinel (Figure 6.2A), tridymite (Figure 6.2B), willemite (Figure 6.2C), and with both spinel and willemite (Figure 6.2D) respectively. The extensive solid solution was measured for spinel and will be further discussed in latter sections.

The liquidus surfaces with 2, 4 and 6 wt pct Al_2O_3 on the ZnO-"FeO"-SiO_2-Al_2O_3 system were constructed based on the data listed in Table 6.1 to Table 6.3, as shown in Figure 6.3 to Figure 6.5. In the Figure 6.3 to Figure 6.5, the thin solid lines are experimental determined isotherms, while the thick solid lines represent the experimentally determined boundaries and the thick dash lines indicate the phase boundaries in the areas without experimental data. It can be seen that, the liquidus temperatures mainly decrease in the spinel primary phase field and increase in the tridymite primary phase field with increasing SiO_2 concentration. In the willemite primary phase field the liquidus temperatures increase with increasing ZnO concentration.

Table 6.1 Experimental determined phases compositions in the ZnO-"FeO"-SiO_2-Al_2O_3 system at 1523 K (1250 °C) under Po_2 10^{-8} atm

Experiment No.	Temperature [K (°C)]	Phase	Composition (wt pct)			
			ZnO	SiO_2	"FeO"	Al_2O_3
240	1523 (1250)	Liquid	22	37.6	36.5	3.9
		Spinel	14.5	0.4	80.5	4.6
241	1523 (1250)	Liquid	21.7	37.1	37.3	3.9
		Spinel	14	0.3	81.3	4.4
242	1523 (1250)	Liquid	22.5	37.5	36.2	3.8
		Spinel	14.5	0.4	80.6	4.5
260	1523 (1250)	Liquid	20	37.2	39.2	3.6
		Spinel	12.9	0.4	82.3	4.4
261	1523 (1250)	Liquid	19.5	37.1	39.7	3.7
		Spinel	12.6	0.5	83.0	4.0
272	1523 (1250)	Liquid	12.6	35.3	50.2	1.9
		Spinel	6.8	0.4	91.2	1.6
276	1523 (1250)	Liquid	12.9	35.0	50.3	1.8
		Spinel	6.7	0.4	91.3	1.5
322	1523 (1250)	Liquid	0	24.6	74.1	1.3
		Spinel	0.0	0.7	97.5	1.7
323	1523 (1250)	Liquid	0	25.5	71.9	2.6
		Spinel	0	0.7	95.7	3.6
334	1523 (1250)	Liquid	0	26	70.2	3.8
		Spinel	0	0.6	93.9	5.5
405	1523 (1250)	Liquid	21.5	37.3	36.6	4.6
		Spinel	14.3	0.3	80.2	5.2
437	1523 (1250)	Liquid	0.0	25.9	72.0	2.0
		Spinel	0	0.7	96.4	2.9
438	1523 (1250)	Liquid	0	26	72	2
		Spinel	0.1	0.5	96.9	2.4
441	1523 (1250)	Liquid	0	25.8	72.1	2.1
		Spinel	0	0.7	96.4	2.9
443	1523 (1250)	Liquid	0.1	31	66.5	2.4
		Spinel	0	0.4	97.6	2
457	1523 (1250)	Liquid	9.1	38.3	46.5	6.1
		Spinel	6.6	0.4	86.9	6.2
458	1523 (1250)	Liquid	0.0	27.5	66.7	5.7
		Spinel	0	0.5	91.6	7.9
474	1523 (1250)	Liquid	9.6	36.1	48.3	6
		Spinel	7.3	0.4	84.6	7.7
476	1523 (1250)	Liquid	10.1	34.9	48.9	6.1
		Spinel	6.8	0.4	85.1	7.7
501	1523 (1250)	Liquid	9.0	34.2	52.6	4.3
		Spinel	4.5	0.5	90.2	4.9
613	1523 (1250)	Liquid	8.1	37.4	51.7	2.8
		Spinel	4.6	0.4	92.4	2.5
212	1523 (1250)	Liquid	26.2	37.3	33.4	3.1
		SiO_2	0.3	99.3	0.4	0
213	1523 (1250)	Liquid	26.2	37.4	33.3	3.1
		SiO_2	0.3	99.4	0.3	0
316	1523 (1250)	Liquid	0	37.9	60.3	1.8
		SiO_2	0	98.9	1.1	0
335	1523 (1250)	Liquid	0	37.2	61.1	1.7

Experiment No.	Temperature [K (°C)]	Phase	Composition (wt pct)			
			ZnO	SiO_2	"FeO"	Al_2O_3
		SiO_2	0	99.2	0.8	0
336	1523 (1250)	Liquid	0.0	38.6	57.9	3.5
		SiO_2	0	99.2	0.8	0
337	1523 (1250)	Liquid	0	39.4	55.4	5.2
		SiO_2	0.0	98.5	1.4	0.1
439	1523 (1250)	Liquid	0	38.6	57.3	4.1
		SiO_2	0.1	99	0.9	0
440	1523 (1250)	Liquid	0	33.5	62	4.5
468	1523 (1250)	Liquid	13.0	36.8	45.7	4.4
		SiO_2	0.3	98.8	0.9	0
469	1523 (1250)	Liquid	11.7	38.4	43.4	6.5
		SiO_2	0.3	98.7	1	0
471	1523 (1250)	Liquid	15.9	37.3	42.2	4.5
		SiO_2	0.5	98.6	0.9	0
539	1523 (1250)	Liquid	24.3	36.5	37.2	2
		SiO_2	0.5	98.8	0.7	0
588	1523 (1250)	Liquid	13.2	38.7	40.5	7.5
		SiO_2	0.5	98.0	1.3	0.2
642	1523 (1250)	Liquid	7.4	36.1	54.3	2.2
		SiO_2	0.2	98.7	1.1	0.0
643	1523 (1250)	Liquid	8.0	37.5	50.4	4.2
		SiO_2	0.2	98.8	0.9	0.0
644	1523 (1250)	Liquid	7.6	38.5	47.8	6.0
		SiO_2	0.2	98.9	0.8	0.1

Table 6.2 Experimental determined phases compositions in the ZnO-"FeO"-SiO_2-Al_2O_3 system at 1543 K (1270 °C) under Po_2 10^{-8} atm

Experiment No.	Temperature [K (°C)]	Phase	Composition (wt pct)			
			ZnO	SiO_2	"FeO"	Al_2O_3
186	1543 (1270)	Liquid	28.5	35.5	33	3
		Spinel	19.3	0.4	75.9	4.5
187	1543 (1270)	Liquid	0.1	22.1	76	1.8
		Spinel	0.1	0.6	96.2	3.1
202	1543 (1270)	Liquid	0.3	23.6	74.5	1.6
		Spinel	0.2	0.6	96.9	2.3
203	1543 (1270)	Liquid	2.2	26.9	69.2	1.6
		Spinel	1.3	0.6	96.1	2.0
206	1543 (1270)	Liquid	20.6	35.5	41.4	2.5
		Spinel	11	0.3	86.4	2.3
207	1543 (1270)	Liquid	20.2	35.1	42.3	2.5
		Spinel	10.7	0.3	87.2	1.8
223	1543 (1270)	Liquid	27.8	36.3	33.4	2.5
		Spinel	17.6	0.3	79.4	2.7
224	1543 (1270)	Liquid	28.0	36.2	33.3	2.5
		Spinel	17.7	0.3	79.3	2.7
225	1543 (1270)	Liquid	29.5	36.2	31.9	2.4
		Spinel	19	0.3	78.1	2.6
226	1543 (1270)	Liquid	28.9	36.3	32.3	2.5
		Spinel	18.4	0.3	78.5	2.8
250	1543 (1270)	Liquid	29.7	35.2	30.9	4.2

Experiment No.	Temperature [K (°C)]	Phase	Composition (wt pct)			
			ZnO	SiO_2	"FeO"	Al_2O_3
		Spinel	20.2	0.3	73.2	6.3
252	1543 (1270)	Liquid	17.6	35.8	43	3.6
		Spinel	11.1	0.4	83.8	4.6
253	1543 (1270)	Liquid	33.9	37.9	21.9	6.3
		Spinel	27.9	0.3	59.3	12.5
300	1543 (1270)	Liquid	0	21.8	76.7	1.5
		Spinel	0	0.7	96.7	2.6
305	1543 (1270)	Liquid	0	22.7	74.5	2.8
		Spinel	0	0.6	94.3	5.1
315	1543 (1270)	Liquid	0	23.9	71.8	4.3
		Spinel	0	0.6	91.6	7.8
502	1543 (1270)	Liquid	11.4	34.8	53.8	11.4
		Spinel	6.6	0.4	88.1	4.9
542	1543 (1270)	Liquid	0	24.3	69.8	5.9
		Spinel	0	0.5	87.6	11.9
582	1543 (1270)	Liquid	7.8	33.2	52.8	6.2
		Spinel	6.4	0.4	83.9	9.3
584	1543 (1270)	Liquid	21.0	36.2	37.3	5.5
		Spinel	14.7	0.6	76.2	8.5
585	1543 (1270)	Liquid	26.5	36.9	30.8	5.7
		Spinel	19.7	0.3	70.9	9.0
598	1543 (1270)	Liquid	19.5	35.9	39.1	5.5
		Spinel	14.2	0.4	76.4	9.0
612	1543 (1270)	Liquid	22.7	34.7	37.3	5.2
		Spinel	17.6	0.3	72.8	9.2
747	1543 (1270)	Liquid	17.6	34.9	45.2	2.3
		Spinel	11.0	0.4	85.5	3.2
211	1543 (1270)	Liquid	25.6	38.1	33.3	3
		SiO_2	0.5	98.9	0.6	0
231	1543 (1270)	Liquid	29	37.5	31.3	2.2
		SiO_2	0.7	98.7	0.6	0
256	1543 (1270)	Liquid	26.4	38.7	30	4.9
		SiO_2	0.6	98.7	0.7	0
321	1543 (1270)	Liquid	0	41	52.8	6.2
		SiO_2	0	99.3	0.7	0
451	1543 (1270)	Liquid	0	38.9	57	4.1
		SiO_2	0.0	99.2	0.8	0.0
499	1543 (1270)	Liquid	0.0	37.7	60.5	1.9
		SiO_2	0.0	99.3	0.7	0.0
540	1543 (1270)	Liquid	23.9	37.1	37	2
		SiO_2	0.5	98.8	0.7	0
572	1543 (1270)	Liquid	0.0	37.2	61.0	1.8
		SiO_2	0.0	99.2	0.8	0.0
583	1543 (1270)	Liquid	14.2	38.9	39.8	7.2
		SiO_2	0.5	98.7	0.8	0.0
586	1543 (1270)	Liquid	12.9	37.5	46.8	2.8
		SiO_2	0.4	98.5	1.1	0.0
646	1543 (1270)	Liquid	6.8	38.7	50.4	4.1
		SiO_2	0.2	99.1	0.7	0.0
647	1543 (1270)	Liquid	0.0	39.3	57.0	3.7
		SiO_2	0.0	99.2	0.8	0.0
648	1543 (1270)	Liquid	6.3	39.1	48.7	5.9

Experiment No.	Temperature [K (°C)]	Phase	Composition (wt pct)			
			ZnO	SiO_2	"FeO"	Al_2O_3
		SiO_2	0.1	99.2	0.7	0.0
673	1543 (1270)	Liquid	10.4	38.6	45.2	5.9
		SiO_2	0.2	99.0	0.8	0.0
680	1543 (1270)	Liquid	9.3	35.9	52.7	2.1
		SiO_2	0.2	99.0	0.8	0.0
205	1543 (1270)	Liquid	34.7	35.9	24.8	4.7
		Spinel	27.3	0.3	58.8	13.5
		Willemite	62.3	28.1	9.4	0.2
289	1543 (1270)	Liquid	0	31.6	66.3	2.1
294	1543 (1270)	Liquid	0	31.9	66	2.1
297	1543 (1270)	Liquid	0	33.4	62.4	4.2
446	1543 (1270)	Liquid	0.0	38.5	57.2	4.2
298	1543 (1270)	Liquid	35.2	38.0	23.0	3.9
		Willemite	63.3	28.8	7.8	0.1
304	1543 (1270)	Liquid	34.8	36	24.5	4.7
		Willemite	61.8	28.9	9.1	0.2
307	1543 (1270)	Liquid	33.6	35.7	26.7	4.0
		Willemite	61.8	28.7	9.3	0.2
309	1543 (1270)	Liquid	35.2	36.6	22.3	6.0
		Willemite	63.5	28.4	7.9	0.2
481	1543 (1270)	Liquid	32.8	37.2	28.7	1.3
		Willemite	60.6	28.9	10.5	0
482	1543 (1270)	Liquid	33.8	37.5	25.2	3.5
		Willemite	61.8	29.1	9.0	0.0
486	1543 (1270)	Liquid	32.2	36.4	29.8	1.6
		Willemite	61.3	28.3	10.4	0
500	1543 (1270)	Liquid	34.5	35.2	25.5	4.8
		Willemite	62.2	28.5	9.1	0.2

Table 6.3 Experimental determined phases compositions in the ZnO-"FeO"-SiO_2-Al_2O_3 system at 1573 K (1300 °C) under Po_2 10^{-8} atm

Experiment No.	Temperature [K (°C)]	Phase	Composition (wt pct)			
			ZnO	SiO_2	"FeO"	Al_2O_3
310	1573 (1300)	Liquid	4.7	28.0	65.0	2.3
		Spinel	2.8	0.4	93.8	3.0
311	1573 (1300)	Liquid	22.8	32.3	40.5	4.4
		Spinel	14.6	0.3	76.7	8.4
312	1573 (1300)	Liquid	5.9	26.4	65.9	1.8
		Spinel	3.1	0.4	94.0	2.6
313	1573 (1300)	Liquid	0.9	23.5	74.0	1.6
		Spinel	0.4	0.4	97.6	1.6
314	1573 (1300)	Liquid	25.6	34.7	34.4	5.2
		Spinel	21.4	0.4	69.3	8.9
317	1573 (1300)	Liquid	6.4	26.5	65.7	1.4
		Spinel	3.3	0.4	94.6	1.7
453	1573 (1300)	Liquid	15.2	30.2	50.5	4.1
		Spinel	10.5	0.3	80.0	9.2
454	1573 (1300)	Liquid	14.3	31.1	48.7	5.9
		Spinel	12.4	0.3	73.1	14.2
456	1573 (1300)	Liquid	24.0	29.6	44.3	2.1

Experiment No.	Temperature [K (°C)]	Phase	Composition (wt pct)			
			ZnO	SiO_2	"FeO"	Al_2O_3
		Spinel	14.2	0.4	81.2	4.2
463	1573 (1300)	Liquid	0.0	15.9	81.1	3.0
		Spinel	0.1	0.4	92.4	7.1
472	1573 (1300)	Liquid	0.0	20.3	73.5	6.2
		Spinel	0.0	0.4	83.0	16.6
474	1573 (1300)	Liquid	0.0	15.7	81.9	2.4
		Spinel	0.1	0.5	93.8	5.7
479	1573 (1300)	Liquid	0.0	17.7	78.1	4.1
		Spinel	0.0	0.4	89.0	10.6
749	1573 (1300)	Liquid	8.3	28.6	60.7	2.4
		Spinel	4.9	0.4	90.9	3.7
750	1573 (1300)	Liquid	36.6	29.5	31.9	2.1
		Spinel	21.8	0.5	74.3	3.5
792	1573 (1300)	Liquid	26.1	31.5	40.1	2.2
		Spinel	16.4	0.4	78.9	4.3
296	1573 (1300)	Liquid	38.1	36.2	21.0	4.7
318	1573 (1300)	Liquid	39.9	36.2	19.0	4.9
		Willemite	65.3	28.1	6.5	0.2
319	1573 (1300)	Liquid	39.5	36.0	19.4	5.2
		Willemite	64.7	28.3	6.8	0.2
324	1573 (1300)	Liquid	38.2	37.9	20.3	3.6
		Willemite	64.6	28.3	7.0	0.1
325	1573 (1300)	Liquid	39.4	36.4	20.4	3.8
		Willemite	64.1	28.3	7.5	0.1
328	1573 (1300)	Liquid	38.9	34.3	22.6	4.3
		Willemite	63.7	28.3	7.8	0.2
329	1573 (1300)	Liquid	39.6	33.4	23.4	3.6
		Willemite	63.6	28.2	8.0	0.2
330	1573 (1300)	Liquid	38.6	32.9	25.1	3.4
		Willemite	63.5	28.0	8.4	0.2
332	1573 (1300)	Liquid	40.1	34.1	20.5	5.3
		Willemite	65.3	27.9	6.7	0.2
333	1573 (1300)	Liquid	40.2	35.4	19.4	5.0
		Willemite	64.8	28.5	6.6	0.2
331	1573 (1300)	Liquid	38.4	33.0	25.3	3.3
		Willemite	63.3	27.9	8.5	0.2
483	1573 (1300)	Liquid	36.3	34.7	28.1	0.8
		Willemite	61.7	29.0	9.3	0.0
484	1573 (1300)	Liquid	38.5	36.2	20.7	4.6
		Willemite	63.8	28.7	7.3	0.2
487	1573 (1300)	Liquid	38.5	32.8	24.5	4.2
		Willemite	63.4	28.2	8.3	0.1
541	1573 (1300)	Liquid	40.5	35.2	17.5	6.8
		Willemite	65.5	28.1	6.2	0.2
751	1573 (1300)	Liquid	38.0	33.1	26.9	1.9
		Willemite	63.0	27.6	9.3	0.1
793	1573 (1300)	Liquid	38.0	33.6	25.9	2.6
		Willemite	63.0	28.7	8.3	0.0
362	1573 (1300)	Liquid	0.0	18.9	78.5	2.6
363	1573 (1300)	Liquid	0.0	18.1	77.7	4.2
448		Liquid	19.0	31.9	46.8	2.3
503		Liquid	3.7	31.6	61.7	3.0

Experiment No.	Temperature [K (°C)]	Phase	Composition (wt pct)			
			ZnO	SiO_2	"FeO"	Al_2O_3
326	1573 (1300)	Liquid	36.4	39.6	19.6	4.4
		SiO_2	1.0	98.6	0.4	0.0
327	1573 (1300)	Liquid	38.0	39.1	18.6	4.3
		SiO_2	0.9	98.8	0.4	0.0
353	1573 (1300)	Liquid	0.0	39.5	58.2	2.2
		SiO_2	0.0	99.1	0.9	0.0
357	1573 (1300)	Liquid	0.0	41.1	54.8	4.0
		SiO_2	0.0	98.5	1.4	0.0
361	1573 (1300)	Liquid	0.0	41.4	52.9	5.6
		SiO_2	0.0	99.1	0.9	0.0
460	1573 (1300)	Liquid	17.2	38.2	40.4	4.2
		SiO_2	0.6	98.3	1.1	0.0
461	1573 (1300)	Liquid	19.6	40.1	34.3	6.0
		SiO_2	0.7	98.5	0.8	0.0
504	1573 (1300)	Liquid	25.0	38.4	34.7	1.9
		SiO_2	0.6	98.8	0.7	0.0
614	1573 (1300)	Liquid	8.3	39.0	48.2	4.6
		SiO_2	0.2	99.0	0.8	0.0
649	1573 (1300)	Liquid	8.9	37.9	50.5	2.7
		SiO_2	0.2	99.0	0.8	0.0
650	1573 (1300)	Liquid	12.5	39.2	43.7	4.6
		SiO_2	0.3	98.8	0.9	0.0
651	1573 (1300)	Liquid	9.5	38.8	45.1	6.7
		SiO_2	0.2	99.1	0.7	0.0
670	1573 (1300)	Liquid	9.0	37.1	51.7	2.1
		SiO_2	0.2	98.9	0.9	0.0
671	1573 (1300)	Liquid	12.8	38.2	44.7	4.2
		SiO_2	0.3	98.7	1.0	0.0
672	1573 (1300)	Liquid	9.2	40.1	44.5	6.3
		SiO_2	0.2	99.0	0.8	0.0

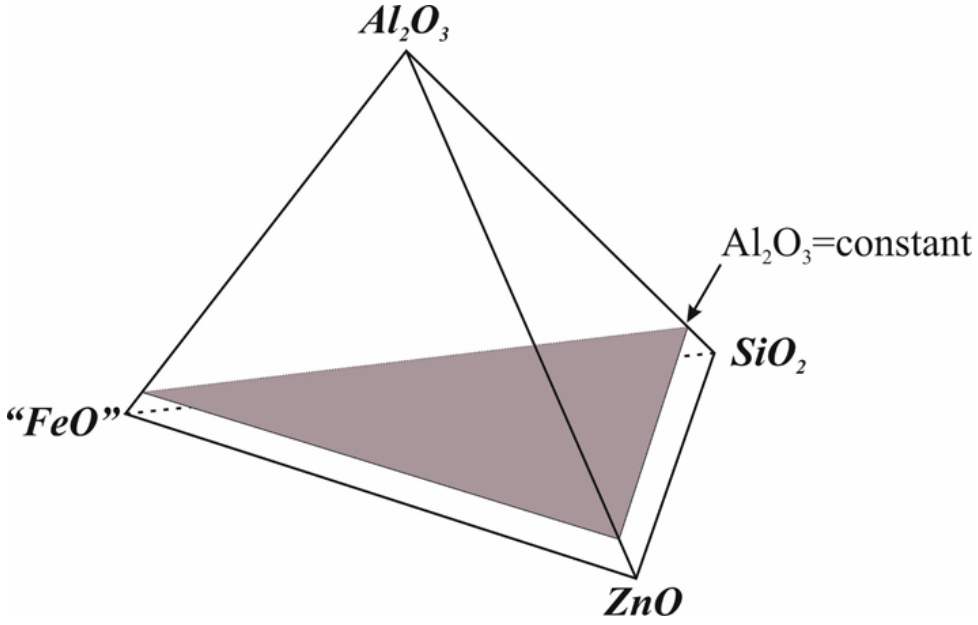

Figure 6.1 Pseudo-ternary section in the "FeO"-ZnO-Al_2O_3-SiO_2 system at constant Al_2O_3 content in liquid under Po_2 10^{-8} atm

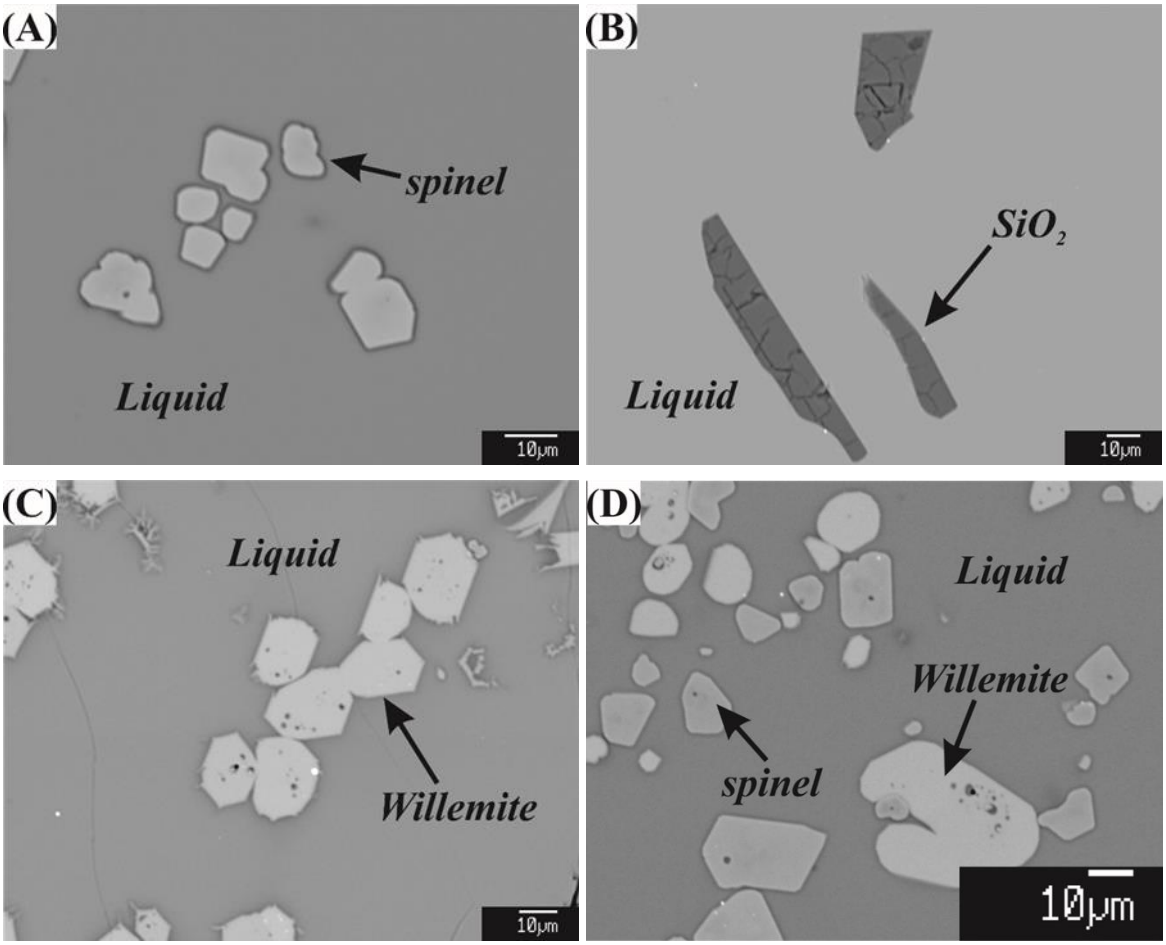

Figure 6.2 Microstructures of quenched samples showing liquid in equilibrium with, (A) - Spinel, (B) - SiO_2, (C) - Willemite, (D) - Spinel and Willemite, under Po_2 10^{-8} atm

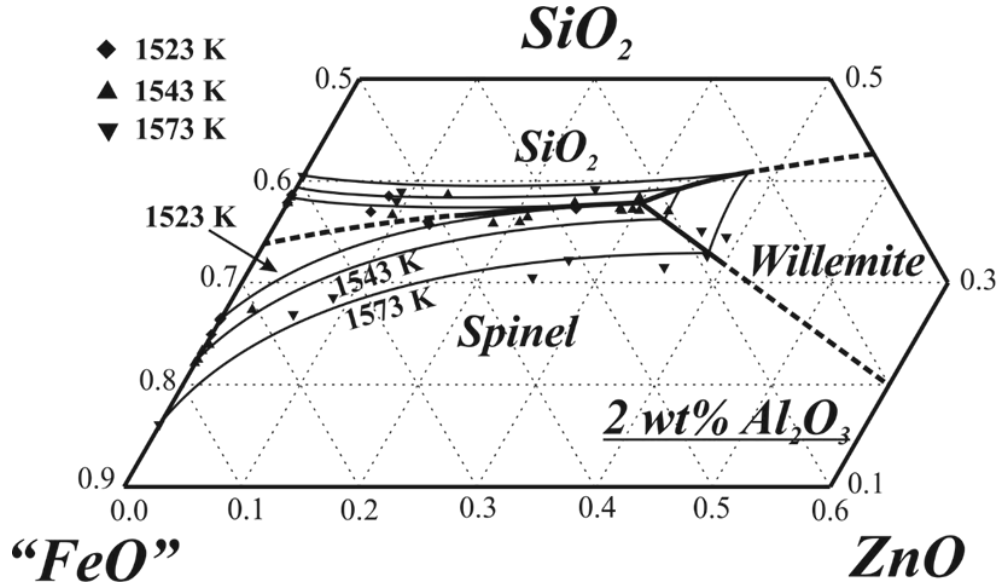

Figure 6.3 Summary of experimental data on the liquidus in the section, "FeO"-ZnO-Al_2O_3-SiO_2 system with 2 wt pct Al_2O_3 in the liquid under Po_2 at 10^{-8} atm

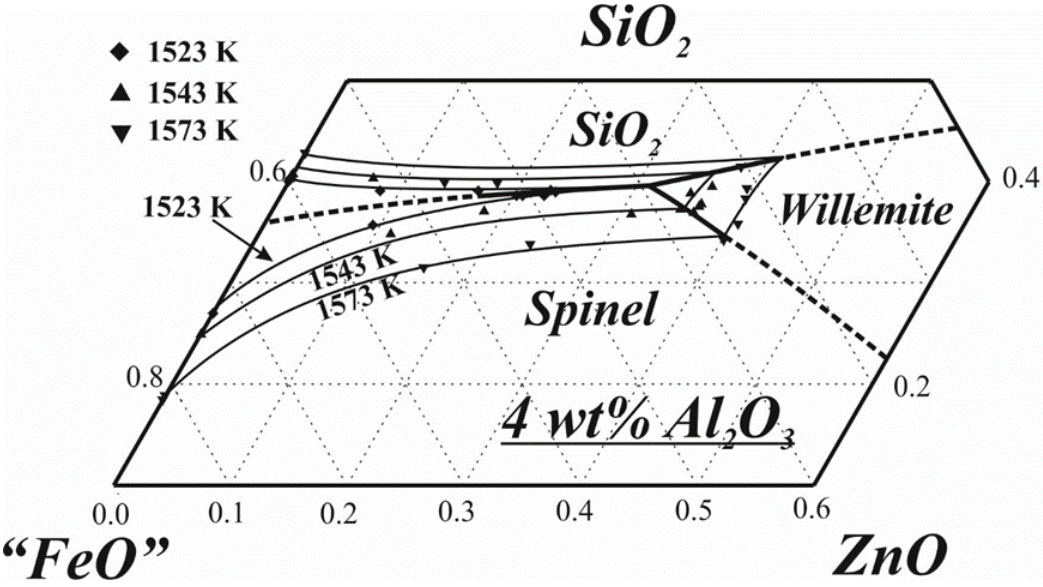

Figure 6.4 Summary of experimental data on the liquidus in the section, "FeO"-ZnO-Al_2O_3-SiO_2 system with 4 wt pct Al_2O_3 in the liquid under Po_2 at 10^{-8} atm

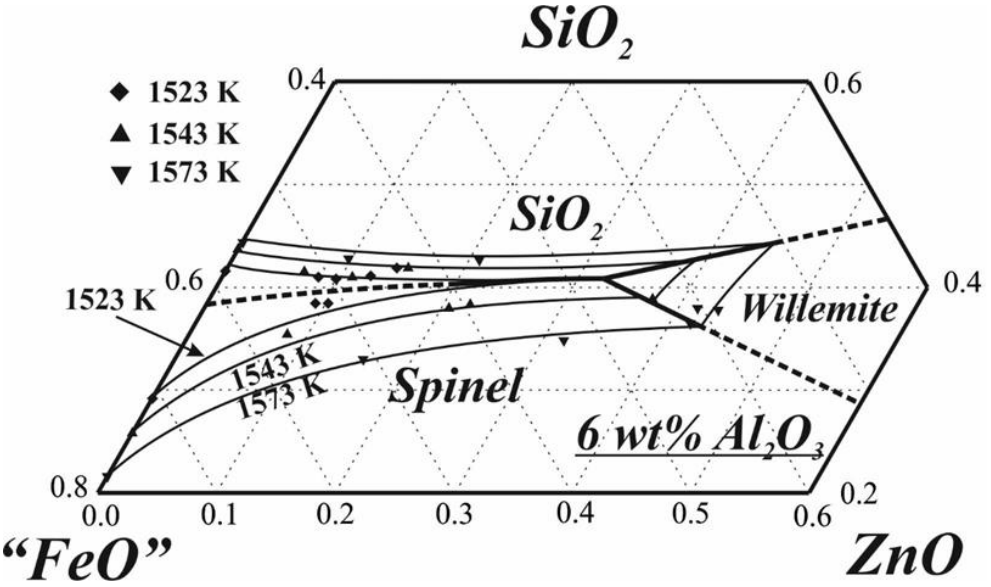

Figure 6.5 Summary of experimental data on the liquidus in the section, "FeO"-ZnO-Al_2O_3-SiO_2 system with 6 wt pct Al_2O_3 in the liquid under Po_2 at 10^{-8} atm

6.3.1 Effects of Al_2O_3 and ZnO content on the primary phase and liquidus temperature

Alumina (Al_2O_3), commonly presents in the copper smelting slags, either introducing by copper concentrate, silica flux or fuel. By using the current experimental data, liquidus surfaces at 1523 K (1250 °C) with varied Al_2O_3 contents are constructed as shown in Figure 6.6. The liquidus temperatures predicted by FactSage[21] are also presented in the figure for comparison. It can be seen from the figure that up to 6 wt pct Al_2O_3 does not have a significant effect on the size of the fully liquid area surrounded by the isotherms in the spinel and tridymite primary phase fields. Both isotherms move towards high SiO_2 direction. The fully liquid area at 1523

K (1250 °C) determined from the present study is much smaller than that from FactSage prediction[21] at Po_2 10^{-8} atm.

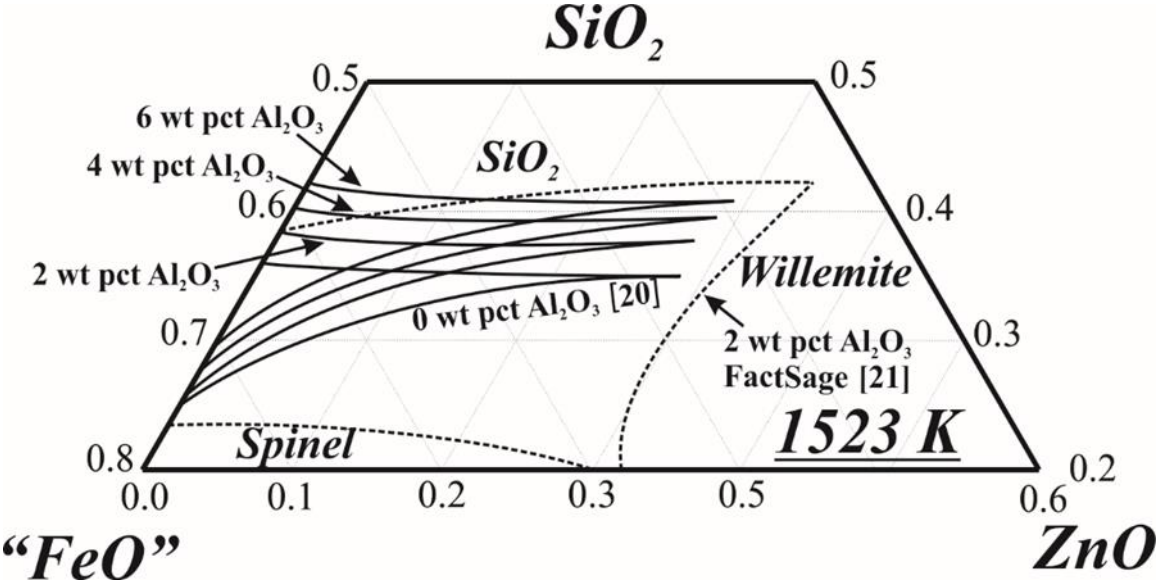

Figure 6.6 Liquidus surfaces at 1523 K (1250 °C) with varied Al_2O_3 contents under Po_2 at 10^{-8} atm

For the industrial implication purposes, the effect of ZnO on the liquidus temperatures in the spinel primary phase field is presented on pseudo-binary sections with Fe/SiO_2 (mass ratio) relevant to the copper smelting slags[4]. It can be seen from Figure 6.7 that, liquidus temperatures in spinel phase filed continuously increase with increasing ZnO concentration regardless Al_2O_3 concentration. However, it can be seen that the spinel liquidus is more sensitive to ZnO concentration if Al_2O_3 is present. In Al_2O_3-free slag the liquidus temperature is increased by approximately 45 K with 10 wt pct ZnO addition. When 6 wt pct Al_2O_3 is present, the liquidus temperature will be increased by approximately 70 K with 10 wt pct ZnO addition. It also can be seen that, FactSage predictions[21] of the spinel liquidus are much lower than the experimental results. For example, at 2 wt pct Al_2O_3 and 10 wt pct ZnO, the liquidus temperature predicted by FactSage is 70 K lower than that determined in the present study.

Figure 6.8 shows the effect of Al_2O_3 on the liquidus temperatures in the spinel primary phase field at Fe/SiO_2 weight ratio of 1.5 in the liquid phase. It can be seen that liquidus temperatures in the spinel primary phase field increase with increasing Al_2O_3 concentration at fixed ZnO concentrations. Addition of 6 wt pct Al_2O_3 in the slag can increase the liquidus temperature by 20 - 50 K depending on the ZnO concentrations in the liquid.

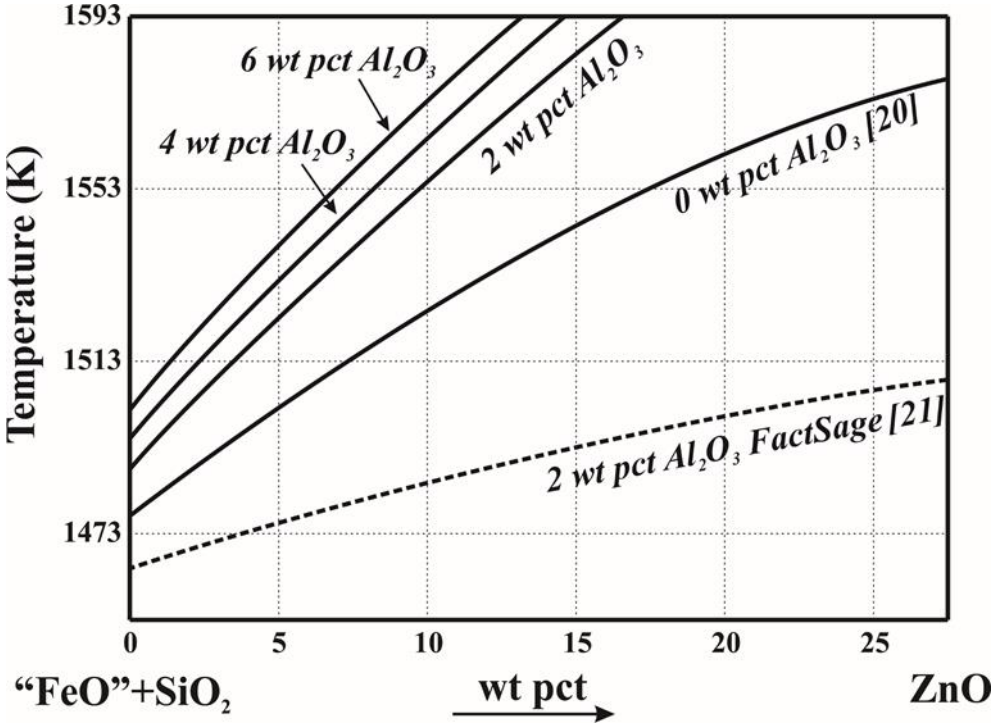

Figure 6.7 Comparison of the pseudo-binary ("FeO"+SiO_2)-ZnO between present study, Al_2O_3-free system[3] and FactSage prediction[14] in spinel primary phase field as a function of ZnO concentration with varied Al_2O_3 content at fixed Fe/SiO_2 = 1.5 and Po_2 = 10^{-8} atm

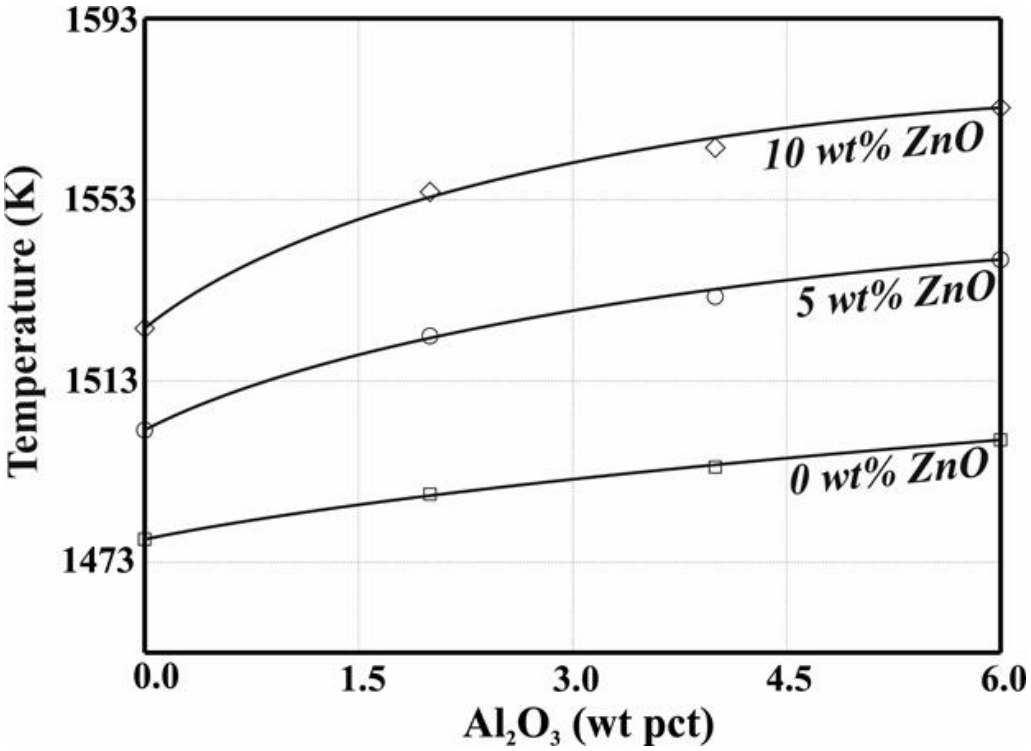

Figure 6.8 Liquidus temperature in spinel primary phase field as a function of Al_2O_3 content at fixed Fe/SiO_2 = 1.5 with varied ZnO content under Po_2 at 10^{-8} atm

Silica is commonly used as a flux in the copper smelting process to control the slag properties. It is convenient for industry to use the correlation between liquidus temperature and SiO_2

concentration. Figure 6.9 shows the liquidus temperature in spinel primary phase field as a function of SiO_2 concentration (Fe/SiO_2 weight ratio) at fixed 5 wt pct ZnO. It can be seen that spinel and SiO_2 are the major primary phases in the composition range investigated (Fe/SiO_2 weight ratio 1.0 to 3.0). In spinel primary phase field the liquidus temperatures increase with increasing Fe/SiO_2 weight ratio. In contrast, the liquidus temperatures in the SiO_2 primary phase field decrease with increasing Fe/SiO_2 weight ratio. The minimum liquidus temperature (eutectic between the primary phase fields of spinel and silica) at a given Al_2O_3 concentration increases with increasing Al_2O_3 and move towards low Fe/SiO_2 weight ratio. Clearly it can be seen from the figure that liquidus temperatures predicted by FactSage[21] are much lower than that determined in the present study in both spinel and silica primary phase fields. The above results suggest that it is an effective way to control the operating temperature by tuning the Fe/SiO_2 ratio in the industrial copper smelting operation to offset the effects of Al_2O_3 and ZnO in the slag.

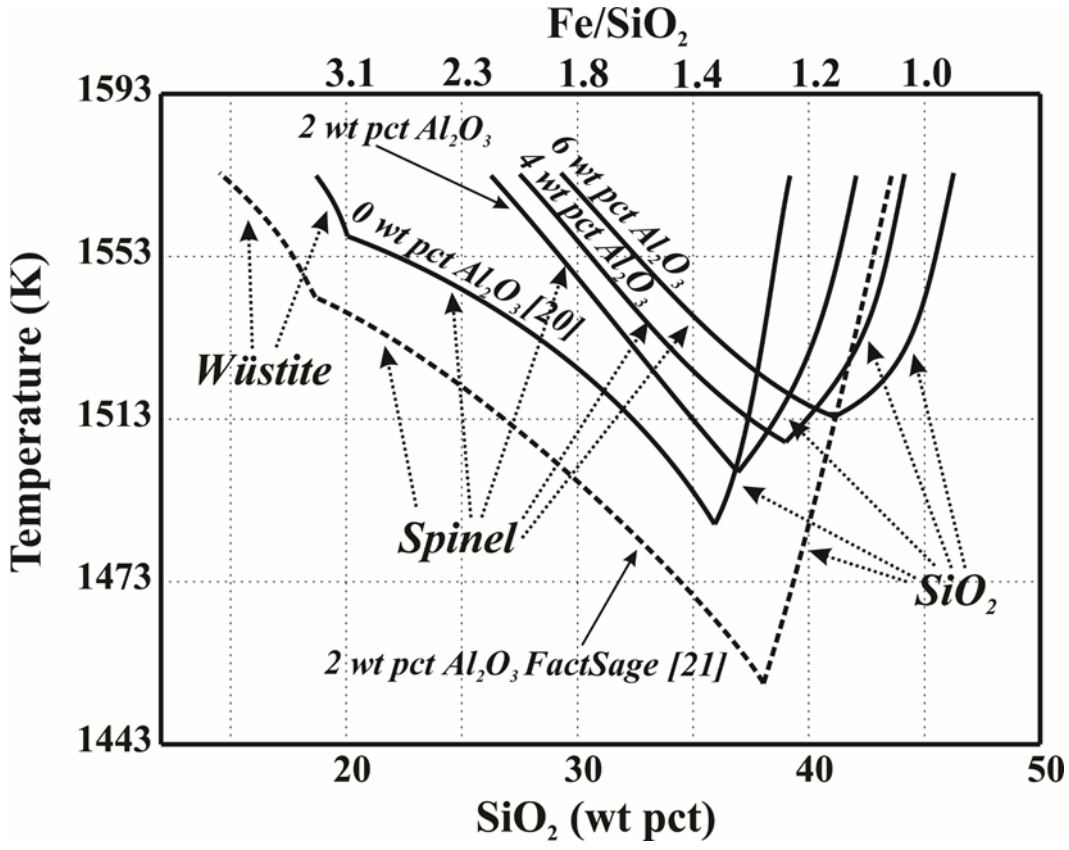

Figure 6.9 Comparison of the liquidus temperature between present studies, Al_2O_3-free system[3] and FactSage prediction[14] as a function of SiO_2 (flux) concentration in the ZnO-"FeO"-SiO_2-Al_2O_3 system with fixed 5.0 wt pct ZnO content under Po_2 10^{-8} atm

6.3.2 Solid-liquid equilibria

One of the advantages by using the present experimental approach is that the compositions of solid phase that in equilibrium with the liquid phase can be measured in the same quenched sample. In the present study, the spinel phase forms an extensive solid solution [(Fe^{2+}, Zn)O•(Fe^{3+}, Al)$_2O_3$] as shown in Table 6.1 to Table 6.3. In other words, by using the current experimental scheme, it is able to provide accurate data on the solid solutions that are very important for the development of thermodynamic modelling.

Copper smelting slags are usually located in the spinel primary phase field which is a solid solution of Fe_3O_4, $ZnFe_2O_4$, $FeAl_2O_4$ and $ZnAl_2O_4$[14]. As an example, the partitioning of ZnO between spinel and liquid is shown in Figure 6.10. The solid symbols in the figure are the present results and the results from Al_2O_3-free system at Po_2 10^{-8} atm[20] and Al_2O_3-ZnO-"FeO"-SiO_2-CaO at metallic iron saturation[3, 10-15] are also shown in the figure for comparison. It appears that Al_2O_3 in liquid can influence the ZnO partitioning and the effect of temperature is not significant. The line passing the symbols represents approximately 5 wt pct Al_2O_3 in the liquid. It can be seen that the ZnO in the spinel is approximately 66 pct of that in the corresponding liquid in the system ZnO-"FeO"-SiO_2-Al_2O_3 at Po_2 10^{-8} atm. This is slightly higher than that in the system ZnO-"FeO"-SiO_2 at Po_2 10^{-8} atm[21], but much lower than that in the system Al_2O_3-ZnO-"FeO"-SiO_2-CaO[3, 10-15] at metallic iron saturation. It appears that the ZnO concentration in the spinel is increased with the presence of Al_2O_3 in the slag which suggests that Al_2O_3 can stabilize the ZnO-containing spinel. As shown in Table 6.4, the Gibbs free energy of formation (ΔG_f) of $ZnAl_2O_4$ is lower than other spinels which indicates the higher stability of $ZnAl_2O_4$. Moreover, A much higher ZnO content in the spinel can be observed in the Al_2O_3-ZnO-"FeO"-SiO_2-CaO system[3, 10-15] at metallic iron saturation as compared to that from higher Po_2. This phenomenon can be explained by the fact that at more reducing condition, e.g., under metallic iron saturation, the Fe_3O_4 and $ZnFe_2O_4$ will be much less stable compared to $ZnAl_2O_4$ and $ZnFe_2O_4$. The results indicate that both Al_2O_3 and Po_2 can affect the ZnO partitioning behaviour and the influence of Po_2 is more significant.

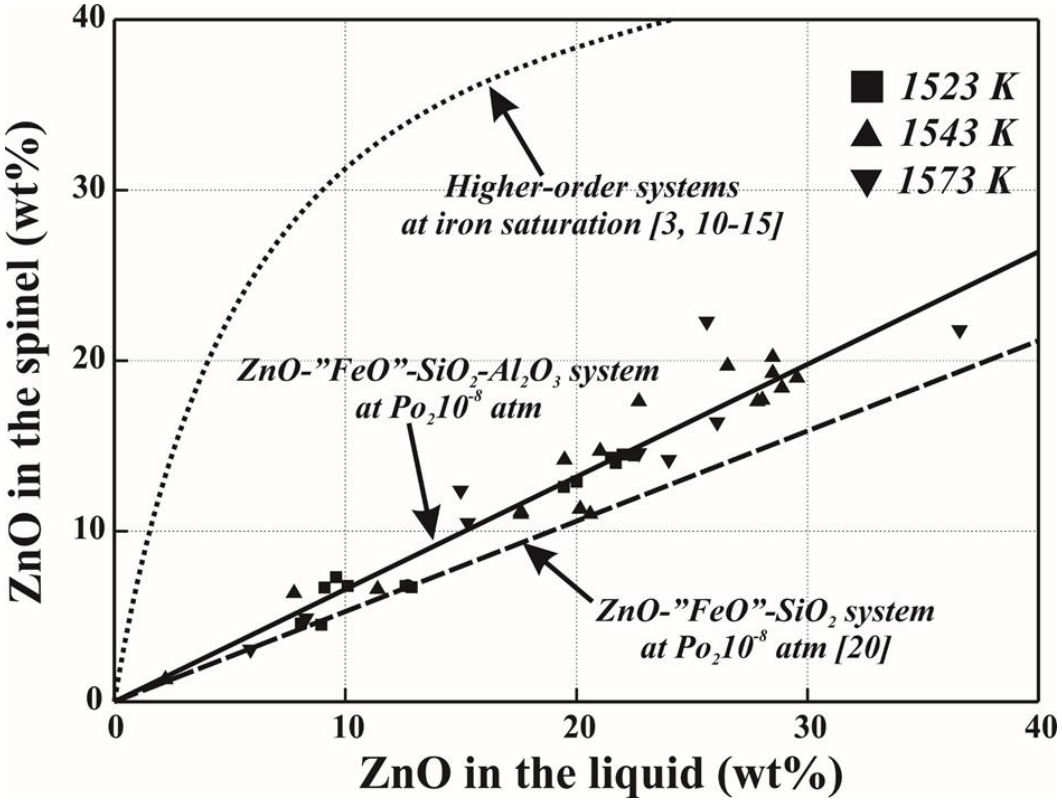

Figure 6.10 ZnO partitioning between spinel and liquid phase in present studies, Al_2O_3-free system[3] at Po_2 10^{-8} atm, and the higher-order systems at metallic iron saturation[4, 8-12] (the labels show the corresponding Al_2O_3 content in the spinel phase)

Table 6.4 The Gibbs Free Energy of Formation (ΔG_f, kJ·mol^{-1}) for varied components of spinel at varied temperatures[21]

Temperature (°C)	Fe_3O_4	$ZnFe_2O_4$	$FeAl_2O_4$	$ZnAl_2O_4$
1250	-1440.1	-1461.9	-2181.2	-2246.8
1270	-1449.6	-1470.6	-2188.9	-2253.8
1300	-1464.0	-1483.8	-2200.6	-2264.5

6.3.3 Industrial implications

The optimisation of pyrometallurgical process is largely depending on the improved understanding of the slag properties. Present study has been carried out to fill the knowledge gap of the phase equilibria for the ZnO-containing copper smelting slags. The results in the present study shown that the introduction of Al_2O_3 in the slag phase increases the liquidus temperatures in spinel primary phase field resulting in the participation of spinel solid phase. Presence of the spinel phase in the slag has been proven to be beneficial to a longer campaign life of the smelting furnace.[22, 23] However, the addition of Al_2O_3 in the slag could lead to a sharp increase of the slag liquidus temperature if ZnO is also present in the slag. Precipitation of the spinel phase may not be easily controlled and it may cause significant operation difficulty.[23] On the other hand, the liquidus temperatures in the spinel primary phase field can

be adjusted by Fe/SiO_2 ratio and the proportion of the spinel solid can be managed to be a proper level.

FactSage[21] is a useful tool for industry to predict the liquidus temperatures and proportion of the solid phase at given temperatures. The present results show that the differences of the liquidus temperatures between FactSage predictions and experimental data are significant. The discrepancies are due to the lack of the accurate data in the ZnO-containing systems under the copper smelting conditions. Experimental results determined in the present study will be used to improve the thermodynamic model to be used for copper industry.

6.4 Conclusion

Phase relations and liquidus temperatures in the ZnO-"FeO"-SiO_2-Al_2O_3 system have been determined at Po_2 10^{-8} atm relevant to copper smelting slags. The results show that, spinel, SiO_2 and willemite are the major primary phase fields in the composition range investigated. The liquidus temperatures increase with the increasing of Al_2O_3 concentration in the liquid phase, accompanying with an extension of the spinel primary phase field. A detailed analysis on partitioning of ZnO between liquid and the conjugated spinel phase shows that ZnO in the spinel is lower than that in the liquid phase. Present study fills the gap of phase equilibria in zinc-containing system at conditions relevant to the copper smelting process. The results will be applied to guide the industrial operation and optimise the thermodynamic database for the zinc-containing system.

6.5 References

1. P. J. Mackey, *Can. Metall. Q.*, 1982, vol. 21, pp. 221-260.

2. T. Barry, A. Dinsdale and J. Gisby, *JOM*, 1993, vol. 45, pp. 32-38.

3. B. Zhao, P. C. Hayes and E. Jak, *Int. J. Mater. Res.*, 2011, vol. 102, pp. 134-142.

4. B. Zhao, Z. Cui and Z. Wang, In *4th International Symposium on High-Temperature Metallurgical Processing*, (John Wiley & Sons, Inc.: 2013), p 10.

5. K. Yamaguchi, M. Kudo, Y. Kimura, S. Ueda and Y. Takeda, In *2006 TMS Fall Extraction & Processing Meeting: Sohn International Symposium*, (Minerals, Metals & Materials Society: San Diego, CA, 2006), pp 199-208.

6. K. Verscheure, M. Van Camp, B. Blanpain, P. Wollants, P. Hayes and E. Jak, *Metall. Mater. Trans. B*, 2007, vol. 38, pp. 13-20.

7. J. Matousek, *JOM*, 2011, vol. 63, pp. 63-67.

8. E. Jak, In *Ninth International Conference on Molten Slags, Fluxes and Salts (MOLTEN12)*, (The Chinese Society for Metals: Beijing, China, 2012), p 28.

9. K. C. Mills, L. Yuan and R. T. Jones, *Journal of the Southern African Institute of Mining and Metallurgy*, 2011, vol. 111, pp. 649-658.

10. B. Zhao, P. C. Hayes and E. Jak, *Int. J. Mater. Res.*, 2011, vol. 102, pp. 269-276.

11. B. Zhao, P. C. Hayes and E. Jak, *Metall. Mater. Trans. B*, 2011, vol. 42, pp. 490-499.

12. B. Zhao, P. C. Hayes and E. Jak, *Metall. Mater. Trans. B*, 2011, vol. 42, pp. 978-986.

13. B. Zhao, P. C. Hayes and E. Jak, *Metall. Mater. Trans. B*, 2010, vol. 41, pp. 386-395.

14. B. Zhao, P. C. Hayes and E. Jak, *Metall. Mater. Trans. B*, 2010, vol. 41, pp. 374-385.

15. B. Zhao, P. C. Hayes and E. Jak, *Metall. Mater. Trans. B*, 2010, vol. 42, pp. 50-67.

16. E. Jak, B. Zhao and P. C. Hayes, *Metall. Mater. Trans. B*, 2002, vol. 33B, pp. 865-876.

17. E. Jak, B. Zhao and P. C. Hayes, *Metall. Mater. Trans. B*, 2002, vol. 33, pp. 877-890.

18. E. Jak, S. Degterov, A. D. Pelton and P. C. Hayes, *Metall. Mater. Trans. B*, 2001, vol. 32, pp. 793-800.

19. S. Degterov, A. Pelton, E. Jak and P. Hayes, *Metall. Mater. Trans. B*, 2001, vol. 32, pp. 643-657.

20. H. Liu, Z. Cui, M. Chen and B. Zhao, *Metall. Mater. Trans. B*, 2016, vol. 47, pp. 164-173.

21. C. W. Bale, E. Bélisle, P. Chartrand, S. A. Decterov, G. Eriksson, K. Hack, I. H. Jung, Y. B. Kang, J. Melançon, A. D. Pelton, C. Robelin and S. Petersen, *CALPHAD: Comput. Coupling Phase Diagrams Thermochem.*, 2009, vol. 33, pp. 295-311.

22. P. Coursol, N. Tripathi, P. Mackey, T. Leggett and A. S. d. Friedberg, *Can. Metall. Q.*, 2010, vol. 49, pp. 255-262.

23. P. Coursol, P. Mackey, Y. Prevost, M. Zamalloa and A. Warner, In *The Carlos Díaz Symposium on Pyrometallurgy, Toronto Canada*, (2007), pp 79-92.

7 Phase Equilibria Study of the ZnO-"FeO"-SiO_2-MgO System at Po_2 10^{-8} atm

Abstract: Experimental studies on the liquidus temperature and phase relations of ZnO-"FeO"-SiO_2-MgO system have been investigated at Po2 10-8 atm related to copper smelting slag. The experimental technique applied in present study involves master slag preparation, high-temperature equilibration, quenching and EPMA analysis. The impact of MgO content on the liquidus temperature and partitioning behaviour of ZnO have been evaluated. It was found that presence of MgO content in the slag can significantly increase liquidus temperature in spinel primary phase field and narrow the full liquid area at a given operating temperature. The ZnO and MgO concentrations in the liquid phase are higher than those in the spinel phase. Present study provides more accurate information for copper smelting slags and optimisation of the thermodynamic modelling.

Key words: phase equilibrium, copper smelting slag, ZnO-"FeO"-SiO_2-MgO, EPMA

7.1 Introduction

Present study is part of a grand research program to characterise the Zn-containing copper smelting slag under conditions relevant to the industrial copper smelter operations. Previous studies have been focused on the ZnO-"FeO"-SiO_2 system[1] and ZnO-"FeO"-SiO_2-Al_2O_3 system[2] at oxygen partial pressure (Po_2) fixed at 10^{-8} atm. Major differences on the liquidus temperatures and phase relations were observed in the previous studies when comparing to those results obtained under iron-saturation, as well as FactSage predictions. With an aim to explore the effect of MgO on the liquidus temperature and phase relations of the Zn-containing slag systems, current experimental work will focus on phase equilibria study of ZnO-"FeO"-SiO_2-MgO system at Po_2 10^{-8} tam.

MgO is commonly present in the pyrometallurgical slags which may be introduced through feeding materials or consumption of refractory linings. Although MgO in these slags are relatively low in quantity[3], its significant effect on the liquidus temperature had been reported in the literatures.[4, 5] Previous studies on the phase equilibria of system ZnO-"FeO"-SiO2-MgO and subsystems had been widely investigated by various researchers. Bowen *et al*[6] experimentally determined the phase diagram of MgO-"FeO"-SiO_2 system under metallic iron saturation. Muan[7] carried out phase equilibria studies on the same system at a broad range of Po_2 ($10^{-6.5}$ to $10^{-10.5}$ atm) controlled by CO_2 and H_2. Significant differences on liquidus temperatures and phase relations from previous studies were observed as the Po_2 varied. Wu *et*

al[8] conducted a thermodynamic evaluation on the MgO-"FeO"-SiO_2 system in metallic iron saturation. Sarver and Hummel[9] investigated the sub-solidus equilibria on willimite-forsterite (Zn_2SiO_4 - Mg_2SiO_4) join with temperature varying from 1123 K (850 °C) to 1743 K (1470 °C). Segnit and Holland[10] investigated the MgO-ZnO-SiO_2 system by quenching method using platinum crucible. Hansson[11] *et al* carried out phase equilibrium studies on the Fe-Mg-Zn-O system at sub-solidus temperature in air, and extensive solid solutions were determined in their study. Jung *et al*[12] thermodynamically evaluated and optimized the FeO-Fe_2O_3-MgO-SiO_2 system under a variety of Po_2.

Only limited information on the MgO-bearing copper smelting slags was found in literatures. Zhao *et al*[5] experimentally investigated the zinc-free, Al_2O_3-MgO-CaO-"FeO"-SiO_2 system under the metallic iron saturation. A further study on the ZnO-Al_2O_3-MgO-CaO-"FeO"-SiO_2 system was carried out by same authors[4] under metallic iron saturation. Both studies in the metallic iron saturation indicated that the MgO could significantly increases the liquidus temperatures. However, no study on the ZnO-"FeO"-SiO_2-MgO system has been experimentally determined at Po_2 10^{-8} tam. For this reason, present studies will focus on the system ZnO-"FeO"-SiO_2-MgO at Po_2 10^{-8} tam.

7.2 Experimental

The detailed experimental procedures used in present study had been adopted by present authors in the previous papers.[1, 2] Briefly, two master slags, zinc silicate master slag and iron silicate master slag, were firstly prepared. When preparing the starting mixture, the desired magnesia (MgO) was mixed with iron-silicate master slag and zinc-silicate master slag using agate mortar and pestle. After pelletising, the mixture (around 0.15 g) was placed in a suitable container. SiO_2 substrates were used for the experiments in SiO_2 primary phase field, and platinum baskets were used in spinel, olivine and willemite primary phase fields. The mixture was then suspended in the hot-zone of reaction tube with the CO_2/CO passing through to maintain Po_2 at 10^{-8} atm to attain final equilibrium. After equilibration, the sample was quenched into ice water. The quenched samples were then mounted in epoxy resin, polished and cleaned for further analyses.

A JXA 8200 Electron Probe Micro-analyser equipped with wavelength-dispersive X-ray spectroscopy (Japan Electron Optics Ltd) was applied to the examinations of microstructures and quantitative measurements of the phase compositions. The working voltage and probe current were 15 kV and 15 nA respectively. The standards used for the analysis were from

Charles M. Taylor Co. (Stanford, California): Fe_2O_3 for Fe, MgO for Mg and $CaSiO_3$ for Si, and Micro-Analysis Consultant Ltd (Cambridge, UK): ZnO for Zn. The ZAF correction procedure supplied with the EPMA was applied. Although Fe^{2+} and Fe^{3+} are both present in the quenched samples, only metal cation concentrations can be measured by EPMA. Therefore, all the iron was recalculated to "FeO" for presentation purpose only.

7.3 Results and Discussion

In the present study, the phase relations and liquidus temperatures of the system ZnO-"FeO"-SiO_2-MgO were experimentally determined with MgO content varying from 2 to 6 wt pct between 1523 K (1250 °C) and 1573 K (1300 °C) under Po_2 fixed at 10^{-8} atm. It was found that five primary phase fields are present in the composition range investigated, including spinel, wüstite, olivine, SiO_2 and willemite. Figure 7.1 shows the typical microstructures of quenched samples with two or three phases in equilibrium. Figure 7.1 (A) shows the liquid in equilibrium with spinel. Figure 7.1 (B) shows the equilibration of liquid with SiO_2. Figure 7.1 (C) shows the equilibrium between liquid and willemite. Figure 7.1 (D) shows the liquid was in equilibrium with wüstite. Figure 7.1 (E) shows the equilibrium between liquid and olivine. Figure 7.1 (F) shows the liquid was equilibrated with both spinal and willemite. Figure 7.1 (G) shows the coexisting of spinel, olivine and liquid under equilibration. Figure 7.1 (H) shows the liquid phase was equilibrated with spinel, olivine and willemite.

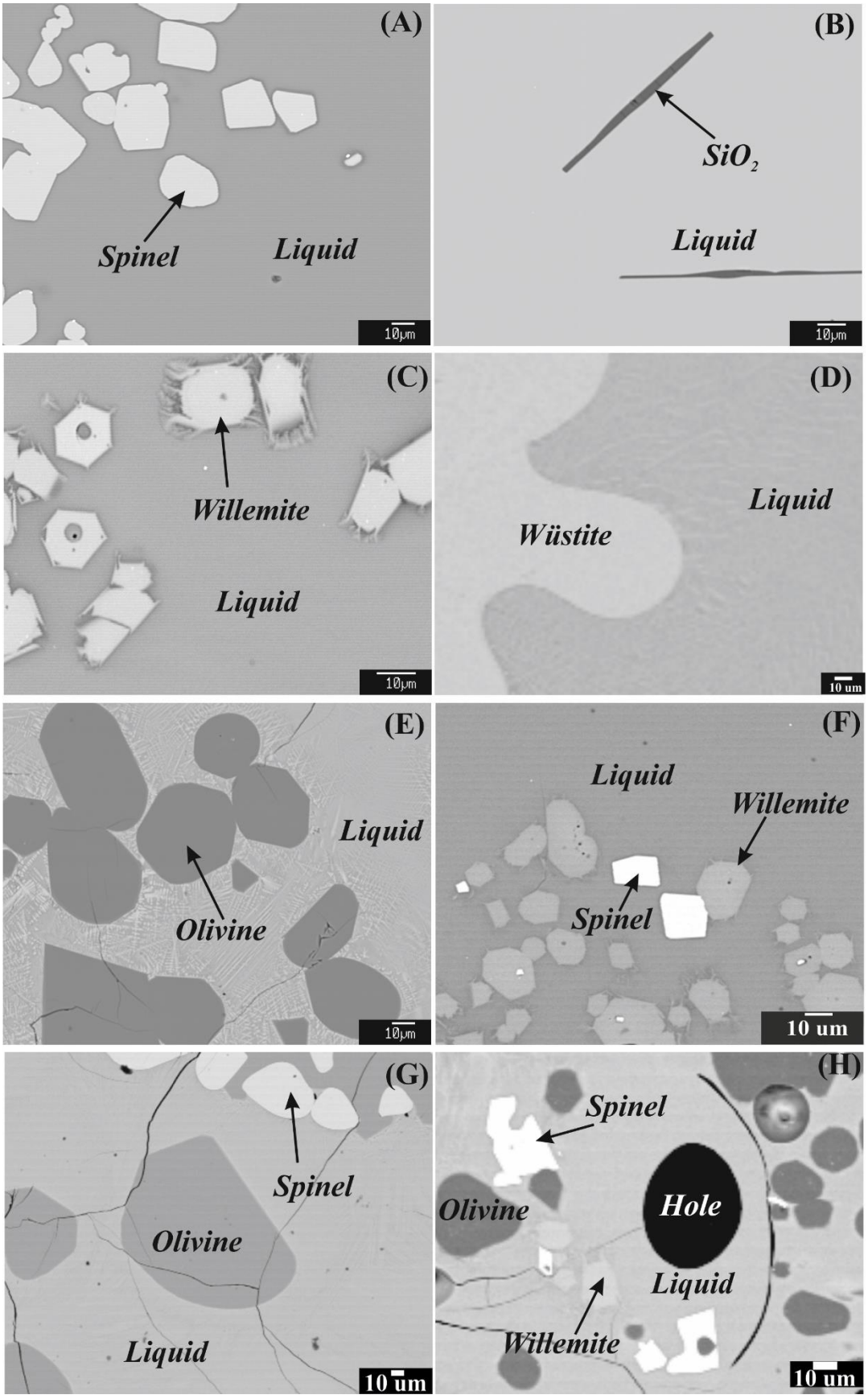

Figure 7.1 Microstructures of quenched samples showing liquid in equilibrium with, (A) - Spinel, (B) - SiO_2, (C) - Willemite, (D) - Wüstite, (E) - Olivine, (F) - Spinel and Willemite, (G) - Spinel and Olivine and (H) - Spinel, Olivine and Willimite at Po_2 10^{-8} atm

The normalized EPMA measurements of the phases in quenched samples are listed in Table 7.1 through Table 7.3. It is noticed that the spinel forms extensive solid solutions which can be commonly present as $(Fe^{2+},Zn,Mg)O•(Fe^{3+}{}_2O_3)$[4], with a maximum 0.8 wt pct of SiO_2 present. Meanwhile, the maximum solubility of "FeO" in the SiO_2 phase (tridymite) was determined to be 1.1 wt pct. The compositions of spinel, willemite and olivine that form extensive solid solution were directly measured by EPMA, of which the information are particularly important for the thermodynamic modelling. As the copper smelter generally operates under conditions that approaching spinel saturation, hence, further discussion will focus on partitioning behaviour of ZnO and MgO between spinel and liquid phases.

Table 7.1 Experimental determined phases compositions in the ZnO-"FeO"-SiO_2-MgO system at 1523 K (1250 °C) under Po_2 10^{-8} atm

Experiment No.	Temperature [K (°C)]	Phase	Composition (Wt Pct)			
			ZnO	SiO_2	"FeO"	MgO
488	1523 (1250)	Liquid	0.0	25.8	72.0	2.2
		Spinel	0.0	0.7	98.6	0.7
489	1523 (1250)	Liquid	7.4	34.4	55.8	2.4
		Spinel	3.6	0.5	95.3	0.5
550	1523 (1250)	Liquid	5.6	34.1	58.5	1.8
		Spinel	2.7	0.6	96.2	0.4
558	1523 (1250)	Liquid	4.5	34.3	58.6	2.6
		Spinel	2.2	0.3	96.9	0.6
579	1523 (1250)	Liquid	13.9	36.1	47.5	2.5
		Spinel	7.2	0.5	91.8	0.6
505	1523 (1250)	Liquid	9.2	33.5	53.9	3.5
		Spinel	4.5	0.5	94.1	0.9
525	1523 (1250)	Liquid	0.0	26.4	70.5	3.1
		Spinel	0.0	0.8	98.2	1.0
551	1523 (1250)	Liquid	0.0	26.1	70.5	3.4
		Spinel	0.0	0.8	98.3	0.9
560	1523 (1250)	Liquid	15.8	37.5	42.6	4.0
		Spinel	9.3	0.4	89.4	1.0
693	1523 (1250)	Liquid	6.7	35.2	53.4	4.6
		Spinel	3.3	0.5	95.1	1.1
723	1523 (1250)	Liquid	6.3	34.5	54.8	4.4
		Spinel	2.9	0.3	95.8	1.0
491	1523 (1250)	Liquid	7.8	34.2	52.8	5.3
		Spinel	3.6	0.4	94.6	1.3
562	1523 (1250)	Liquid	14.7	38.4	41.3	5.7
		Spinel	8.3	0.4	89.9	1.5
580	1523 (1250)	Liquid	14.0	37.4	42.4	6.2
		Spinel	7.8	0.4	90.3	1.5
692	1523 (1250)	Liquid	6.5	35.5	52.1	5.9
		Spinel	2.9	0.4	95.2	1.5
		Olivine	4.1	33.5	41.9	20.5
490	1523 (1250)	Liquid	11.8	35.2	50.9	2.2
		SiO_2	0.3	98.6	1.1	0.0
548	1523 (1250)	Liquid	0.0	37.9	60.3	1.7

Experiment No.	Temperature [K (°C)]	Phase	Composition (Wt Pct)			
			ZnO	SiO_2	"FeO"	MgO
		SiO_2	0.0	99.1	0.9	0.0
549	1523 (1250)	Liquid	9.1	36.8	52.0	2.1
		SiO_2	0.2	98.8	0.9	0.0
508	1523 (1250)	Liquid	13.9	37.7	44.3	4.2
		SiO_2	0.4	98.6	1.0	0.0
543	1523 (1250)	Liquid	0.1	40.0	55.8	4.2
		SiO_2	0.0	99.3	0.7	0.0
658	1523 (1250)	Liquid	6.4	37.8	51.7	4.1
		SiO_2	0.1	99.4	0.6	0.0
492	1523 (1250)	Liquid	12.6	39.0	42.1	6.3
		SiO_2	0.3	98.8	0.9	0.0
510	1523 (1250)	Liquid	11.9	39.4	42.5	6.3
		SiO_2	0.3	98.9	0.8	0.0
544	1523 (1250)	Liquid	0.0	41.7	52.5	5.8
		SiO_2	0.0	99.3	0.7	0.0
659	1523 (1250)	Liquid	5.9	39.5	48.8	5.8
		SiO_2	0.1	99.0	0.8	0.0

Table 7.2 Experimental determined phases compositions in the ZnO-"FeO"-SiO_2-MgO system at 1543 K (1270 °C) under Po_2 10^{-8} atm

Experiment No.	Temperature [K (°C)]	Phase	Composition (Wt Pct)			
			ZnO	SiO_2	"FeO"	MgO
605	1543 (1270)	Liquid	25.6	37.3	31.0	6.1
655	1543 (1270)	Liquid	26.6	36.5	32.9	4.1
721	1543 (1270)	Liquid	26.8	36.4	32.4	4.4
788	1543 (1270)	Olivine	0.0	34.3	46.8	18.8
		Spinel	0.0	0.7	97.9	1.4
373	1543 (1270)	Liquid	0.0	20.9	77.0	2.0
		Spinel	0.0	0.7	98.5	0.8
493	1543 (1270)	Liquid	10.2	32.3	55.6	1.9
		Spinel	5.0	0.4	94.1	0.5
514	1543 (1270)	Liquid	8.9	33.3	53.4	4.4
		Spinel	4.3	0.4	94.2	1.1
513	1543 (1270)	Liquid	8.3	34.3	51.1	6.3
		Spinel	4.2	0.5	93.7	1.6
516	1543 (1270)	Liquid	0.0	21.5	76.7	1.8
		Spinel	0.0	0.6	98.7	0.7
522	1543 (1270)	Liquid	0.0	22.4	74.2	3.3
		Spinel	0.0	0.7	97.9	1.4
554	1543 (1270)	Liquid	4.4	30.7	62.9	2.1
		Spinel	2.0	0.5	97.0	0.6
699	1543 (1270)	Liquid	6.3	33.0	55.3	5.3
		Spinel	3.1	0.5	95.0	1.4
568	1543 (1270)	Liquid	4.6	32.6	57.5	5.3
		Spinel	2.2	0.4	96.1	1.3
569	1543 (1270)	Liquid	19.2	35.8	40.5	4.5
		Spinel	11.1	0.4	87.3	1.2
570	1543 (1270)	Liquid	19.6	36.6	36.8	7.0
		Spinel	11.4	0.4	86.2	1.9
719	1543 (1270)	Liquid	9.6	33.1	53.5	3.8
		Spinel	5.2	0.5	93.3	1.0

Experiment No.	Temperature [K (°C)]	Phase	Composition (Wt Pct)			
			ZnO	SiO_2	"FeO"	MgO
720	1543 (1270)	Liquid	20.2	34.7	41.1	4.0
		Spinel	11.1	0.4	87.5	1.1
841	1543 (1270)	Liquid	19.3	34.9	40.3	5.4
		Spinel	10.8	0.4	87.4	1.4
638	1543 (1270)	Liquid	29.5	36.0	30.3	4.1
		Willemite	54.6	29.2	10.8	5.4
654	1543 (1270)	Liquid	30.8	36.3	30.7	2.2
		Willemite	57.1	29.4	10.7	2.9
656	1543 (1270)	Liquid	26.9	37.1	29.9	6.1
		Willemite	50.3	30.5	10.7	8.4
696	1543 (1270)	Liquid	27.3	38.7	27.8	6.3
		Willemite	42.5	34.2	9.8	13.5
722	1543 (1270)	Liquid	27.0	38.2	28.8	6.0
		Willemite	51.5	30.0	10.7	7.8
380	1543 (1270)	Liquid	0.0	38.7	59.3	2.0
		SiO_2	0.0	99.2	0.7	0.0
381	1543 (1270)	Liquid	0.0	39.2	57.6	3.2
		SiO_2	0.0	99.1	0.9	0.0
382	1543 (1270)	Liquid	0.0	39.2	57.6	3.2
		SiO_2	0.0	99.1	0.9	0.0
515	1543 (1270)	Liquid	14.5	39.2	40.0	6.4
		SiO_2	0.4	98.7	0.9	0.0
536	1543 (1270)	Liquid	0.0	38.7	58.9	2.3
		SiO_2	0.0	99.3	0.7	0.0
564	1543 (1270)	Liquid	0.2	41.5	53.0	5.3
		SiO_2	0.3	98.7	1.0	0.0
537	1543 (1270)	Liquid	16.0	38.0	41.8	4.2
		SiO_2	0.4	98.6	1.0	0.0
538	1543 (1270)	Liquid	14.6	39.6	39.6	6.2
		SiO_2	0.5	98.7	0.8	0.0
545	1543 (1270)	Liquid	0.0	40.6	55.3	4.0
		SiO_2	0.1	98.9	1.0	0.0
546	1543 (1270)	Liquid	0.0	42.1	51.9	6.0
		SiO_2	0.0	99.0	0.9	0.0
565	1543 (1270)	Liquid	11.1	40.3	41.7	6.9
		SiO_2	0.3	98.7	0.9	0.0
573	1543 (1270)	Liquid	13.7	37.7	46.1	2.5
		SiO_2	0.3	98.8	0.8	0.0
660	1543 (1270)	Liquid	6.4	40.0	47.9	5.6
		SiO_2	0.1	98.9	0.9	0.0
694	1543 (1270)	Liquid	8.5	37.3	51.9	2.3
		SiO_2	0.1	99.0	1.0	0.0
695	1543 (1270)	Liquid	8.6	38.9	48.7	3.8
		SiO_2	0.1	99.1	0.8	0.0
602	1543 (1270)	Liquid	29.9	34.5	33.3	2.2
		Willemite	55.2	29.2	12.5	3.1
		Spinel	16.9	0.3	82.3	0.5
603	1543 (1270)	Liquid	27.8	34.7	33.6	3.9
		Willemite	52.6	29.9	12.0	5.5
		Spinel	16.1	0.3	82.6	1.1

Table 7.3 Experimental determined phases compositions in the ZnO-"FeO"-SiO_2-MgO system at 1573 K (1300 °C) under Po_2 10^{-8} atm

Experiment No.	Temperature [K (°C)]	Phase	Composition (Wt Pct)			
			ZnO	SiO_2	"FeO"	MgO
578	1573 (1300)	Liquid	25.3	33.7	35.7	5.4
685	1573 (1300)	Liquid	0.0	21.7	74.6	3.7
494	1573 (1300)	Liquid	15.3	30.3	52.8	1.7
		Spinel	8.0	0.4	91.1	0.5
517	1573 (1300)	Liquid	13.4	29.8	53.2	3.6
		Spinel	6.4	0.4	92.1	1.1
518	1573 (1300)	Liquid	9.5	30.5	54.4	5.6
		Spinel	5.2	0.4	92.7	1.6
523	1573 (1300)	Liquid	0.1	19.4	77.4	3.1
		Spinel	0.1	0.7	96.5	2.8
531	1573 (1300)	Liquid	25.4	31.6	39.0	4.0
		Spinel	14.0	0.5	84.3	1.2
532	1573 (1300)	Liquid	26.2	30.9	36.7	6.2
		Spinel	14.0	0.4	83.7	1.9
567	1573 (1300)	Liquid	0.0	20.1	75.9	4.0
		Spinel	0.0	0.7	96.4	2.9
574	1573 (1300)	Liquid	9.5	28.6	60.3	1.5
		Spinel	5.0	0.5	94.0	0.5
575	1573 (1300)	Liquid	4.9	27.9	62.7	4.5
		Spinel	2.7	0.5	95.4	1.4
576	1573 (1300)	Liquid	6.5	27.8	59.7	6.1
		Spinel	2.9	0.4	94.8	1.8
577	1573 (1300)	Liquid	17.5	31.2	45.4	5.9
		Spinel	9.8	0.3	88.0	1.8
604	1573 (1300)	Liquid	6.0	27.4	63.8	2.7
		Spinel	3.0	0.5	95.7	0.8
606	1573 (1300)	Liquid	6.0	27.8	62.3	3.9
		Spinel	3.1	0.5	95.2	1.2
619	1573 (1300)	Liquid	8.5	27.9	61.6	2.0
		Spinel	4.3	0.4	94.6	0.7
620	1573 (1300)	Liquid	1.8	21.1	74.7	2.4
		Spinel	0.8	0.5	97.7	1.0
843	1573 (1300)	Liquid	29.8	30.2	38.2	1.7
		Spinel	16.3	0.3	82.9	0.5
765	1573 (1300)	Liquid	0.0	19.9	76.1	4.0
		Olivine	0.0	34.6	41.9	23.5
511	1573 (1300)	Liquid	0.0	17.0	81.2	1.8
		Wüstite	0.0	0.6	97.9	1.5
497	1573 (1300)	Liquid	17.1	37.5	43.6	1.9
		SiO_2	0.5	98.5	1.0	0.0
519	1573 (1300)	liquid	15.5	38.3	41.9	4.3
		SiO_2	0.4	98.6	1.0	0.0
520	1573 (1300)	Liquid	18.6	40.9	34.0	6.5
		SiO_2	0.6	98.6	0.9	0.0
533	1573 (1300)	Liquid	0.0	40.2	57.5	2.3
		SiO_2	0.0	98.9	1.1	0.0
534	1573 (1300)	liquid	0.0	41.6	54.0	4.3
		SiO_2	0.0	99.1	0.8	0.0
547	1573 (1300)	Liquid	0.1	42.7	51.6	5.6

Experiment No.	Temperature [K (°C)]	Phase	Composition (Wt Pct)			
			ZnO	SiO_2	"FeO"	MgO
		SiO_2	0.0	99.2	0.8	0.0
622	1573 (1300)	Liquid	6.5	38.0	53.7	1.8
		SiO_2	0.1	99.2	0.6	0.0
663	1573 (1300)	Liquid	5.8	41.1	47.2	5.9
		SiO_2	0.1	99.1	0.8	0.0
697	1573 (1300)	Liquid	9.0	39.6	47.3	4.1
		SiO_2	0.2	99.1	0.8	0.0
698	1573 (1300)	Liquid	6.7	37.9	53.2	2.3
		SiO_2	0.1	99.0	0.9	0.0
844	1573 (1300)	Liquid	23.0	38.0	36.9	2.2
		SiO_2	0.5	98.9	0.7	0.0
845	1573 (1300)	Liquid	24.8	39.1	32.0	4.1
		SiO_2	0.8	98.4	0.7	0.0
593	1573 (1300)	Liquid	30.1	33.4	32.2	4.4
		Willemite	52.9	30.1	11.0	6.0
595	1573 (1300)	Liquid	25.2	34.0	32.5	8.3
		Willemite	46.0	31.2	11.7	11.1
621	1573 (1300)	Liquid	33.6	32.5	32.1	1.8
		Willemite	57.9	29.2	10.4	2.4
657	1573 (1300)	Liquid	29.2	38.1	26.6	6.1
		Willemite	52.0	30.4	9.5	8.1
842	1573 (1300)	Liquid	36.3	29.2	3.7	30.9
		Willemite	29.4	10.2	4.7	55.7
662	1573 (1300)	Liquid	0.0	20.2	76.0	3.8
		Wüstite	0.0	0.7	96.3	3.0
		Olivine	0.0	34.5	42.6	22.9
690	1573 (1300)	Liquid	0.0	20.2	76.0	3.8
		Wüstite	0.0	0.7	96.3	3.0
		Olivine	0.0	34.5	42.6	22.9
496	1573 (1300)	Liquid	7.5	31.0	54.4	7.1
		Spinel	3.9	0.5	93.5	2.1
		Olivine	4.5	17.5	70.7	7.3
524	1573 (1300)	Liquid	0.0	20.4	75.4	4.1
		Spinel	0.0	0.7	96.1	3.2
		Olivine	0.1	34.8	42.2	22.9
607	1573 (1300)	Liquid	32.3	30.8	34.8	2.0
		Willemite	55.3	29.3	11.6	3.8
		Spinel	18.3	0.3	80.8	0.6
608	1573 (1300)	Liquid	27.9	32.5	33.5	6.1
		Willemite	49.9	30.4	11.3	8.5
		Spinel	16.4	0.4	81.5	1.8
596	1573 (1300)	Liquid	24.7	34.2	31.8	9.2
		Spinel	14.8	0.4	82.0	2.9
		Olivine	15.8	35.6	20.2	28.5
		Willemite	44.7	31.6	11.0	12.7

The normalized EPMA measurements of the liquid phase were used to construct the liquidus surfaces at fixed MgO content in the liquid phase of the ZnO-"FeO"-SiO_2-MgO system at Po_2 10^{-8} atm, as illustrated Figure 7.2. Some of the measured MgO concentrations in liquid phase were deviated from the target values and they were not used in constructing the liquidus

surfaces. However, these results can still be useful for the thermodynamical modelling. As shown in Figure 7.3 to Figure 7.5, the thin solid lines are experimentally determined isotherms, while the thin dash lines are hypothetical isotherms. The thick solid lines in the figures represent the experimentally determined boundaries and the thick dash lines indicate the boundaries in the areas where there is no experimental data.

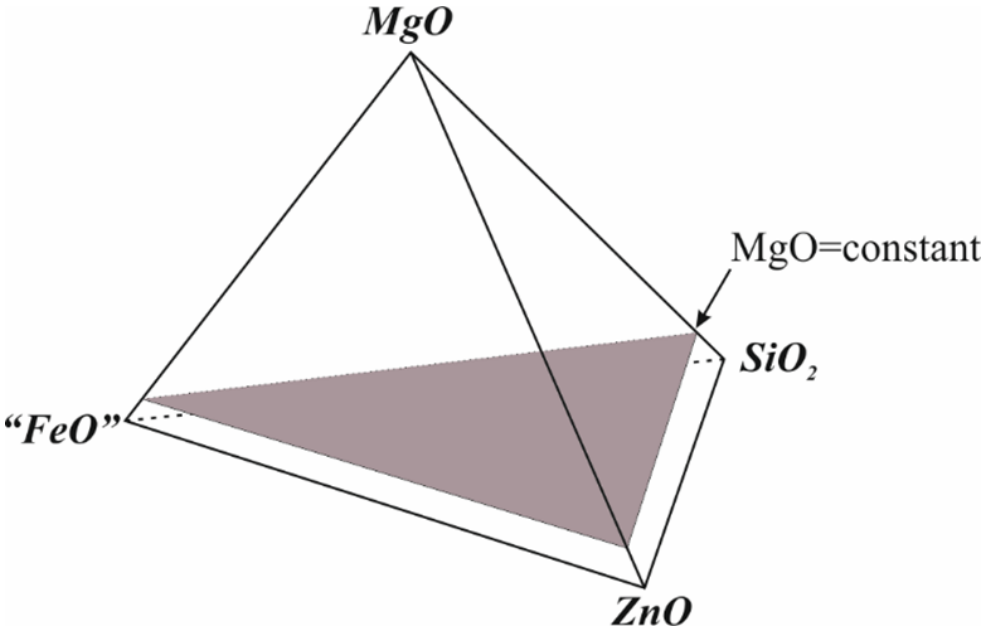

Figure 7.2 Pseudo-ternary section in the MgO-ZnO-"FeO"-SiO_2 system at constant MgO content in liquid under Po_2 10^{-8} atm

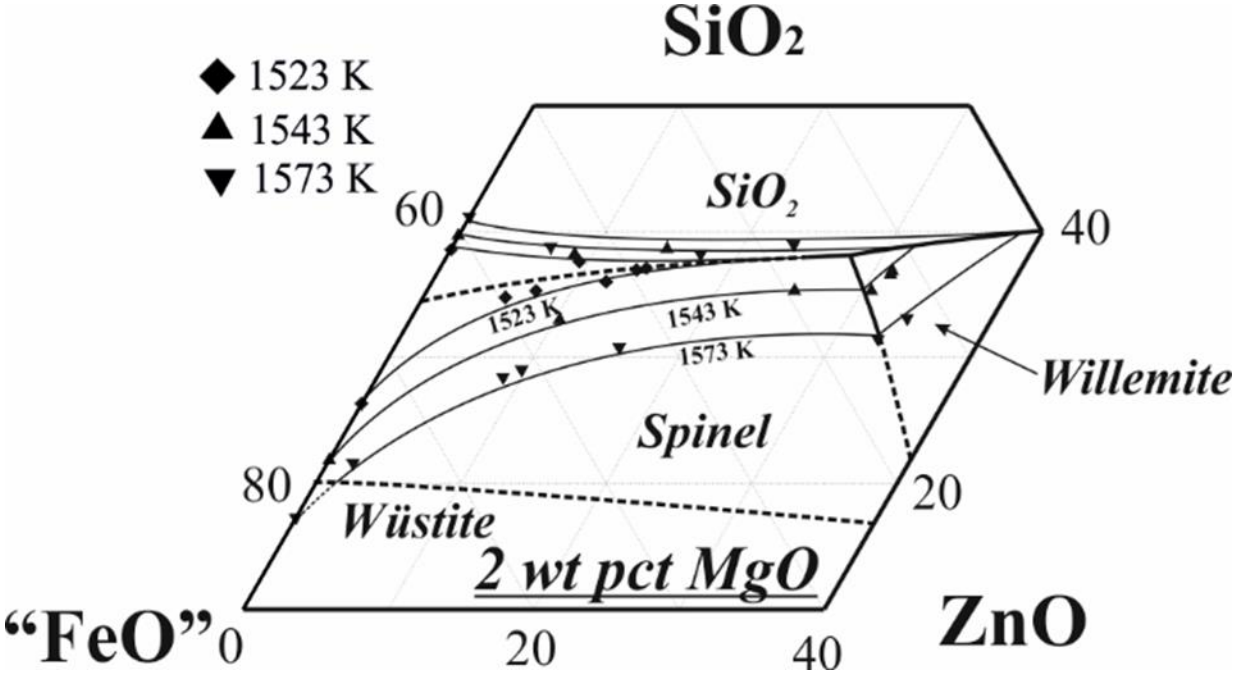

Figure 7.3 Summary of experimental data on the liquidus in the section, ZnO-"FeO"-SiO_2-MgO with 2 wt pct MgO in the liquid under Po_2 at 10^{-8} atm

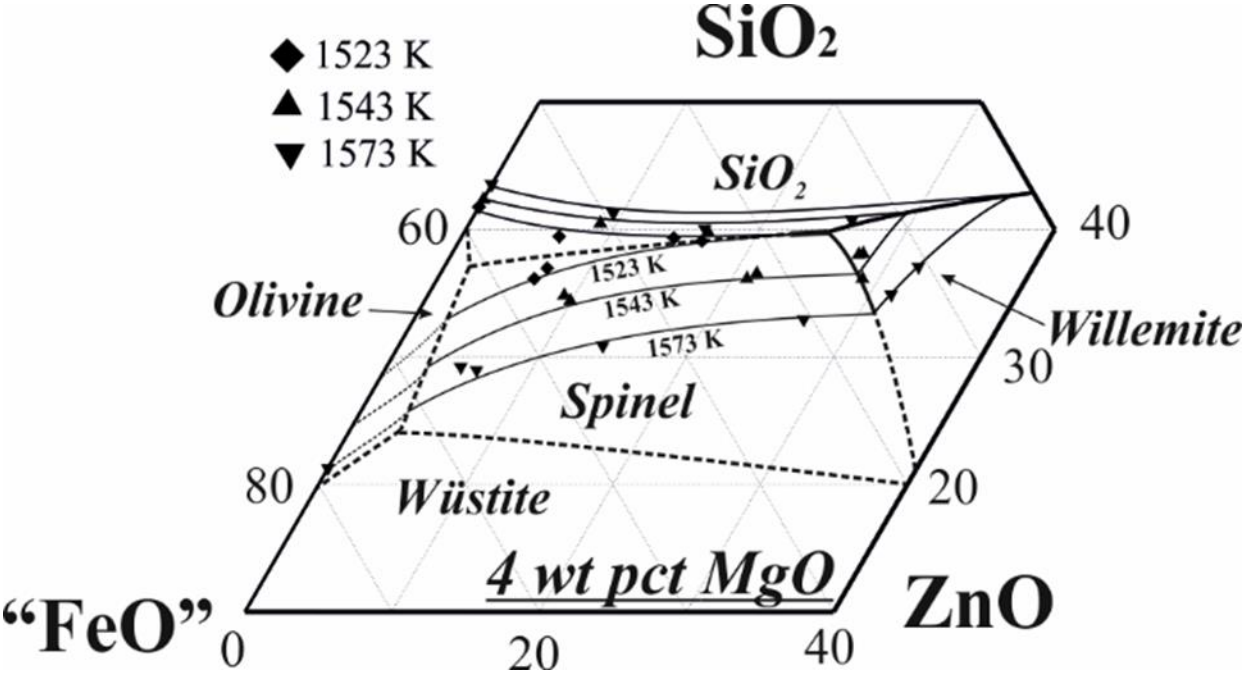

Figure 7.4 Summary of experimental data on the liquidus in the section, ZnO-"FeO"-SiO_2-MgO with 4 wt pct MgO in the liquid under Po_2 at 10^{-8} atm

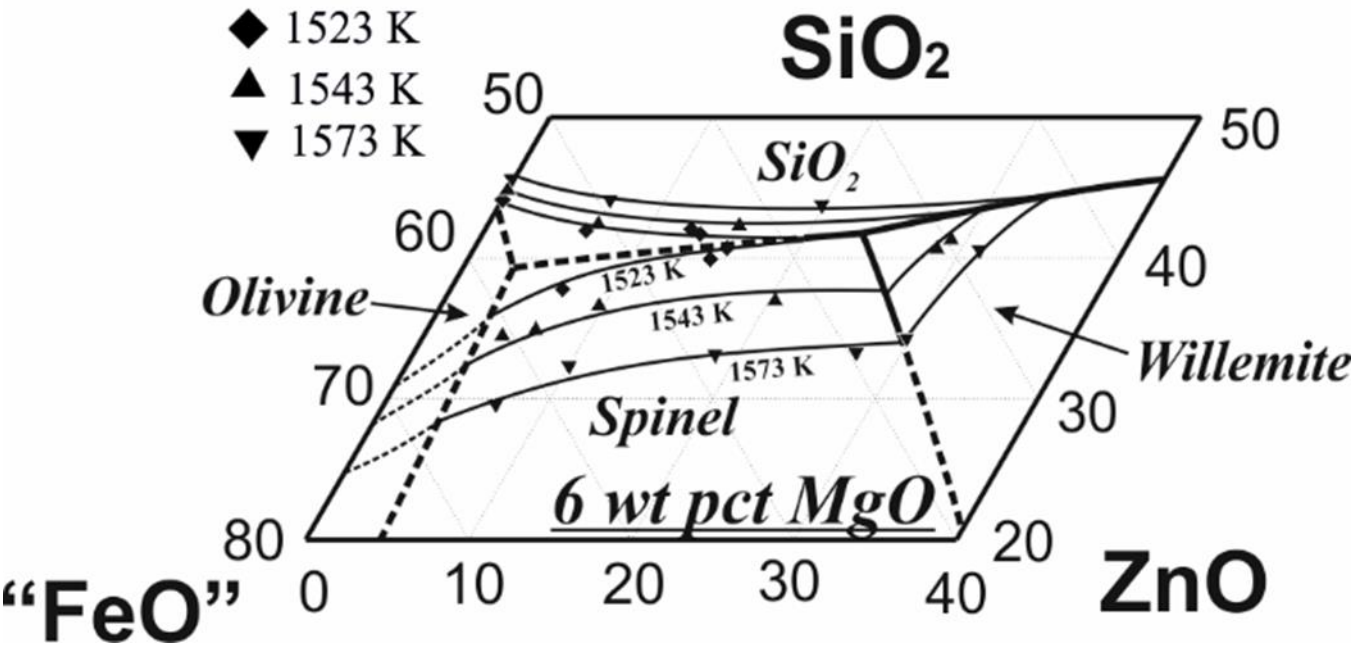

Figure 7.5 Summary of experimental data on the liquidus in the section, ZnO-"FeO"-SiO_2-MgO with 6 wt pct MgO in the liquid under Po_2 at 10^{-8} atm

7.3.1 Effect of MgO and ZnO content on the primary phase and liquidus temperature

By using present experimental results, the effect of MgO content on the phase relation and liquidus temperatures can be evaluated. Figure 7.6 shows the comparison of 1523 K (1250 °C) isotherm between present study, MgO-free[1] system and FactSage prediction[13] at Po_2 10^{-8} atm. It can be seen that spinel isotherm and SiO_2 isotherm are joined directly according to the

present results. Both spinel and SiO_2 isotherms move towards high- SiO_2 direction with increasing MgO in the liquid. In contrast, FactSage predicted that the spinel and SiO_2 isotherms at 1523 K (1250 °C) are joined through willemite isotherm. The full liquid area formed by the isotherms in different primary phase fields indicates the operation window of slag compositions at a given temperature. It can be seen that the full liquid area substantially decreases with increasing MgO content. Besides, the full liquid area with 2 wt pct MgO determined in the present study is smaller than that predicted by FactSage 6.2.[13] The results suggest that the database of FactSage 6.2 needs to be improved to correctly characterize the copper smelting slags.

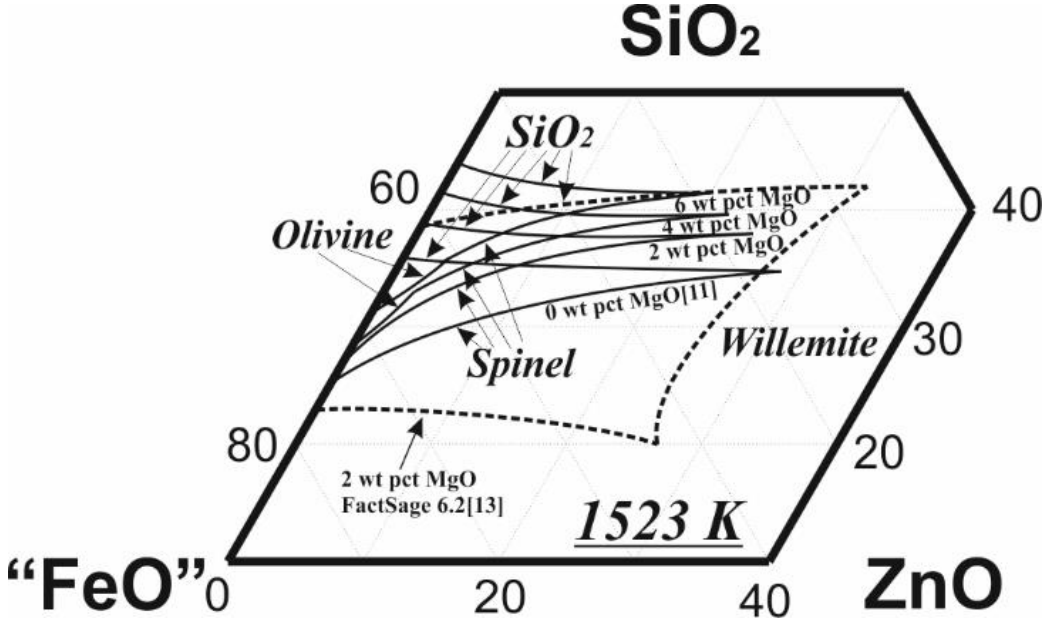

Figure 7.6 Liquidus surfaces at 1250 °C with varied MgO contents under Po_2 at 10^{-8} atm

For the convenience of applying present study to industrial operations, different types of pseudo-binary phase diagrams are constructed. Figure 7.7 shows the pseudo-binary ("FeO"+SiO_2)-ZnO with fixed Fe/SiO_2 = 1.3 (mass). The dash line indicates the liquidus in the olivine primary phase filed, and the dot-dash line shows the FactSage predictions with 2 wt pct MgO[13]. It can be seen that olivine primary phase field tends to show up at higher MgO content. A wide olivine primary phase field is predicted at 2 wt pct MgO by FactSage[13], but not observed in the present study. The liquidus temperatures increase in spinel phase filed with the increase of ZnO content in all MgO contents. The experimentally determined liquidus temperatures can be 80 degrees higher than that predicted by.

The impact of MgO on the liquidus temperatures in the spinel primary phase field is shown in Figure 7.8. It can be seen that an increase of the MgO content in slag will significantly

increase liquidus temperatures in the spinel phase field. For example, the liquidus temperature is increased by 30 K when MgO content increases from 0 to 2 wt pct at 10 wt pct ZnO.

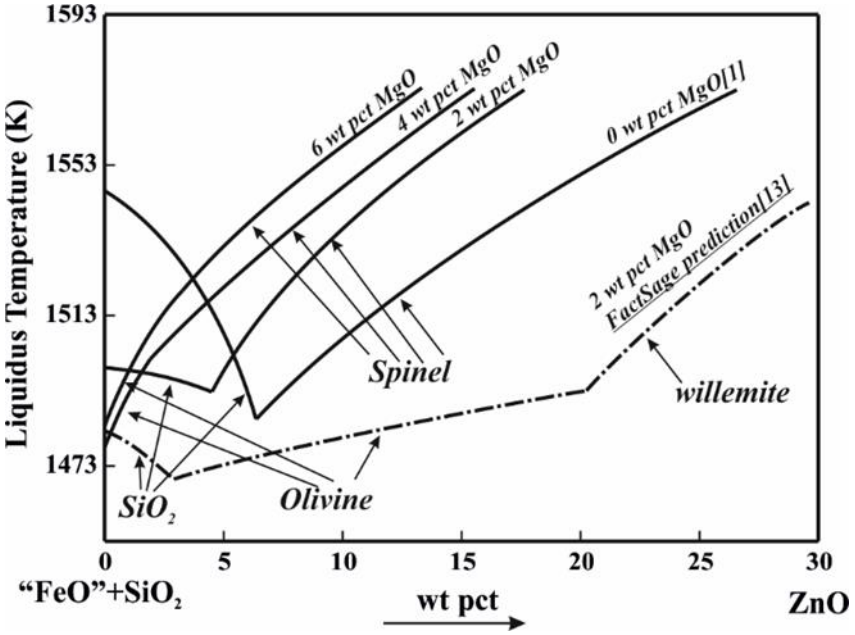

Figure 7.7 Comparisons of pseudo-binary ("FeO"+SiO_2)-ZnO at fixed Fe/SiO_2 = 1.3 (mass) between present study, MgO-free[1] and FactSage prediction[13] at $Po_2 10^{-8}$ atm

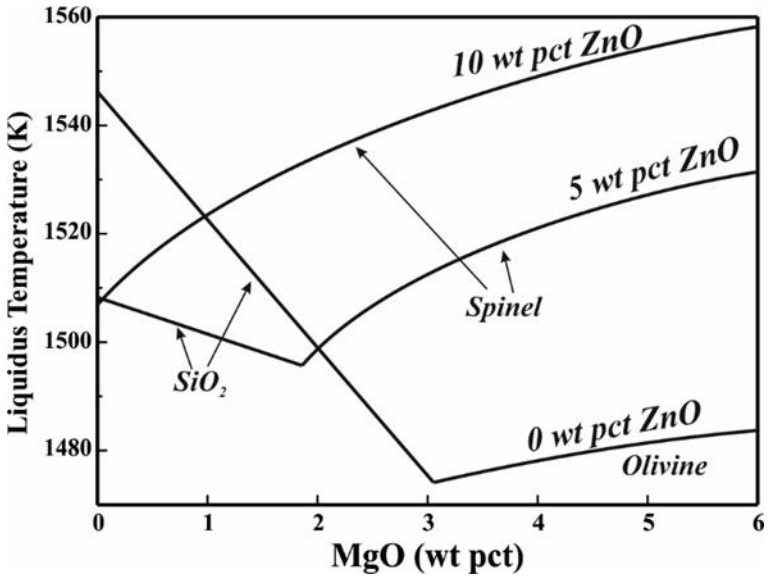

Figure 7.8 Liquidus temperature as function of magnesia (MgO) contents with varied ZnO content and Fe/SiO_2 = 1.3 (mass)

Figure 7.9 shows the comparisons of MgO and Al_2O_3 on the liquidus temperature at fixed Fe/SiO_2 = 1.3 under Po_2 10^{-8} atm. It can be seen that MgO and Al_2O_3 both increase the liquidus temperatures in the spinel primary phase field. It seems that liquidus temperatures in the spinel primary phase field of the ZnO-"FeO"-SiO_2-MgO system are generally higher than the ZnO-"FeO"-SiO_2-Al_2O_3 system[2], especially at low ZnO content. For instance, the liquid

temperature in MgO-containing system is about 13 K higher than that in the system ZnO-"FeO"-SiO_2-Al_2O_3 system[2] at 5 wt pct ZnO.

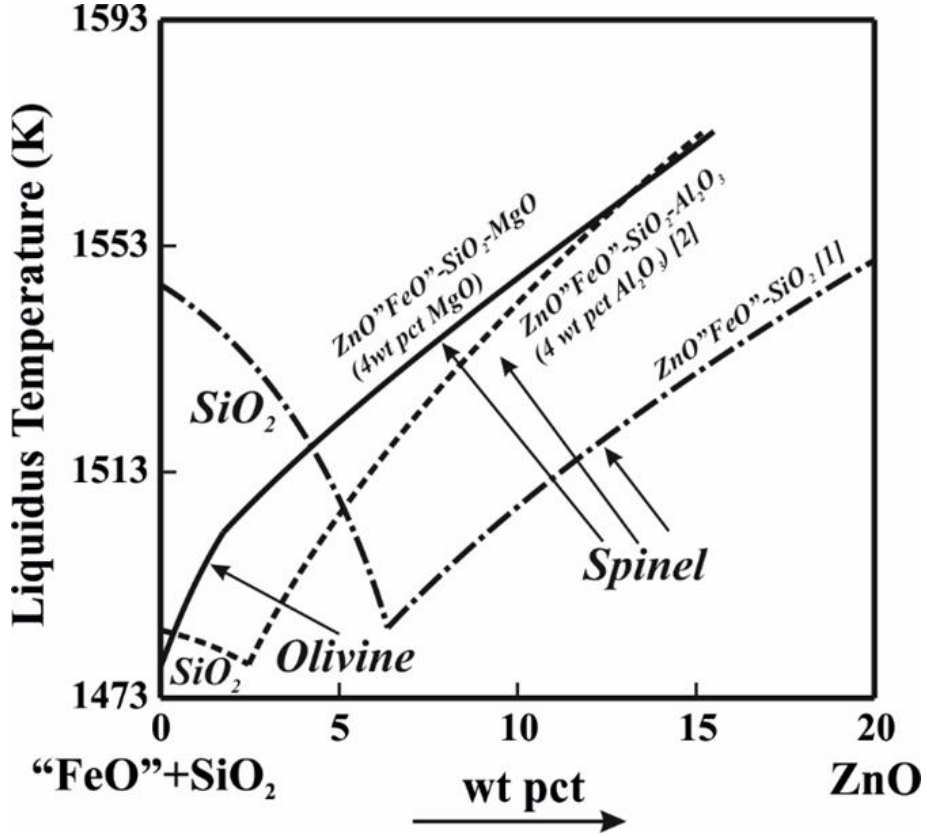

Figure 7.9 Comparisons of liquidus temperatures at fixed Fe/SiO_2 = 1.3 (mass) between present study (4 wt pct MgO), system ZnO-"FeO"-SiO_2-Al_2O_3 (4 wt pct Al_2O_3)[2] and system ZnO-"FeO"-SiO_2[1] at Po_2 10^{-8} atm

To evaluate the effect of fluxing condition (commonly represented by Fe/SiO_2 ratio in industrial practice) on the liquidus temperatures, pseudo-binary phase diagrams "FeO"-SiO_2 at fixed 5 wt pct ZnO and various MgO are constructed and shown the Figure 7.10. It can be seen that the liquidus temperatures continuously decrease in spinel phase field and increase dramatically in SiO_2 primary phase field with increasing SiO_2 concentration (decreasing Fe/SiO_2 ratio). For instance, the liquidus temperature is decreased by 50 K when the SiO_2 content increasing from 28 to 36 wt pct at 2 wt pct MgO. Figure 7.10 shows that the joint between spinel and silica primary phase fields moves towards low Fe/SiO_2 ratio when MgO in slag is increased. This means that more SiO_2 is required to keep the same liquidus temperature in the spinel primary phase field if MgO is present. For example, the MgO-free slag with 32 wt pct SiO_2 has a liquidus temperature 1513 K. However, when 6 wt pct MgO is present, the SiO_2 concentration needs to be increased to 41 wt pct to keep the same liquidus temperature for the slag. Clearly it can be seen that the experimental liquidus temperatures and phases

relations are significantly different from those predicted by FactSage[13] in primary phase and liquidus temperature.

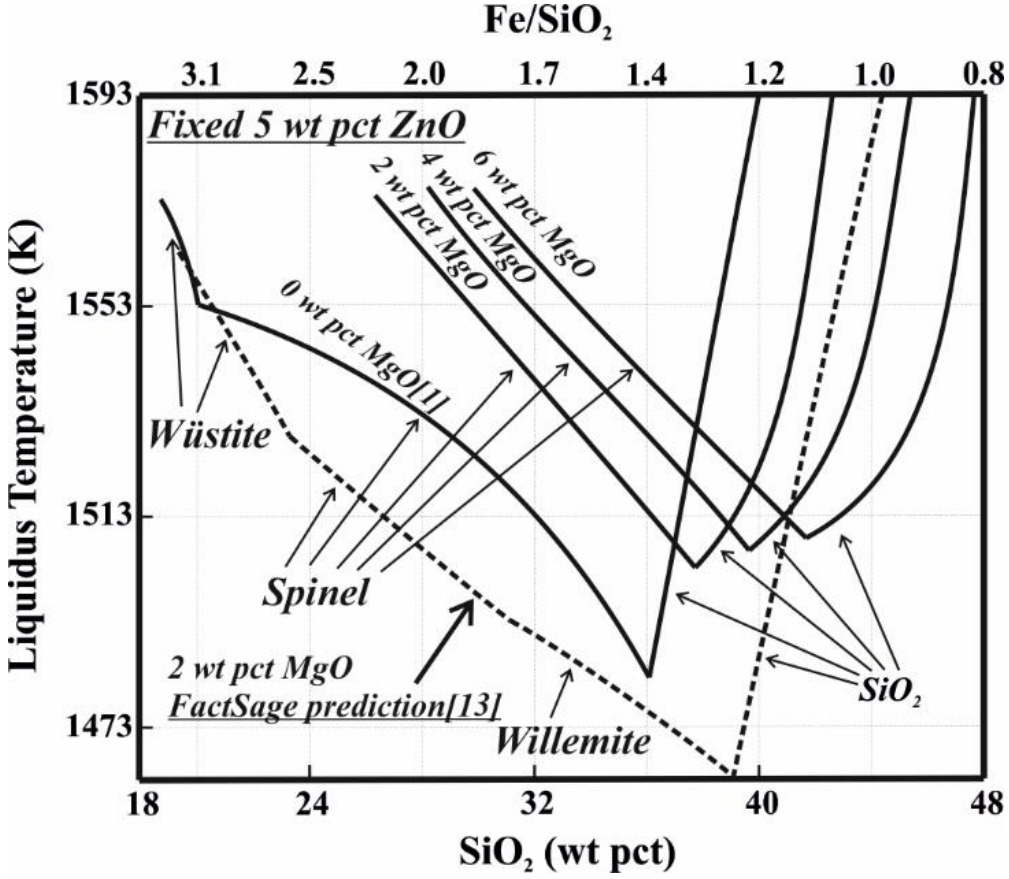

Figure 7.10 Pseudo-binary "FeO"-SiO_2 at fixed 5 wt pct ZnO under Po_2 at 10^{-8} atm from present study, MgO-fee system[1] and FactSage prediction[13]

7.3.2 Solid-liquid equilibria

Partitioning behaviour of slag components between the liquid phase and solid phase will provide useful information for development of thermodynamic modelling. One of the advantages by using EPMA technique approach is that the compositions of the solid phase that in equilibrium with the liquid phase can be measured in the same sample. By using the present experimental techniques, these information can be accurately obtained with high efficiency.

The spinel phase that commonly present in the copper smelting slags[3], forms extensive solid solution as shown in the Table 7.1 to Table 7.3, with formula $(Fe^{2+},Zn,Mg)O•Fe^{3+}{}_2O_3$[4]. Figure 7.11 shows the partitioning effect of ZnO between spinel and liquid phases from present study and MgO-free system[1] at Po_2 10^{-8} atm and also Zn-containing system under metallic iron saturation[4, 14-19]. It can be seen that the ZnO partitioning behaviour from the present study is similar to that in the MgO-free system[1] where quasi-linear relationship was observed. The ZnO concentration in the spinel from the ZnO-"FeO"-SiO_2-Al_2O_3 system[2] is slightly higher

than that in present study and MgO-free system[1] at the same ZnO content in the liquid. However, the ZnO concentrations in spinel phase are higher than those in the liquid phase under metallic iron saturation[4, 14-19]. For example, the ZnO concentrations in spinel at iron saturation are about 3.5 times higher than that obtained under Po_2 10^{-8} atm with 14 wt pct ZnO in the liquid.

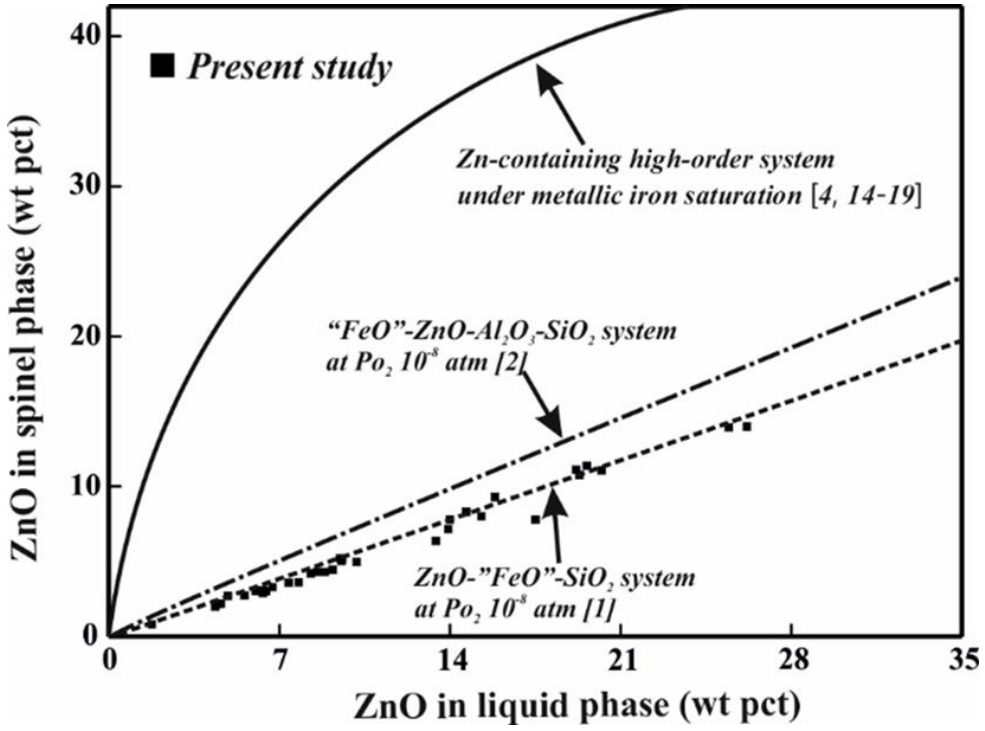

Figure 7.11 ZnO partitioning effect between spinel and liquid phases from present study, MgO-free system[1], ZnO-"FeO"-SiO_2-Al_2O_3 system[2] at Po_2 10^{-8} atm and Zn-containing high-order system under metallic iron saturation[4, 14-19]

Figure 7.12 shows the partitioning of MgO between spinel and liquid phases. As shown in Figure 7.12 (A), the MgO concentration in the spinel phase from the present study is much lower than that obtained at metallic iron saturation[4]. For instance, the MgO partitioning ratio ($\frac{MgO\ concentration\ in\ liquid}{MgO\ concentration\ in\ spinel}$) at metallic iron saturation[4] is about 5 times higher than that obtained in present study at Po_2 10^{-8} atm with 3.0 wt pct in the liquid. Moreover, as shown in the Figure 7.12 (B), the MgO partitioning coefficients from current study slightly increases with increasing equilibration temperature, which can be explained by an increasing on Gibbs Energy of Formation with temperature. The results obtained in present study will provide an insight to understand the interaction between Zn-containing copper smelting slags and the refractory linings in copper smelter where magnesia-chromite refractories are commonly used[20].

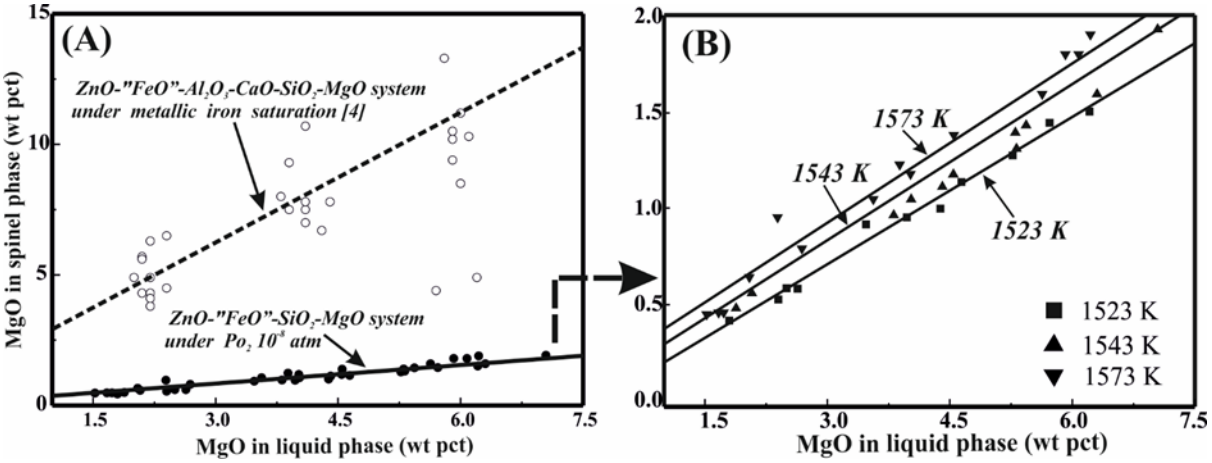

Figure 7.12 MgO partitioning effect between spinel and liquid phases, (A) - comparison between present study at Po_2 10^{-8} atm and Zn-containing high-order systems under metallic iron saturation[4]; (B) at varied equilibration temperature, 1523, 1543 and 1573 K

7.4 Summary

Phase equilibria and liquidus temperatures on the ZnO-"FeO"-SiO_2-MgO system with MgO content up to 6 wt pct have been experimentally determined at Po_2 10^{-8} atm which is directly relevant to copper smelting process. Spinel, SiO_2 and willemite are the major primary phase fields in the composition range investigated and wüstite is only observed at lower MgO content. The full liquid area continuously reduces with increasing MgO content from 2 to 6 wt pct. Besides, the liquidus temperatures in spinel primary phase field increase with increasing MgO content in the liquid phase. The ZnO concentration in liquid phase is higher than that in the spinel phase at Po_2 10^{-8} atm, and the MgO shows similar partitioning behaviour to that of ZnO. Present study will improve the understanding of phase equilibria for MgO- and ZnO-containing copper smelting slags under conditions relevant to the industrial practices.

7.5 References

1. H. Liu, Z. Cui, M. Chen and B. Zhao, *Metall. Mater. Trans. B*, 2016, vol. 47, pp. 164-173.

2. H. Liu, Z. Cui, M. Chen and B. Zhao, *Metall. Mater. Trans. B*, 2016, vol. 47, pp. 1113-1123.

3. B. Zhao, Z. Cui and Z. Wang, In *4th International Symposium on High-Temperature Metallurgical Processing*, (John Wiley & Sons, Inc.: 2013), p 10.

4. B. Zhao, P. C. Hayes and E. Jak, *Metall. Mater. Trans. B*, 2011, vol. 42, pp. 490-499.

5. B. Zhao, E. Jak and P. C. Hayes, *Metall. Mater. Trans. B*, 1999, vol. 30, pp. 1017-1026.

6. N. L. Bowen and J. F. Schairer, *Am. J. Sci.*, 1935, vol. 29, pp. 151-217.

7. A. Muan and E. F. Osborn, *J. Am. Ceram. Soc.*, 1956, vol. 39, pp. 121-40.

8. P. Wu, G. Eriksson, A. D. Pelton and M. Blander, *ISIJ Int.*, 1993, vol. 33, pp. 26-35.

9. J. F. Sarver and F. A. Hummel, *J. Am. Ceram. Soc.*, 1962, vol. 45, pp. 304-304.

10. E. R. Segnit and A. E. Holland, *J. Am. Ceram. Soc.*, 1965, vol. 48, pp. 409-413.

11. R. Hansson, P. C. Hayes and E. Jak, *Scand. J. Metall.*, 2004, vol. 33, pp. 355-361.

12. I.-H. Jung, S. Decterov and A. Pelton, *Metall. Mater. Trans. B*, 2004, vol. 35, pp. 877-889.

13. C. W. Bale, E. Bélisle, P. Chartrand, S. A. Decterov, G. Eriksson, K. Hack, I. H. Jung, Y. B. Kang, J. Melançon, A. D. Pelton, C. Robelin and S. Petersen, *CALPHAD: Comput. Coupling Phase Diagrams Thermochem.*, 2009, vol. 33, pp. 295-311.

14. B. Zhao, P. C. Hayes and E. Jak, *Int. J. Mater. Res.*, 2011, vol. 102, pp. 134-142.

15. B. Zhao, P. C. Hayes and E. Jak, *Int. J. Mater. Res.*, 2011, vol. 102, pp. 269-276.

16. B. Zhao, P. C. Hayes and E. Jak, *Metall. Mater. Trans. B*, 2011, vol. 42, pp. 978-986.

17. B. Zhao, P. C. Hayes and E. Jak, *Metall. Mater. Trans. B*, 2010, vol. 41, pp. 386-395.

18. B. Zhao, P. C. Hayes and E. Jak, *Metall. Mater. Trans. B*, 2010, vol. 41, pp. 374-385.

19. B. Zhao, P. C. Hayes and E. Jak, *Metall. Mater. Trans. B*, 2010, vol. 42, pp. 50-67.

20. A. Malfliet, S. Lotfian, L. Scheunis, V. Petkov, L. Pandelaers, P. T. Jones and B. Blanpain, *J. Eur. Ceram. Soc.*, 2014, vol. 34, pp. 849-876.

8 Phase Equilibria Study of the ZnO-"FeO"-SiO_2-CaO System at Po_2 10^{-8} atm

Abstract: Experimental investigations on the phase equilibria behaviours of the system ZnO-"FeO"-SiO_2-CaO system have been carried out with CaO content at 2, 4 and 6 wt pct CaO in the temperatures, 1543 (1250), 1543 (1270) and 1573 K (1300 °C) under Po_2 at 10^{-8} atm. The experimental techniques adopted in present study involve high-temperature equilibration, quenching and Electron Probe X-ray Microanalysis (EPMA). The results indicate that the liquidus temperatures increase in spinel primary phase field and decrease in the SiO_2 primary phase field when the CaO content in liquid phase increasing; the presence of sulphur in the slag phase, however, significantly decrease the liquidus temperature in the spinel phase field. The ZnO concentrations in the liquid phase is higher than that in the spinel phase. Results present in current study can be applied to improve the accuracy of FactSgae in predicting the copper smelting slags under intermediate Po_2.

Key words: phase equilibrium, copper smelting slag, ZnO-"FeO"-SiO_2-CaO, EPMA

8.1 Introduction

Present study is extend of the research project to characterise the slag chemistry of the Zn-containing copper smelting slags under conditions relevant to the industrial copper smelting operation. The system ZnO-"FeO"-SiO_2-CaO forms the basis of slag compositions in non-ferrous metals smelting.[1] In the copper smelting processes, the lime (CaO) was added to the charge as modulator of slag viscosity;[2, 3] meanwhile, appreciable amount of CaO also present in the flux. For these reasons, it is necessary to investigate its impact on the phase equilibria of Zn-containing smelting slags.

Limited phase equilibria studies on the ZnO-"FeO"-SiO_2-CaO system had been reported. Dobrotsvetov *et al*[4] firstly investigated the system along the join $CaFeSiO_4$ - Zn_2SiO_4 by applying DTA, microscopy, chemical analysis and XRD. A second study on the system was performed by Lenz and Lee[5] under the stream of 90 pct N_2, 5.2 pct CO_2 and 4.8 pct CO using DTA technique. Only liquidus temperatures were measured in the study without attempt to examine the phases after experiments. Jak *et al*[1, 6] conducted phase equilibrium studies in ZnO-"FeO"-(SiO_2 + CaO) system with varied CaO/SiO_2 ratio under metallic iron saturation by applying "pie-type" sample method[7]. Their results suggest that wüstite and fayalite are the primary phase fields at the "FeO-rich side, and the increase of CaO/SiO_2 will decrease the full liquid area in the 1523 K (1250 °C). Extensive experimental studies on the sub-system CaO-

ZnO-SiO_2 was conducted by Segnit[8] with temperatures ranging from 1433 K (1160 °C) to 1863 K (1590 °C) in platinum crucible. By using the quenching technique, the phase assemblages were examined by petrographic microscope. An assessment on the Ca-Fe-O-Si system was performed by Selleby[9] under air condition, CO_2 atmosphere and iron saturation respectively. An investigation on density and surface tension of CaO-FeO-Fe_2O_3-ZnO was performed by Pavol *et al*[10] at 1573 K (1300 °C) using maximum bubble pressure method under N_2 atmosphere. No liquidus information and phase relations were reported in their study. Apart from these studies, a numerous experimental works[11-17] have been carried out on the high order systems of ZnO-"FeO"-CaO-SiO_2 under metallic iron saturation which were reviewed in our previous papers[18, 19].

Although extensive studies[1, 6] had been performed on ZnO-"FeO"-SiO_2-CaO system under metallic iron saturation, there are no studies on the ZnO-"FeO"-SiO_2-CaO system have been experimentally performed at conditions close to that in the copper smelting process. Phase equilibria behaviours of the Zn-containing slags in our previous studies at Po_2 10^{-8} atm[18, 19] showed major differences with those obtained under iron-saturation or FactSage predictions[20]. Moreover, the sulphur also commonly present in the copper smelting slags.[21] As such, with an aim to further improve the understanding of Zn-containing smelting slags, current study will focus on the ZnO-"FeO"-SiO_2-CaO system at Po_2 10^{-8} tam, following by a preliminary investigation on the ZnO-"FeO"-SiO_2-CaO-S system at Po_2 10^{-8} tam.

8.2 Experimental

The experimental techniques applied in present study have been described in our previous articles[18, 19]. The generally procedures applied in present work can briefly be described as follow. The zinc silicate master slag and iron master slag were firstly prepared. The starting mixtures for the system ZnO-"FeO"-CaO-SiO_2 were prepared by mixing the as-prepared master slags with additional components by agate mortar and pestle. The CaO was obtained by heating the calcium carbonate at 1173 K (900 °C) for overnight. The ZnS was used as the sulphur source in present study. After pelletized, the mixture was placed in suitable container, and suspended at hot-zone of gas-tight vertical furnace tube with CO_2/CO passing through. The mixture was then quenched into ice water after equilibration. At last, quantitative analyses on the quenched sample were performed on JXA 8200 Electron Probe Micro-analyser equipped with wavelength-dispersive X-ray spectroscopy (Japan Electron Optics Ltd). The standards used for the analysis were from Charles M. Taylor Co. (Stanford, California): Fe_2O_3 for Fe,

$CaSiO_3$ for Si and Ca and $CuFeS_2$ for sulphur, and Micro-Analysis Consultant Ltd (Cambridge, UK): ZnO for Zn. The ZAF correction procedure supplied with the EPMA was applied. Although both as Fe^{2+} and Fe^{3+} present in the quenched sample, for the presentation purpose, all Fe was calculated into FeO.

8.3 Results and Discussion

Present studies have been experimentally determined the phase relations and liquidus temperatures of the system ZnO-"FeO"-SiO_2-CaO with CaO content varied from 2 to 6 wt pct between 1523 K (1250 °C) and 1573 K (1300 °C) under Po_2 fixed at 10^{-8} atm. Four primary phase fields were observed in the composition range investigated, including spinel [$(Fe^{2+},Zn)O\bullet Fe^{3+}{}_2O_3$], wüstite [$(Fe^{2+},Zn)O$], tridymite ($SiO_2$) and willemite [$(Zn,Fe^{2+})_2SiO_4$]. The wüstite was only observed at 1573 K (1300 °C) on the join "FeO"-SiO_2-CaO. Figure 8.1 shows the typical microstructures of quenched samples with two or three phases in equilibrium. The Figure 8.1 (A) shows the liquid in equilibrium with the spinel. Figure 8.1 (B) shows the equilibration of liquid with SiO_2. Figure 8.1 (C) shows the equilibria between liquid and willemite. Figure 8.1 (D) shows the liquid is in equilibrium with both spinal and willemite. The Figure 8.1 (E) shows the liquid is equilibrated with wüstite.

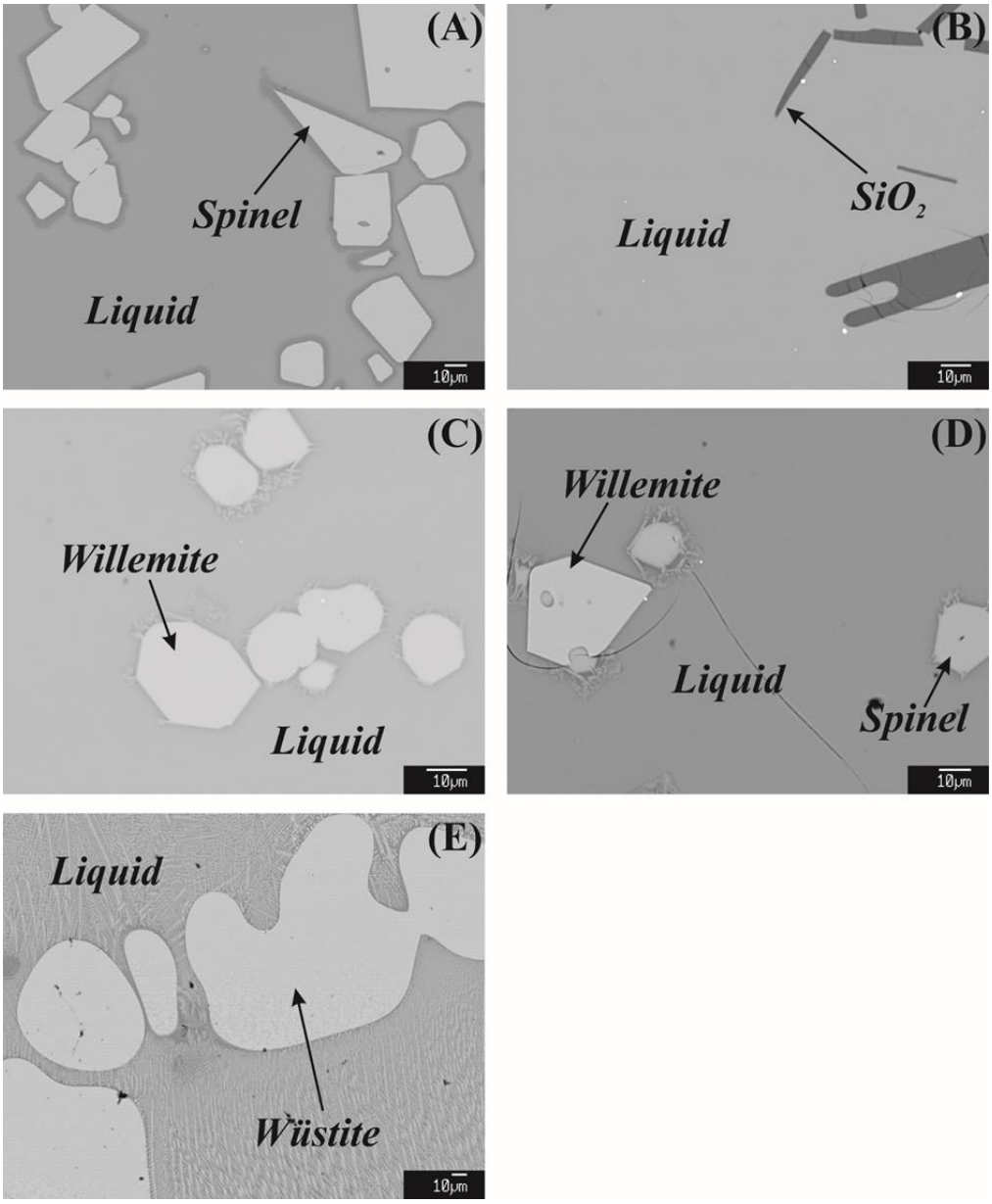

Figure 8.1 Microstructures of quenched samples showing liquid in equilibrium with, (A) - Spinel, (B) - SiO_2, (C) - Willemite, (D) - Spinel and Willemite and (E) - Wüstite under Po_2 10^{-8} atm

The normalized compositions of the phase assemblages present in the quenched samples measured by EPMA were listed in Table 8.1 through Table 8.3 based on equilibration temperatures for the system ZnO-"FeO"-SiO_2-CaO, while that for system ZnO-"FeO"-SiO_2-CaO-S was listed in Table 8.4. It can be seen that the spinel [$(Fe^{2+},Zn)O•(Fe^{3+}{}_2O_3)$] forms extensive solid that commonly presents in the copper slag smelting[21]. The measured maximum solubility of SiO_2 in spinel phase is 0.7 wt pct, while that of "FeO" in the SiO_2 phase (tridymite) is 1.1 wt pct. By using present experimental methodology, the solid solutions in equilibrium with the liquid phase can be accurately measured at high efficiency. These information are particularly important to the thermodynamic modelling of the Zn-containing copper smelting

slags since scarce information is available on the system ZnO-"FeO"-SiO_2-CaO under intermediate Po_2. Further discussion on partitioning behaviour of ZnO will be present in the lateral session.

Table 8.1 Experimental determined phases compositions in the ZnO-"FeO"-SiO_2-CaO system at 1523 K (1250 °C) under Po_2 10^{-8} atm

Experiment No.	Temperature [K (°C)]	Phase	Composition (Wt Pct)			
			ZnO	SiO_2	"FeO"	CaO
599	1523 (1250)	Liquid	0.0	26.3	71.4	2.3
		Spinel	0.0	0.7	99.3	0.0
600	1523 (1250)	Liquid	0.0	28.2	64.1	7.6
		Spinel	0.0	0.5	99.5	0.0
616	1523 (1250)	Liquid	14.2	37.8	45.2	2.8
		Spinel	7.6	0.4	92.0	0.0
623	1523 (1250)	Liquid	4.5	34.9	56.9	3.7
		Spinel	2.3	0.5	97.2	0.0
629	1523 (1250)	Liquid	0.0	26.5	69.6	3.9
		Spinel	0.0	0.6	99.4	0.0
630	1523 (1250)	Liquid	0.0	27.6	66.0	6.4
		Spinel	0.0	0.6	99.4	0.0
632	1523 (1250)	Liquid	11.8	38.1	46.0	4.1
		Spinel	6.5	0.4	93.1	0.0
633	1523 (1250)	Liquid	23.6	37.1	36.8	2.6
		Spinel	12.6	0.3	87.1	0.0
687	1523 (1250)	Liquid	15.4	36.3	45.7	2.5
		Spinel	8.2	0.4	91.4	0.0
702	1523 (1250)	Liquid	11.7	36.3	49.5	2.5
		Spinel	6.2	0.4	93.3	0.0
712	1523 (1250)	Liquid	10.2	35.8	51.7	2.3
		Spinel	5.4	0.4	94.3	0.0
725	1523 (1250)	Liquid	11.3	35.4	51.5	1.8
		Spinel	6.0	0.3	93.7	0.0
732	1523 (1250)	Liquid	10.2	36.2	51.7	1.9
		Spinel	5.1	0.3	94.6	0.0
733	1523 (1250)	Liquid	6.1	35.9	53.2	4.7
		Spinel	3.2	0.5	96.2	0.0
734	1523 (1250)	Liquid	16.7	38.9	39.5	4.9
		Spinel	9.9	0.2	89.9	0.0
735	1523 (1250)	Liquid	5.6	36.5	50.5	7.4
		Spinel	3.3	0.4	96.3	0.0
741	1523 (1250)	Liquid	8.2	35.8	53.9	2.1
		Spinel	4.2	0.3	95.5	0.0
753	1523 (1250)	Liquid	11.4	35.6	51.0	2.1
		Spinel	5.9	0.3	93.9	0.0
754	1523 (1250)	Liquid	7.8	36.3	51.6	4.2
		Spinel	4.1	0.3	95.6	0.0
770	1523 (1250)	Liquid	5.1	34.4	58.5	2.1
		Spinel	2.6	0.4	97.0	0.0
771	1523 (1250)	Liquid	5.3	35.0	56.1	3.6
		Spinel	2.9	0.3	96.7	0.0
772	1523 (1250)	Liquid	4.6	34.7	55.0	5.7
		Spinel	2.2	0.2	97.6	0.0

Experiment No.	Temperature [K (°C)]	Phase	Composition (Wt Pct)			
			ZnO	SiO_2	"FeO"	CaO
773	1523 (1250)	Liquid	18.7	38.0	37.9	5.4
		Spinel	10.9	0.3	88.8	0.0
601	1523 (1250)	Liquid	0.0	38.5	59.5	2.0
		SiO_2	0.1	99.0	0.9	0.0
617	1523 (1250)	Liquid	10.6	37.6	50.0	1.7
		SiO_2	0.2	98.9	1.0	0.0
625	1523 (1250)	Liquid	7.8	37.8	52.4	2.0
		SiO_2	0.1	99.3	0.6	0.0
675	1523 (1250)	Liquid	0.0	39.5	56.7	3.7
		SiO_2	0.0	99.2	0.8	0.0
689	1523 (1250)	Liquid	0.1	40.4	54.8	4.6
		SiO_2	0.1	99.2	0.7	0.0
743	1523 (1250)	Liquid	11.9	39.8	43.2	5.1
		SiO_2	0.3	99.0	0.8	0.0
755	1523 (1250)	Liquid	0.0	40.7	53.4	5.8
		SiO_2	0.0	98.8	1.1	0.0
769	1523 (1250)	Liquid	8.5	40.5	44.9	6.0
		SiO_2	0.2	99.2	0.6	0.0

Table 8.2 Experimental determined phases compositions in the ZnO-"FeO"-SiO_2-CaO system at 1543 K (1270 °C) under Po_2 10^{-8} atm

Experiment No.	Temperature [K (°C)]	Phase	Composition (Wt Pct)			
			ZnO	SiO_2	"FeO"	CaO
667	1543 (1270)	Liquid	0.0	22.1	73.4	4.5
		Spinel	0.0	0.5	99.4	0.0
716	1543 (1270)	Liquid	0.0	21.9	74.2	3.9
		Spinel	0.1	0.5	99.5	0.0
717	1543 (1270)	Liquid	0.0	22.3	71.6	6.1
		Spinel	0.0	0.5	99.5	0.0
729	1543 (1270)	Liquid	10.9	32.5	54.8	1.8
		Spinel	4.6	0.3	95.1	0.0
736	1543 (1270)	Liquid	9.0	34.4	51.1	5.4
		Spinel	4.5	0.3	95.1	0.0
737	1543 (1270)	Liquid	27.6	33.9	33.7	4.8
		Spinel	15.9	0.3	83.8	0.0
738	1543 (1270)	Liquid	6.1	34.4	51.2	8.3
		Spinel	3.1	0.3	96.6	0.0
756	1543 (1270)	Liquid	9.9	33.3	54.3	2.5
		Spinel	5.2	0.3	94.5	0.0
758	1543 (1270)	Liquid	0.0	21.2	77.1	1.7
		Spinel	0.0	0.6	99.4	0.0
774	1543 (1270)	Liquid	5.7	31.6	60.1	2.5
		Spinel	3.0	0.4	96.6	0.0
775	1543 (1270)	Liquid	19.2	34.5	44.1	2.2
		Spinel	10.4	0.3	89.3	0.0
776	1543 (1270)	Liquid	3.8	31.1	60.8	4.2
		Spinel	1.9	0.3	97.7	0.0
777	1543 (1270)	Liquid	27.8	33.8	34.2	4.2
		Spinel	15.5	0.1	84.3	0.0
778	1543 (1270)	Liquid	7.0	32.8	54.2	6.0
		Spinel	3.5	0.3	96.2	0.0

Experiment No.	Temperature [K (°C)]	Phase	Composition (Wt Pct)			
			ZnO	SiO_2	"FeO"	CaO
779	1543 (1270)	Liquid	29.3	34.3	30.8	5.6
		Spinel	17.4	0.2	82.5	0.0
797	1543 (1270)	Liquid	22.3	35.1	39.2	3.4
		Spinel	12.6	0.2	87.3	0.0
628	1543 (1270)	Liquid	9.2	37.8	51.0	2.0
		SiO_2	0.2	98.9	0.9	0.0
631	1543 (1270)	Liquid	0.0	38.9	59.0	2.1
		SiO_2	0.0	99.2	0.8	0.0
668	1543 (1270)	Liquid	0.0	39.7	56.7	3.5
		SiO_2	0.0	99.2	0.8	0.0
674	1543 (1270)	Liquid	0.0	40.6	54.6	4.8
		SiO_2	0.0	98.9	1.1	0.0
707	1543 (1270)	Liquid	7.9	39.2	49.2	3.8
		SiO_2	0.2	99.1	0.8	0.0
746	1543 (1270)	Liquid	0.0	42.0	52.4	5.6
		SiO_2	0.0	99.3	0.7	0.0
780	1543 (1270)	Liquid	11.4	41.7	40.5	6.4
		SiO_2	0.2	99.2	0.7	0.0
803	1543 (1270)	Liquid	19.0	38.1	40.8	2.2
		SiO_2	0.4	99.0	0.6	0.0
804	1543 (1270)	Liquid	19.1	40.2	36.4	4.3
		SiO_2	0.4	98.9	0.7	0.0
805	1543 (1270)	Liquid	22.0	41.4	30.6	6.0
		SiO_2	0.5	98.9	0.5	0.0
820	1543 (1270)	Liquid	33.0	35.1	30.0	1.8
		Willemite	61.5	28.2	10.3	0.0
821	1543 (1270)	Liquid	34.3	34.8	27.2	3.7
		Willemite	62.4	28.1	9.4	0.0
802	1543 (1270)	Liquid	35.1	39.6	19.4	5.9
		Willemite	64.7	28.3	7.0	0.0
822	1543 (1270)	Liquid	34.2	36.3	23.3	6.2
		Willemite	63.9	28.2	7.8	0.0
730	1543 (1270)	Liquid	33.3	33.1	31.5	2.2
		Spinel	18.8	0.3	81.0	0.0
		Willemite	60.3	28.4	11.2	0.0
763	1543 (1270)	Liquid	34.2	33.2	27.1	5.5
		Willemite	62.4	28.3	9.3	0.0
		Spinel	20.9	0.2	78.9	0.0
796	1543 (1270)	Liquid	32.7	33.3	31.7	2.4
		Spinel	18.6	0.3	81.1	0.0
		Willemite	62.7	28.2	9.1	0.0
800	1543 (1270)	Liquid	33.3	33.8	30.9	1.9
		Spinel	19.7	0.3	80.0	0.0
		Willemite	61.0	28.5	10.5	0.0
762	1543 (1270)	Liquid	33.2	33.0	30.0	3.8
		Spinel	18.9	0.3	80.8	0
		Willemite	61.5	28.4	10.1	0

Table 8.3 Experimental determined phases compositions in the ZnO-"FeO"-SiO_2-CaO system at 1573 K (1300 °C) under Po_2 10^{-8} atm

Experiment No.	Temperature [K (°C)]	Phase	Composition (Wt Pct)			
			ZnO	SiO_2	"FeO"	CaO
664	1573 (1300)	Liquid	0.0	16.2	82.0	1.8
		Wüstite	0.0	0.5	99.5	0.0
676	1573 (1300)	Liquid	0.0	16.0	80.6	3.3
		Wüstite	0.0	0.4	99.5	0.1
678	1573 (1300)	Liquid	0.0	17.5	77.7	4.8
		Wüstite	0.0	0.4	99.5	0.1
700	1573 (1300)	Liquid	0.0	16.5	80.1	3.4
		Wüstite	0.0	0.4	99.6	0.0
701	1573 (1300)	Liquid	0.0	17.4	77.3	5.3
		Wüstite	0.0	0.4	99.6	0.0
635	1573 (1300)	Liquid	2.6	23.1	72.1	2.2
		Spinel	1.2	0.4	98.4	0.0
677	1573 (1300)	Liquid	23.7	30.5	43.1	2.7
		Spinel	12.3	0.4	87.2	0.0
704	1573 (1300)	Liquid	10.6	28.6	58.4	2.3
		Spinel	6.3	0.4	93.3	0.0
731	1573 (1300)	Liquid	10.7	27.9	59.2	2.2
		Spinel	5.9	0.3	93.8	0.0
739	1573 (1300)	Liquid	11.3	28.5	58.2	2.1
		Spinel	6.3	0.4	93.3	0.0
740	1573 (1300)	Liquid	32.4	29.8	36.3	1.6
		Spinel	17.7	0.3	82.0	0.0
744	1573 (1300)	Liquid	33.8	30.2	31.8	4.3
		Spinel	19.4	0.3	80.4	0.0
745	1573 (1300)	Liquid	8.6	28.7	56.4	6.3
		Spinel	4.4	0.2	95.4	0.0
757	1573 (1300)	Liquid	9.2	28.4	23.7	2.4
		Spinel	4.5	0.2	95.3	0.0
759	1573 (1300)	Liquid	0.0	18.0	76.4	5.6
		Spinel	0.0	0.3	99.7	0.0
760	1573 (1300)	Liquid	0.0	17.1	79.2	3.7
		Spinel	0.0	0.4	99.6	0.0
764	1573 (1300)	Liquid	32.6	29.5	36.1	1.8
		Spinel	17.6	0.2	82.1	0.0
781	1573 (1300)	Liquid	4.6	25.1	67.7	2.6
		Spinel	2.4	0.4	97.2	0.0
783	1573 (1300)	Liquid	28.9	29.8	39.4	1.9
		Spinel	15.5	0.3	84.3	0.0
782	1573 (1300)	Liquid	3.1	25.1	68.2	3.6
		Spinel	2.0	0.3	97.7	0.0
799	1573 (1300)	Liquid	27.0	30.7	39.3	3.1
		Spinel	15.3	0.3	84.4	0.0
828	1573 (1300)	Liquid	26.2	31.2	36.6	6.1
		Spinel	15.6	0.2	84.2	0.0
827	1573 (1300)	Liquid	27.6	30.7	37.5	4.2
		Spinel	16.0	0.2	83.7	0.0
846	1573 (1300)	Liquid	10.6	29.1	56.5	3.8
		Spinel	5.3	0.3	94.3	0.1
711	1573 (1300)	Liquid	0.0	17.1	79.1	3.8

Experiment No.	Temperature [K (°C)]	Phase	Composition (Wt Pct)			
			ZnO	SiO_2	"FeO"	CaO
636	1573 (1300)	Liquid	8.1	38.6	51.2	2.1
		SiO_2	0.2	99.0	0.8	0.0
679	1573 (1300)	liquid	0.0	40.5	55.8	3.7
		SiO_2	0.0	99.1	0.9	0.0
691	1573 (1300)	Liquid	0.0	40.0	58.0	2.0
		SiO_2	0.0	99.2	0.7	0.0
705	1573 (1300)	Liquid	0.0	42.8	51.7	5.5
		SiO_2	0.0	99.3	0.7	0.0
767	1573 (1300)	Liquid	34.2	38.5	24.8	2.5
		SiO_2	1.0	98.4	0.6	0.0
823	1573 (1300)	Liquid	8.7	38.6	50.4	2.3
		SiO_2	0.1	99.3	0.6	0.0
824	1573 (1300)	Liquid	20.0	38.3	39.6	2.1
		SiO_2	0.2	99.1	0.7	0.0
825	1573 (1300)	Liquid	20.5	40.2	35.0	4.3
		SiO_2	0.3	99.1	0.6	0.0
826	1573 (1300)	Liquid	27.3	42.1	25.3	5.4
		SiO_2	0.7	98.7	0.6	0.0
708	1573 (1300)	Liquid	35.4	30.4	32.4	1.8
		Willemite	61.4	28.6	10.1	0.0
815	1573 (1300)	Liquid	36.4	33.5	27.9	2.1
		Willemite	61.9	28.9	9.3	0.0
816	1573 (1300)	Liquid	37.0	34.0	25.0	4.0
		Willemite	63.5	28.8	7.7	0.0
817	1573 (1300)	Liquid	38.3	35.3	20.8	5.6
		Willemite	65.1	28.7	6.2	0.0
768	1573 (1300)	Liquid	38.3	30.2	25.8	5.6
		Spinel	22.5	0.2	77.3	0.0
		Willemite	64.8	28.5	6.7	0.1
798	1573 (1300)	Liquid	36.5	29.9	31.7	1.9
		Spinel	21.1	0.2	78.7	0.0
		Willemite	63.7	28.2	8.1	0.0
818	1573 (1300)	Liquid	36.5	29.9	31.7	1.9
		Spinel	21.1	0.2	78.7	0.0
		*Willemite	9.7	63.9	26.4	0.0

Table 8.4 Experimental determined phases compositions in the ZnO-"FeO"-SiO_2-CaO-S system at 1473 K (1200 °C) under Po_2 10^{-8} atm

Experiment No.	Temperature [K (°C)]	Phase	Composition (Wt Pct)				
			ZnO	SiO_2	"FeO"	CaO	S
813	1473 (1200)	Liquid	0.1	19.8	76.6	1.7	1.8
		Wüstite	0.0	0.6	99.4	0.0	0.0
814	1473 (1200)	Liquid	0.0	19.6	77.3	1.4	1.7
		Wüstite	0.1	0.7	99.3	0.0	0.0
829	1473 (1200)	Liquid	0.2	18.8	77.4	1.6	2.0
		Wüstite	0.1	0.6	99.3	0.0	0.0
847	1473 (1200)	Liquid	8.3	18.9	68.6	1.9	2.3
		Spinel	4.3	0.5	95.1	0.1	0.0

By using the normalized compositions of the liquid phase measured by EPMA, liquidus surfaces of the system ZnO-"FeO"-SiO_2-CaO were constructed with fixed CaO content in the liquid phase at Po_2 10^{-8} atm, as illustrated in Figure 8.2. There are three pseudo-sections investigated in present study, including 2, 4 and 6 wt pct CaO in the liquid phase. Although those results with CaO deviating to the target values were not applied to construct the liquidus surfaces, they are included in the Table 8.1 to Table 8.3 due to the importance to thermodynamical modelling of copper smelting slags.

The constructed liquidus surfaces with fixed CaO content (2, 4 and 6 wt pct) in the liquid phase of the system ZnO-"FeO"-SiO_2-CaO at Po_2 10^{-8} atm were shown in Figure 8.3 to Figure 8.5. The thin solid lines are experimental determined isotherms, while the thin dash lines are hypothetical isotherms, and the thick solid lines represent the experimentally decided boundaries, while the thick dash lines indicating the boundaries in areas where there is no experimental data available. It can be seen that the spinel primary phase field substantially increases with the CaO content. In addition, the liquidus temperatures increase in spinel primary phase field and decrease in the SiO_2 and willemite primary phase fields.

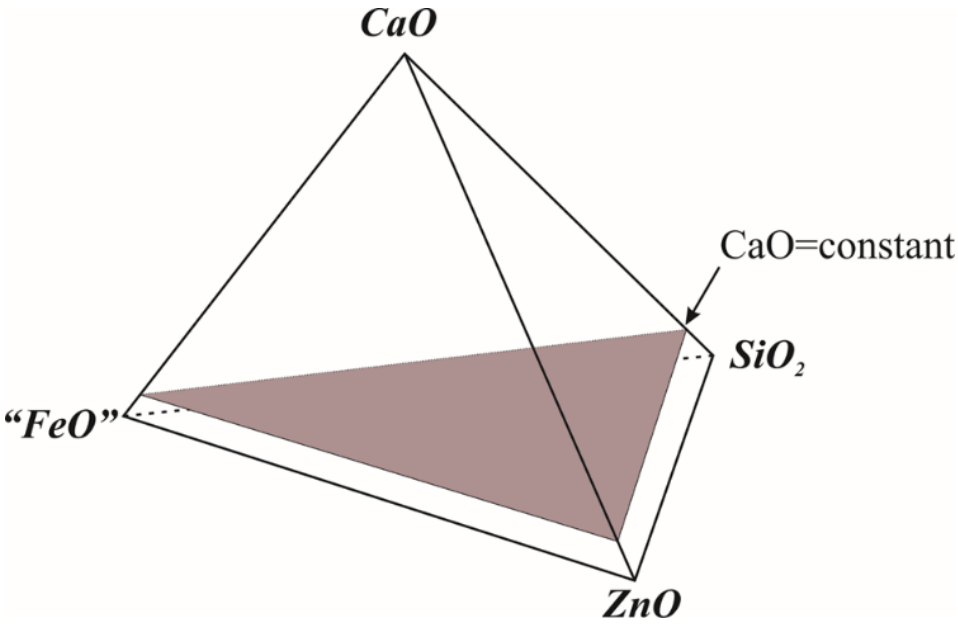

Figure 8.2 Pseudo-ternary section in the ZnO-"FeO"-SiO_2-CaO system at constant CaO content in liquid under Po_2 10^{-8} atm

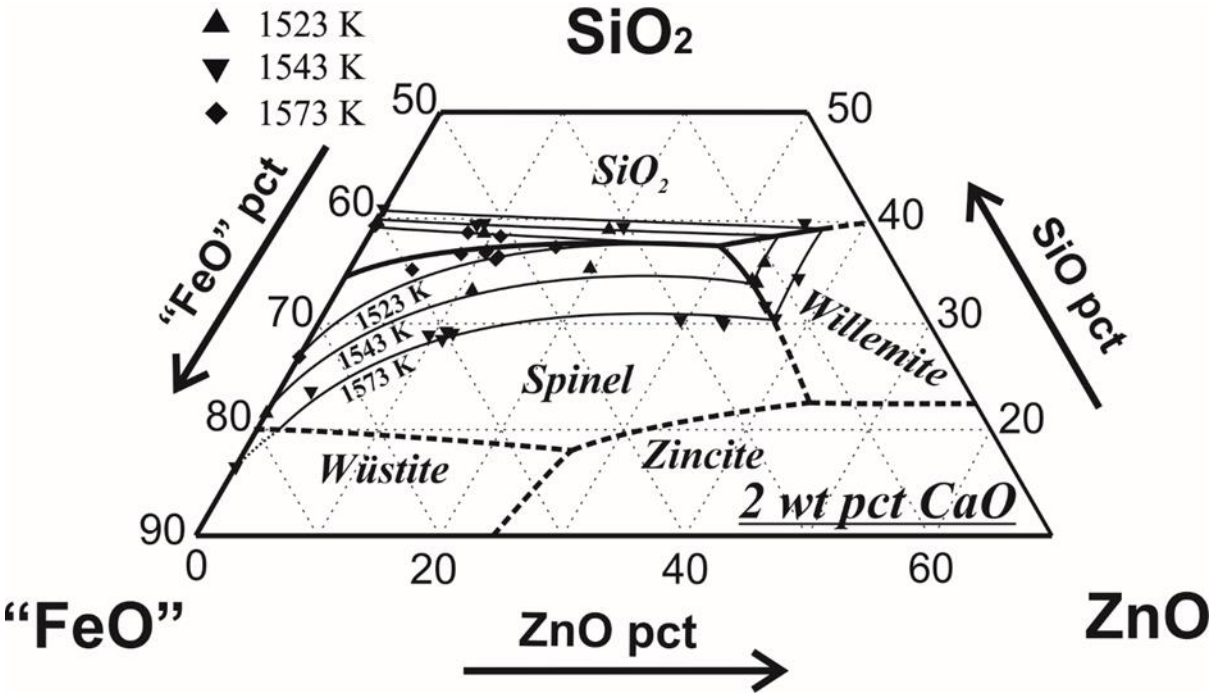

Figure 8.3 Summary of experimental data on the liquidus in the section, ZnO-"FeO"-SiO_2-CaO with 2 wt pct CaO in the liquid under Po_2 at 10^{-8} atm

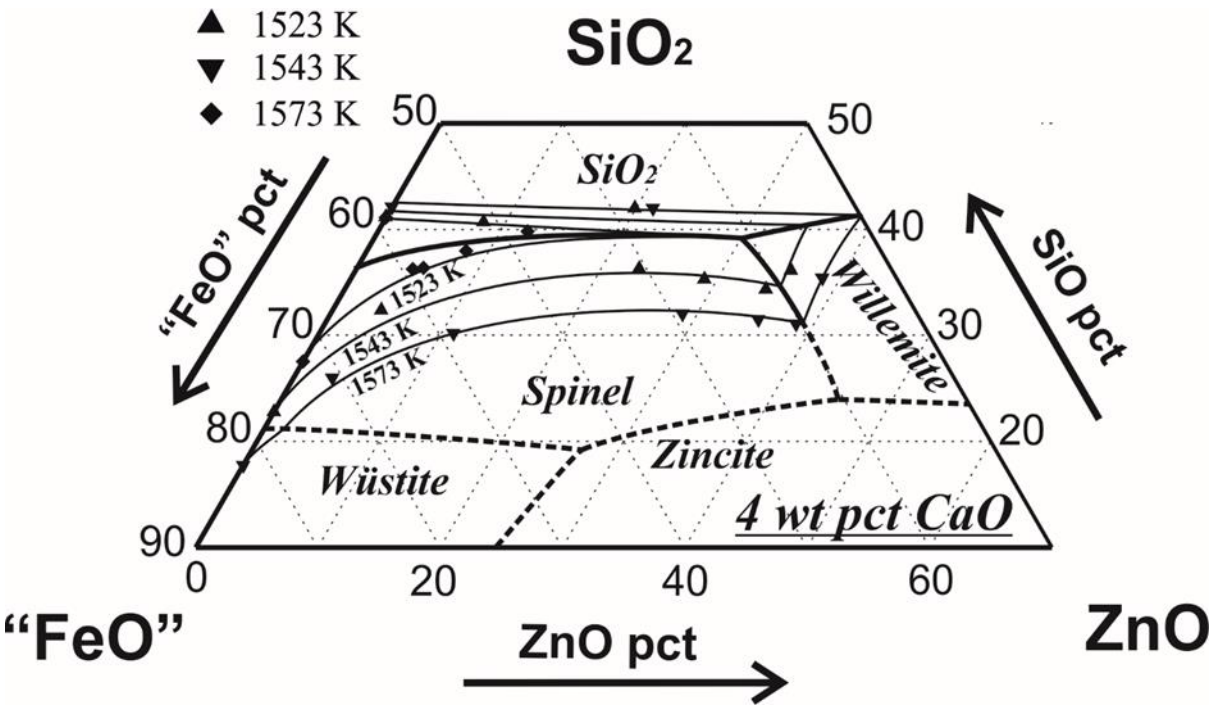

Figure 8.4 Summary of experimental data on the liquidus in the section, ZnO-"FeO"-SiO_2-CaO with 4 wt pct CaO in the liquid under Po_2 at 10^{-8} atm

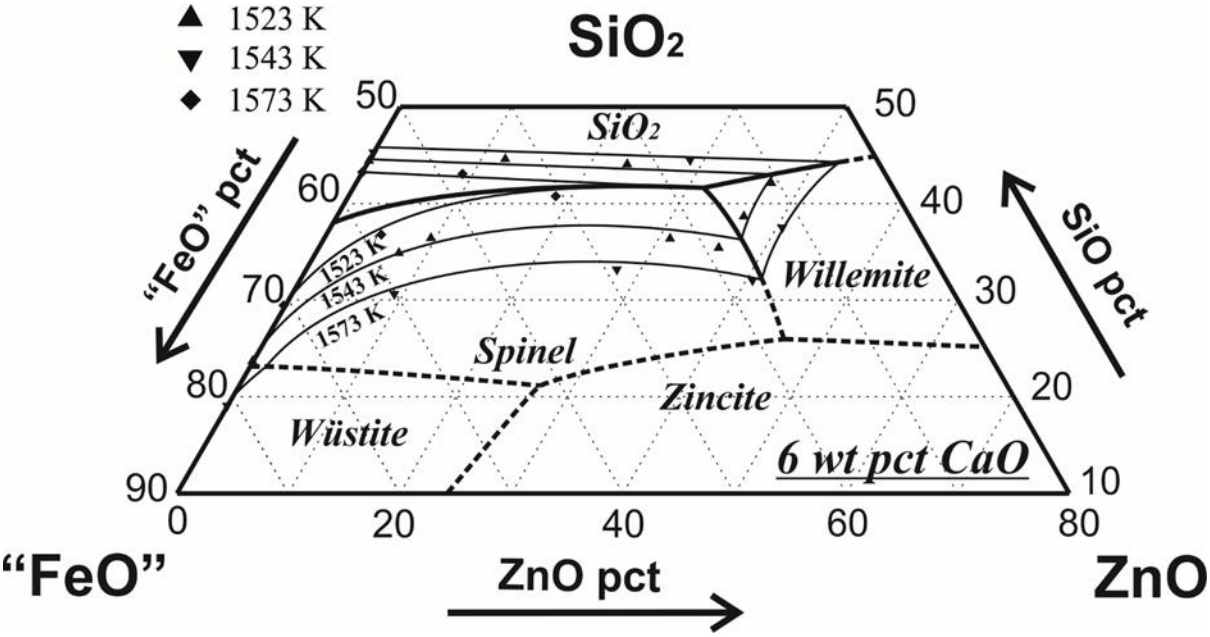

Figure 8.5 Summary of experimental data on the liquidus in the section, ZnO-"FeO"-SiO_2-CaO with 6 wt pct CaO in the liquid under Po_2 at 10^{-8} atm

8.3.1 Effect of CaO, ZnO and sulphur on the primary phase and liquidus temperature

The effect of CaO content on the phase relation and liquidus temperatures of the Zn-content smelting slag at Po_2 10^{-8} atm can be effectively evaluated using present study. Figure 8.6 shows a comparison of the isotherm at 1523 K (1250 °C) between present study, CaO-free[19] system and FactSage prediction[20] under Po_2 10^{-8} atm. It can be seen that the liquidus temperatures increase in spinel primary phase field while decrease in the SiO_2 primary phase field when CaO content increasing. The full liquid areas that represent the operation window of slag compositions in industrial copper smelting at this temperature seems to be independent of the CaO content. However, the full liquid areas determined by present authors tend be smaller than that predicted by FactSage 6.2[20]. As such, the accuracy of FactSage 6.2 prediction[20] on Zn-containing copper smelting slags at intermediate Po_2 can be improved using the experimental results present in current study.

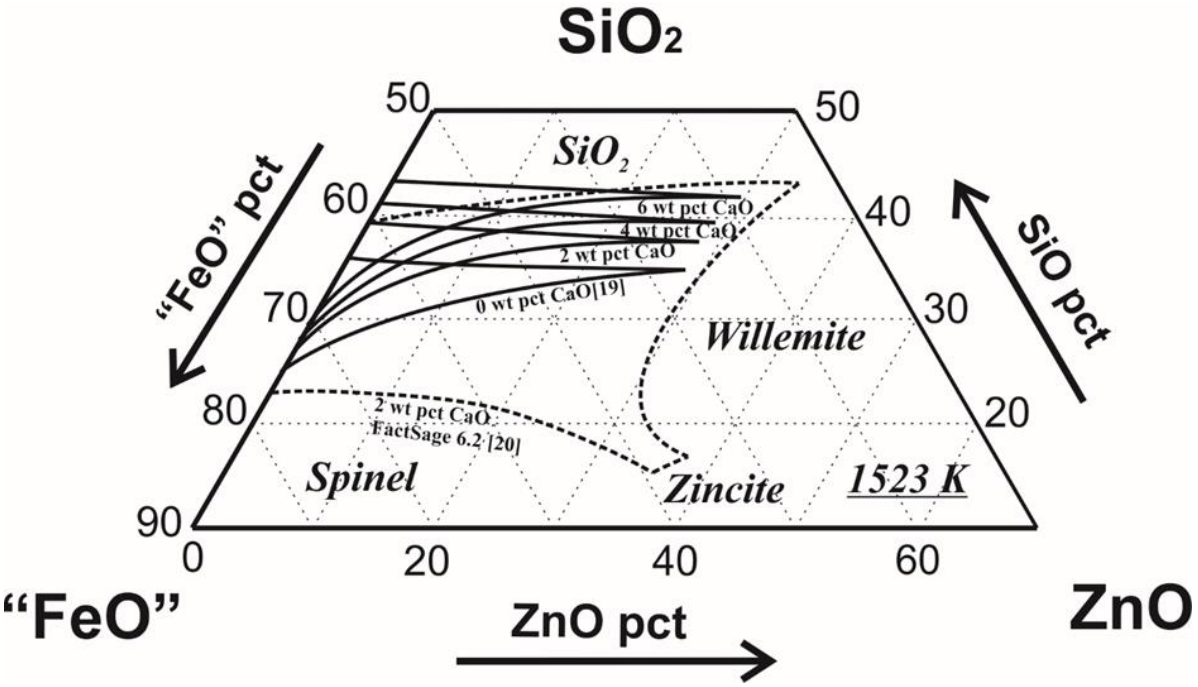

Figure 8.6 Liquidus surfaces at 1250 °C with varied CaO contents under Po_2 at 10^{-8} atm

Pseudo-binary phase diagrams provide a more conceivable way for the industrial to apply the experimental results in present study to industrial practices. Figure 8.7 shows the pseudo-binary ("FeO"+SiO_2)-ZnO with fixed Fe/SiO_2 = 1.5 (mass), where the dash line shows prediction from FactSage 6.2[20]. It is obvious that the liquidus temperatures in spinel phsae continuously increases with ZnO content in all cases. For example, with fixed 2 wt pct CaO in present study, the liquidus temperature increases by 26 K when ZnO content increases from 5 to 10 wt pct. Meanwhile, the liquidus temperatures in present study are higher than those predicted by FactSage 6.2[20]. As an example, with 5 wt pct ZnO in the liquid phase of the 2 wt pct CaO section, the liquidus temperature determined in present study is 29 K higher than that by FactSage 6.2 prediction[20].

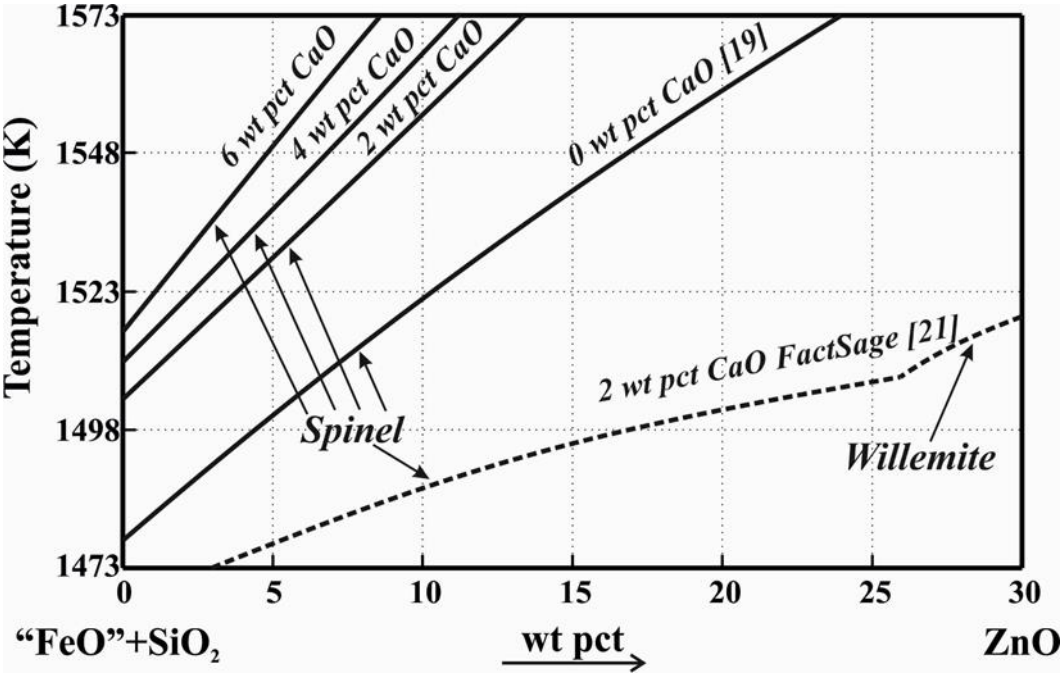

Figure 8.7 Comparisons of pseudo-binary ("FeO"+SiO_2)-ZnO at fixed Fe/SiO_2 = 1.5 (mass) between present study, CaO-free[19] and FactSage prediction[20] at $Po_2 10^{-8}$ atm

The effect of CaO content on the liquidus temperature was shown in the Figure 8.8. It can be seen that the liquidus temperatures increase with the CaO content at fixed ZnO concentration. For instance, the liquidus temperature increases by 39 K when CaO content increases from 0 to 4 wt pct with 5 wt pct ZnO present in the liquid phase.

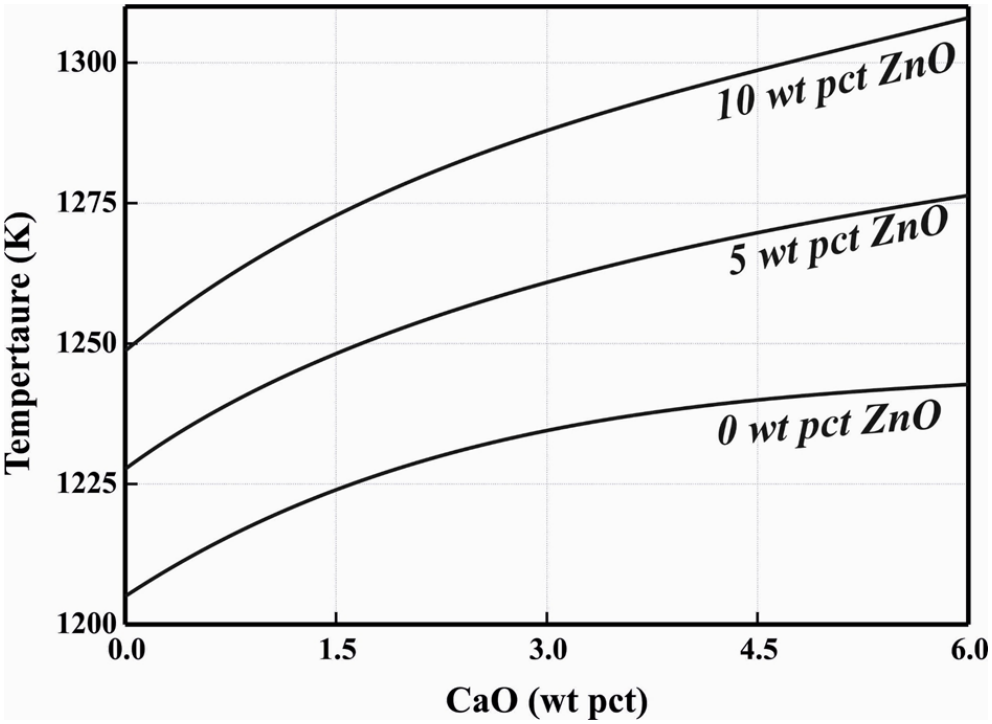

Figure 8.8 Liquidus temperature in the spinel primary phase field as function of magnesia (CaO) content with varied ZnO and Fe/SiO_2 = 1.5 (mass)

Figure 8.9 shows the comparison of liquidus temperatures between present system with 4 wt pct CaO, system ZnO-"FeO"-SiO_2-MgO with 4 wt pct MgO[22], system ZnO-"FeO"-SiO_2-Al_2O_3 with 4 wt pct Al_2O_3[18] and system ZnO-"FeO"-SiO_2[19] at fixed Fe/SiO_2 = 1.5 (mass) under Po_2 10^{-8} atm. It can be seen that the introduction of CaO, MgO or Al_2O_3 will increases the liquidus temperature in spinel primary phase field. The liquidus temperatures from present system are higher than those in the system ZnO-"FeO"-SiO_2-Al_2O_3[18]. Meanwhile, the liquidus temperatures obtained in present study tends to be close to those obtained in system ZnO-"FeO"-SiO_2-MgO[22].

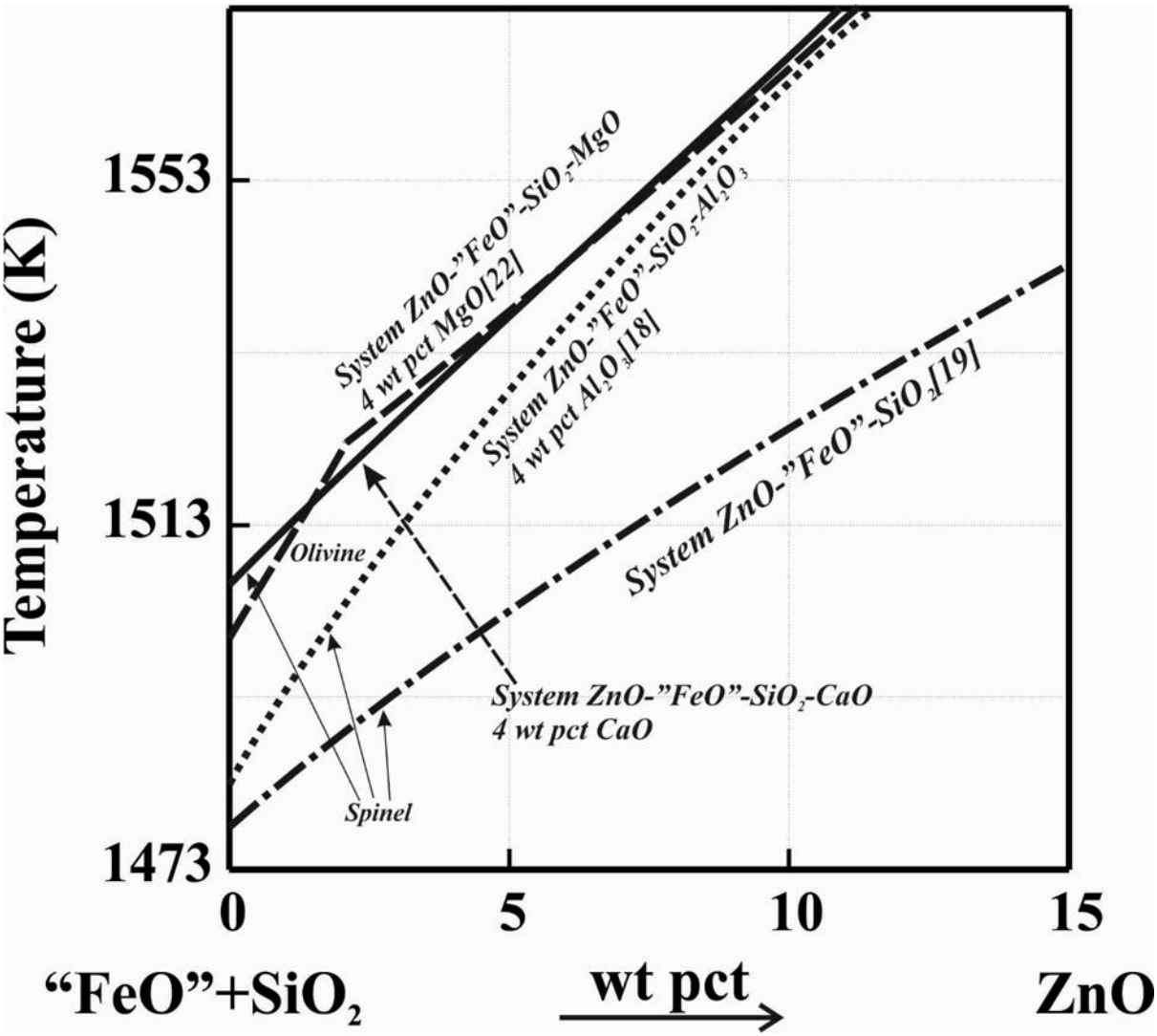

Figure 8.9 Comparison of liquidus temperatures at fixed Fe/SiO_2 = 1.5 (mass) between present system, system ZnO-"FeO"-SiO_2-MgO with 4 wt pct MgO[22], system ZnO-"FeO"-SiO_2-Al_2O_3 with 4 wt pct Al_2O_3[18] and system ZnO-"FeO"-SiO_2[19] at Po_2 10^{-8} atm

The Fe/SiO_2 ratio is commonly used as fluxing condition in the copper smelting operation. As such, pseudo-binary diagram was constructed to evaluate the impact of Fe/SiO_2 ratio on the liquidus temperature at fixed 5 wt pct ZnO in liquid, as shown in the Figure 8.10. Apparently,

the liquidus temperatures decrease in the spinel primary phase field and increases in SiO_2 primary phase field when SiO_2 content increasing (towards to lower Fe/SiO_2 ratio) in all cases. For instance, the liquidus temperature decreases by 27 K when the SiO_2 content increasing from 30 to 35 wt pct (or Fe/SiO_2 ratio, 1.8 to 1.4) in 2 wt pct CaO section. Meanwhile, liquidus temperatures in spinel primary phase field from present study are higher than those in CaO-free system[19] and FactSage 6.2[20]. As an example, with fixed Fe/SiO_2 ratio at 1.8, the liquidus temperature in spinel primary phase field on 2 wt pct CaO section in present study is 26 K higher than CaO-free system[19], and 52 K higher than FactSage prediction[20].

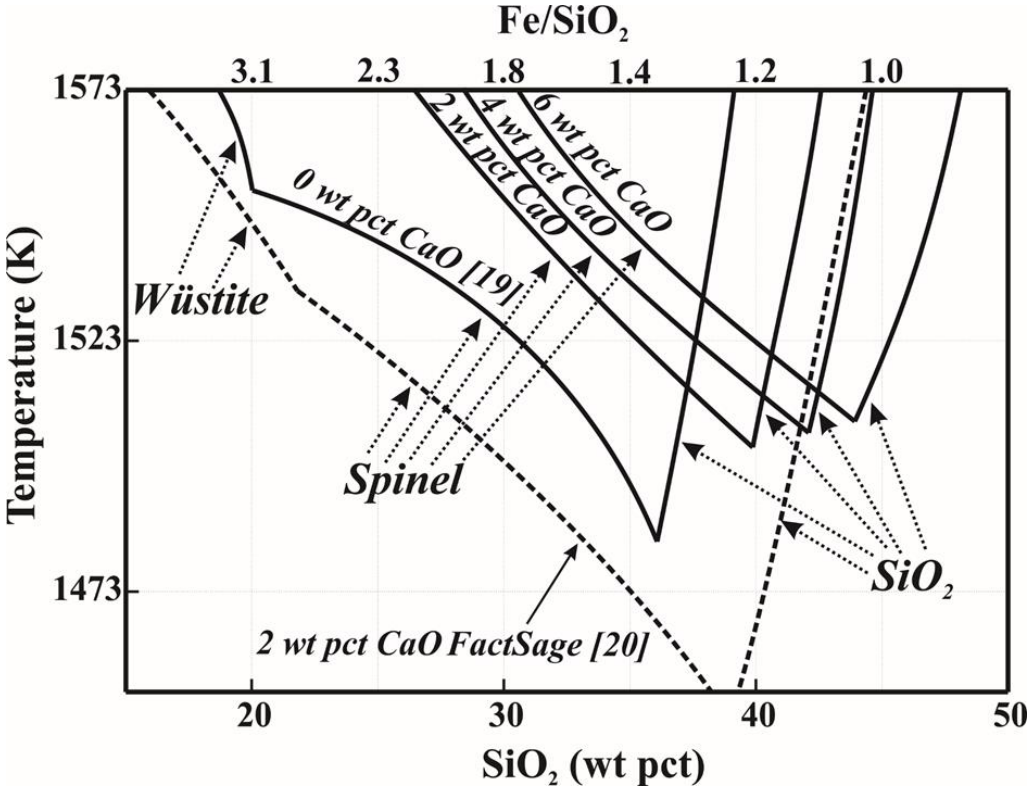

Figure 8.10 Pseudo-binary "FeO"-SiO_2 at fixed 5 wt pct ZnO under Po_2 at 10^{-8} atm from present study, CaO-fee system[19] and FactSage prediction[20]

As the sulphur also commonly presents in the copper smelting slags, so that its impact on the liquidus temperature should be evaluated.[17, 21] Figure 8.11 (A) shows pseudo-binary diagram of the ZnO-"FeO"-SiO_2-CaO-S system with 2 wt pct CaO and 0 wt pct ZnO in liquid phase at Po_2 10^{-8} atm. The solid lines show the experimentally determined liquidus, while the dash lines show extends of solid lines. It can be seen that the liquidus temperatures shows good agreement with those determined by Hidayat *et al*[23] at 0 wt pct sulphur in liquid phase. Moreover, the liquidus temperature with 2 wt pct sulphur in liquid is about 75 K lower than that in the sulphur-free system. Figure 8.11 (B) shows the pseudo-binary diagram of the ZnO-"FeO"-SiO_2-CaO-S system with 2 wt pct CaO and 8.8 wt pct ZnO in liquid phase at Po_2 10^{-8} atm. It is obvious

that the liquidus temperature in sulphur-free is much higher than that with the 2 wt pc sulphur, which is close to 160 K. Such phenomenon was also observed in the study by Zhao *et al*.[17]

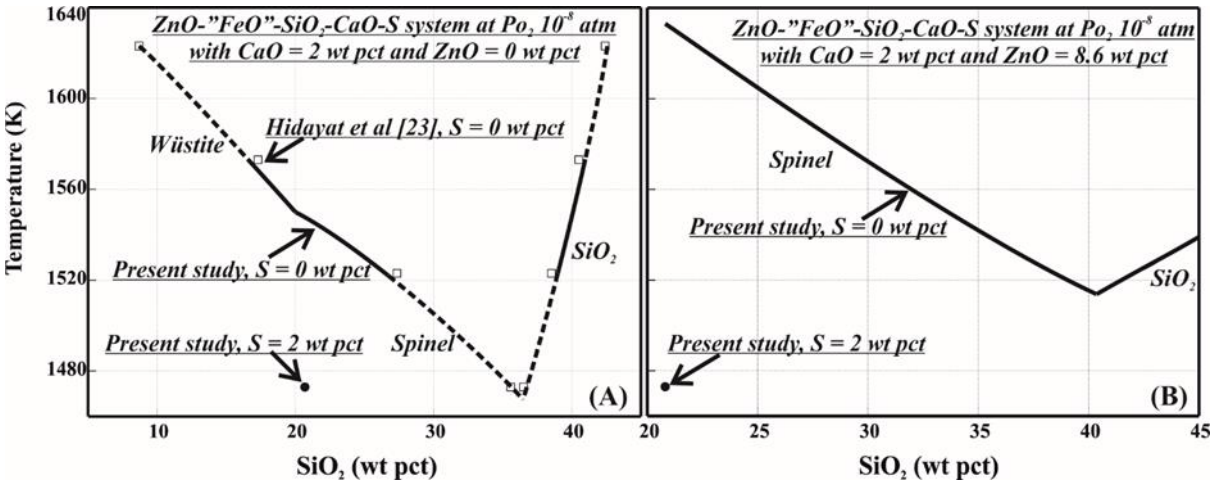

Figure 8.11 Pseudo-binary diagrams of the ZnO-"FeO"-SiO_2-CaO-S system with 2 wt pct CaO, (A) - 0 wt pct ZnO and (B) - 8.8 wt pct ZnO under Po_2 10^{-8} atm

8.3.2 Solid-Liquid Equilibria

As can be seen in section 8.1, there is limited information on the system ZnO-"FeO"-SiO_2-CaO under intermediate Po_2 which might lead to the significant discrepancy between current study and predictions by FactSage 6.2, as present in 8.3.1. Meanwhile, the development of thermodynamic modelling requires comprehensive knowledge on the solid-liquid equilibria behaviour. By applying present experimental methodology, the information of solid-liquid equilibria can be well attained at high efficiency.

The spinel forms extensive solid solution as shown in the Table 8.1 to Table 8.3, with formula $(Fe^{2+},Zn,Mg)O•(Fe^{3+}, Al)_2O_3$[16]. Information on the partitioning effect of ZnO between spinel and liquid phases, not only can benefit the thermodynamic modelling of the copper smelting slags, but also important to the management of ZnO during copper smelting processes. The Figure 8.12 shows the partitioning effect of ZnO between spinel and liquid phases from present study and CaO-free system[19] at Po_2 10^{-8} atm and Zn-containing high-order systems under metallic iron saturation[11-17]. It can be seen that the ZnO partitioning behaviour from present study is similar to that in the CaO-free system[19] and ZnO-"FeO"-SiO_2-MgO where quasi-linear relationships were observed. Meanwhile, the ZnO concentration in the spinel from the ZnO-"FeO"-SiO_2-Al_2O_3 system[18] is slightly higher than that in present study and CaO-free system[19]. It can be concluded that the ZnO concentrations in spinel phase are generally lower than that in the liquid phase at Po_2 10^{-8} atm. The ZnO concentrations in spinel phase of the Zn-containing high-order systems, however, are higher than those in the liquid phase under

metallic iron saturation[11-17], which are also much higher than that from present work. For example, that is 3.5 times higher than that in present study with14 wt pct ZnO in the liquid, as can be seen in the Figure 8.12.

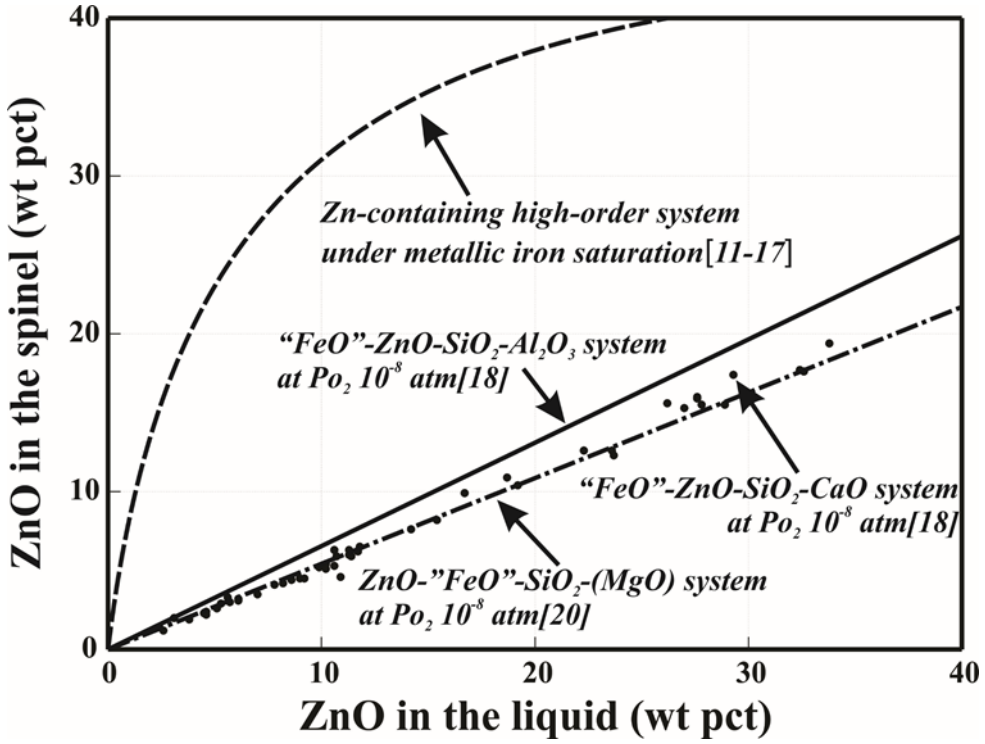

Figure 8.12 ZnO partitioning effect between spinel and liquid phases from present study, CaO-free system[19], ZnO-"FeO"-SiO_2-Al_2O_3 system[18] at Po_2 10^{-8} atm and Zn-containing high-order systems under metallic iron saturation[11-17]

8.3.3 Industrial Implications

The smooth operation at low energy consumption has been the first priority in the industrial copper smelting processes. The attainment of such goal requires comprehensive understanding on the copper smelting slags under operating conditions. Using the knowledge obtained in present study on the Zn-containing copper smelting slags, the industrial can better manage the operational parameters to approach the goal.

The introduction of CaO into slag systems, although could decrease the viscosity of the copper smelting slags[2, 3], will increase the liquidus temperature by 40 K when CaO increases from 0 to 4 wt pct at fixed Fe/SiO_2 = 1.5 according to present study. Such effect should be carefully evaluated during the copper smelting processes to avoid the aggressive deposit of spinel phase which tends to decrease in the effective vessel volume and blockage of slag tapping hole[24]. In the meanwhile, current studies also indicate that the liquidus temperature is closely related to the Fe/SiO_2 ratio. A continuously decrease of liquidus in the spinel phase was

observed when Fe/SiO_2 decreases. By using current experimental results, a proper Fe/SiO_2 ratio can be selected to maintain a moderate solid proportion in the copper smelter.

The introduction of sulphur into the slags system will significantly decreases the liquidus temperature as shown in present study. A 2 wt pct of sulphur in the Zn-containing slag can reduce the liquidus temperature in the spinel phase by 160 K. Such phenomenon explains the smooth operation of industrial copper smelting can be maintain at low temperature operation. As such, operating parameters that increase the sulphur capacity in the slag might be applied during the copper smelting process.

In the meanwhile, major differences between current studies and the FactSage prediction[20] were observed in both phase relations and liquidus temperature. The discrepancies are due to the lack of the information in the ZnO-containing systems under the copper smelting conditions. By applying current experimental results, more accurate thermodynamic modelling on the zinc-containing copper smelting slag can be attained.

8.4 Summary

Phase equilibria and liquidus temperatures on the ZnO-"FeO"-SiO_2-CaO system with CaO content varying from 2 to 6 wt pct have been experimentally determined at the temperatures, 1523 (1250), 1543 (1270) and 1573 K (1300 °C) under Po_2 10^{-8} atm relevant to the industrial copper smelting processes. The results suggest that the liquidus temperatures in the increase in the spinel primary phase field, while decrease in the SiO_2 primary phase field when the CaO content in liquid phase increases. The introduction of 2 wt pct sulphur into the slag systems can significantly decrease the liquidus temperature in the spinel phase by 160 K. The partitioning effect of ZnO between spinel and liquid phases tends be similar to those in the CaO-free system where the concentrations of ZnO in the liquid phase are higher than those in the spinel phase. The findings in present study can improve the understanding of copper smelting slags and aid the development of thermodynamic modelling on the Zn-containing copper smelting slags.

8.5 References

1. E. Jak, B. Zhao and P. C. Hayes, *Metall. Mater. Trans. B*, 2002, vol. 33, pp. 877-890.
2. M. Kucharski, N. M. Stubina and J. M. Toguri, *Can. Metall. Q.*, 1989, vol. 28, pp. 7-11.
3. G. H. Kaiura, J. M. Toguri and G. Marchant, *Can. Metall. Q.*, 1977, vol. 16, pp. 156-160.

4. B. L. Dobrotsvetov, E. I. Bogoslovskaya and V. E. Rudnichenko, *Zh. Neorg. Khim.*, 1967, vol. 12, pp. 2190-8.

5. J. G. Lenz and I. Lee, In *Metall. Slags Fluxes, Int. Symp., Proc., 2nd*, ed. H. Alan; Gaskell Fine, David R (Metall. Soc. AIME: 1984), pp 823-35.

6. E. Jak, B. Zhao and P. C. Hayes, *Metall. Mater. Trans. B*, 2002, vol. 33B, pp. 865-876.

7. E. Jak, B. Zhao and P. Hayes, *Metall. Mater. Trans. B*, 2000, vol. 31, pp. 1195-1201.

8. E. R. Segnit, *J. Am. Ceram. Soc.*, 1954, vol. 37, p. 5.

9. M. Selleby, *Metall. Mater. Trans. B*, 1997, vol. 28, pp. 577-596.

10. P. Vadász, M. Havlík and V. Daněk, *cent.eur.j.chem.*, 2006, vol. 4, pp. 174-193.

11. B. Zhao, P. C. Hayes and E. Jak, *Int. J. Mater. Res.*, 2011, vol. 102, pp. 134-142.

12. B. Zhao, P. C. Hayes and E. Jak, *Int. J. Mater. Res.*, 2011, vol. 102, pp. 269-276.

13. B. Zhao, P. C. Hayes and E. Jak, *Metall. Mater. Trans. B*, 2010, vol. 41, pp. 386-395.

14. B. Zhao, P. C. Hayes and E. Jak, *Metall. Mater. Trans. B*, 2010, vol. 41, pp. 374-385.

15. B. Zhao, P. C. Hayes and E. Jak, *Metall. Mater. Trans. B*, 2010, vol. 42, pp. 50-67.

16. B. Zhao, P. C. Hayes and E. Jak, *Metall. Mater. Trans. B*, 2011, vol. 42, pp. 490-499.

17. B. Zhao, P. C. Hayes and E. Jak, *Metall. Mater. Trans. B*, 2011, vol. 42, pp. 978-986.

18. H. Liu, Z. Cui, M. Chen and B. Zhao, *Metall. Mater. Trans. B*, 2016, vol. 47, pp. 1113-1123.

19. H. Liu, Z. Cui, M. Chen and B. Zhao, *Metall. Mater. Trans. B*, 2016, vol. 47, pp. 164-173.

20. C. W. Bale, E. Bélisle, P. Chartrand, S. A. Decterov, G. Eriksson, K. Hack, I. H. Jung, Y. B. Kang, J. Melançon, A. D. Pelton, C. Robelin and S. Petersen, *CALPHAD: Comput. Coupling Phase Diagrams Thermochem.*, 2009, vol. 33, pp. 295-311.

21. B. Zhao, Z. Cui and Z. Wang, In *4th International Symposium on High-Temperature Metallurgical Processing*, (John Wiley & Sons, Inc.: 2013), p 10.

22. H. Liu, Z. Cui, M. Chen and B. Zhao, Phase Equilibrium Study of ZnO-"FeO"-SiO_2-MgO System at Po_2 10^{-8} atm, *Metall. Mater. Trans. B*, Summited, 2016.

23. T. Hidayat, P. Hayes and E. Jak, *Metall. Mater. Trans. B*, 2012, vol. 43, pp. 27-38.

24. P. Coursol, P. Mackey, Y. Prevost, M. Zamalloa and A. Warner, In *The Carlos Díaz Symposium on Pyrometallurgy, Toronto Canada*, (2007), pp 79-92.

9 Arsenic and Zinc Distribution Behaviour in the Copper Smelting Process

Abstract: An extensive review has been carried out on the thermodynamic behaviour of As and Zn in the copper smelting process. Present review covers three different aspects of the minor elements during the copper smelting processes, including the occurrence manners and the partitioning effect, with particular interest on fractional distribution behaviours. Generally trends of the correlations between operating parameters and minor elements distribution were obtained for the industrial smelting practices. The matte grade in the continuously copper smelting operation and sulphur dioxide partial pressure (Pso_2) both have major impact on the minor elements distribution which should be careful controlled to maximise to total elimination. Other operating parameters, such as the ratios of Fe/SiO_2 and CaO/SiO_2 in slag, seems to have minor effect on total elimination of the minor elements, which can be applied as useful tool in the management of minor elements in the copper smelting operations.

Key words: arsenic, zinc, occurrence manner, distribution coefficient, fractional distribution

9.1 Introduction

During the pyrometallurgical copper production processes, the minor elements, such as arsenic (As) and zinc (Zn) that commonly present in the copper ores could pose issues on the industrial operation.[1, 2] It has been well known that the As content in the final copper product should be carefully controlled for marketing, and that in the slag should also well controlled to meet the environmental regulation for safety disposal.[3, 4] Meanwhile, the Zn tends to have major effect on the slag liquidus temperature[5] which plays crucial role in the industrial operation. Hence, the management and control of minor elements in the pyrometallurgical production processes are critically important, not only to the final copper quality and smooth operation, but also to the environmental protection and public health[4].

The attainment of management and control of minor elements in the pyrometallurgical copper production processes requires comprehensive understanding on the thermodynamic behaviour of these elements in the copper production circuit. As the conventional pyrometallurgical copper production generally involves copper matte-making and matte-converting processes in sequences, so that a good elimination of these elements is desirable at matte-making process. Present review will focus on the fractional distribution* behaviour of As and Zn in the matte-making process.

* Fractional distribution": normalized mass proportion of minor elements to each phase.

In the matte-making (or smelting) process where multi-phases coexisting, including the copper matte, slag (the solid phase was not considered for simplification) and off-gas, such complexity at smelting temperature brings difficulty in experimental studies on the fractional distribution behaviour of minor elements. For this reason, the thermodynamic model become a powerful tool, not only to predict the fractional distribution behaviour of minor elements, but also to cognize the correlations between the fractional distribution behaviour and the industrial operating parameters. Several studies[6-11] have been developed by varied authors to prediction the distribution behaviour in the copper smelting process.

However, the development of thermodynamic model to predict the fractional distribution behaviour of minor elements requires information of thermodynamic basis, such as the occurrence of minor elements in each phases and partitioning coefficients under the conditions relevant to those in the industrial smelting. Meanwhile, the knowledge on thermodynamic basis of minor elements in smiting process is also vital to interpret the thermodynamic predictions and comprehend the impacts by the operating parameters.

As such, present paper firstly review the occurrence manners of minor elements in the copper smelting process. The compiled information of the partitioning coefficients was then present at the Section 9.2. At last, the fractional distribution of minor elements from both thermodynamic modelling and industrial (or lab-scale) observations was reviewed. Further comparisons were also conducted between the FactSage 6.4[12] and results from other sources.

9.2 Occurrences Of As and Zn in Copper Smelting Processes

The occurrence manners of the minor elements in the copper smelting forms the basic knowledge to understand the correlations between Previous review on the probable forms of copper smelting in the copper smelting process had been conducted by Steinhauser *et al*[13] since 1982, where the occurrence of arsenic was not included. Hence, review was further improved based on their work by incorporating new findings with As included, as listed in the Table 9.1. The As in the gas, as suggested by Nagamori and Chaubal[14] the sulfidic arsenic (AsS) tends to be the predominant species with minor oxidic arsenic (AsO); for zinc, the Zn gas has the highest partial pressure with ZnS in subsequent.

The forms of minor elements in the condensed phases in the copper smelting, as shown in the Table 9.1, both As and Zn tends to be in oxidic form in the slag phase. Meanwhile, the As present as AsCu3 molecular cluster in the matte phase according to the study performed by Nagamori.[15] The Zn in the matte phase, however, tends to be stable as ZnS according those studies by Yazawa[16, 17].

Table 9.1 Probable forms of arsenic and zinc during copper smelting process

Phase	Znic[13]	Arsenic[2, 13-15, 18]
Gas	Zn, ZnS, ZnO	AsS, AsO
Slag	ZnO	$AsO_{1.5}$
Matte	ZnS	$AsCu_3$

9.3 Distribution Coefficients Of As and Zn in Copper Smelting Processes

The partitioning effects of minor elements under conditions relavent to that in the copper smelting process are particularly important for the development of thermodynamic model. Moreover, the distribution coefficicents - the presentation of partitioning effects, can be experimentally determined and derived from the thermodynamic properties. Hence, the accurracy of the distribution coefficients of minor elements should be the first priority when developing the thermodynamic model in prediction the fractional distribution.

The Table 9.2 and Table 9.3 show the distribution coefficients of As and Zn respectively, under typical conditions relevant to that in industrial copper smelting. As shown in Table 9.2, good consistency can be seen between varied sources except the value reported by Roine[19] which wad derived from the empirical equation. The matte grade in continuously smelting operation, as reported by Font and Reddy[20, 21] and Chen *et al*[6] tends to have minor impact on the distribution coefficient of As until that approach 70 pct of Cu in matte where significantly drop was observed.

As shown in the Table 9.3, the distribution coefficients of Zn between slag and matte phases are much higher than those of As as shown in the Table 9.2, which suggest that the ZnO tends to be stable under the copper smelting conditions.[16, 17] The value of distribution coefficient determined by Nagamori and Mackey[22], seems to have good consistent with the industrial observation. The value reported by Yazawa and Azakami[17] tends to have big deviation to the industrial observation which is due to the lack of activity coefficient data.

It should be noticed those values in Table 9.2 and Table 9.3 only present the typical distribution coefficient of As and Zn respectively, more delicate models have be developed by Nagamori and Mackey[22] and chen *et al*[6] to predict the distribution coefficients at given conditions.

Table 9.2 Distribution coefficients of As between slag and matte phase under copper smelting conditions

Temperature (°C)	Matte grade (%Cu)	$L_{Slag/Matte}$	Reference
1200	68	0.6	Nagamori and Mackey[22]
1300	60	0.6	Roghani *et al*[23, 24]
1300	60	0.6	Font and Reddy[20, 21]
1250	75	0.6	Acuna and Sherrington[25]
1250	60	0.2	Roine[19]

Table 9.3 Distribution coefficients of Zn between slag and matte phase under copper smelting conditions

Temperature (°C)	Matte grade (%Cu)	$L_{slag/Matte}$	Reference
1200	Intermediate matte grade	2.0	Yazawa and Azakami[17]
1200	68	7.1	Nagamori and Mackey[22]
1200	68	5.9	Industrial observation[22]

9.4 Fractional Distribution Behaviours of As and Zn during Copper Smelting Processes

To management and control the minor elements during the industrial copper smelting, it is imperative to comprehend the correlations between operating parameter and fractional distribution behaviour of those elements. Several thermodynamic models[6, 8-10, 25-28] have been developed to investigate the effects of operating parameters, including matte grade, smelting temperature, slag compositions (Fe/SiO_2 ratio and slag basicity), Pso_2 (or the oxygen enrichment in tuyere gas) and initial content of minor elements in the charge, on the distribution behaviour of As and Zn in the copper smelting process. However, limited information on the fractional distribution in copper smelting was reported by the experimental studies[11, 29] or industrial observations[9, 10].

In present study, the FactSage 6.4 was also applied to predict the fractional distribution of As and Zn under the conditions relevant to the industrial copper smelting. All these information were compiled together on operating-parameter-basis for further comparisons. However, when comparing the results between varied sources, the parameters applied to should be considered, so that these information were listed in the Table 9.4 and Table 9.5 for the investigation of As, and Table 9.6 that of Zn.

Table 9.4 Detailed parameters applied in predicting fractional distribution of arsenic (As)

Reference	Processing Parameters
FactSage 6.4[12]	1523 K, 0.2 %As in charge, Pso_2 = 0.1 atm, Fe/SiO_2 = 1.8
Itagaki and Yazawa[10]	1573 K, 0.1 %As in charge, Pso_2 = 0.1 atm, 55 %Cu
Nagamori and Chaubal[9]	1473 K, Pso_2 = 0.12 atm, 72 %Cu, 21 $\%O_2$ in tuyere air
Itagaki[30]	1573 K, 0.3 %As in charge, Pso_2 = 0.12 atm, 60 %Cu
Sohn *et al*[8]	1473 K, 0.14 %As in charge, Pso_2 = 0.15 atm, 21 $\%O_2$ in tuyere air
Nagamori *et al*[28]	1453 K, Fe/SiO_2 = 1.2, Pso_2 = 0.2 atm, 40% O_2 in tuyere air
Cerna *et al*[27]	1523 K, 0.15 %As in charge, Pso_2 = 0.25 atm, 72 %Cu, 32.2 $\%O_2$ in tuyere air
Acuna and Sherrington[25]	1523 K, 0.2 – 1.2 %As in charge, 75 %Cu, 32 $\%O_2$ in tuyere air
Chen *et al*[6]	1523 K, Pso_2 = 0.1 atm, 0.2 %As in charge, 60 %Cu, 21 $\%O_2$ in tuyere air

Table 9.5 Detailed parameters applied in observations of fractional distribution of arsenic (As)

Sources	Processing Parameters
Nagmori and Chaubal[9]	1473 K, 0.14 %As in charge, 72 %Cu, 21 %O_2 in tuyere air
Itagaki and Yazawa[10]	70 %Cu (KCS process)
	0.2 – 2 %As in charge, 40 - 45 %Cu (TBRC process)
	0.1 – 0.17 %As in charge, 45 %Cu (Outokumpu flash smelting)
Moyano *et al*[26]	1523 K, Pso_2 = 0.27 atm, 61 – 76 %Cu, 37 %O_2 in tuyere air (lab-scale)
	1523 K, Pso_2 = 0.27 atm, Fe/SiO_2 = 1.7, 68 – 71 %Cu, 36 %O_2 in tuyere air
Montenegro[11]	1523 K, Pso_2 = 0.1 atm, Fe/SiO_2 = 2, 61 %Cu, 21% O_2 in tuyere air

Table 9.6 Detailed parameters applied in investigations of fractional distribution of zinc (Zn)

Sources	Processing Parameters
FactSage 6.4[12]	1523 K, 0.2 %Zn in charge, Pso_2 = 0.1 atm, Fe/SiO_2 = 1.8
Nagamori and Chaubal[9]	1473 K, Pso_2 = 0.12 atm, 72 %Cu, 21 %O_2 in tuyere air
Sohn *et al*[8]	1473 K, 1 %Zn in charge, Pso_2 = 0.15 atm, 21 %O_2 in tuyere air
Nagamori *et al*[28]	1453 K, Fe/SiO_2 = 1.2, Pso_2 = 0.2 atm, 40% O_2 in tuyere air
Montenegro *et al*[11]	1523 K, Pso_2 = 0.1 atm, 3.06 %Zn in the charge, Fe/SiO_2 = 2, 61 %Cu, 21% O_2 in tuyere air (lab-scale study)

9.4.1 Fractional distribution and matte grade

In the steady-state or continuously copper smelting operation, the matte grade can be treated as constant. In the meanwhile, the matte grade almost depends on the oxygen potential. As such, the impact of matte grade on the fractional distribution of minor element should be deliberately considered. Comparisons on the fractional distributions of minor element behaviour between the thermodynamic modellings, industrial and lab-scale observations and FactSage 6.4 predictions[12] were carried out, as shown in in Figure 9.1 and Figure 9.3 respectively. The length of bar itself corresponds to the deportment of minor elements to the slag phase, where the solid bars (sparse bar was used instead where overlap happens) represent those results obtained by thermodynamic modelling and the hollow bars represent those by industrial or lab-scale observations. The dash lines and dot-dash lines represent the continuously predictions by thermodynamic models, while the dot lines represents those results from industrial or lab-scale observation. The gap between the paired lines stands for the proportion of minor element in the slag phase and that above and below denotes the proportion of minor elements in the gas phase and matte phase respectively. Such rules were applied all through the discussions in Section 9.4.

Figure 9.1 and Figure 9.2 show the fractional distribution of arsenic as function of matte grade at 1523 K and 1473 K respectively. It can be seen that all continuous thermodynamic predictions suggest higher deportment of As to slag phase and lower that to gas phase when matte grade increases. Meanwhile, good consistent between varied models and industrial or lab-scale observations can be seen at matte grade lower than 70 pct of Cu except the prediction by FactSage 6.4[12] which shows poor consistency with industrial observations through all matte grade. A much lower total

elimination* was observed in Itagaki's model[10] where low gas saturation factor was applied. The Chen's model[6] shows that the total elimination significantly decreases when the matte grade approaching white metal, which can be explained by the fact that the higher grade matte generally has higher affinity to As[6, 17].

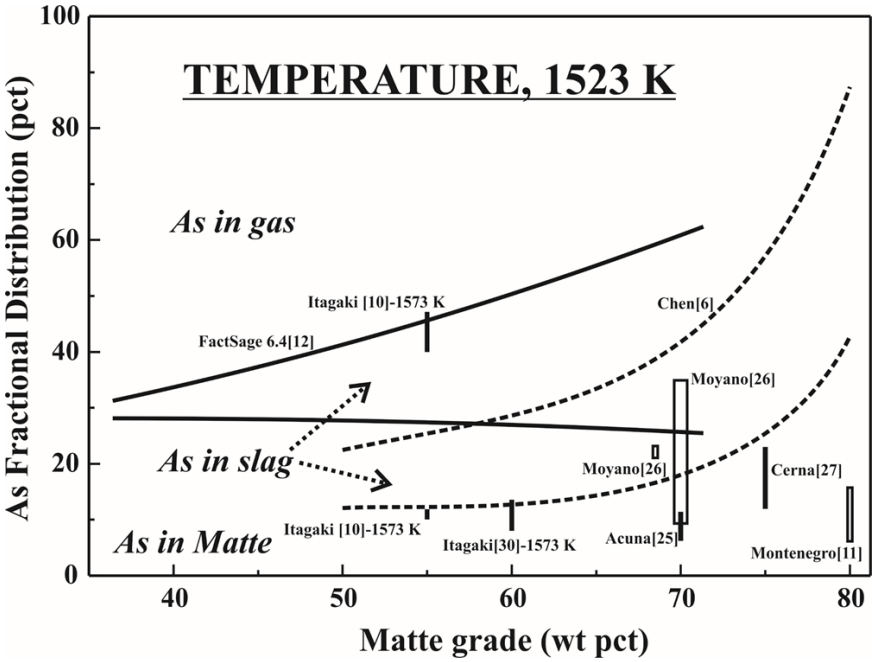

Figure 9.1 Fractional distribution of arsenic during copper smelting as function of matte grade at 1523 K

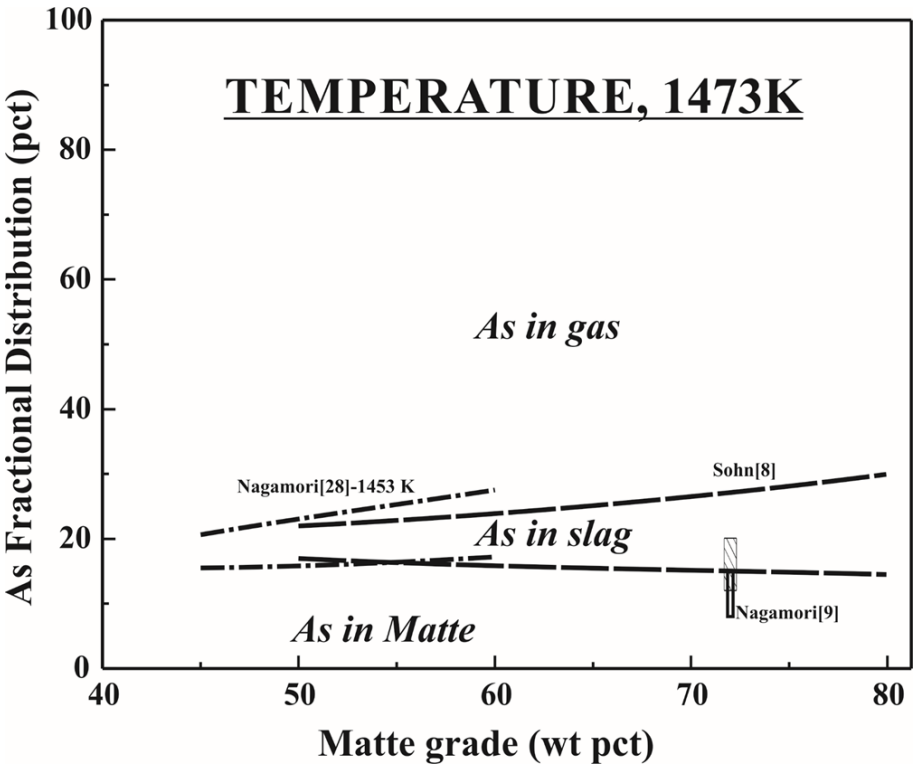

Figure 9.2 Fractional distribution of arsenic during copper smelting as function of matte grade at 1473 K

* total elimination: the sum of fractional distributions of minor element in gas and slag phases

The effect of matte grade in the copper smelting on the fractional distribution of zinc was shown in the Figure 9.3. It is worth noted that the prediction by FactSage 6.4 suggests that only negligible zin will report to the gas phase, so that only the deportment of zinc to slag phase was illustrated Figure 9.3. It can be seen that both the modellings by Nagamori *et al*[28] and Sohn *et al*[8] suggest that the deportment of Zn to the slag phase substantially increase with the matte grade accompanying with an increasing on the overall elimination. The deportment of Zn to the slag phase predicted by FactSage 6.4[12] also substantially increases when matte grade increasing. The volatilization effect of Zn in the dust-circulation tests by Montenegro *et al*[11, 29] that tends to be much higher than others. The reason could be the high kinetics of volatilization under the gas flushing as the volatilization effect in the settling zone in the copper smelter could be much lower compared to that in the circulation tests. Such phenomenon was also observed in our phase equilibria studies on Zn-containing slag under Po_2 10^{-8} atm[5, 31]. It can be seen that the volatilization rate of Zn under such conditions ranges from 22 to 80 wt pct which are comparable to those obtained by Montenergro *et al*[11, 29].

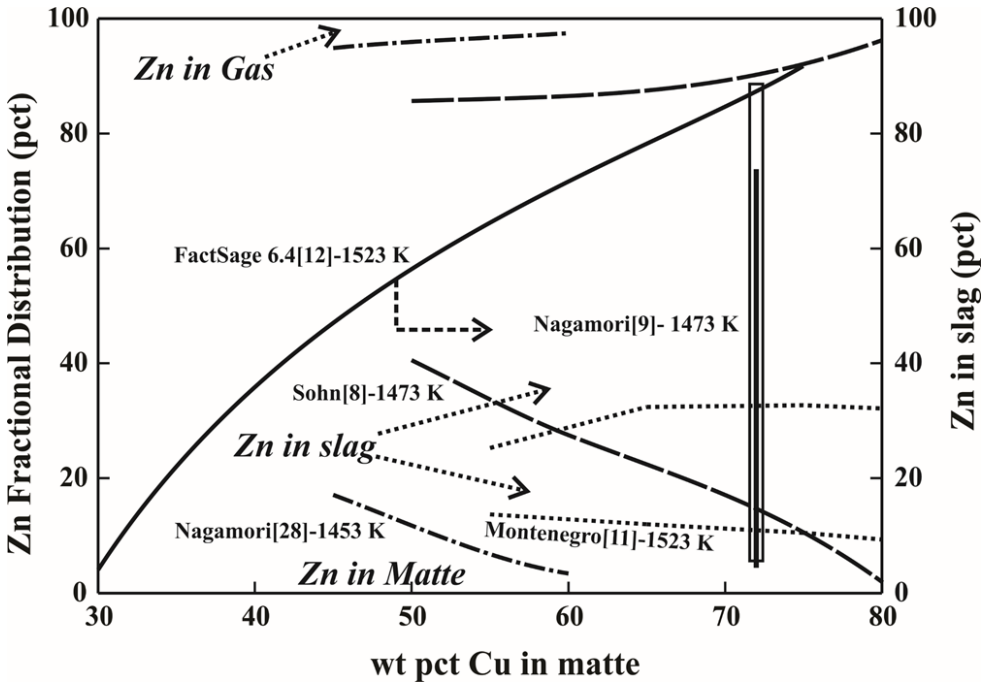

Figure 9.3 Fractional distribution of arsenic during copper smelting as function of matte grade

9.4.2 Fractional distribution and Fe/SiO_2 ratio of slag

The Fe/SiO_2 ratio of the slag plays crucial in the smooth operation of industrial smelting. As such, it is necessary to investigate to the correlation between Fe/SiO_2 and fractional distribution of minor element. Figure 9.4 shows the fractional distribution of arsenic as function of Fe/SiO_2. It can be seen that both predictions by Chen *et al*[6] and FactSage 6.4[12] suggest that high Fe/SiO_2 tends to increase the deportment of As to the slag phase, while has minor effect on the total elimination rate. The enhanced slagging effect is contributed by the decrease of activity coefficient at higher Fe/SiO_2.[6]

The effect of Fe/SiO_2, according to the prediction by Nagamori *et al*[28], appears to have minor impact to the fractional distribution of Zn in the copper smelting. The prediction by FactSage 6.4[12] suggests that the deportment of Zn to matte phase will slightly increase when Fe/SiO_2 increases. This discrepancy could due to the lack of experimental data for thermodynamic modelling.

The Fe/SiO_2 ratio of slag phase, although has minor impact on the total elimination of minor element, tends to have major effect on the deportment of As to the slag phase. For this reason, the Fe/SiO_2 ratio can be a useful tool to control the As content in the slag to meet the environmental regulation for safety disposal.

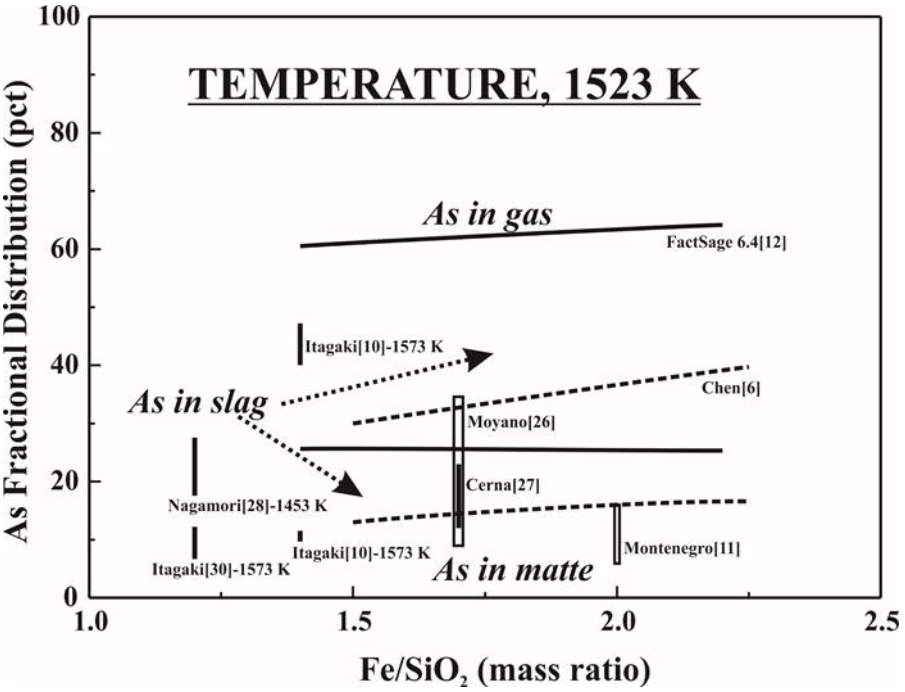

Figure 9.4 Fractional distribution of arsenic during copper smelting as function of Fe/SiO_2 (mass)

9.4.3 Fractional distribution and slag basicity (CaO/SiO_2)

The addition of CaO to non-ferrous smelting slag has been an effective way to modulate the slag viscosity.[32, 33] For this reason, appreciable amount of CaO generally present in the copper smelting slag.[34, 35] As such, it is important to investigate the impact of CaO (or slag basicity) on the fractional distribution of minor element.

Figure 9.5 shows the correlation between the slag basicity and fractional distribution of As. Both predictions by Chen *et al*[6] and FactSage 6.4 suggest that higher deportment of As to slag phase when CaO/SiO_2 increases. Such phenomenon can be explained by the decreasing on activity coefficient of As in the slag when increasing slag basicity[6, 20] which will promote the slagging effect. The total elimination, however, tends to be stable with CaO/SiO_2 increasing.

The slag basicity, based on the FactSage 6.4 prediction[12], tends to slightly decrease the total elimination of Zn in copper smelting process. No other information is available. Similar to that of Fe/SiO_2, slag basicity can be an effective approach to management the deportment of minor elements to the off-gas or slag phase in the industrial practices.

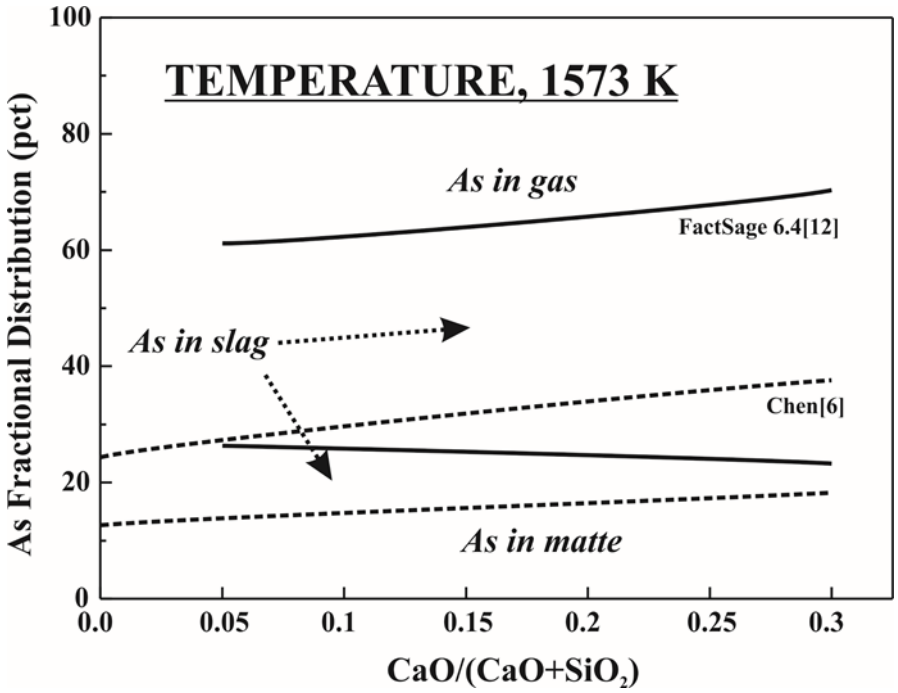

Figure 9.5 Fractional distribution of arsenic as function of $CaO/(CaO+SiO_2)$ (mass) in copper smelting

9.4.4 Fractional distribution and Pso_2 (Sulphur dioxide partial pressure)

The oxygen enrichment in the tuyere gas (submerged-tuyere smelting) play vital role in the smelting process, not only to control the matte grade, but also to the Pso_2 in the off-gas in meeting requirement of sulfuric acid making. Meanwhile, the Pso_2 can be treated as function of oxygen enrichment in the tuyere gas when the feeding materials fixed[36], which generally tends to be when higher oxygen enrichment applied. For this reason, the correlation between Pso_2 and fractional distribution of minor elements.

Figure 9.6 shows the fractional distribution of arsenic as function of the Pso_2. Generally, good consistency can be between predictions except that by FactSage 6.4[12] The prediction by FactSage 6.4 shows poor agreement with others, particularly at higher Pso_2 as the volatilization kinetics effect was not included. The continuous predictions by Nagamori[28] and Chen *et al*[6] suggest that the deportment of As to the gas significantly decreases with the increasing Pso_2. During the copper smelting process, when higher oxygen enrichment applied at fixed gas flow rate, the volume of the off-gas will decrease which is detrimental for the volatilization. The variation of total elimination when Pso_2 increasing, however, tends to substantially decrease as predicted by Nagamori[28] and be stable in prediction by Chen *et al*[6].

Figure 9.7 shows the impact of Pso_2 on the fractional distribution of Zn in the matte-making process. It can be seen that studies by Nagamori *et al*[28] and Montenegro *et al*[29] both suggest that the deportment of Zn to the slag phase increases with Pso_2. Similar trend can also be observed in the prediction by FactSage 6.4[12]. The high volatilization of Zn in the dust-circulation test by Montenegro *et al*[29] should be due to the high vaporization kinetics.

It can be concluded that the Pso_2 that closely the oxygen enrichment in the tuyere gas has major impact on the volatilization of the minor elements. The impact of that on the total elimination of minor elements, however, tends to be inconsistent between thermodynamic models.

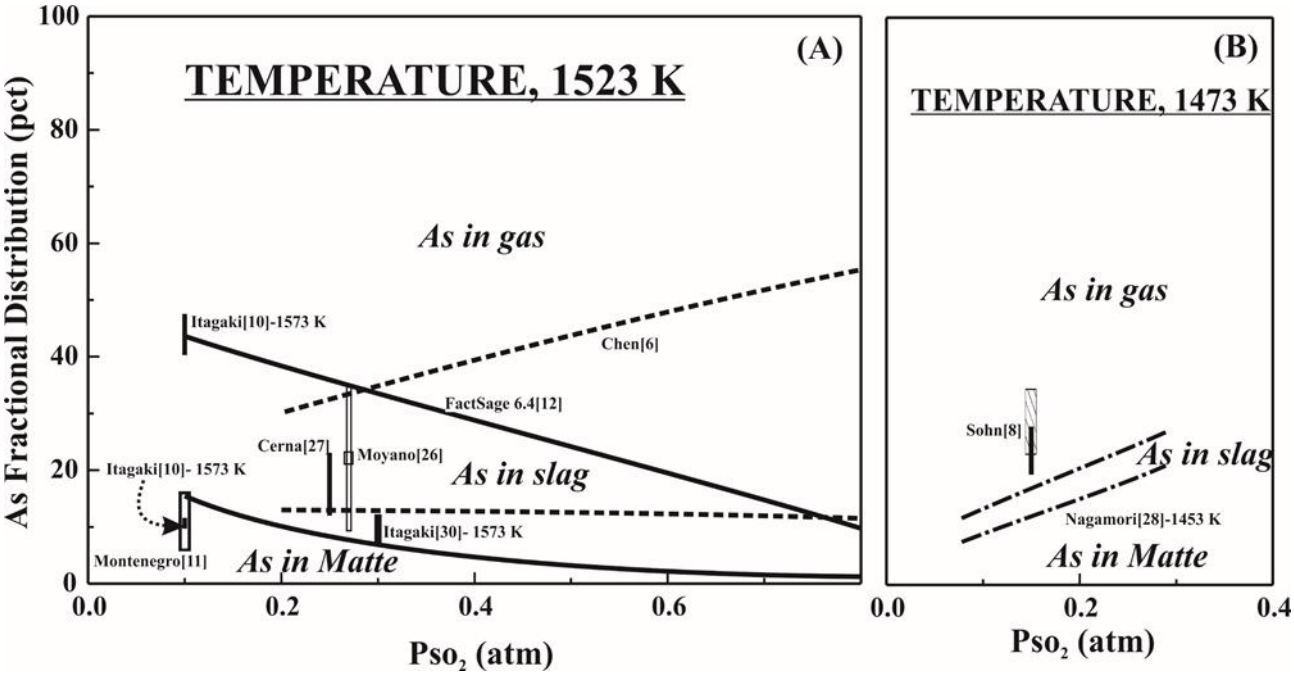

Figure 9.6 Fractional distribution of arsenic during copper smelting as function of Pso_2, (a) - 1523 K and (B) - 1473 K

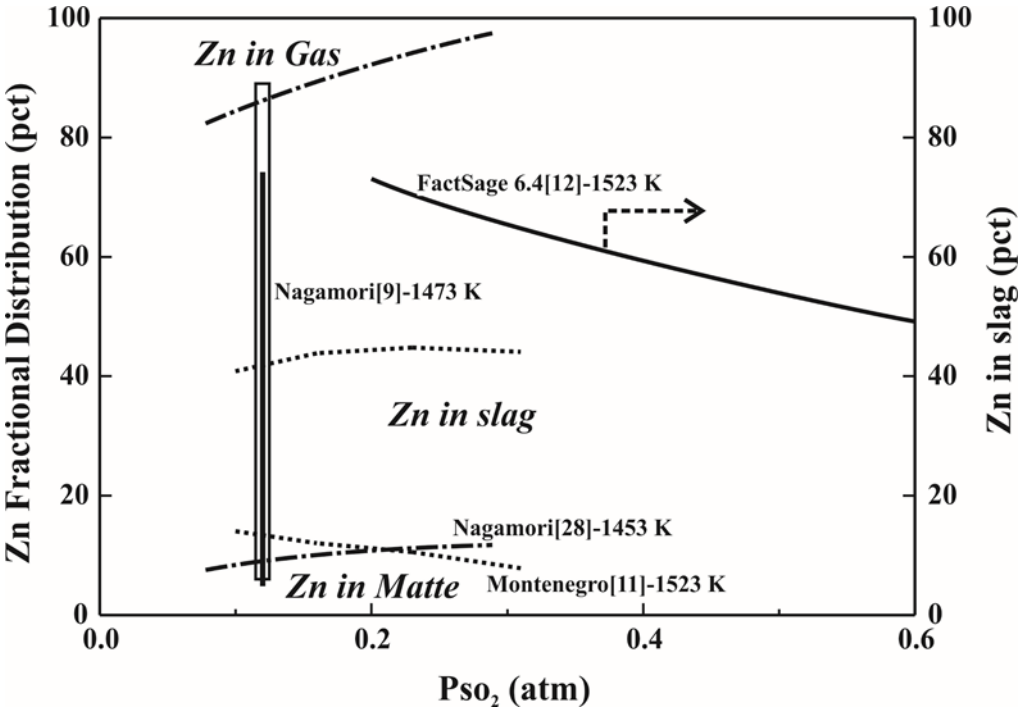

Figure 9.7 Fractional distribution of zinc as function of Pso_2 during matte-making

9.4.5 Fractional distribution and initial content in the charge

Due to the depletion of high grade copper ore, the chance of processing copper ore with high impurities level will likely increase in the future.[37] Moreover, the recirculation of the dust generated in the off-gas streams during smelting and converting processes to recover the copper, could also lead to abnormal high of impurities level in the charge.[11, 29] As such, it is essential to investigate the correlation between fractional distribution of minor element and its initial content in the charge.

Figure 9.8 shows effect of on its fractional distribution of arsenic as function of the initial content in charge. It can be seen that all the thermodynamic modellings suggest that a higher deportment of As to the gas phase when the initial content in charge increases. Such phenomenon can be explained by the fact that partial pressure of As-bearing gas species increases with the As content in the charge. Meanwhile, the total elimination also increases with increasing initial content in charge. However, the study by Montenegro *et al*[11] suggests a maximum total elimination at 1.6 wt pct of As in charge which could origin from the saturation of gas species. The FactSage 6.4[12] seems to have better prediction at higher As content as compared to other results. It should be noted that although the total elimination of As increase with the initial content, the concentration of As in copper matte at the end of smelting could also significantly increase.[11, 26, 29] For this reason, special care should be paid the subsequently matte-converting process to make sure the final copper productivity are suitable for the marketing.

No information on the relationship between Zn initial content and its fractional distribution was reported. The prediction by FactSage 6.4[12] that the fractional distribution hardly depend on the initial content in charge.

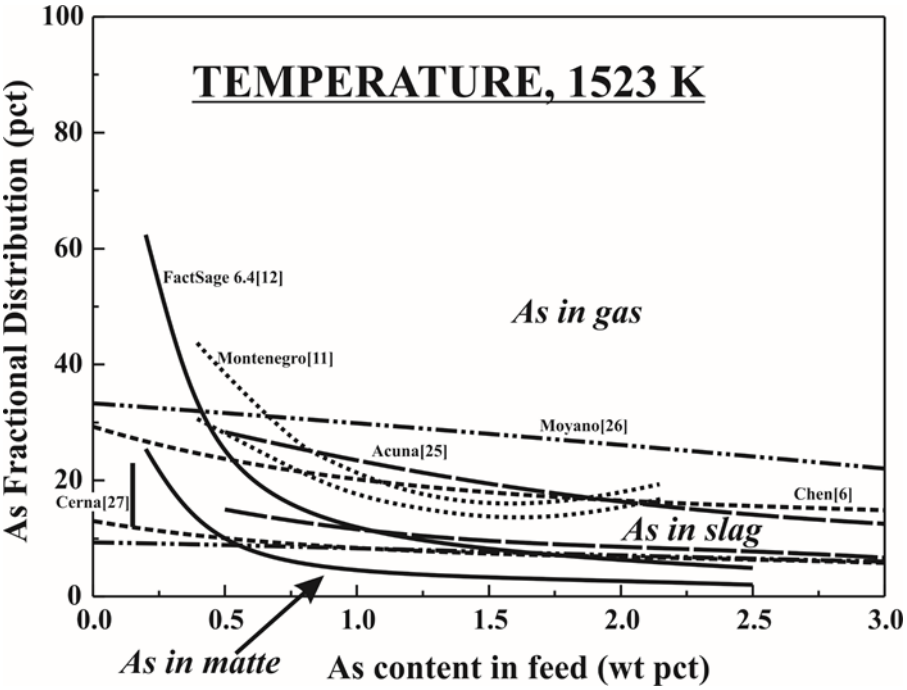

Figure 9.8 Fractional distribution of arsenic during copper smelting as function of As content in the charge

9.4.6 Fractional distribution and operating temperature

The operating temperature of copper smelting process generally varies between different types of smelting processes. For instance, the operating temperature is close to 1180 °C in the Fangyuan Bottom Blowing, while that in the Noranda matte-mode process is around 1200 °C and 1250 °C for the Teniente Converter.[9, 25, 38] As such, it is necessary to consider the impact of operating temperature on the fractional distribution of minor elements.

Figure 9.9 shows the relationship between operating temperature and fractional distribution of As. It is notable that a higher deportment of As to the gas phase when the smelting temperature increases as the partial pressure of As-bearing gas species increases at elevated temperature. The total elimination rate, however, tends to be steady when the operating temperature increases in all studies.

Figure 9.10 shows the distribution behaviour of zinc as function of operating temperature. The studies by Nagamori *et al*[28] and Montenegro *et al*[11] both suggest that deportment of Zn to the gas phase increases when operating temperature increases accompanying with inhibited slagging effect. Meanwhile, the overall elimination of Zn, however, tends to be steady when the operating temperature increasing. However, the prediction by FactSage 6.4 shows that the total elimination significantly

with smelting temperature increasing, of which the discrepancy should be due to its deficiency in prediction vaporization kinetics.

It can be concluded that the volatilization of minor elements can be promoted at elevated operating temperature with minor impact on the total elimination. As such, smelting operating temperature could be a useful approach in management and control of minor element during copper smelting when other conditions permit.

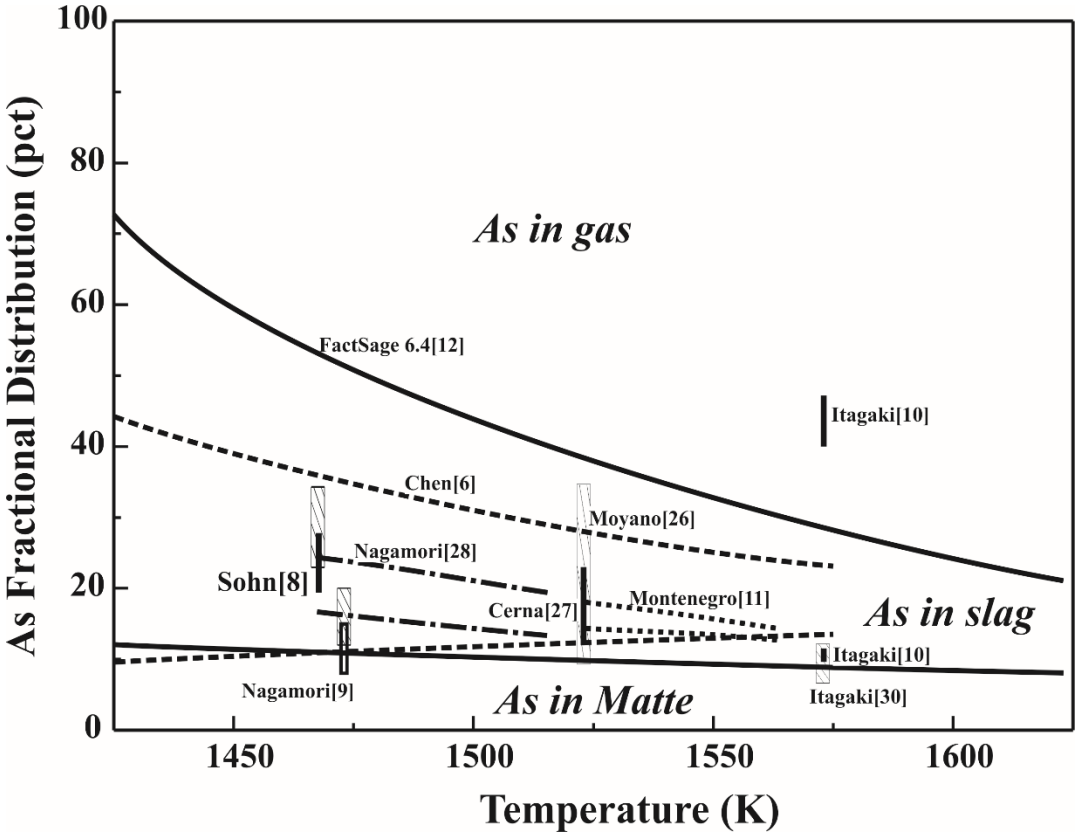

Figure 9.9 Fractional distribution of arsenic during copper smelting as function of smelting temperature

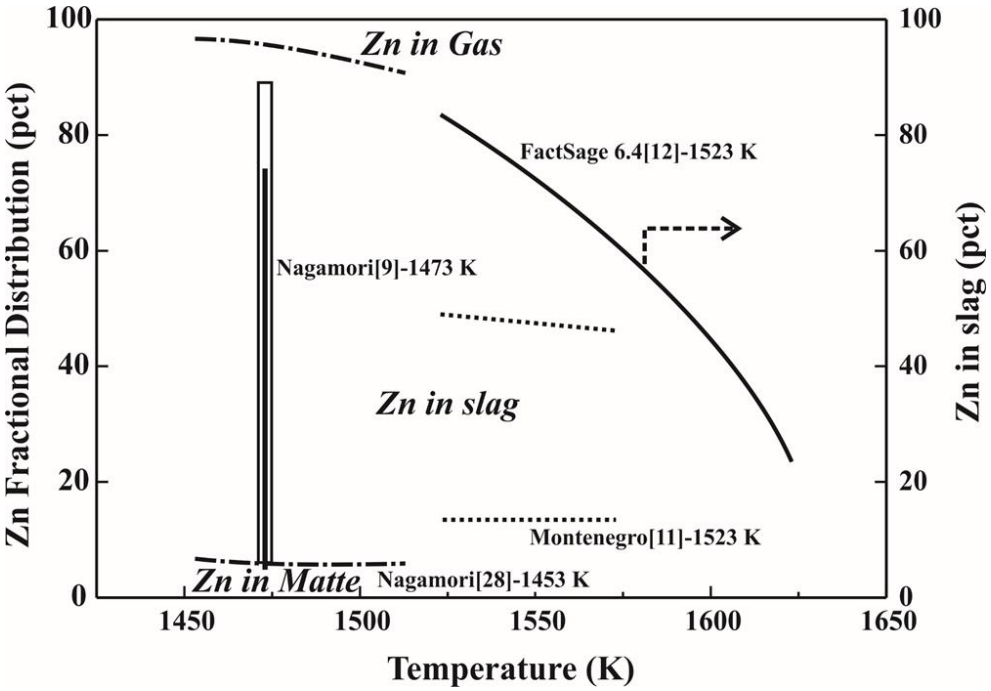

Figure 9.10 Fractional distribution of zinc as function of operating temperature during matte-making

9.5 Summary

Current paper presents an extensive literature review on the thermodynamic behaviour of minor elements relevant to that in the copper smelting process. Present review covers the key information on three aspects of thermodynamic behaviour of arsenic and zinc during copper smelting, the occurrence manners, partitioning effect and fractional distribution. Special attention has been paid on the impact of operating parameters on fractional distribution in the copper smelting process. Major findings on the correlations between operating parameters and fractional distribution behaviour of minor elements are summarized in the Table 9.7.

Table 9.7 Correlations between fractional distribution of minor elements and industrial operating parameters

Operating Parameter	Slagging Effect		Volatilization Effect		Total Elimination	
	Positive	Negative	Positive	Negative	Positive	Negative
Matte grade	As, Zn			As, Zn	Zn	As
Pso_2	As, Zn			As, Zn		As
Fe/SiO_2	As			As		—
$CaO/(CaO+SiO_2)$	As			As		—
Initial content in feed		As	As		As	
Temperature		As, Zn	As, Zn		As	

Note: bars stand for those where minor impact observed.

Generally, good total elimination of zinc (Zn) can be attained during the copper matte-smelting process due to the magnificent slagging effect. That of arsenic (As), however, tends be highly dependent on the matte grade and Pso_2. As such, these two parameters should be well-controlled

during in the matte-making. Other factors, such as Fe/SiO_2 and slag basicity, however, tend to have minor impact on the total elimination of minor elements which can be applied as tools to the management of arsenic in the industrial smelting operation. In the meanwhile, accurate thermodynamic information of As at higher matte grade is required as large discrepancy has been observed in area where matte grade approaching 60 pct of Cu.

9.6 References

1. P. C. Chaubal and M. Nagamori, *Metall. Trans., B*, 1982, vol. 13B, pp. 339-48.

2. D. C. Lynch, S. Akagi and W. G. Davenport, *Metallurgical Transactions B*, 1991, vol. 22, pp. 677-688.

3. M. Free, *JOM*, 2011, vol. 63, pp. 89-89.

4. J. M. Pacyna, *SCOPE*, 1987, vol. 31, pp. 69-87.

5. H. Liu, Z. Cui, M. Chen and B. Zhao, *Metall. Mater. Trans. B*, 2016, vol. 47, pp. 164-173.

6. C. Chen, L. Zhang and S. Jahanshahi, *Metall. Mater. Trans. B*, 2010, vol. 41, pp. 1175-1185.

7. A. K. Kyllo and G. G. Richards, *Metall. Mater. Trans. B*, 1998, vol. 29, pp. 261-268.

8. H. Y. Sohn, H. Kim and K. W. Seo, In *EMC '91: Non-Ferrous Metallurgy—Present and Future*, (Springer Netherlands: 1991), pp 205-217.

9. M. Nagamori and P. C. Chaubal, *Metallurgical Transactions B*, 1982, vol. 13, pp. 331-338.

10. K. Itagaki and A. Yazawa, *Trans. Jpn. Inst. Met.*, 1982, vol. 23, pp. 759-67.

11. V. Montenegro, H. Sano and T. Fujisawa, *Mater. Trans.*, 2008, vol. 49, pp. 2112-2118.

12. C. W. Bale, E. B. P. Chartrand, S. A. Decterov, G. Eriksson, A. Gheribi, K. Hack, I. H. Jung, J. Melançon, A. D. Pelton, S. Petersen and C. Robelin, In *Celebrating the Megascale*, (John Wiley & Sons, Inc.: 2014), pp 141-148.

13. J. Steinhauser, A. Vartiainen and W. Wuth, *JOM*, 1984, vol. 36, pp. 54-61.

14. M. Nagamori and P. C. Chaubal, *Metallurgical Transactions B*, 1982, vol. 13, pp. 319-329.

15. M. Nagamori, *Can. Metall. Q.*, 2001, vol. 40, pp. 499-522.

16. A. Yazawa, *Can. Metall. Q.*, 1974, vol. 13, pp. 443-453.

17. A. Yazawa and T. Azakami, *Can. Metall. Q.*, 1969, vol. 8, pp. 257-261.

18. C. Chen and S. Jahanshahi, *Metall. Mater. Trans. B*, 2010, vol. 41, pp. 1166-1174.

19. A. Roine, *Metallurgical Transactions B*, 1987, vol. 18, pp. 213-223.

20. J. C. Font and R. G. Reddy, (Minerals, Metals & Materials Society: 2005), pp 51-60.

21. R. Reddy and J. Font, *Metall. Mater. Trans. B*, 2003, vol. 34, pp. 565-571.

22. M. Nagamori and P. J. Mackey, *Metallurgical Transactions B*, 1978, vol. 9, pp. 567-579.

23. G. Roghani, Y. Takeda and K. Itagaki, *Metall. Mater. Trans. B*, 2000, vol. 31, pp. 705-712.

24. G. Roghani, M. Hino and K. Itagaki, *Mater. Trans. JIM*, 1997, vol. 38, pp. 707-713.

25. C. M. Acuna and M. Sherrington, In *The Carlos Diaz Symposium on Pyrometallurgy*, (Canadian Institute of Mining, Metallurgy and Petroleum: 2007), pp 273-285.

26. A. Moyano, C. Caballero, R. Mackay, P. Morales and K. ltagaki, In *The Carlos Diaz Symposium on Pyrometallurgy*, (Canadian Institute of Mining, Metallurgy and Petroleum: 2007), pp 301-313.

27. M. Cerna, R. Bustos, G. Riveros and J. Soto, *Proceedings of the Pyrometallurgy 95,(Cambridge, England: The Institution of Mining and Metallurgy, IMM, 1995), 143-156*, 1995, pp. 143-156.

28. M. Nagamori, W. J. Errington, P. J. Mackey and D. Poggi, *Metall. Mater. Trans. B*, 1994, vol. 25B, pp. 839-53.

29. V. Montenegro, H. Sano and T. Fujisawa, *Miner. Eng.*, 2013, vol. 49, pp. 184-189.

30. K. Itagaki, *Metall. Rev. MMIJ*, 1986, vol. 3, pp. 87-100.

31. H. Liu, Z. Cui, M. Chen and B. Zhao, *Metall. Mater. Trans. B*, 2016, vol. 47, pp. 1113-1123.

32. M. Kucharski, N. M. Stubina and J. M. Toguri, *Can. Metall. Q.*, 1989, vol. 28, pp. 7-11.

33. G. H. Kaiura, J. M. Toguri and G. Marchant, *Can. Metall. Q.*, 1977, vol. 16, pp. 156-160.

34. B. Zhao, P. Hayes and E. Jak, *Journal of Mining and Metallurgy, Section B: Metallurgy*, 2013, vol. 49, pp. 153-159.

35. Z. Cui, Z. Wang and B. Zhao, In *Copper 2013: Copper International Conference*, (2013), pp 923-933.

36. M. Nagamori and P. J. Mackey, *Metallurgical Transactions B*, 1978, vol. 9, pp. 255-265.

37. W. J. Bruckard, K. J. Davey, F. R. A. Jorgensen, S. Wright, D. R. M. Brew, N. Haque and E. R. Vance, *Miner. Eng.*, 2010, vol. 23, pp. 1167-1173.

38. B. Zhao, Z. Cui and Z. Wang, In *4th International Symposium on High-Temperature Metallurgical Processing*, (John Wiley & Sons, Inc.: 2013), p 10.

10 Summary

In the present study, extensive experimental works on the phase equilibria of Zn-containing copper smelting slags have been carried out at Po_2 10^{-8} atm relevant to that in the copper smelting. Advanced experimental techniques were developed and adopted in present study to enable the exploration of phase equilibria behaviour on the Zn-containing copper smelting slags at reducing conditions. The experimental methodology applied in present studies involves master slags preparation, high temperature equilibration, quenching and electron probe X-ray microanalysis (EPMA). Such approach enables the analysis of phase assemblages and the corresponding compositions can be measured in the same sample.

The liquidus temperatures and phase relations of the systems "FeO"-SiO_2, ZnO-"FeO"-SiO_2, ZnO-"FeO"-SiO_2-Al_2O_3, ZnO-"FeO"-SiO_2-MgO and ZnO-"FeO"-SiO_2-CaO relating to the copper smelting slags were studied at a broad range of temperatures under Po_2 10^{-8} atm. The major findings in the present study can be summarized as follow:

(1) A reinvestigation on "FeO"-SiO_2 system at temperature range from 1473 K (1200 °C) to 1573 K (1300 °C) under Po_2 10^{-8} atm shows good agreement with the reported results, and fills the gap where no data available.

(2) Phase equilibria study on ZnO-"FeO"-SiO_2 system at temperature range from 1443 K (1170 °C) to 1573 K (1300 °C) shows that the presence of ZnO in the slag will increase the liquidus temperatures in the spinel phase compared to those in the "FeO"-SiO_2 system; the liquidus temperatures in the spinel phase increase with the ZnO content; the ZnO concentrations in liquid phase are about 2 times to those in spinel phase.

(3) Phase equilibria study on ZnO-"FeO"-SiO_2-Al_2O_3 system at temperatures, 1523 K (1250 °C), 1543 K (1270 °C) and 1573 K (1300 °C) with Al_2O_3 varying from 2 to 6 wt pct suggests that the introduction of Al_2O_3 into the slag phase increase the liquidus temperatures in the spinel phase compared to those in ZnO-"FeO"-SiO_2 system; the increase of Al_2O_3 content in the slag phase increases the liquidus temperature in the spinel phase; the ZnO concentration in the spinel phase of the ZnO-"FeO"-SiO_2-Al_2O_3 system is higher than that in ZnO-"FeO"-SiO_2 system.

(4) Phase equilibria study on ZnO-"FeO"-SiO_2-MgO system at temperatures, 1523 K (1250 °C), 1543 K (1270 °C) and 1573 K (1300 °C) with MgO varying from 2 to 6 wt pct indicates that the liquidus temperatures in spinel phase field are higher than those in the ZnO-"FeO"-SiO_2 system; the liquidus temperature in the spinel phase increases with MgO content in the slag

phase; the partitioning effect of ZnO between spinel and liquid phases behaves similarly to that in the ZnO-"FeO"-SiO_2 system.

(5) Phase equilibria study on ZnO-"FeO"-SiO_2-CaO system at temperatures, 1523 K (1250 °C), 1543 K (1270 °C) and 1573 K (1300 °C) with CaO varying from 2 to 6 wt pct shows that the presence of CaO in the slag increases the liquidus temperature in the spinel phase compared to ZnO-"FeO"-SiO_2 system; increasing CaO content in liquid phase will increase the lqiudus temperatures in the spinel phase field; similar partitioning effect of ZnO between spinel and liquid phases as to that in ZnO-"FeO"-SiO_2 system.

(6) Preliminary Phase equilibria study on ZnO-"FeO"-SiO_2-CaO-S system at temperatures 1443 K (1170 °C) and 1473 K (1200 °C) suggests that introduction of 2 wt pct of sulphur in the liquid phase dramatically decrease the liquidus temperature by 160 K compared the ZnO-"FeO"-SiO_2-CaO system.

The extensive literature review on the thermodynamic behaviour of minor elements relevant to that in the copper smelting process suggests than good total elimination of zinc (Zn) can generally be attained during the copper matte-smelting process due to the magnificent slagging effect. That of arsenic (As), however, tends be highly dependent on the matte grade and Pso_2. As such, these two parameters should be well-controlled during in the matte-making. Other factors, such as Fe/SiO_2 and slag basicity, nevertheless, tend to have minor impact on the total elimination of minor elements which can be applied as tools to the management of arsenic in the industrial smelting operation.